Enriching Majorana Zero Modes

Thesis by
Aaron Chew

In Partial Fulfillment of the Requirements for the
Degree of
Doctor of Philosophy

Caltech

CALIFORNIA INSTITUTE OF TECHNOLOGY
Pasadena, California

2020
Defended 11 May 2020

© 2020

Aaron Chew
ORCID: 0000-0003-0448-6215

ACKNOWLEDGEMENTS

I owe an immense amount of my success in grad school to the tireless efforts of my advisor, Jason Alicea. Without his guidance, dedication, and optimism, I would have been lost many times over these past years. I also profitted immensely from discussions with my collaborators: David Mross, Andrew Essin, Christina Knapp, and Wenyu He. I hope they enjoyed working together as much as I did.

I also would like to thank the friends I have made at Caltech, especially Joe Iverson and Loly Ekmekjian; their companionship offered a welcome reprieve from the day-to-day of graduate school. And finally, I would like to thank my family for their constant support. This thesis, the denouement of years of research, would not have been possible without their hard work and patience. Thank you.

ABSTRACT

My various projects in graduate school have centered around a common theme: harnessing relatively well-understood phases of matter and combining them to create exotic physics. They also involve Majoranas, or more accurately, defects that bind Majorana zero modes and are the centerpiece for topological quantum computation. We exploit and enrich this Majorana zero mode by employing topological superconductors, time crystals, and quantum dots and combining them together. Our first project involved joining Majorana nanowires and quantum dots to simulate the SYK model, a zero-dimensional strongly interacting phase with connections to black holes and holography. We follow by explaining how to combine spontaneous symmetry-breaking with topological superconductivity to recover parafermion physics in one dimension. We explain an exact mapping that relates fermions to parafermions, illustrating a deep connection between different one-dimensional phases of matter. We finally show that enhancing the topological superconductor with a time crystal, a phase of matter that spontaneously breaks time-translation symmetry, creates an anomalous zero mode that displays $4T$ periodicity in the Floquet drive. By combining these different phases in judicious ways we achieve exotic physics unattainable by the constituent parts. Our work thus illustrates profitable directions for harnessing Majorana zero modes to study the physics of exotic matter.

PUBLISHED CONTENT AND CONTRIBUTIONS

[1] Aaron Chew, Andrew Essin, and Jason Alicea. Approximating the sachdev-ye-kitaev model with majorana wires. *Phys. Rev. B*, 96:121119, Sep 2017. doi: 10.1103/PhysRevB.96.121119. URL https://link.aps.org/doi/10.1103/PhysRevB.96.121119.
A.C. participated in numerics, theoretical calculations, and manuscript preparation. Copyright 2017, APS Physical Review B.

[2] Aaron Chew, David F. Mross, and Jason Alicea. Fermionized parafermions and symmetry-enriched majorana modes. *Phys. Rev. B*, 98:085143, Aug 2018. doi: 10.1103/PhysRevB.98.085143. URL https://link.aps.org/doi/10.1103/PhysRevB.98.085143.
A.C. participated in numerics, theoretical calculations, and manuscript preparation. Copyright 2018, APS Physical Review B.

[3] Aaron Chew, David F. Mross, and Jason Alicea. Time-crystalline topological superconductors. *Phys. Rev. Lett.*, 124:096802, Mar 2020. doi: 10.1103/PhysRevLett.124.096802. URL https://link.aps.org/doi/10.1103/PhysRevLett.124.096802.
A.C. participated in numerics, theoretical calculations, and manuscript preparation. Copyright 2020, APS Physical Review Letters.

TABLE OF CONTENTS

LIST OF ILLUSTRATIONS

LIST OF TABLES

C h a p t e r   1

INTRODUCTION

	Standard Model	Condensed Matter System
ground state	vacuum	$\sim 10^{23}$ electrons
excitations	elementary particles	quasiparticles allowed
exchange	bosonic/fermionic	anyonic allowed
dimensions	$3 + 1D$	lower dimensions allowed

Table 11: A short comparison between the standard model and a typical condensed matter system.

The elementary particles of the standard model can be classified by their behavior under exchange. If two identical bosons are exchanged with one another, then the wavefunction of the system remains the same, while if two identical fermions are interchanged the wavefunction accumulates a global minus sign. This theorem is fundamental and all particles can be classified in this manner; the two options of plus and minus one are intimately tied to the fact that all closed paths in three dimensions can be deformed around the particles under exchange and into a point.

In condensed matter physics, the situation is far richer. Even though our Hamiltonians are still typically built from electrons, the ground state of the system is no longer the vacuum. This allows for the existence of quasiparticles—emergent degrees of freedom that cannot exist outside the condensed matter system. A typical example is a phonon in a metal, a quanta of vibration. While for all intents and purposes the phonon behaves as a bosonic particle, it cannot be "pulled out" of the metal and into the vacuum, as phonons require a lattice to vibrate.

These quasiparticles can thus behave in manners that standard particles cannot, and their exotic physics can be exploited to our ends. In two dimensions one escapes the restriction that exchange accumulates only a sign; quasiparticles with richer exchange are termed anyons [40, 63, 64]. Examples of these particles are the collective excitations that emerge in the Quantum Hall effect [46, 52, 53, 62], bound to vortices in a p+ip superconductor [31], in models like the toric code or Kitaev honeycomb [36, 38], or even in designer heterostructures [15, 18, 41, 45, 61] that combine these phases together, among many, many other suggestions [5, 6].
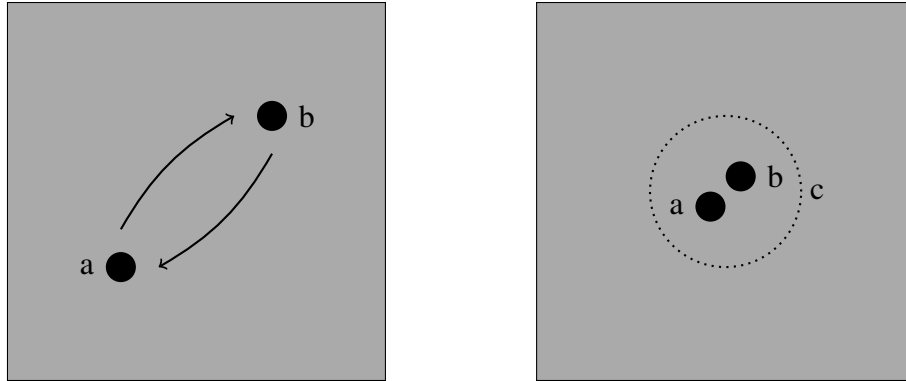
Figure 11: Anyonic exchange and fusion. Abelian anyons simple accumulate a phase, while non-Abelian anyons rotate the ground state with a unitary transformation. When Abelian anyons are fused, their result is deterministic; when non-Abelian anyons are fused, there are multiple possible outcomes.

These anyons are further classified into two types, Abelian and non-Abelian, which are intimately related to how they behave under exchange. Particle exchange in two dimensions is characterized by the braid group, and the representations of this group distinguish the different types of anyons [27, 66]. Abelian anyons accumulate a global phase when exchanged, yet in some sense this is still 'uninteresting' as global phases cannot be measured and generally do not affect measurement outcomes. Non-Abelian anyons, on the other hand, encode a non-local ground state degeneracy in the condensed matter system. Exhange of two non-Abelian anyons implements a unitary rotation of the ground state. This has led to the idea of implementing anyons for topological quantum computation: an adiabatic exchange of these anyons implements a protected unitary gate on the ground state subspace [23, 38, 48].

1.1 Topological quantum computation

Though anyons are exciting in their own right (with their bizarre physics and experimental signaures), by far and large their greatest application is in quantum computation. Simulating quantum systems with classical computers comes with immense difficulty; the size of the Hilbert space grows exponentially in system size and performing quantum operations involves matrix multiplication on that Hilbert space. While many clever simplifications exist for Hamiltonians that are local or obey some physical property that makes them tractable, a generic quantum evolution is computationally intractable on a classical computer. However, one may turn this problem on its head, instead proposing a quantum computer that manipulates a quantum system to solve problems that are expensive for a classical computer.

Unlike standard computers, which use binary arithmetic to compute, a quantum computer will involve unitary operations on a Hilbert space, thus opening a new paradigm of probabilistic algorithms. There are already incredible breakthroughs in the realm of quantum algorithms, most notably Shor's algorithm, a method of factoring prime numbers that far surpasses any known classical algorithm [58].

Manipulating a quantum system is fraught with difficulty. Even ignoring the precise control one must have over the quantum mechanical degrees of freedom, quantum systems by their nature are sensitive to even the smallest perturbation. Key to the power of quantum computers is the ability to maintain coherence of quantum states. Coupling to the environment will inevitably destroy our quantum superpositions. There have been several avenues suggested to solve the problem: one prominent technique is quantum error correction, where in essence the quantum system is redundantly coded to protect against environmental perturbations [59]. If the protection is acceptable to a certain degree, then quantum computation is possible.

The other technique, topological quantum computation, exploits the striking properties of non-Abelian anyons [38]. As mentioned earlier, well-separated non-Abelian anyons encode a degenerate ground state; this is the Hilbert space employed for quantum computation. Unlike systems with fermionic or bosonic zero modes, non-Abelian anyons cannot occur outside the system and cannot couple easily with environmental perturbations. If the anyons are separated in space by macroscopic distance L these perturbations are suppressed in system size. The system is also gapped, meaning thermal activations are suppressed in temperature. Thus, condensed matter systems hosting non-Abelian anyons are a promising avenue for fault-tolerant quantum computation.

Braiding

The mathematical theory behind non-Abelian anyons is incredibly rich [1, 9, 19, 20, 22, 25, 38, 42, 64]. Here we will review two key properties that will occur in later chapters: braiding and fusion. The exchange of two anyons (or any identical particle in general) implements a unitary rotation of the ground state subspace. These unitary operators form a representation of the braid group, as the worldlines in two dimensions form the strings that are braided around each other. It is these operations that we use to implement the quantum gates for computing. Depending on the type of non-Abelian anyon, one will have access to certain unitaries for gates. If these

gates can approximate any unitary operation with sufficient applications, then the gate set is universal. The braiding operation is also insensitive to local perturbations. If the anyons are kept far apart during the evolution, the braid operation depends only on the topology of the worldlines of the anyons and not the minutiae of the process.

Being able to braid non-Abelian anyons requires the ability to capture anyons and manipulate their locations. One of the most promising avenues concerns one-dimensional topological superconductors, which can host Majorana zero modes at their ends [2, 37, 43, 49, 55]. These zero modes can be braided by adjusting voltages and couplings in one-dimensional wire networks [4, 17, 30, 56], or via measurement-based protocols [8, 32].

Fusion

To implement quantum readout, anyons can also be brought together, or 'fused'. By bringing two anyons close together in position, we allow for perturbations that mix the anyons, lifting the ground state degeneracy and allowing us to collapse onto a quantum state. If the anyon is Abelian, there is only one result of fusion. If the anyon is non-Abelian, there are multiple outcomes of this process. The Majorana zero mode captures an Ising-type anyon, two of which can fuse into two possible channels [47].

1.2 Majorana zero modes

Majorana zero modes have been found to capture non-Abelian statistics and have thus received immense amount of attention in the literature, especially as a vehicle for quantum computation [3, 7, 39, 54, 60]. Their greatest advantage lies in that Majorana fermions can be captured in one-dimensional, non-interacting fermionic Hamiltonians (though superconductivity is necessary). While it may seem odd to imagine 'braiding' in one dimension, the Majoranas in our wires are not true anyons in the sense of quasiparticle excitations. It is more accurate to describe them as defects that bind zero modes, and 'braiding' is an adiabatic evolution of the Hamiltonian in parameter space. The non-Abelian defects in modern literature have similar flavors: some one-dimensional system (it could be a wire, or the edge of a topological insulator, or a trench carved in a quantum Hall fluid) is gapped with two different mechanisms on either side of a domain wall (for example, backscattering and pairing) [15, 18, 41, 50, 61, 68]. At the domain wall the gap must close and this 'zero mode' is what captures the non-Abelian statistics. Majorana nanowires are

especially alluring as one-dimensional systems are more tractable both theoretically and experimentally. Even though Ising anyons cannot achieve universal quantum computation alone via braiding and fusion, they can be supplemented with non-protected operations (such as magic-state injection) that can offer a high degree of fidelity at the cost of some overhead, or other techniques [10–13, 24, 48].

Algebra

Fermion creation operators may be decomposed as

$$c_j = \frac{1}{2}(\gamma_{2j} + i\gamma_{2j-1}) \tag{1.1}$$

$$\gamma_{2j-1} = -i(c_j - c_j^\dagger) \tag{1.2}$$

$$\gamma_{2j} = c_j + c_j^\dagger. \tag{1.3}$$

These new Majorana operators are self-Hermitian, anticommute, and square to unity:

$$\{\gamma_j, \gamma_k\} = 2\delta_{jk}, \quad j \neq k \tag{1.4}$$

$$\gamma_j = \gamma_j^\dagger. \tag{1.5}$$

A single Dirac fermion is equivalent to two Majoranas; the Fock space they generate is identical. An example of where Majorana fermions can emerge in two dimensional systems is in a p+ip superconductor, where Majorana zero modes are bound to vortices [31]. Pairs of these fermions may be grouped together to create a fermionic description of the low-energy Hilbert space.

Nanowire setups

In this section, we will detail schemes to realize Majorana zero modes in nanowire geometries. The simplest model that realizes Majorana zero modes in a wire is the Kitaev chain, a one-dimensional chain of spinless fermions [37]. The Hamiltonian reads

$$H = \sum_{j=1}^{L-1} -tc_j^\dagger c_{j+1} - \Delta c_j c_{j+1} + H.c. - \mu c_j^\dagger c_j, \tag{1.6}$$

where hopping and pairing are supplemented by p-wave pairing. The fermions are spinless. In the limit where $t = \Delta$, $\mu = 0$, the Hamiltonian becomes particularly simple:

$$H = \sum_{j=1}^{L-1} -it\gamma_{2j}\gamma_{2j+1}, \tag{1.7}$$

where γ_1, γ_{2L} do not appear in the Hamiltonian and thus are zero modes. As the two Majorana zero modes combine into a Dirac fermion ($\psi = \frac{1}{2}(\gamma_1 + i\gamma_{2L})$), there is a two-fold ground state degeneracy, and this cannot be lifted without hybridizing the Majoranas separated by length L. If we tune slightly away from this perfect limit the Majorana modes still persist, but their wavefunctions will bleed into the interior of the wire. The zero modes will commute with the Hamiltonian up to an exponentially suppressed correction. Tuning the parameters greatly will push the system through a topological phase transition, turning the system into a trivial insulator and removing the Majorana zero modes.

Despite the simple form of the Hamiltonian it is difficult to realize in experiment. The Kitaev model requires spinless fermions c and a special pairing mechanism that is not very natural. Great progress was made when it was realized that the p-wave pairing could be replaced by coupling a spin-orbit coupled spinful nanowire system to an s-wave superconductor [2, 43, 49, 55]. A wire is endowed with spin orbit coupling, which shifts the spin up and spin down bands to the left and right in momentum space. The chemical potential is dropped in the middle of the wire, yielding four low-energy fermionic movers; this is reduced to two by gapping out the interior modes at momentum $k = 0$ pair via a Zeeman coupling to a magnetic field. The remaining modes are gapped with an s-wave superconductor, yielding Majorana modes at the ends. The Hamiltonian reads

$$H = \int_x \psi^\dagger \left(-\frac{\partial_x^2}{2m} - \mu - h\sigma^x - i\alpha\sigma^y\partial_x \right)\psi + \Delta(\psi_\uparrow\psi_\downarrow + H.c.), \qquad (1.8)$$

and we will revisit this Hamiltonian in future parts of this thesis.

Braiding and Fusion

Braiding and fusion take on slightly different interpretations in nanowire networks: the wire Hamiltonians are subjected to an adiabatic cycle which rotates the ground state while mapping the Hamiltonian back to itself. A simple example of such a cycle would be endowing the superconductor with phase φ and winding the phase from 0 to 2π. The Kitaev chain Hamiltonian with superconducting phase reads

$$H = \sum_j -tc_j^\dagger c_{j+1} - \Delta e^{i\varphi}c_j c_{j+1} + H.c. - \mu c_j^\dagger c_j, \qquad (1.9)$$

and the superconducting phase can be gauged away by a redefinition of c:

$$c \rightarrow e^{-i\varphi/2}c \tag{1.10}$$

$$\gamma_1 = -i(e^{i\varphi/2}c_1 - e^{-i\varphi/2}c_1^\dagger) \tag{1.11}$$

$$\gamma_{2L} = e^{i\varphi/2}c_L + e^{-i\varphi/2}c_L^\dagger \tag{1.12}$$

and it becomes clear that the Majorana modes accumulate a minus sign after one evolution, though the Hamiltonian remains the same [3].

A braiding protocol involves shuttling zero modes around each other, sometimes using special wire network geometries like T-junctions [4, 17, 26, 30, 56]. We can, however, argue the form of the braid matrix without appealing to microscopic calculations. Two Majorana modes γ_1, γ_2 will combine to form a Dirac fermion ψ, which can be occupied or unoccupied. However, since no other Majorana modes are involved in braiding γ_1 and γ_2, fermion parity must be conserved. Also, the self-Hermitian square-to-one properties of the Majorana modes greatly constrains their form after braiding. This restricts the braid operation to be (up to an overall sign)

$$\gamma_1 \rightarrow \gamma_2 \tag{1.13}$$

$$\gamma_2 \rightarrow -\gamma_1. \tag{1.14}$$

Two of these braids yields the same result as winding the phase by 2π.

Fusion is also straightforward: we can shrink the topological regions and allow two zero modes to hybridize:

$$H_{\text{pert}} = -t_{hyb}i\gamma_1\gamma_2, \tag{1.15}$$

which splits the states in energy according to whether ψ is occupied or unoccupied. Hence, we have a simple mechanism for readout of Majorana zero modes.

Fractional Josephson effect

One key signature of the Majorana zero mode is its effect on Josephson junctions [37]. In a conventional Josephson junction, the current between the two supercon-ductors is 2π periodic in the phase difference. In a topological Josephson junction, two topological superconductors are allowed to contact and the two Majorana zero modes at the junction are allowed to hybridize. There are thus two bound states at the junction, corresponding to an occupied fermion or unoccupied. If the two

Majorana modes are denoted as γ_2, γ_3, then the occupation of $\psi_M = \frac{1}{2}(\gamma_2 + i\gamma_3)$ dictates the energy of the system.

However, as the phase difference is varied by 2π, the Majorana mode $\gamma_3 \rightarrow -\gamma_3$, and thus the fermion $\psi_M \rightarrow \psi_M^\dagger$. Physically, this means the occupation of the junction switches under a 2π evolution, that is, a fermion is 'pumped' to the outer edge. Thus, even though the Hamiltonian is 2π periodic, it takes a 4π evolution, a double winding, for the ground state to map back into itself.

1.3   This Thesis

In this thesis we recount three of our research projects, all of which involve exploiting the Majorana zero mode in some fashion to achieve even richer physics. All of our setups are heterostructures built from tabletop condensed matter systems. We begin by demonstrating how to recreate the SYK model out of Majorana nanowires. The SYK model is a zero-dimensional, strongly interacting Hamiltonian whose physics relates to those of black holes and is thus of immense interest to high-energy theorists [35, 44]. We then proceed to illustrate an exact mapping between parafermions, non-Abelian anyons that generalize the Majorana mode, and Majoranas intertwined with symmetry breaking. We propose simple models that capture the physics of this new phase and the implications of the enhancement on Majorana braiding and fusion. Our results link together many different types of one-dimensional phases, illustrating deep relations between, for example, the TRITOPS phase [14, 16, 28, 29, 33, 51, 69] and other SPT's. We finally promote symmetry-breaking to time-translation breaking by harnessing the physics of time crystals [21, 34, 57, 65, 67], creating a new type of anomalous Majorana zero mode that exhibits previously unforetold quadrupled periodicity in the Floquet drive.

BIBLIOGRAPHY

[1] F. Alexander Bais, Peter van Driel, and Mark de Wild Propitius. Quantum symmetries in discrete gauge theories. *Physics Letters B*, 280(1):63 – 70, 1992. ISSN 0370-2693. doi: https://doi.org/10.1016/0370-2693(92)90773-W. URL http://www.sciencedirect.com/science/article/pii/037026939290773W.

[2] Jason Alicea. Majorana fermions in a tunable semiconductor device. *Phys. Rev. B*, 81:125318, 2010. doi: 10.1103/PhysRevB.81.125318.

[3] Jason Alicea. New directions in the pursuit of majorana fermions in solid state systems. *Reports on Progress in Physics*, 75(7):076501, jun 2012. doi: 10.1088/0034-4885/75/7/076501. URL https://doi.org/10.1088%2F0034-4885%2F75%2F7%2F076501.

[4] Jason Alicea, Yuval Oreg, Gil Refael, Felix von Oppen, and Matthew P. A. Fisher. Non-abelian statistics and topological quantum information processing in 1d wire networks. *Nature Physics*, 7(5):412–417, 2011. doi: 10.1038/nphys1915. URL https://doi.org/10.1038/nphys1915.

[5] Maissam Barkeshli and Xiao-Liang Qi. Topological nematic states and non-Abelian lattice dislocations. *Phys. Rev. X*, 2:031013, Aug 2012. doi: 10.1103/PhysRevX.2.031013.

[6] Maissam Barkeshli and Xiao-Liang Qi. Synthetic topological qubits in conventional bilayer quantum Hall systems. *Phys. Rev. X*, 4:041035, Nov 2014. doi: 10.1103/PhysRevX.4.041035. URL http://link.aps.org/doi/10.1103/PhysRevX.4.041035.

[7] C. W. J. Beenakker. Search for Majorana fermions in superconductors. *Annu. Rev. Con. Mat. Phys.*, 4:113–136, 2013. doi: 10.1146/annurev-conmatphys-030212-184337.

[8] Parsa Bonderson. Measurement-only topological quantum computation via tunable interactions. *Phys. Rev. B*, 87:035113, Jan 2013. doi: 10.1103/PhysRevB.87.035113.

[9] Parsa Bonderson, Kirill Shtengel, and J.K. Slingerland. Interferometry of non-abelian anyons. *Annals of Physics*, 323(11):2709 – 2755, 2008. ISSN 0003-4916. doi: https://doi.org/10.1016/j.aop.2008.01.012. URL http://www.sciencedirect.com/science/article/pii/S0003491608000171.

[10] Parsa Bonderson, David J. Clarke, Chetan Nayak, and Kirill Shtengel. Implementing arbitrary phase gates with ising anyons. *Phys. Rev. Lett.*, 104:180505, May 2010. doi: 10.1103/PhysRevLett.104.180505. URL https://link.aps.org/doi/10.1103/PhysRevLett.104.180505.

[11] P. Oscar Boykin, Tal Mor, Matthew Pulver, Vwani Roychowdhury, and Farrokh Vatan. On universal and fault-tolerant quantum computing, 1999.

[12] Sergey Bravyi. Universal quantum computation with the ν=5/2 fractional quantum hall state. *Phys. Rev. A*, 73:042313, Apr 2006. doi: 10.1103/PhysRevA. 73.042313. URL https://link.aps.org/doi/10.1103/PhysRevA.73. 042313.

[13] Sergey Bravyi and Alexei Kitaev. Universal quantum computation with ideal clifford gates and noisy ancillas. *Phys. Rev. A*, 71:022316, Feb 2005. doi: 10. 1103/PhysRevA.71.022316. URL https://link.aps.org/doi/10.1103/ PhysRevA.71.022316.

[14] Alberto Camjayi, Liliana Arrachea, Armando Aligia, and Felix von Oppen. Fractional spin and Josephson effect in time-reversal-invariant topological superconductors. *Phys. Rev. Lett.*, 119:046801, Jul 2017. doi: 10.1103/ PhysRevLett.119.046801. URL https://link.aps.org/doi/10.1103/ PhysRevLett.119.046801.

[15] Meng Cheng. Superconducting proximity effect on the edge of fractional topological insulators. *Phys. Rev. B*, 86:195126, Nov 2012. doi: 10. 1103/PhysRevB.86.195126. URL https://link.aps.org/doi/10.1103/ PhysRevB.86.195126.

[16] Suk Bum Chung, Joshua Horowitz, and Xiao-Liang Qi. Time-reversal anomaly and Josephson effect in time-reversal-invariant topological superconductors. *Phys. Rev. B*, 88:214514, Dec 2013. doi: 10.1103/PhysRevB.88.214514. URL https://link.aps.org/doi/10.1103/PhysRevB.88.214514.

[17] David J. Clarke, Jay D. Sau, and Sumanta Tewari. Majorana fermion exchange in quasi-one-dimensional networks. *Phys. Rev. B*, 84:035120, Jul 2011. doi: 10.1103/PhysRevB.84.035120.

[18] David J. Clarke, Jason Alicea, and Kirill Shtengel. Exotic non-Abelian anyons from conventional fractional quantum Hall states. *Nature Commun.*, 4:1348, 2013. doi: 10.1038/ncomms2340.

[19] Mark de Wild Propitius and F. Alexander Bais. Discrete gauge theories, 1995.

[20] R. Dijkgraaf, V. Pasquier, and P. Roche. Quasi-hopf algebras, group cohomology and orbifold models. *Nuclear Physics B - Proceedings Supplements*, 18(2): 60 – 72, 1991. ISSN 0920-5632. doi: https://doi.org/10.1016/0920-5632(91) 90123-V. URL http://www.sciencedirect.com/science/article/ pii/092056329190123V.

[21] Dominic V. Else, Bela Bauer, and Chetan Nayak. Floquet time crystals. *Phys. Rev. Lett.*, 117:090402, Aug 2016. doi: 10.1103/PhysRevLett. 117.090402. URL https://link.aps.org/doi/10.1103/PhysRevLett. 117.090402.

[22] K. Fredenhagen, K. H. Rehren, and B. Schroer. Superselection sectors with braid group statistics and exchange algebras. *Communications in Mathematical Physics*, 125(2):201–226, 1989. doi: 10.1007/BF01217906. URL https://doi.org/10.1007/BF01217906.

[23] M H Freedman. P/np, and the quantum field computer. *Proceedings of the National Academy of Sciences of the United States of America*, 95(1):98–101, 01 1998. doi: 10.1073/pnas.95.1.98. URL https://pubmed.ncbi.nlm.nih.gov/9419335.

[24] Michael Freedman, Chetan Nayak, and Kevin Walker. Towards universal topological quantum computation in the $\nu = \frac{5}{2}$ fractional quantum hall state. *Phys. Rev. B*, 73:245307, Jun 2006. doi: 10.1103/PhysRevB.73.245307. URL https://link.aps.org/doi/10.1103/PhysRevB.73.245307.

[25] J. Fröhlich and F. Gabbiani. Braid statistics in local quantum theory. *Reviews in Mathematical Physics*, 02(03):251–353, 1990. doi: 10.1142/S0129055X90000107. URL https://doi.org/10.1142/S0129055X90000107.

[26] Liang Fu and C. L. Kane. Superconducting proximity effect and majorana fermions at the surface of a topological insulator. *Phys. Rev. Lett.*, 100: 096407, Mar 2008. doi: 10.1103/PhysRevLett.100.096407. URL https://link.aps.org/doi/10.1103/PhysRevLett.100.096407.

[27] Gerald A. Goldin, Ralph Menikoff, and David H. Sharp. Comments on "general theory for quantum statistics in two dimensions". *Phys. Rev. Lett.*, 54:603–603, Feb 1985. doi: 10.1103/PhysRevLett.54.603. URL https://link.aps.org/doi/10.1103/PhysRevLett.54.603.

[28] Arbel Haim, Anna Keselman, Erez Berg, and Yuval Oreg. Time-reversal-invariant topological superconductivity induced by repulsive interactions in quantum wires. *Phys. Rev. B*, 89:220504, Jun 2014. doi: 10.1103/PhysRevB.89.220504. URL https://link.aps.org/doi/10.1103/PhysRevB.89.220504.

[29] Arbel Haim, Erez Berg, Karsten Flensberg, and Yuval Oreg. No-go theorem for a time-reversal invariant topological phase in noninteracting systems coupled to conventional superconductors. *Phys. Rev. B*, 94:161110, Oct 2016. doi: 10.1103/PhysRevB.94.161110. URL https://link.aps.org/doi/10.1103/PhysRevB.94.161110.

[30] Bertrand I. Halperin, Yuval Oreg, Ady Stern, Gil Refael, Jason Alicea, and Felix von Oppen. Adiabatic manipulations of Majorana fermions in a three-dimensional network of quantum wires. *Phys. Rev. B*, 85:144501, Apr 2012. doi: 10.1103/PhysRevB.85.144501.

[31] D. A. Ivanov. Non-Abelian statistics of half-quantum vortices in *p*-wave superconductors. *Phys. Rev. Lett.*, 86:268–271, Jan 2001. doi: 10.1103/ PhysRevLett.86.268.

[32] Torsten Karzig, Christina Knapp, Roman M. Lutchyn, Parsa Bonderson, Matthew B. Hastings, Chetan Nayak, Jason Alicea, Karsten Flensberg, Stephan Plugge, Yuval Oreg, Charles M. Marcus, and Michael H. Freedman. Scalable designs for quasiparticle-poisoning-protected topological quantum computation with majorana zero modes. *Phys. Rev. B*, 95:235305, Jun 2017. doi: 10.1103/PhysRevB.95.235305. URL https://link.aps.org/doi/ 10.1103/PhysRevB.95.235305.

[33] Anna Keselman, Liang Fu, Ady Stern, and Erez Berg. Inducing time-reversal-invariant topological superconductivity and fermion parity pumping in quantum wires. *Phys. Rev. Lett.*, 111:116402, Sep 2013. doi: 10.1103/PhysRevLett.111.116402. URL https://link.aps.org/doi/10. 1103/PhysRevLett.111.116402.

[34] Vedika Khemani, Achilleas Lazarides, Roderich Moessner, and S. L. Sondhi. Phase structure of driven quantum systems. *Phys. Rev. Lett.*, 116:250401, Jun 2016. doi: 10.1103/PhysRevLett.116.250401. URL https://link.aps. org/doi/10.1103/PhysRevLett.116.250401.

[35] A. Kitaev. A simple model of quantum holography. *http://online.kitp.ucsb.edu/online/entangled15/ kitaev/, http://online.kitp.ucsb.edu/online/entangled15/ kitaev2/*, 2015.

[36] Alexei Kitaev. Anyons in an exactly solved model and beyond. *Annals of Physics*, 321(1):2 – 111, 2006. ISSN 0003-4916. doi: https: //doi.org/10.1016/j.aop.2005.10.005. URL http://www.sciencedirect. com/science/article/pii/S0003491605002381. January Special Issue.

[37] Alexei Yu Kitaev. Unpaired Majorana fermions in quantum wires. *Sov. Phys.– Uspeki*, 44(10S):131, October 2001. doi: 10.1070/1063-7869/44/10S/S29.

[38] Alexei Yu Kitaev. Fault-tolerant quantum computation by anyons. *Ann. Phys.*, 303:2–30, 2003. doi: 10.1016/S0003-4916(02)00018-0.

[39] Martin Leijnse and Karsten Flensberg. Introduction to topological superconductivity and majorana fermions. *Semiconductor Science and Technology*, 27(12):124003, nov 2012. doi: 10.1088/0268-1242/27/12/124003. URL https://doi.org/10.1088%2F0268-1242%2F27%2F12%2F124003.

[40] J. M. Leinaas and J. Myrheim. On the theory of identical particles. *Il Nuovo Cimento B (1971-1996)*, 37(1):1–23, 1977. doi: 10.1007/BF02727953. URL https://doi.org/10.1007/BF02727953.

[41] Netanel H. Lindner, Erez Berg, Gil Refael, and Ady Stern. Fractionalizing Majorana fermions: Non-Abelian statistics on the edges of Abelian quantum Hall states. *Phys. Rev. X*, 2:041002, Oct 2012. doi: 10.1103/PhysRevX.2.041002.

[42] Hoi-Kwong Lo and John Preskill. Non-abelian vortices and non-abelian statistics. *Phys. Rev. D*, 48:4821–4834, Nov 1993. doi: 10.1103/PhysRevD.48.4821. URL https://link.aps.org/doi/10.1103/PhysRevD.48.4821.

[43] Roman M. Lutchyn, Jay D. Sau, and S. Das Sarma. Majorana fermions and a topological phase transition in semiconductor-superconductor heterostructures. *Phys. Rev. Lett.*, 105:077001, 2010. doi: 10.1103/PhysRevLett.105.077001.

[44] Juan Maldacena and Douglas Stanford. Remarks on the sachdev-ye-kitaev model. *Phys. Rev. D*, 94:106002, Nov 2016. doi: 10.1103/PhysRevD.94.106002. URL http://link.aps.org/doi/10.1103/PhysRevD.94.106002.

[45] Roger S. K. Mong, David J. Clarke, Jason Alicea, Netanel H. Lindner, Paul Fendley, Chetan Nayak, Yuval Oreg, Ady Stern, Erez Berg, Kirill Shtengel, and Matthew P. A. Fisher. Universal topological quantum computation from a superconductor-Abelian quantum Hall heterostructure. *Phys. Rev. X*, 4:011036, Mar 2014. doi: 10.1103/PhysRevX.4.011036.

[46] G. Moore and N. Read. Nonabelions in the fractional quantum Hall effect. *Nucl. Phys. B*, 360:362, 1991.

[47] Chetan Nayak and Frank Wilczek. "$2n$ quasihole states realize $2n - 1$ dimensional spinor braiding statistics in paired quantum hall states". *Nuclear Physics B*, 479(3):529 – 553, 1996. ISSN 0550-3213. doi: https://doi.org/10.1016/0550-3213(96)00430-0. URL http://www.sciencedirect.com/science/article/pii/0550321396004300.

[48] Chetan Nayak, Steven H. Simon, Ady Stern, Michael Freedman, and Sankar Das Sarma. Non-Abelian anyons and topological quantum computation. *Rev. Mod. Phys.*, 80:1083–1159, Sep 2008.

[49] Yuval Oreg, Gil Refael, and Felix von Oppen. Helical liquids and Majorana bound states in quantum wires. *Phys. Rev. Lett.*, 105:177002, 2010. doi: 10.1103/PhysRevLett.105.177002.

[50] Christoph P. Orth, Rakesh P. Tiwari, Tobias Meng, and Thomas L. Schmidt. Non-Abelian parafermions in time-reversal-invariant interacting helical systems. *Phys. Rev. B*, 91:081406, Feb 2015. doi: 10.1103/PhysRevB.91.081406.

[51] Xiao-Liang Qi, Taylor L. Hughes, S. Raghu, and Shou-Cheng Zhang. Time-reversal-invariant topological superconductors and superfluids in two

and three dimensions. *Phys. Rev. Lett.*, 102:187001, May 2009. doi: 10.1103/PhysRevLett.102.187001. URL https://link.aps.org/doi/10.1103/PhysRevLett.102.187001.

[52] N. Read and Dmitry Green. Paired states of fermions in two dimensions with breaking of parity and time-reversal symmetries and the fractional quantum Hall effect. *Phys. Rev. B*, 61(15):10267–10297, 2000. doi: 10.1103/PhysRevB.61.10267.

[53] N. Read and E. Rezayi. Beyond paired quantum hall states: Parafermions and incompressible states in the first excited landau level. *Phys. Rev. B*, 59:8084–8092, Mar 1999. doi: 10.1103/PhysRevB.59.8084. URL https://link.aps.org/doi/10.1103/PhysRevB.59.8084.

[54] Sankar Das Sarma, Michael Freedman, and Chetan Nayak. Majorana zero modes and topological quantum computation. *npj Quantum Information*, 1 (1):15001, 2015. doi: 10.1038/npjqi.2015.1. URL https://doi.org/10.1038/npjqi.2015.1.

[55] Jay D. Sau, Roman M. Lutchyn, Sumanta Tewari, and S. Das Sarma. Generic new platform for topological quantum computation using semiconductor heterostructures. *Phys. Rev. Lett.*, 104:040502, Jan 2010. doi: 10.1103/PhysRevLett.104.040502. URL https://link.aps.org/doi/10.1103/PhysRevLett.104.040502.

[56] Jay D. Sau, David J. Clarke, and Sumanta Tewari. Controlling non-abelian statistics of majorana fermions in semiconductor nanowires. *Phys. Rev. B*, 84:094505, Sep 2011. doi: 10.1103/PhysRevB.84.094505. URL https://link.aps.org/doi/10.1103/PhysRevB.84.094505.

[57] Alfred Shapere and Frank Wilczek. Classical time crystals. *Phys. Rev. Lett.*, 109:160402, Oct 2012. doi: 10.1103/PhysRevLett.109.160402. URL https://link.aps.org/doi/10.1103/PhysRevLett.109.160402.

[58] P. W. Shor. Algorithms for quantum computation: discrete logarithms and factoring. In *Proceedings 35th Annual Symposium on Foundations of Computer Science*, pages 124–134, 1994.

[59] Peter W. Shor. Scheme for reducing decoherence in quantum computer memory. *Phys. Rev. A*, 52:R2493–R2496, Oct 1995. doi: 10.1103/PhysRevA.52.R2493. URL https://link.aps.org/doi/10.1103/PhysRevA.52.R2493.

[60] T D Stanescu and S Tewari. Majorana fermions in semiconductor nanowires: fundamentals, modeling, and experiment. *Journal of Physics: Condensed Matter*, 25(23):233201, may 2013. doi: 10.1088/0953-8984/25/23/233201. URL https://doi.org/10.1088%2F0953-8984%2F25%2F23%2F233201.

[61] Abolhassan Vaezi. Fractional topological superconductor with fractionalized Majorana fermions. *Phys. Rev. B*, 87:035132, Jan 2013. doi: 10.1103/PhysRevB.87.035132.

[62] Abolhassan Vaezi and Maissam Barkeshli. Fibonacci anyons from Abelian bilayer quantum Hall states. *Phys. Rev. Lett.*, 113:236804, Dec 2014. doi: 10.1103/PhysRevLett.113.236804.

[63] F. Wilczek. Magnetic Flux, Angular Momentum, and Statistics. *prl*, 48(17): 1144–1146, April 1982. doi: 10.1103/PhysRevLett.48.1144.

[64] F. Wilczek. *Fractional statistics and anyon superconductivity*. World Scientific, Singapore, 1990.

[65] Frank Wilczek. Quantum time crystals. *Phys. Rev. Lett.*, 109:160401, Oct 2012. doi: 10.1103/PhysRevLett.109.160401. URL https://link.aps.org/doi/10.1103/PhysRevLett.109.160401.

[66] Yong-Shi Wu. General theory for quantum statistics in two dimensions. *Phys. Rev. Lett.*, 52:2103–2106, Jun 1984. doi: 10.1103/PhysRevLett.52.2103. URL https://link.aps.org/doi/10.1103/PhysRevLett.52.2103.

[67] N. Y. Yao, A. C. Potter, I.-D. Potirniche, and A. Vishwanath. Discrete time crystals: Rigidity, criticality, and realizations. *Phys. Rev. Lett.*, 118:030401, Jan 2017. doi: 10.1103/PhysRevLett.118.030401. URL https://link.aps.org/doi/10.1103/PhysRevLett.118.030401.

[68] Fan Zhang and C. L. Kane. Time-reversal-invariant Z_4 fractional josephson effect. *Phys. Rev. Lett.*, 113:036401, Jul 2014. doi: 10.1103/PhysRevLett.113.036401. URL https://link.aps.org/doi/10.1103/PhysRevLett.113.036401.

[69] Fan Zhang, C. L. Kane, and E. J. Mele. Time-reversal-invariant topological superconductivity and Majorana Kramers pairs. *Phys. Rev. Lett.*, 111:056402, Aug 2013. doi: 10.1103/PhysRevLett.111.056402. URL https://link.aps.org/doi/10.1103/PhysRevLett.111.056402.

Chapter 2

APPROXIMATING THE SACHDEV-YE-KITAEV MODEL WITH MAJORANA NANOWIRES

2.1 Introduction

Majorana fermions provide building blocks for many novel phenomena. As one notable example, Majorana-fermion zero modes [38, 53] capture the essence of non-Abelian statistics and topological quantum computation [39, 47], and correspondingly now form the centerpiece of a vibrant experimental effort [1, 11, 14, 16, 17, 20, 31, 41, 42, 45, 46, 62]. More recently, randomly interacting Majorana fermions governed by the 'Sachdev-Ye-Kitaev (SYK) model' [36, 44, 55] were shown to exhibit sharp connections to chaos, quantum-information scrambling, and black holes—naturally igniting broad interdisciplinary activity (see, e.g., [4, 8, 12, 13, 15, 21–24, 27, 29, 32–35, 40, 49, 51, 61, 63]). The goal of this paper is to exploit hardware components of a Majorana-based topological quantum computer for a tabletop implementation of the SYK model, thus uniting these very different topics.

The SYK Hamiltonian reads

$$H_{SYK} = \sum_{1 \leq i < j < k < l \leq N} J_{ijkl} \gamma_i \gamma_j \gamma_k \gamma_l, \tag{2.1}$$

where $\gamma_{i=1,...,N}$ denote Majorana fermions with 'all-to-all', Gaussian-distributed random couplings J_{ijkl} satisfying

$$\langle J_{ijkl} \rangle = 0, \quad \langle J_{ijkl} J_{i'j'k'l'} \rangle = \delta_{i,i'} \delta_{j,j'} \delta_{k,k'} \delta_{l,l'} \frac{3! \bar{J}^2}{N^3}. \tag{2.2}$$

At large N the model is solvable and exhibits rich behavior. Most remarkably, for temperatures satisfying $\bar{J}/N \ll T \ll \bar{J}$ the SYK model enjoys approximate conformal symmetry and, similar to black holes, is maximally chaotic as diagnosed by out-of-time-ordered correlators. These properties are expected for a holographic dual to quantum gravity, and there has been much interest in the corresponding bulk theory [28, 33].

Laboratory realizations of Eq. (2.1) face intertwined hurdles: First, hybridizing Majorana fermions naively yields bilinears of the form $iM_{jk} \gamma_j \gamma_k$ as the dominant

couplings, yet these are absent from the Hamiltonian. Second, generating all-to-all couplings requires abandoning locality for the Majorana fermions. And finally, the host platform must carry sufficient disorder to at least approximate independence among the large number of random J_{ijkl}'s. References [13, 49] proposed SYK-model platforms using cold atoms and topological insulators, respectively, while Ref. [22] suggested a qubit simulation of the model capable of probing correlations. We instead envision a realization [Fig. 21(a)] that exploits Majorana zero modes germinated in proximitized semiconductor nanowires [43, 48]—a leading experimental architecture for topological quantum information applications [1, 11, 14, 16, 20, 31, 41, 42, 45].

More precisely, we explore an array of such wires interfaced with a disordered quantum dot that mediates coupling among the constituent Majorana modes and randomizes the corresponding zero-mode wavefunctions. Unwanted Majorana bilinears are suppressed by an approximate time-reversal symmetry [59] that, importantly, is preserved by the dominant sources of disorder expected in the dot. Interactions intrinsic to the dot instead generate the desired all-to-all four-Majorana couplings, thus approximating the SYK model up to corrections that we quantify (and which appear generic for any physical realization). We discuss several future directions that our approach spotlights, including tunneling experiments that provide a natural first probe of SYK physics.

2.2 Setup

We begin with the Hamiltonian for a clean, single-subband proximitized wire:

$$H_{\text{wire}} = \int_x \left[\psi^\dagger \left(-\frac{\partial_x^2}{2m} - \mu - h\sigma^x - i\alpha\sigma^y\partial_x \right)\psi + \Delta(\psi_\uparrow\psi_\downarrow + H.c.) + \cdots \right], \quad (2.3)$$

which features Zeeman coupling h generated by a magnetic field **B**, spin-orbit coupling α, and proximity-induced pairing Δ. Together these ingredients allow the formation of Majorana zero modes $\gamma, \tilde{\gamma}$ at the wire ends over a chemical potential window centered around $\mu = 0$ [43, 48]. Crucially, the terms explicitly displayed above respect a time-reversal transformation $\mathcal{T}$ that sends $\psi \to \psi$, $i \to -i$ and thus satisfies $\mathcal{T}^2 = +1$ [59]. Additional couplings denoted by the ellipsis can in general violate $\mathcal{T}$ since it is not a true microscopic symmetry. Nevertheless, we will assume that such perturbations are negligible, which is not unreasonable at low densities appropriate for the topological regime. (See Discussion for further comments.) Under the approximate $\mathcal{T}$ symmetry the Majorana-zero-mode operators transform
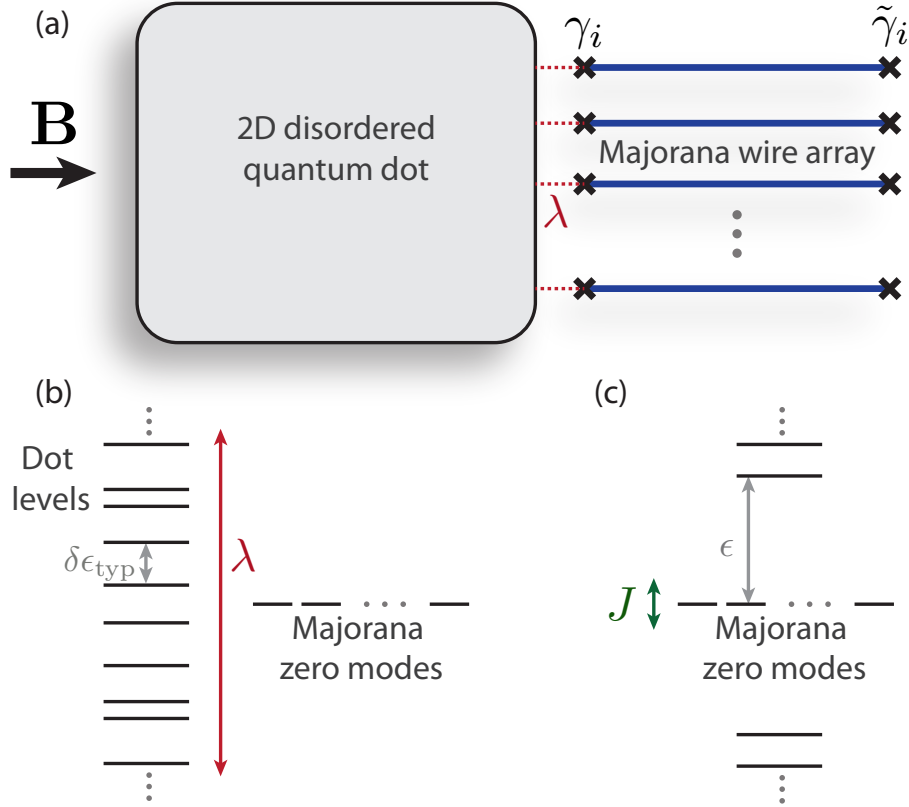
Figure 21: (a) Device that approximates the SYK model using topological wires interfaced with a 2D quantum dot. The dot mediates disorder and four-fermion interactions among Majorana modes $\gamma_{1,\ldots,N}$ inherited from the wires, while Majorana bilinears are suppressed by an approximate time-reversal symmetry. (b) Energy levels pre-hybridization. The dot-Majorana hybridization energy λ is large compared to $N\delta\epsilon_{\text{typ}}$, where N is the number of Majorana modes and $\delta\epsilon_{\text{typ}}$ is the typical dot level spacing; this maximizes leakage into the dot. (c) Energy levels post-hybridization. The N absorbed Majorana modes enhance the energy ϵ to the next excited dot state via level repulsion; four-Majorana interactions occur on a scale $J < \epsilon$.

as $\gamma \to \gamma$ and $\tilde{\gamma} \to -\tilde{\gamma}$. The opposite signs acquired by $\gamma, \tilde{\gamma}$ ensure that $\mathcal{T}$ commutes with the ground-state fermion parity $P = i\gamma\tilde{\gamma}$, as it must.

Consider now N topological wires 'plugged into' a 2D disordered quantum dot [Fig. 21(a)], such that the Majoranas $\gamma_{1,\ldots,N}$ that are even under $\mathcal{T}$ hybridize with the dot while their partners $\tilde{\gamma}_{1,\ldots,N}$ decouple completely. The full architecture continues to approximately preserve $\mathcal{T}$ provided (*i*) the dot carries negligible spin-orbit coupling and (*ii*) the **B** field orients in the plane of the dot so that orbital effects are absent. Here the setup falls into class BDI, which in the free-fermion limit admits an integer topological invariant $\nu \in \mathbb{Z}$ [37, 54] that counts the number of Majorana zero modes at each end; interactions collapse the classification to $\mathbb{Z}_8$ [18, 19]. In essence

our device leverages nanowires to construct a topological phase with a free-fermion invariant $\nu = N$: All bilinear couplings $iM_{jk}\gamma_j\gamma_k$ are forbidden by $\mathcal{T}$ and thus *cannot* be generated by the dot under the conditions specified above. We exploit the resulting N Majorana zero modes to simulate SYK-model physics mediated by disorder and interactions native to the dot, similar in spirit to Refs. [49, 63].

Figures 21(b) and (c) illustrate the relevant parameter regime. The dot-Majorana hybridization energy λ satisfies $\lambda \gg N\delta\epsilon_{typ}$, where $\delta\epsilon_{typ}$ denotes the typical dot level spacing. This criterion enables the dot to absorb a substantial fraction of *all* N Majorana zero modes as shown below. The dot's disordered environment then efficiently 'scrambles' the zero-mode wavefunctions, though we assume that their localization length ξ exceeds the dot size L. More quantitatively, we take the mean-free path $\ell_{mfp} \ll L$ to maximize randomness and the dimensionless conductance $g = k_F\ell_{mfp} > 1$ such that $L < \xi$. Turning on four-fermion interactions couples the disordered Majorana modes with typical J_{ijkl}'s that are smaller than the energy ϵ to the next excited state (which as we will see is enhanced by level repulsion compared to $\delta\epsilon_{typ}$). This separation of scales allows us to first analyze the disordered wavefunctions in the non-interacting limit and then explore interactions projected onto the zero-mode subspace. We next carry out this program using random-matrix theory, which is expected to apply in the above regime [2, 5].

2.3 Random-matrix-theory analysis

We model the dot as a 2D lattice composed of $N_{dot} \gg N$ sites hosting fermions $c_{a=1,\ldots,N_{dot}}$ [1]. In terms of physical dot parameters we have $N_{dot} \sim (L/\ell_{mfp})^2$— that is, the fermions represent degrees of freedom coarse-grained on a length scale of order the mean-free path. The Hamiltonian governing the dot-Majorana system is $H = H_0 + H_{int}$, with H_0 and H_{int} the free and interacting pieces, respectively. We employ a Majorana basis and write $c_a = (\eta_a + i\tilde{\eta}_a)/2$, where η_a is even under $\mathcal{T}$ while $\tilde{\eta}_a$ is odd (similarly to $\gamma_i, \tilde{\gamma}_i$). In terms of

$$\Gamma = [\eta_1 \cdots \eta_{N_{dot}}; \gamma_1 \cdots \gamma_N]^T, \quad \tilde{\Gamma} = [\tilde{\eta}_1 \cdots \tilde{\eta}_{N_{dot}}]^T, \quad (2.4)$$

H_0 takes the form

$$H_0 = \frac{i}{4}\begin{bmatrix} \Gamma^T & \tilde{\Gamma}^T \end{bmatrix}\begin{bmatrix} 0 & M \\ -M^T & 0 \end{bmatrix}\begin{bmatrix} \Gamma \\ \tilde{\Gamma} \end{bmatrix}. \quad (2.5)$$

---

[1]We assume spinless fermions for simplicity; spin can be introduced trivially since we impose $\mathcal{T}^2 = 1$ symmetry.

Time-reversal $\mathcal{T}$ fixes the zeros above but allows for a general real-valued $(N_{\mathrm{d}ot} + N) \times N_{\mathrm{d}ot}$-dimensional matrix M. (The matrix is not square since we discarded the $\tilde{\gamma}_i$ modes that trivially decouple.) One can perform a singular-value decomposition of M by writing $\Gamma = O\Gamma'$ and $\tilde{\Gamma} = \tilde{O}\tilde{\Gamma}'$. Here $O, \tilde{O}$ denote orthogonal matrices consisting of singular vectors, i.e., the matrix $\Lambda \equiv O^T M \tilde{O}$ only has non-zero entries along the diagonal. Writing $\Gamma' = [\eta_1' \cdots \eta_{N_{\mathrm{d}ot}}'; \gamma_1' \cdots \gamma_N']^T$ and similarly for $\tilde{\Gamma}'$, the Hamiltonian becomes

$$H_0 = \frac{i}{2} \sum_{a=1}^{N_{\mathrm{d}ot}} \epsilon_a \eta_a' \tilde{\eta}_a', \tag{2.6}$$

where $\epsilon_a \equiv \Lambda_{aa}$ are the non-zero dot energies. Most importantly, $\gamma_{i=1,...,N}'$ drop out and form the modified N Majorana zero modes guaranteed by $\mathcal{T}$ symmetry.

We are interested in statistical properties of the associated Majorana wavefunctions in the presence of strong randomness. To make analytic progress we assume (for now) that all elements of M in Eq. (3.40) are independent, Gaussian-distributed random variables with zero mean and the same variance, corresponding to the chiral orthogonal ensemble [57, 60]. This form permits Cooper pairing of dot fermions—an inessential detail for our purposes—and also does not enforce the strong-hybridization criterion $\lambda \gg N\delta\epsilon_{\mathrm{typ}}$. We will see that the Majorana wavefunctions nevertheless live almost entirely in the dot as appropriate for the latter regime.

The probability density for such a random matrix M is [6] $P(M)$, which is proportional to $\exp(-\frac{\pi^2}{8N_{\mathrm{d}ot}\delta\epsilon_{\mathrm{typ}}^2}\mathrm{Tr}(M^T M))$. Because $P(M)$ is invariant under $M \rightarrow O^T M \tilde{O}$, the singular-vector matrices $O, \tilde{O}$ are uniformly distributed over the spaces $O(N_{\mathrm{d}ot} + N)$ and $O(N_{\mathrm{d}ot})$, respectively. In particular, the Majorana wavefunctions ϕ_i corresponding to γ_i' are the final N columns of a random element of $O(N_{\mathrm{d}ot} + N)$. For large $N_{\mathrm{d}ot} + N$ the distribution of wavefunction components is asymptotically Gaussian [5, 30]:

$$\langle \phi_{i,I} \rangle = 0, \quad \langle \phi_{i,I} \phi_{j,J} \rangle = \frac{\delta_{i,j}\delta_{I,J}}{N_{\mathrm{d}ot} + N} \approx \frac{\delta_{i,j}\delta_{I,J}}{N_{\mathrm{d}ot}}. \tag{2.7}$$

Summing $\phi_{i,I}^2$ over the dot sites thus gives unity up to corrections of order $N/N_{\mathrm{d}ot}$, i.e., the dot swallows the Majorana modes as claimed.

Once absorbed by the dot, the N Majorana zero modes repel the nearby energy levels. Random matrix theory allows us to estimate the energy ϵ to the first excited dot state. References [3, 56] show that the smallest eigenvalue for the Wishart matrix $M^T M$ approaches $(\sqrt{a} - \sqrt{b})^2 v$, where M is an $a \times b$ matrix with variance v for each

element. The energy ϵ is the square root of this eigenvalue. For our matrix M we thus obtain

$$\epsilon \approx \frac{1}{\pi} N \delta \epsilon_{typ}. \tag{2.8}$$

The enhancement compared to $\delta \epsilon_{typ}$ [sketched in Fig. 21(c)] isolates the N Majorana modes from adjacent levels, justifying projection onto the zero-energy subspace.

Let us now examine a general $\mathcal{T}$-invariant four-fermion interaction among dot fermions, $H_{int} = \sum_{abcd} U_{abcd} c_a^\dagger c_b^\dagger c_c c_d$. Projection follows from $c_a \rightarrow \frac{1}{2} \sum_i \phi_{i,a} \gamma_i'$, which yields

$$H \rightarrow \sum_{1 \leq i < j < k < l \leq N} J_{ijkl} \gamma_i' \gamma_j' \gamma_k' \gamma_l' \tag{2.9}$$

$$J_{ijkl} = \frac{1}{2^4} \sum_{abcd} U_{abcd} \sum_p s_p \phi_{p(i)a} \phi_{p(j)b} \phi_{p(k)c} \phi_{p(l)d}. \tag{2.10}$$

The p sum runs over permutations of $ijkl$, and $s_p = \pm 1$ is the parity of permutation p. Notice that only the part of U_{abcd} that is asymmetric under swapping any pair of indices contributes to J_{ijkl}. For density-density interactions among the coarse-grained fermions—where $U_{abcd} \propto \delta_{ad} \delta_{bc}$—all J_{ijkl} consequently vanish. This in fact is a virtue that underlies compatibility of SYK physics with randomness in our setup. Density-density interactions would project nontrivially only if potential disorder $\delta \mu_a c_a^\dagger c_a$ did as well, but the latter would generate unwanted Majorana bilinears that tend to spoil SYK properties. Other physical couplings such as current-current interactions produce non-zero J_{ijkl}. We stress, however, that *microscopic* density-density interactions will generically contribute to J_{ijkl} after coarse graining.

Emulating the SYK model requires that the J_{ijkl}'s encode all-to-all Majorana interactions and form independent random variables whose correlations obey Wick's theorem. Using Eq. (2.7) one reproduces Eq. (2.2) with

$$\bar{J}^2 = \frac{3N^3}{8N_{dot}^4} \sum_{abcd} (U_{abcd}^{as})^2 \sim \frac{N^3}{N_{dot}^\alpha}. \tag{2.11}$$

Here U_{abcd}^{as} denotes the antisymmetric part of U_{abcd}. The exponent α on the right side is interaction-dependent. An (unphysical) non-local interaction with $(U_{abcd}^{as})^2 = constant$ yields $\alpha = 0$, while a local U_{abcd}^{as} with support only for bcd 'near' a instead yields $\alpha = 3$.

Equation (2.11) implies all-to-all coupling but does not guarantee independence of the J_{ijkl}'s. Since there are $\binom{N}{4} \sim N^4$ such couplings and $N \times N_{dot}$ independent
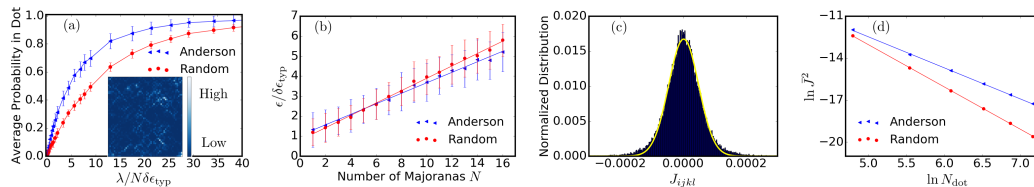
Figure 22: (a) Average absorption of Majorana wavefunctions into the dot versus the hybridization strength λ with $N = 16$ zero modes. Inset: probability density for a Majorana wavefunction swallowed and randomized by the dot of size 51×51. (b) Enhanced level repulsion of the first excited dot state ϵ by N absorbed Majorana modes; cf. Figs. 21(b) and (c). (c) Histogram of J_{ijkl} couplings obtained from local current-current interactions on a dot of size 21×21, together with a Gaussian fit (solid line). (d) Scaling of the variance $\propto \bar{J}^2$ of these couplings versus N_{dot}.

Majorana-wavefunction components in the dot, a necessary condition for the latter property is

$$N_{dot} \gtrsim N^3. \tag{2.12}$$

Corrections to Wick's theorem persist even in this regime, however. For example, Eq. (2.7) yields

$$\langle J_{ijkl} J_{klmn} J_{ijmn} \rangle \propto \frac{1}{N_{dot}^6} \sum_{abcdef} U_{abcd}^{as} U_{cdef}^{as} U_{abef}^{as} \sim \frac{1}{N_{dot}^\beta}, \tag{2.13}$$

whereas in the SYK model such correlations vanish. (Note that our system still preserves the statistical SO(N) 'flavor' symmetry corresponding to rotations among the Majorana fermions that is present in the SYK model.) A local interaction implies $\beta = 5$; Eq. (2.13) then decays faster with N_{dot} compared with $\langle J_{ijkl}^2 \rangle^{3/2}$. In this sense the J_{ijkl}'s asymptotically form independent Gaussian random variables as in Ref. [13]. Corrections to Wick's theorem do nevertheless introduce a proliferation of new Feynman diagrams that may qualitatively alter SYK-model physics over some energy scales [2].

---

[2] See Section 2.6 for a discussion of corrections to Wick's theorem for J_{ijkl} couplings.

2.4 Numerics

We now semi-quantitatively validate random-matrix-theory predictions using a more physically motivated Hamiltonian. Consider first the free part,

$$H_0 = -\sum_{a \neq b} t_{ab} c_a^\dagger c_b + \sum_a V_a c_a^\dagger c_a + \lambda \sum_{i=1}^{N} \gamma_i (c_{a_i} - c_{a_i}^\dagger). \tag{2.14}$$

Here V_a is an uncorrelated Gaussian disorder landscape with zero mean and variance $\bar{V}^2$. In the λ hybridization term, Majorana γ_i couples to a single dot site a_i. For the hoppings t_{ab}, we consider uniform nearest-neighbor tunnelings of strength t (yielding an Anderson model) and compare results with purely random, arbitrary-range hopping satisfying $\langle t_{ab} \rangle = 0, \langle t_{ab} t_{a'b'} \rangle = t^2$ (yielding a random-matrix model). All data below correspond to $\bar{V} = t$ with adjacent Majorana modes separated by two or three dot sites. Unless specified otherwise $\lambda = t/2$, the dot system size is 31×31, and results are disorder-averaged over many configurations [20 for Fig. 22(a), 50 for (b) and (d), and 500 for (c)].

Figure 22(a) corresponds to $N = 16$ and plots the fraction of the Majorana mode wavefunctions absorbed by the dot—averaged over all 16 zero modes—versus $\lambda/(N\delta\epsilon_{\text{typ}})$. For both the Anderson and random-matrix models the fraction is of order one at $\lambda/(N\delta\epsilon_{\text{typ}}) \gtrsim 4$, eventually saturating to unity as in random matrix theory. The inset shows the probability density for a zero-mode wavefunction nearly fully absorbed by the dot, obtained from an $N = 1$ Anderson model; the wavefunction appears thoroughly randomized and loses all information about its original position (in this case, the center). Figure 22(b) illustrates level repulsion of the excitation energy ϵ (normalized by the level spacing $\delta\epsilon_{\text{typ}}$) versus N. Note that the dot almost completely absorbs all zero modes up to the largest N shown. The random matrix model yields a slope that agrees within $\sim 5\%$ with Eq. (2.8) obtained from random matrix theory, while the Anderson model agrees within $\sim 20\%$.

Next we include a local current-current interaction

$$H_{\text{int}} = U \sum_{\langle ab \rangle} c_a^\dagger \nabla c_a \cdot c_b^\dagger \nabla c_b, \tag{2.15}$$

with ∇ a lattice gradient, projected into the zero-mode subspace. Figure 22(c) plots a histogram of the resulting J_{ijkl} couplings (in units of U) using an Anderson model with $N = 8$ and a 21×21 dot. The data agrees well with a Gaussian distribution; see solid line. Finally, Fig. 22(d) illustrates the N_{dot}-dependence of the variance $\propto \bar{J}$ for J_{ijkl} [recall Eq. (2.2)] with $N = 8$. The Anderson model yields a scaling

close $1/N_{\text{d}ot}^2$—slower than $1/N_{\text{d}ot}^3$ result from random matrix theory [Eq. (2.11)]. We attribute this difference primarily to localization effects that effectively reduce the system area. As a check, the random-matrix model, which should not suffer localization due to the non-local hoppings, indeed yields the expected $1/N_{\text{d}ot}^3$ scaling.

2.5 Discussion

We showed that in certain regimes our Majorana wire/quantum dot setup can emulate the SYK model up to very generic corrections. Chiefly, we invoked an approximate time-reversal symmetry that suppresses bilinears, strong dot-Majorana coupling that delocalizes and randomizes the wavefunctions, level repulsion that suppresses pollution of the zero-mode subspace by additional dot levels, and sufficient randomness to approximate independent, random all-to-all couplings J_{ijkl}. Regarding the last property, Eqs. (2.11) and (2.12) imply that independence requires $\bar{J} \sim 1/N^3$ for a dot with local interactions. Since $\bar{J} \ll \epsilon$ excited dot states indeed can be safely ignored. We saw that level repulsion of the dot states scales with N, implying that one can enlarge the dot to accommodate arbitrarily many wires without spoiling this property, provided the system size does not exceed the localization length. (For larger scales we lose all-to-all coupling, as the Majorana wavefunctions localize.) However, increasing N rapidly diminishes the strong-coupling temperature window $T \ll \bar{J}$—where much of the interesting physics emerges. This challenge can be alleviated with long-range interactions, which lead to slower decay with N. Alternatively, one can intentionally abandon independence to boost $\bar{J}$, though the fate of SYK physics in such cases remains to be systematically understood.

To maintain approximate $\mathcal{T}$ symmetry graphene-based dots appear ideal due to their strict two-dimensionality and extremely weak spin-orbit coupling. In this case the dominant source of $\mathcal{T}$ violation will likely originate from the Majorana wires. We can crudely assess the impact of such perturbations by adding local $\mathcal{T}$-breaking terms for the dot in the vicinity of the wires and projecting, e.g.,

$$\delta H = \chi \sum_{i=1}^{N} (ic_{a_i}^\dagger c_{a_i+1} + H.c.) \rightarrow \sum_{1 \le j < k \le N} iM_{jk}\gamma_j'\gamma_k'$$

$$M_{jk} = \chi \sum_{i=1}^{N} (\phi_{j,a_i}\phi_{k,a_i+1} - \phi_{k,a_i}\phi_{j,a_i+1}). \tag{2.16}$$

The M_{jk} bilinear couplings are random with zero mean and variance $2\chi^2 N/N_{\text{d}ot}^2 \sim 1/N^5$, where we used Eq. (2.12). The correction to the two-point correlation function $\langle\gamma_i(t)\gamma_i(0)\rangle$ is thus $\propto N(\chi^2/N^5)$, and should be compared to the contribution $\bar{J}^2 \sim$

U^2/N^6 (for local interactions) from four-Majorana interactions. This correction is small provided $\chi \lesssim U/N$; longer-range interactions relax the criterion further. Tunneling into the dot provides an appealing benchmark of proximity to SYK physics: the conductance approaches a constant at zero bias if bilinears dominate but diverges as $V^{-1/2}$ for the large-N SYK model [44].

The setup we propose suggests several other tantalizing applications. First, with relatively few wires ($N \leq 8$) one can experimentally explore the $\mathbb{Z} \to \mathbb{Z}_8$ reduction of the BDI classification by interactions [18, 19], very similar to Refs. [10, 50]. One can also investigate quantum quenches as a possible probe of SYK physics by disconnecting or reconnecting the dot and wires to effectively freeze the zero modes or restore their coupling. Finally, much work has been done regarding measuring out-of-time-order correlators in cold atoms and qubit systems; see, e.g., [25, 58, 64, 65]. Our setup offers the exciting prospect of exploiting Majorana hardware and topological quantum information ideas to measure such quantities in pursuit of the SYK model's hallmark maximal chaos. Developing protocols to this end poses an interesting challenge highlighted by our study.

2.6 Corrections to Wick's theorem

In this Section we discuss the asymptotically small corrections to Wick's theorem for the J_{ijkl} couplings. Our treatment is quite general and does not rely on our particular proposed realization. We will take the best-case scenario for randomness, invoking Eq. (2.12) and assuming completely disordered and independent zero-mode wavefunctions ϕ_i that obey Eq. (2.7). In practice the ϕ_i's also suffer subdominant correlations and will not be truly Gaussian; these corrections can be studied using techniques described, e.g., in Refs. [26, 52] but are neglected for simplicity.

Using Eq. (2.10) we see that correlations among m J_{ijkl}'s satisfy

$$\langle \prod_{f=1}^{m} J_{i_f j_f k_f l_f} \rangle = \left(\frac{4!}{2^4} \right)^m \prod_f U^{\text{as}}_{a_f b_f c_f d_f} \langle \prod_f \phi_{i_f a_f} \phi_{j_f b_f} \phi_{k_f c_f} \phi_{l_f d_f} \rangle, \qquad (2.17)$$

where repeated indices are summed. The assumption of i.i.d. Gaussian wavefunction components $\phi_{i,I}$ allows us to simply apply Wick's theorem to evaluate the right-hand side—though this does not mean the J_{ijkl} couplings are independent. Each $U^{\text{as}}_{a_f b_f c_f d_f}$ connects to four wavefunction elements ϕ_{i_f, a_f}, etc., and each wavefunction element contracts with another. The disorder average on the right side of Eq. (2.17) thus pairs all the a_f, b_f, c_f, d_f indices in some manner and also forces all of the i_f, j_f, k_f, l_f indices to similarly pair together (otherwise the average vanishes trivially).

Wick-theorem-obeying correlations among J_{ijkl}'s occur when all four indices of each $U^{as}_{a_f b_f c_f d_f}$ pair with all four indices of another. For a local interaction such cases yield

$$\langle \prod_{f=1}^{m} J_{i_f j_f k_f l_f} \rangle_{\text{Wick}} \sim N_{\text{d}ot}^{g-2m}, \tag{2.18}$$

where g is the number of connected pieces in the diagram and m must be even [3]. Note that the maximally disconnected pieces with $g = m/2$ minimize the decay with $N_{\text{d}ot}$ and reduce to $\langle J_{ijkl}^2 \rangle^{m/2}$.

Non-Wick correlations arise when more than two J_{ijkl}'s share indices. Equation (2.13) gives one example. Another is

$$\langle J_{ijkl} J_{inkp} J_{mjol} J_{mnop} \rangle \quad \propto \frac{1}{N_{\text{d}ot}^8} \sum_{abcdefgh} U^{as}_{abcd} U^{as}_{ebgd} U^{as}_{afch} U^{as}_{efgh} \sim N_{\text{d}ot}^{-7}, \tag{2.19}$$

where we again used a local interaction. By contrast, Eqs. (2.13) and (2.19) both vanish in the SYK model. Such non-Wick contributions are generically suppressed by some power of $N_{\text{d}ot}$ compared to $\langle J_{ijkl}^2 \rangle^{m/2}$. Naively, this analysis suggests that the Wick contributions dominate the Feynman-diagram expansion of the model, and that hence we can use the 'melon diagram' formalism [36, 44, 51] that yields the large-N SYK solution.

However, at increasingly high order in the diagrammatic expansion, non-Wick correlations lead to a proliferation of new diagrams. Though each individual contribution is small in the above sense, the number of allowed graphs grows far faster than the suppression in $1/N_{\text{d}ot}$. References [7, 9] discuss the asymptotic number of simple regular graphs, that is, graphs with each vertex connected to a fixed number of edges. In our case we are concerned with 4-regular graphs: the number scales as

$$P(m) \sim \frac{(4m)!}{(2m)!(m)!C^m} \sim m^m \tag{2.20}$$

for some constant C. Note that this result underestimates the number of graphs since it excludes the ones that have multiple edges that join the same vertices. Thus while each graph is, at best, suppressed exponentially in m (i.e., by a factor $1/N_{\text{d}ot}^{const \times m}$), the number of such graphs grows combinatorially, and it becomes very nontrivial to resum the Feynman diagrams for the two and four point functions. Hence the melon and ladder diagram resummations may need to be amended.

---

[3] Here connectedness refers to the way the U tensors are contracted.

What fate befalls the SYK model in the large-N limit in the presence of the corrections identified above, which are likely present in any physical realization? Possible ways of addressing this important question include (*i*) developing a controlled scheme for analytically including residual correlations among J_{ijkl}'s and (*ii*) numerically studying the evolution of two- and four-point functions for finite-N in the presence of correlated disorder. While both schemes lie beyond the scope of our work, we offer some speculations here. Plausible outcomes include a reduction from the maximal chaos present in the 'pure' SYK model, corrections to scaling of the two-point function, and possibly new physics setting in at the lowest energy scales (e.g., spin-glass behavior). Understanding such issues provides yet additional motivation for pursuing experimental realizations of the SYK model and variations thereof.

2.7 Acknowledgments

BIBLIOGRAPHY

[1] S. M. Albrecht, A. P. Higginbotham, M. Madsen, F. Kuemmeth, T. S. Jespersen, J. Nygård, P. Krogstrup, and C. M. Marcus. Exponential protection of zero modes in majorana islands. *Nature*, 531:206–209, March 2016. doi: 10.1038/nature17162.

[2] I.L. Aleiner, P.W. Brouwer, and L.I. Glazman. Quantum effects in coulomb blockade. *Physics Reports*, 358(5–6):309 – 440, 2002. ISSN 0370-1573. doi: http://dx.doi.org/10.1016/S0370-1573(01)00063-1. URL http://www.sciencedirect.com/science/article/pii/S0370157301000631.

[3] Z. D. Bai and Y. Q. Yin. Limit of the smallest eigenvalue of a large dimensional sample covariance matrix. *Ann. Probab.*, 21(3):1275–1294, 07 1993. doi: 10.1214/aop/1176989118. URL http://dx.doi.org/10.1214/aop/1176989118.

[4] Sumilan Banerjee and Ehud Altman. Solvable model for a dynamical quantum phase transition from fast to slow scrambling. *Phys. Rev. B*, 95:134302, Apr 2017. doi: 10.1103/PhysRevB.95.134302. URL https://link.aps.org/doi/10.1103/PhysRevB.95.134302.

[5] C. W. J. Beenakker. Random-matrix theory of quantum transport. *Rev. Mod. Phys.*, 69:731–808, Jul 1997. doi: 10.1103/RevModPhys.69.731. URL http://link.aps.org/doi/10.1103/RevModPhys.69.731.

[6] C. W. J. Beenakker. Random-matrix theory of majorana fermions and topological superconductors. *Rev. Mod. Phys.*, 87:1037–1066, Sep 2015. doi: 10.1103/RevModPhys.87.1037. URL http://link.aps.org/doi/10.1103/RevModPhys.87.1037.

[7] Edward A Bender and E.Rodney Canfield. The asymptotic number of labeled graphs with given degree sequences. *Journal of Combinatorial Theory, Series A*, 24(3):296 – 307, 1978. ISSN 0097-3165. doi: http://dx.doi.org/10.1016/0097-3165(78)90059-6. URL http://www.sciencedirect.com/science/article/pii/0097316578900596.

[8] Zhen Bi, Chao-Ming Jian, Yi-Zhuang You, Kelly Ann Pawlak, and Cenke Xu. Instability of the non-fermi-liquid state of the sachdev-ye-kitaev model. *Phys. Rev. B*, 95:205105, May 2017. doi: 10.1103/PhysRevB.95.205105. URL https://link.aps.org/doi/10.1103/PhysRevB.95.205105.

[9] Bela Bollobas. The asymptotic number of unlabelled regular graphs. *Journal of the London Mathematical Society*, s2-26(2):201–206, 1982. ISSN 1469-7750. doi: 10.1112/jlms/s2-26.2.201. URL http://dx.doi.org/10.1112/jlms/s2-26.2.201.

[10] Ching-Kai Chiu, D. I. Pikulin, and M. Franz. Proposed platform to study interaction-enabled topological phases with fermionic particles. *Phys. Rev. B*, 92:241115, Dec 2015. doi: 10.1103/PhysRevB.92.241115. URL http://link.aps.org/doi/10.1103/PhysRevB.92.241115.

[11] H. O. H. Churchill, V. Fatemi, K. Grove-Rasmussen, M. T. Deng, P. Caroff, H. Q. Xu, and C. M. Marcus. Superconductor-nanowire devices from tunneling to the multichannel regime: Zero-bias oscillations and magnetoconductance crossover. *Phys. Rev. B*, 87:241401, Jun 2013. doi: 10.1103/PhysRevB.87.241401.

[12] Jordan S. Cotler, Guy Gur-Ari, Masanori Hanada, Joseph Polchinski, Phil Saad, Stephen H. Shenker, Douglas Stanford, Alexandre Streicher, and Masaki Tezuka. Black holes and random matrices. *Journal of High Energy Physics*, 2017(5):118, 2017. doi: 10.1007/JHEP05(2017)118. URL https://doi.org/10.1007/JHEP05(2017)118.

[13] Ippei Danshita, Masanori Hanada, and Masaki Tezuka. Creating and probing the Sachdev–Ye–Kitaev model with ultracold gases: Towards experimental studies of quantum gravity. *Progress of Theoretical and Experimental Physics*, 2017(8), 08 2017. ISSN 2050-3911. doi: 10.1093/ptep/ptx108. URL https://doi.org/10.1093/ptep/ptx108. 083I01.

[14] A. Das, Y. Ronen, Y. Most, Y. Oreg, M. Heiblum, and H. Shtrikman. Zero-bias peaks and splitting in an Al-InAs nanowire topological superconductor as a signature of Majorana fermions. *Nat. Phys.*, 8:887–895, 2012. doi: 10.1038/nphys2479.

[15] Richard A. Davison, Wenbo Fu, Antoine Georges, Yingfei Gu, Kristan Jensen, and Subir Sachdev. Thermoelectric transport in disordered metals without quasiparticles: The sachdev-ye-kitaev models and holography. *Phys. Rev. B*, 95:155131, Apr 2017. doi: 10.1103/PhysRevB.95.155131. URL https://link.aps.org/doi/10.1103/PhysRevB.95.155131.

[16] M. T. Deng, S. Vaitiekenas, E. B. Hansen, J. Danon, M. Leijnse, K. Flensberg, J. Nygård, P. Krogstrup, and C. M. Marcus. Majorana bound state in a coupled quantum-dot hybrid-nanowire system. *Science*, 354(6319):1557–1562, 2016. doi: 10.1126/science.aaf3961. URL http://science.sciencemag.org/content/354/6319/1557.

[17] Benjamin E. Feldman, Mallika T. Randeria, Jian Li, Sangjun Jeon, Yonglong Xie, Zhijun Wang, Ilya K. Drozdov, B. Andrei Bernevig, and Ali Yazdani. *Nature Physics*, 13:286–291, 2017. doi: 10.1038/nphys3947.

[18] Lukasz Fidkowski and Alexei Kitaev. Effects of interactions on the topological classification of free fermion systems. *Phys. Rev. B*, 81:134509, Apr 2010. doi: 10.1103/PhysRevB.81.134509.

[19] Lukasz Fidkowski and Alexei Kitaev. Topological phases of fermions in one dimension. *Phys. Rev. B*, 83:075103, Feb 2011. doi: 10.1103/PhysRevB.83. 075103.

[20] A. D. K. Finck, D. J. Van Harlingen, P. K. Mohseni, K. Jung, and X. Li. Anomalous modulation of a zero-bias peak in a hybrid nanowire-superconductor device. *Phys. Rev. Lett.*, 110:126406, Mar 2013. doi: 10.1103/PhysRevLett.110.126406.

[21] Wenbo Fu and Subir Sachdev. Numerical study of fermion and boson models with infinite-range random interactions. *Phys. Rev. B*, 94:035135, Jul 2016. doi: 10.1103/PhysRevB.94.035135. URL http://link.aps.org/doi/10. 1103/PhysRevB.94.035135.

[22] L. García-Álvarez, I. L. Egusquiza, L. Lamata, A. del Campo, J. Sonner, and E. Solano. Digital quantum simulation of minimal AdS/CFT. *Phys. Rev. Lett.*, 119:040501, Jul 2017. doi: 10.1103/PhysRevLett.119.040501. URL https://link.aps.org/doi/10.1103/PhysRevLett.119.040501.

[23] Antonio M. García-García and Jacobus J. M. Verbaarschot. Spectral and thermodynamic properties of the sachdev-ye-kitaev model. *Phys. Rev. D*, 94:126010, Dec 2016. doi: 10.1103/PhysRevD.94.126010. URL http: //link.aps.org/doi/10.1103/PhysRevD.94.126010.

[24] Antonio M. García-García and Jacobus J. M. Verbaarschot. Analytical spectral density of the sachdev-ye-kitaev model at finite n. *Phys. Rev. D*, 96:066012, Sep 2017. doi: 10.1103/PhysRevD.96.066012. URL https://link.aps. org/doi/10.1103/PhysRevD.96.066012.

[25] Martin Gärttner, Justin G. Bohnet, Arghavan Safavi-Naini, Michael L. Wall, John J. Bollinger, and Ana Maria Rey. Measuring out-of-time-order correlations and multiple quantum spectra in a trapped-ion quantum magnet. *Nature Physics*, 13(8):781–786, 2017. doi: 10.1038/nphys4119. URL https://doi.org/10.1038/nphys4119.

[26] T. Gorin. Integrals of monomials over the orthogonal group. *Journal of Mathematical Physics*, 43(6):3342–3351, 2002. doi: 10.1063/1.1471367. URL http://dx.doi.org/10.1063/1.1471367.

[27] David J. Gross and Vladimir Rosenhaus. A generalization of sachdev-ye-kitaev. *Journal of High Energy Physics*, 2017(2):93, 2017. doi: 10.1007/ JHEP02(2017)093. URL https://doi.org/10.1007/JHEP02(2017)093.

[28] David J. Gross and Vladimir Rosenhaus. The bulk dual of syk: cubic couplings. *Journal of High Energy Physics*, 2017(5):92, 2017. doi: 10.1007/ JHEP05(2017)092. URL https://doi.org/10.1007/JHEP05(2017)092.

[29] Yingfei Gu, Xiao-Liang Qi, and Douglas Stanford. Local criticality, diffusion and chaos in generalized sachdev-ye-kitaev models. *Journal of High Energy Physics*, 2017(5):125, 2017. doi: 10.1007/JHEP05(2017)125. URL https://doi.org/10.1007/JHEP05(2017)125.

[30] Thomas Guhr, Axel Muller-Groeling, and Hans A. Weidenmuller. Random-matrix theories in quantum physics: common concepts. *Physics Reports*, 299(4–6):189 – 425, 1998. ISSN 0370-1573. doi: http://dx.doi.org/10.1016/S0370-1573(97)00088-4. URL http://www.sciencedirect.com/science/article/pii/S0370157397000884.

[31] Önder Gül, Hao Zhang, Jouri D. S. Bommer, Michiel W. A. de Moor, Diana Car, Sébastien R. Plissard, Erik P. A. M. Bakkers, Attila Geresdi, Kenji Watanabe, Takashi Taniguchi, and Leo P. Kouwenhoven. Ballistic majorana nanowire devices. *Nature Nanotechnology*, 13(3):192–197, 2018. doi: 10.1038/s41565-017-0032-8. URL https://doi.org/10.1038/s41565-017-0032-8.

[32] Razvan Gurau. The complete 1/n expansion of a syk–like tensor model. *Nuclear Physics B*, 916:386 – 401, 2017. ISSN 0550-3213. doi: http://dx.doi.org/10.1016/j.nuclphysb.2017.01.015. URL http://www.sciencedirect.com/science/article/pii/S0550321317300299.

[33] Kristan Jensen. Chaos in ads$_2$ holography. *Phys. Rev. Lett.*, 117:111601, Sep 2016. doi: 10.1103/PhysRevLett.117.111601. URL http://link.aps.org/doi/10.1103/PhysRevLett.117.111601.

[34] Antal Jevicki and Kenta Suzuki. Bi-local holography in the syk model: perturbations. *Journal of High Energy Physics*, 2016(11):46, 2016. doi: 10.1007/JHEP11(2016)046. URL https://doi.org/10.1007/JHEP11(2016)046.

[35] Shao-Kai Jian and Hong Yao. Solvable sachdev-ye-kitaev models in higher dimensions: From diffusion to many-body localization. *Phys. Rev. Lett.*, 119:206602, Nov 2017. doi: 10.1103/PhysRevLett.119.206602. URL https://link.aps.org/doi/10.1103/PhysRevLett.119.206602.

[36] A. Kitaev. A simple model of quantum holography. *http://online.kitp.ucsb.edu/online/entangled15/ kitaev/, http://online.kitp.ucsb.edu/online/entangled15/ kitaev2/*, 2015.

[37] Alexei Kitaev. Periodic table for topological insulators and superconductors. *AIP Conference Proceedings*, 1134(1):22–30, May 2009. doi: 10.1063/1.3149495.

[38] Alexei Yu Kitaev. Unpaired Majorana fermions in quantum wires. *Sov. Phys.–Uspeki*, 44(10S):131, October 2001. doi: 10.1070/1063-7869/44/10S/S29.

[39] Alexei Yu Kitaev. Fault-tolerant quantum computation by anyons. *Ann. Phys.*, 303:2–30, 2003. doi: 10.1016/S0003-4916(02)00018-0.

[40] Chethan Krishnan, Sambuddha Sanyal, and P. N. Bala Subramanian. Quantum chaos and holographic tensor models. *Journal of High Energy Physics*, 2017 (3):56, 2017. doi: 10.1007/JHEP03(2017)056. URL https://doi.org/10.1007/JHEP03(2017)056.

[41] C. Kurter, A. D. K. Finck, Y. S. Hor, and D. J. Van Harlingen. Evidence for an anomalous current-phase relation in topological insulator josephson junctions. *Nature Communications*, 6:7130, 2015. doi: 10.1038/ncomms8130.

[42] Eduardo J. H. Lee, Xiaocheng Jiang, Manuel Houzet, Ramon Aguado, Charles M. Lieber, and Silvano De Franceschi. Spin-resolved Andreev levels and parity crossings in hybrid superconductor-semiconductor nanostructures. *Nature Nanotech.*, 9:79, 2014. doi: 10.1038/nnano.2013.267.

[43] Roman M. Lutchyn, Jay D. Sau, and S. Das Sarma. Majorana fermions and a topological phase transition in semiconductor-superconductor heterostructures. *Phys. Rev. Lett.*, 105:077001, 2010. doi: 10.1103/PhysRevLett.105.077001.

[44] Juan Maldacena and Douglas Stanford. Remarks on the sachdev-ye-kitaev model. *Phys. Rev. D*, 94:106002, Nov 2016. doi: 10.1103/PhysRevD.94.106002. URL http://link.aps.org/doi/10.1103/PhysRevD.94.106002.

[45] V. Mourik, K. Zuo, S. M. Frolov, S. R. Plissard, E. P. A. M. Bakkers, and L. P. Kouwenhoven. Signatures of Majorana fermions in hybrid superconductor-semiconductor nanowire devices. *Science*, 336:1003–1007, 2012. doi: 10.1126/science.1222360.

[46] Stevan Nadj-Perge, Ilya K. Drozdov, Jian Li, Hua Chen, Sangjun Jeon, Jungpil Seo, Allan H. MacDonald, B. Andrei Bernevig, and Ali Yazdani. Observation of Majorana fermions in ferromagnetic atomic chains on a superconductor. *Science*, 346:602, 2014. doi: 10.1126/science.1259327.

[47] Chetan Nayak, Steven H. Simon, Ady Stern, Michael Freedman, and Sankar Das Sarma. Non-Abelian anyons and topological quantum computation. *Rev. Mod. Phys.*, 80:1083–1159, Sep 2008. doi: 10.1103/RevModPhys.80.1083.

[48] Yuval Oreg, Gil Refael, and Felix von Oppen. Helical liquids and Majorana bound states in quantum wires. *Phys. Rev. Lett.*, 105:177002, 2010. doi: 10.1103/PhysRevLett.105.177002.

[49] D. I. Pikulin and M. Franz. Black hole on a chip: Proposal for a physical realization of the sachdev-ye-kitaev model in a solid-state system. *Phys. Rev. X*, 7:031006, Jul 2017. doi: 10.1103/PhysRevX.7.031006. URL https://link.aps.org/doi/10.1103/PhysRevX.7.031006.

[50] D. I. Pikulin, Ching-Kai Chiu, Xiaoyu Zhu, and M. Franz. Interaction-enabled topological phases in topological insulator/superconductor heterostructures. *Phys. Rev. B*, 92:075438, Aug 2015. doi: 10.1103/PhysRevB.92.075438. URL http://link.aps.org/doi/10.1103/PhysRevB.92.075438.

[51] Joseph Polchinski and Vladimir Rosenhaus. The spectrum in the sachdev-ye-kitaev model. *Journal of High Energy Physics*, 2016(4):1, 2016. doi: 10.1007/JHEP04(2016)001. URL https://doi.org/10.1007/JHEP04(2016)001.

[52] T. Prosen, T. H. Seligman, and H. A. Weidenmuller. Integration over matrix spaces with unique invariant measures. *Journal of Mathematical Physics*, 43(10):5135–5144, 2002. doi: 10.1063/1.1506955. URL http://aip.scitation.org/doi/abs/10.1063/1.1506955.

[53] N. Read and Dmitry Green. Paired states of fermions in two dimensions with breaking of parity and time-reversal symmetries and the fractional quantum hall effect. *Phys. Rev. B*, 61:10267–10297, Apr 2000. doi: 10.1103/PhysRevB.61.10267. URL http://link.aps.org/doi/10.1103/PhysRevB.61.10267.

[54] Shinsei Ryu, Andreas P Schnyder, Akira Furusaki, and Andreas W W Ludwig. Topological insulators and superconductors: tenfold way and dimensional hierarchy. *New Journal of Physics*, 12(6):065010, 2010.

[55] Subir Sachdev and Jinwu Ye. Gapless spin-fluid ground state in a random quantum heisenberg magnet. *Phys. Rev. Lett.*, 70:3339–3342, May 1993. doi: 10.1103/PhysRevLett.70.3339. URL http://link.aps.org/doi/10.1103/PhysRevLett.70.3339.

[56] Jack W. Silverstein. The smallest eigenvalue of a large dimensional wishart matrix. *The Annals of Probability*, 13(4):1364–1368, 1985. ISSN 00911798. URL http://www.jstor.org/stable/2244186.

[57] M. A. Stephanov, J. J. M. Verbaarschot, and T. Wettig. *Random Matrices*. American Cancer Society, 1999. ISBN 9780471346081. doi: 10.1002/047134608X.W2447. URL https://onlinelibrary.wiley.com/doi/abs/10.1002/047134608X.W2447.

[58] Brian Swingle, Gregory Bentsen, Monika Schleier-Smith, and Patrick Hayden. Measuring the scrambling of quantum information. *Phys. Rev. A*, 94:040302, Oct 2016. doi: 10.1103/PhysRevA.94.040302. URL http://link.aps.org/doi/10.1103/PhysRevA.94.040302.

[59] Sumanta Tewari and Jay D. Sau. Topological invariants for spin-orbit coupled superconductor nanowires. *Phys. Rev. Lett.*, 109:150408, Oct 2012. doi: 10.1103/PhysRevLett.109.150408. URL http://link.aps.org/doi/10.1103/PhysRevLett.109.150408.

[60] Jacobus Verbaarschot. Spectrum of the qcd dirac operator and chiral random matrix theory. *Phys. Rev. Lett.*, 72:2531–2533, Apr 1994. doi: 10.1103/PhysRevLett.72.2531. URL http://link.aps.org/doi/10.1103/PhysRevLett.72.2531.

[61] Edward Witten. An syk-like model without disorder. 2016.

[62] Jin-Peng Xu, Mei-Xiao Wang, Zhi Long Liu, Jian-Feng Ge, Xiaojun Yang, Canhua Liu, Zhu An Xu, Dandan Guan, Chun Lei Gao, Dong Qian, Ying Liu, Qiang-Hua Wang, Fu-Chun Zhang, Qi-Kun Xue, and Jin-Feng Jia. Experimental detection of a majorana mode in the core of a magnetic vortex inside a topological insulator-superconductor $bi_2te_3/nbse_2$ heterostructure. *Phys. Rev. Lett.*, 114:017001, Jan 2015. doi: 10.1103/PhysRevLett.114.017001. URL http://link.aps.org/doi/10.1103/PhysRevLett.114.017001.

[63] Yi-Zhuang You, Andreas W. W. Ludwig, and Cenke Xu. Sachdev-ye-kitaev model and thermalization on the boundary of many-body localized fermionic symmetry-protected topological states. *Phys. Rev. B*, 95:115150, Mar 2017. doi: 10.1103/PhysRevB.95.115150. URL https://link.aps.org/doi/10.1103/PhysRevB.95.115150.

[64] Nicole Yunger Halpern, Brian Swingle, and Justin Dressel. Quasiprobability behind the out-of-time-ordered correlator. *Phys. Rev. A*, 97:042105, Apr 2018. doi: 10.1103/PhysRevA.97.042105. URL https://link.aps.org/doi/10.1103/PhysRevA.97.042105.

[65] Guanyu Zhu, Mohammad Hafezi, and Tarun Grover. Measurement of many-body chaos using a quantum clock. *Phys. Rev. A*, 94:062329, Dec 2016. doi: 10.1103/PhysRevA.94.062329. URL https://link.aps.org/doi/10.1103/PhysRevA.94.062329.

C h a p t e r   3

FERMIONIZING PARAFERMIONS

3.1   Introduction

Interacting quantum systems in two dimensions can host quasiparticle excitations whose properties are seemingly at odds with their microscopic origin. In particular, ground states characterized by a subtle non-local entanglement structure—i.e., topological order—host 'anyon' excitations that not only carry fractional quantum numbers, but additionally exhibit exchange statistics that is neither bosonic nor fermionic. An especially interesting example is provided by 'non-Abelian anyons', which display a number of fascinating properties. First, non-Abelian anyons carry exotic zero-energy degrees of freedom that generate a space of locally indistinguishable ground states. Second, braiding the anyons rotates the system within this ground-state space—yielding the remarkable phenomenon of non-Abelian statistics. And third, they exhibit nontrivial fusion rules, i.e., pairs of non-Abelian anyons can combine to form multiple quasiparticle types. The above characteristics are also technologically relevant as they form the basis for inherently fault-tolerant topological quantum computation [59, 85]. An experimentally relevant setting where such exotic excitations emerge is the Moore-Read fractional-quantum-Hall state [75]. There, charge-$e/4$ quasiparticles harbor Majorana zero modes that endow them with the braiding and fusion properties of 'Ising' non-Abelian anyons.

One can alternatively harness non-Abelian-anyon physics through defects in simpler topological phases [13]. Consider, for example, the Kitaev chain [58], which describes a spinless one-dimensional (1D) p-wave superconductor. Domain walls separating topological and trivial phases of the model harbor Majorana zero modes, and hence behave very similarly to non-Abelian anyons in the Moore-Read state. The pursuit of Majorana modes in 1D superconducting devices has correspondingly become a vibrant (and oft-reviewed [2, 5, 14, 30, 32, 64, 66, 95, 99]) enterprise. A more exotic example arises from 'parafermion' chains [6, 34]—1D systems with degrees of freedom that possess an intrinsic, unbreakable $\mathbb{Z}_N$ charge symmetry, analogous to the unbreakable $\mathbb{Z}_2$ parity symmetry of fermions. Domain walls between topological and trivial phases for the chain bind *parafermion zero modes*, which are $\mathbb{Z}_N$ Majorana generalizations that generate larger ground-state degeneracy, denser

2D topologically
ordered host

α_1 α_2

$\mathbb{Z}_{\mathrm{even}}$ parafermion
zero modes

γ_1 $\langle \mathcal{O} \rangle \neq 0$ γ_2

Symmetry-enriched
Majorana zero modes
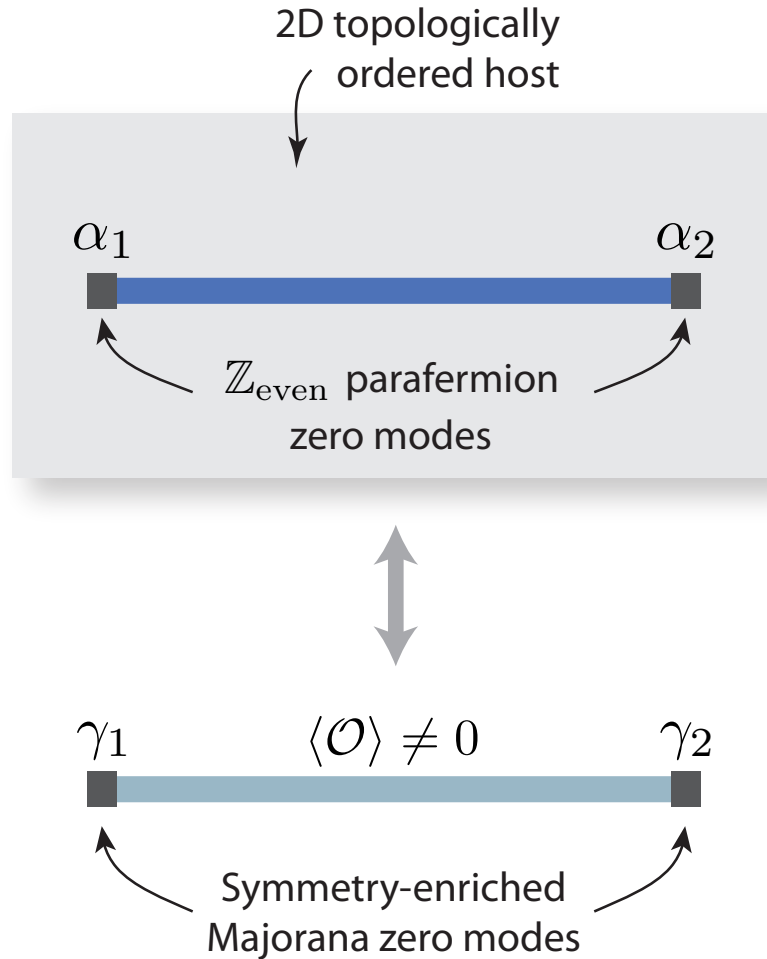
Figure 31: Correspondence between non-Abelian defects in 2D topologically ordered phases and in strictly 1D fermionic systems. Parafermion zero modes $\alpha_{1,2}$ translate into symmetry-enriched Majorana zero modes $\gamma_{1,2}$ intertwined with an order parameter $\mathcal{O}$. We show that symmetry-enriched Majorana zero modes underlie physical properties not possible from conventional Majorana systems, including an enlarged set of braid transformations and anomalous pumping protocols that are closely related to nontrivial fusion rules in the associated parafermion platform.

braid transformations, and richer fusion rules. Because the chain is built from neither bosons nor fermions, realizing these non-Abelian defects is more challenging. Nevertheless, numerous blueprints now exist for stabilizing parafermion zero modes at line defects within a two-dimensional, *Abelian* topologically ordered host. Possible host platforms include the toric code [16], fractional Chern insulators [10], quantum-Hall bilayers [11], quantum-Hall/superconductor hybrids [24, 29, 65, 104], and more [67, 110].

Here we rigorously establish a link between non-Abelian defects in such 2D topolog-

ically ordered phases and those that can arise in *strictly 1D* fermion systems. To this end, we introduce exact, non-local mappings between arbitrary $\mathbb{Z}_{\text{even}}$ parafermion chains and microscopic 1D fermionic models. This machinery provides a 'dictionary' connecting observables, phases, and any other quantity of interest between the two representations. We in particular find that $\mathbb{Z}_{\text{even}}$ parafermion zero modes translate into 'symmetry-enriched Majorana zero modes' whose wavefunctions depend nontrivially on a spontaneously chosen order parameter for the fermions; see Fig. 31. Although the degeneracy in the latter setting enjoys only partial topological protection, we demonstrate that symmetry-enriched Majorana modes give rise to phenomena that are not possible in conventional Majorana platforms.

For one, braiding processes can alter the order-parameter configuration, thereby rotating the system within an enlarged subspace (though the braid matrices do *not* match those arising from parafermions for reasons that we explain). Moreover, we show that the richer fusion rules stemming from parafermion zero modes are directly manifested in the 1D fermion setting. Imagine fusing two non-Abelian defects that bind parafermion zero modes. One can define a pumping cycle that returns the Hamiltonian to its original form yet modifies the fusion channel for the defects. The system thus exhibits an anomalous periodicity set by the number of available fusion channels. Interestingly, one can realize pumping cycles with exactly the same periodicity by hybridizing symmetry-enriched Majorana modes in 1D fermion systems. We study two implementations of such anomalous fermionic pumps. One requires symmetry protection to maintain the same periodicity as in the parafermion realization, while the other relies only on locality and fermion-parity conservation.

Useful insights can be obtained by specializing to the $\mathbb{Z}_4$ case, which we primarily focus on in this paper. In this limit the correspondences highlighted above can be anticipated from several angles. First, each pair of $\mathbb{Z}_4$ parafermions contributes four states to the Hilbert space, just like two species of fermions. Second, Ref. [69] used complementary analytical and numerical methods to infer that the eigenstates of certain $\mathbb{Z}_4$ parafermion chains can be described in terms of free fermions. Third, Zhang and Kane [111] and Orth et al. [87] showed that proximitized edge states of a two-dimensional quantum-spin-Hall insulator can support zero modes reminiscent of $\mathbb{Z}_4$ parafermions (see also Refs. [46, 90, 105]). Finally, parafermion chains are related to bosonic clock models (for any $\mathbb{Z}_N$) [34, 37]—a relation that we will frequently exploit. In the $\mathbb{Z}_4$ limit one can decompose clock spins into two sets of

Pauli matrices [48, 62, 108] that can be fermionized by standard methods [1]. We will later draw further connections to all of these works, particularly the results for quantum-spin-Hall systems.

While the 'fermionizability' of $\mathbb{Z}_4$ parafermion chains is thus natural, it is not clear a priori whether the associated 1D fermionic systems are at all physically relevant. Importantly, in our fermionization scheme (which differs from the strategy noted above) $\mathbb{Z}_4$ parafermions map onto ordinary spinful electrons with familiar symmetries including time reversal and spin rotations. Our dictionary thus indeed relates phases for parafermions to interesting, and in some cases already well-studied, 1D electronic states of matter. The phase that supports symmetry-enriched Majorana modes (see again Fig. 31) corresponds to a topological superconductor accessed by spontaneously breaking time-reversal symmetry, which may already be realized in atomic-chain experiments [33, 51, 83, 88, 94]. As another noteworthy example, the parafermion chain supports a symmetry-protected topological phase that translates into a time-reversal invariant topological superconductor (TRITOPS) [19, 27, 40, 41, 57, 92, 112] with a Kramers pair of Majorana zero modes at each end. One of the anomalous pumping cycles we introduce involves modulating a fermionic wire between trivial and TRITOPS phases; the magnetization at the ends of the system exhibits quadrupled periodicity—reflecting the four fusion channels available in the corresponding parafermion platform. We note that this pump is a strict-1D analogue of the 8π-periodic Josephson effect identified for quantum-spin-Hall edges in Refs. [87, 111]. The experimental requirements for implementing the cycle are surprisingly minimal, thus providing a tantalizing opportunity for exploring certain aspects of parafermion physics using non-fractionalized 1D systems.

We organize the remainder of the paper as follows. In Secs. 3.2 through 3.4 we exclusively treat the $\mathbb{Z}_4$-parafermion case. Section 3.2 details our fermionization scheme, while Sec. 3.3 derives the correspondence between various phases in the clock, parafermion, and electronic representations. We then turn to experimental implications in Sec. 3.4. There we contrast the non-Abelian braiding properties arising from $\mathbb{Z}_4$ parafermion zero modes and symmetry-enriched Majorana modes, and analyze the anomalous pumping cycles. Section 3.5 generalizes these results to arbitrary $\mathbb{Z}_{\text{even}}$ parafermions. An executive summary appears in Sec. 3.6 along with several future directions. Finally, Sections 3.7 through 3.16 contain supplemental results and technical details.

---

[1] For yet another take on fermionizing parafermions, see Ref. [18].

3.2 Operator Mappings

This section introduces non-local mappings that link bosonic $\mathbb{Z}_4$ clock operators, $\mathbb{Z}_4$ parafermions, and spinful fermions residing on a 1D lattice. In what follows we primarily flesh out these mappings without recourse to specific Hamiltonians, which will instead be constructed and analyzed in Sec. 3.3. Sections 3.2 and 3.2 below largely parallel the treatment of $\mathbb{Z}_3$ parafermions in Ref. [73].

$\mathbb{Z}_4$ clock operators

We first review the $\mathbb{Z}_4$ clock representation. Each lattice site, labeled by integers a, contains a four-state 'spin'. The Hilbert space is spanned by unitary clock operators σ_a and τ_a that satisfy

$$\sigma_a^4 = \tau_a^4 = 1 \tag{3.1}$$

along with the commutation relation

$$\sigma_a \tau_a = i\tau_a \sigma_a \ . \tag{3.2}$$

(Off site, the clock operators commute.) The relations above imply that σ_a and τ_a both exhibit eigenvalues $\pm 1, \pm i$, with τ_a 'winding' the eigenvalue of σ_a and vice versa.

We will be particularly interested in chains that exhibit a global $\mathbb{Z}_4$ symmetry, generated by

$$Q = \prod_a \tau_a^\dagger \ , \tag{3.3}$$

as well as an antiunitary time-reversal symmetry $\mathcal{T}$ that satisfies $\mathcal{T}^2 = +1$. The former acts according to

$$Q\sigma_a Q^\dagger = i\sigma_a \ , \qquad Q\tau_a Q^\dagger = \tau_a \ . \tag{3.4}$$

Note that if clock spins constitute physical degrees of freedom, $\mathbb{Z}_4$ symmetry can be broken either spontaneously or explicitly—a situation that we will later contrast with the cases where parafermions and fermions form the physical objects. Time reversal transforms clock operators as

$$\mathcal{T}\sigma_a \mathcal{T} = \sigma_a^\dagger \ , \qquad \mathcal{T}\tau_a \mathcal{T} = \tau_a \ . \tag{3.5}$$

We will also invoke a 'charge conjugation' symmetry C that yields

$$C\sigma_a C = \sigma_a^\dagger \ , \qquad C\tau_a C = \tau_a^\dagger \ . \tag{3.6}$$
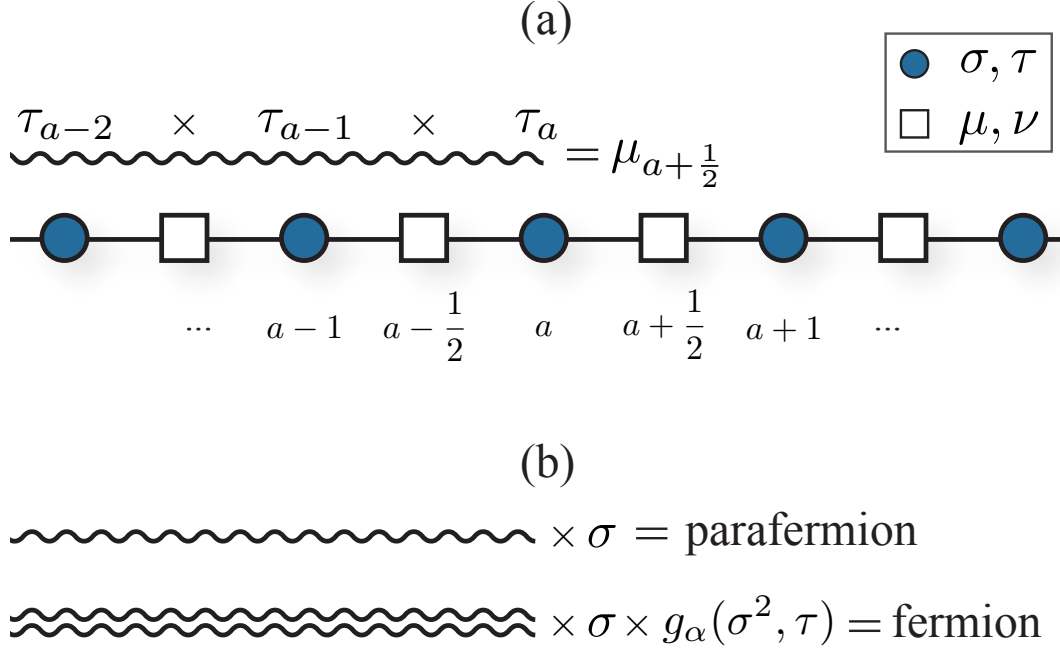
Figure 32: (a) Chain of clock operators σ_a, τ_a together with their dual counterparts $\mu_{a+\frac{1}{2}}$, $\nu_{a+\frac{1}{2}}$, which live on the dual lattice. The dual operator $\mu_{a+\frac{1}{2}}$ corresponds to a non-local τ string (wavy line). (b) Binding σ and μ yields parafermion operators; attaching the double string μ^2 to $\sigma \times g_\alpha(\sigma^2, \tau)$, where $g_\alpha(\sigma^2, \tau)$ is a local function of clock operators, gives fermions with spin α. See Secs. 3.2 and 3.2 for precise expressions relating parafermions and fermions to clock variables.

Table 31 summarizes these symmetry properties.

One can equivalently describe the system with dual operators

$$\mu_{a+\frac{1}{2}} = \prod_{b < a+\frac{1}{2}} \tau_b, \qquad \nu_{a+\frac{1}{2}} = \sigma_a^\dagger \sigma_{a+1} \tag{3.7}$$

that reside on dual-lattice sites labeled by half-integers [see Fig. 32(a)]. Similar to the original clock variables, the dual operators are unitary and satisfy

$$\mu_{a+\frac{1}{2}}^4 = \nu_{a+\frac{1}{2}}^4 = 1, \qquad \mu_{a+\frac{1}{2}} \nu_{a+\frac{1}{2}} = i \nu_{a+\frac{1}{2}} \mu_{a+\frac{1}{2}}. \tag{3.8}$$

Their symmetry properties follow straightforwardly from Eqs. (3.4) through (3.6) and are also listed in Table 31.

Suppose that $\mathbb{Z}_4$ symmetry is spontaneously broken, leading to $\langle \sigma_a \rangle \neq 0$. Starting from such a broken-symmetry phase, the dual operator $\mu_{a+\frac{1}{2}}$ creates a domain-wall defect that winds all clock spins to the left of the dual site $a + \frac{1}{2}$. Proliferation of

	$\mathbb{Z}_4$	C	$\mathcal{T}$
$\sigma \rightarrow$	$i\sigma$	$\sigma^\dagger$	$\sigma^\dagger$
$\tau \rightarrow$	τ	$\tau^\dagger$	τ
$\mu \rightarrow$	μ	$\mu^\dagger$	μ
$\nu \rightarrow$	ν	$\nu^\dagger$	$\nu^\dagger$
$\alpha \rightarrow$	$i\alpha$	$\alpha^\dagger$	$\alpha'^\dagger$
$\alpha' \rightarrow$	$i\alpha'$	$\alpha'^\dagger$	$\alpha^\dagger$
$f_\uparrow \rightarrow$	$ie^{i\pi n_\downarrow} f_\uparrow$	$e^{i\pi n_\uparrow} f_\downarrow$	$ie^{i\pi n_\uparrow} f_\downarrow$
$f_\downarrow \rightarrow$	$-ie^{i\pi n_\uparrow} f_\downarrow$	$e^{i\pi n_\downarrow} f_\uparrow$	$ie^{i\pi n_\downarrow} f_\uparrow$

Table 31: Action of primitive symmetries on clock operators σ, τ; dual clock operators μ, ν; two representations of parafermion operators α, α'; and spinful fermions $f_{\uparrow,\downarrow}$. Site labels are suppressed for brevity here and in other tables below.

these defects—i.e., $\langle \mu_{a+\frac{1}{2}} \rangle \neq 0$—destroys the order and restores $\mathbb{Z}_4$ symmetry. In this sense σ and μ respectively represent order and disorder operators. Combining order and disorder operators generates $\mathbb{Z}_4$ parafermions [34, 37], to which we turn next.

$\mathbb{Z}_4$ parafermions

We have some freedom for how to construct parafermions from order and disorder operators. One choice binds σ and μ to define lattice $\mathbb{Z}_4$ parafermions

$$\alpha_{2a-1} = \sigma_a \mu_{a-\frac{1}{2}}, \qquad \alpha_{2a} = e^{-i\frac{\pi}{4}} \sigma_a \mu_{a+\frac{1}{2}}, \tag{3.9}$$

as sketched in Fig. 32(b). Like the clock variables, these unitary operators obey

$$\alpha_a^4 = 1. \tag{3.10}$$

The τ string encoded in the disorder operators, however, yields the *non-local* commutation relation

$$\alpha_a \alpha_{b>a} = i\alpha_b \alpha_a. \tag{3.11}$$

We could equally well bind σ and $\mu^\dagger$ to define a non-locally related set of $\mathbb{Z}_4$ parafermion operators

$$\alpha'_{2a-1} = \sigma_a \mu^\dagger_{a-\frac{1}{2}}, \qquad \alpha'_{2a} = e^{i\frac{\pi}{4}} \sigma_a \mu^\dagger_{a+\frac{1}{2}} \tag{3.12}$$

that similarly obey

$$\alpha'^4_a = 1, \qquad \alpha'_a \alpha'_{b>a} = -i\alpha'_b \alpha'_a. \tag{3.13}$$

While not independent, both representations are useful to consider since they transform into one another under time reversal $\mathcal{T}$. Table 31 lists their transformation properties, which are inherited from those of the clock operators and their duals. Throughout this paper we mainly focus on the α_a representation for concreteness.

Hereafter, we will define parafermions as physical degrees of freedom if the host system exhibits a $\mathbb{Z}_4$ symmetry (which sends $\alpha_a \to i\alpha_a$) that can never be broken *explicitly* by any local perturbation. Consider, for example, $\mathbb{Z}_4$ parafermions germinated from extrinsic defects in a parent fractional-quantum-Hall medium. The parafermion operator α_a^n adds nontrivial anyon charge to position a provided $n \neq 0$ mod 4, while $(\alpha_a^\dagger)^n$ adds the opposite anyon charge. Since the total anyon charge for the system must be trivial, all physical terms in the Hamiltonian must be invariant under $\mathbb{Z}_4$ symmetry.

Next we discuss *spontaneous* $\mathbb{Z}_4$ symmetry breaking, closely following Ref. [77] (see also Refs. [4, 17, 70]). Due to the non-local commutation relation in Eq. (3.11), a parafermion system cannot spontaneously develop an expectation value $\langle \alpha_a \rangle \neq 0$ across the chain. To see this, note that $\langle \alpha_a^\dagger \alpha_b \rangle = \pm i \langle \alpha_b \alpha_a^\dagger \rangle$; when $|a - b| \to \infty$, factorizing the left and right sides yields $\langle \alpha_a^\dagger \rangle \langle \alpha_b \rangle = \pm i \langle \alpha_b \rangle \langle \alpha_a^\dagger \rangle$, which admits only trivial solutions. Since $[\alpha_a^2, \alpha_b^2] = 0$, however, no such obstruction exists for spontaneously developing an expectation value $\langle \alpha_a^2 \rangle \neq 0$. The resulting 'parafermion condensate' phase spontaneously breaks $\mathbb{Z}_4$ symmetry, but in a way that necessarily preserves $\mathbb{Z}_4^2$. This is the maximal extent to which $\mathbb{Z}_4$ can be broken in a parafermion chain.

Parafermions loosely exhibit a 'self-dual structure' in that they arise from combinations of clock operators and their duals. For a more precise statement consider the quantities

$$e^{i\frac{\pi}{4}}\alpha_{2a-1}^\dagger \alpha_{2a} = \tau_a\,, \quad e^{i\frac{\pi}{4}}\alpha_{2a}^\dagger \alpha_{2a+1} = \sigma_a^\dagger \sigma_{a+1}\,. \tag{3.14}$$

Duality swaps the role of the right-hand sides above, and hence implements a simple spatial translation of parafermion operators.

Spinful fermions

In the previous subsection we saw that parafermionic commutation relations [Eq. (3.11) or (3.13)] emerge upon combining the bosonic operator σ with a string of τ's or $\tau^\dagger$'s. 'Doubling' the string as sketched in Fig. 32(b)—i.e., attaching τ^2's to clock operators—instead naturally generates objects with fermionic statistics. Since the doubled string is Hermitian, the freedom that led to multiple parafermion represen-
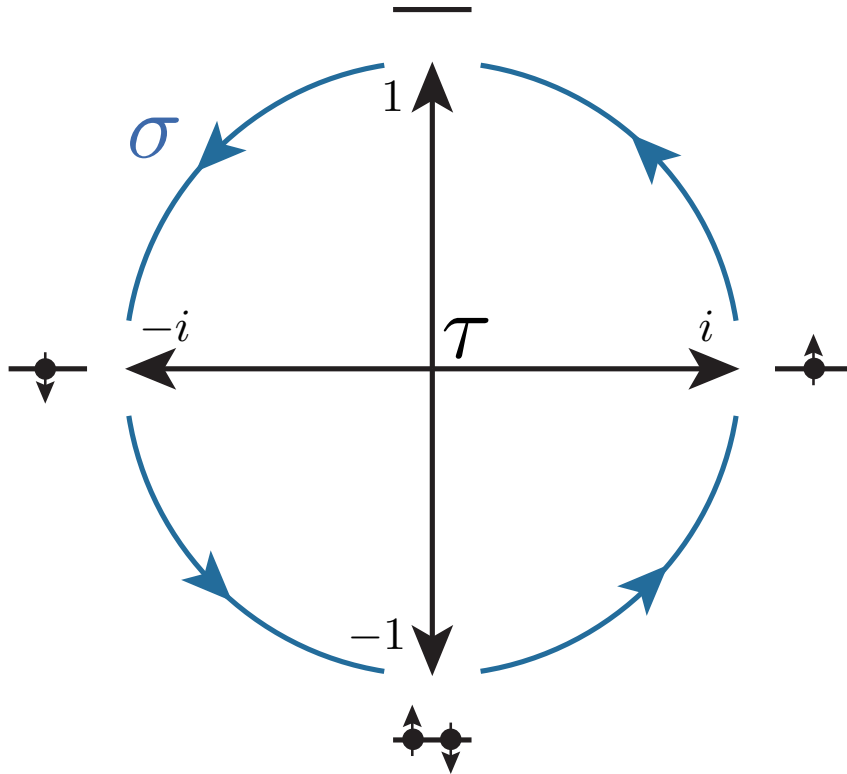
Figure 33: Representation of $\mathbb{Z}_4$ clock-model operators in terms of spinful hard-core bosons. Eigenstates of τ are encoded through boson number eigenstates, e.g., $\tau = +1$ is the boson vacuum while $\tau = -1$ corresponds to a state with both spins populated. The operator σ cycles through τ eigenstates and hence adds and removes bosons in a state-dependent fashion.

tations no longer exists here. Recovering the full clock Hilbert space with four states per site, however, requires that the fermions carry an internal label that is profitably viewed as an electronic spin-1/2 degree of freedom.

As a first step to formalizing this heuristic picture, we introduce spinful hard-core *bosons* $b_{a,\uparrow}$ and $b_{a,\downarrow}$. Observe that one can decompose the τ_a clock operator via

$$\tau_a = e^{i\frac{\pi}{2}(n_{a,\uparrow} - n_{a,\downarrow} + 2n_{a,\uparrow}n_{a,\downarrow})}, \tag{3.15}$$

where $n_{a,\alpha} = b_{a,\alpha}^\dagger b_{a,\alpha}$ denote boson occupation numbers. In this representation $\tau_a = +1$ corresponds to the boson vacuum. Starting from this state, adding a spin-down boson yields $\tau_a = -i$, further adding a spin-up boson yields $\tau_a = -1$, removing the spin-down boson gives $\tau_a = +i$, and finally removing the spin-up boson returns the $\tau_a = +1$ state. This sequence of τ_a windings is implemented by the conjugate clock operator σ_a as Fig. 33 illustrates [2]. To express σ_a in terms of

---

[2]This decomposition of σ_a and τ_a in terms of hard-core bosons is not unique. We could have

bosons it is convenient to introduce operators $P_\alpha(0) = 1 - n_{a,\alpha}$ and $P_\alpha(1) = n_{a,\alpha}$ that respectively project onto the subspace with occupation numbers 0 and 1 for spin α. From Fig. 33 we see that

$$
\begin{aligned}
\sigma_a &= b^\dagger_{a,\downarrow} P_\uparrow(0) P_\downarrow(0) + b^\dagger_{a,\uparrow} P_\uparrow(0) P_\downarrow(1) \\
&\quad + b_{a,\downarrow} P_\uparrow(1) P_\downarrow(1) + b_{a,\uparrow} P_\uparrow(1) P_\downarrow(0) \\
&= (b^\dagger_{a,\downarrow} + b_{a,\uparrow}) + (b^\dagger_{a,\uparrow} - b_{a,\uparrow}) n_{a,\downarrow} + (b_{a,\downarrow} - b^\dagger_{a,\downarrow}) n_{a,\uparrow} \ .
\end{aligned}
\tag{3.16}
$$

As described in Section 3.7, Eqs. (3.15) and (3.16) can be inverted to yield

$$
b_{a,\uparrow} = \left[\sigma_a \frac{1 - \tau_a^2}{4} + H.c. \right] + i \left[\sigma_a \frac{\tau_a^\dagger - \tau_a}{4} + H.c. \right]
\tag{3.17}
$$

$$
b_{a,\downarrow} = \left[\frac{1 - \tau_a^2}{4} \sigma_a + H.c. \right] + i \left[\frac{\tau_a^\dagger - \tau_a}{4} \sigma_a + H.c. \right] .
\tag{3.18}
$$

We can now define spinful fermions

$$
f_{a,\uparrow} = e^{-i\frac{\pi}{4}} S_a b_{a,\uparrow}
\tag{3.19}
$$

$$
f_{a,\downarrow} = e^{-i\frac{\pi}{4}} S_a e^{i\pi n_{a,\uparrow}} b_{a,\downarrow}.
\tag{3.20}
$$

The $e^{-i\frac{\pi}{4}}$ phases are introduced for later convenience, the factor $e^{i\pi n_{a,\uparrow}}$ in Eq. (3.20) enforces anticommutation of spin-up and spin-down fermions on the same site [3], and

$$
S_a = e^{i\pi \sum_{b<a}(n_{b,\uparrow} + n_{b,\downarrow})} = \prod_{b<a} \tau_b^2 = \mu^2_{a-\frac{1}{2}}
\tag{3.21}
$$

is a Jordan-Wigner string that ensures off-site anticommutation. Note the 'doubled' string relative to the α_a operators, consistent with our heuristic picture above.

Section 3.8 derives the action of $\mathbb{Z}_4$, $\mathcal{T}$, and C on the fermions; see Table 31 for a summary. With our conventions all three symmetries act nontrivially, in the sense that the fermions acquire a phase factor dependent on the occupation of the opposite spin species. Combinations of these symmetries nevertheless correspond to familiar operations. First, the generator Q of $\mathbb{Z}_4$ symmetry squares to

$$
Q^2 = \prod_a \tau_a^2 = e^{i\pi \sum_a (n_{a,\uparrow} + n_{a,\downarrow})} = \text{fermion parity.}
\tag{3.22}
$$

---

instead expressed σ_a in terms of boson densities and τ_a in terms of creation and annihilation operators that cycle σ_a eigenvalues. The latter parametrization is problematic, however, in that $\mathbb{Z}_4$-symmetric terms such as $-f(\tau_a + \tau_a^\dagger)$ become nonlocal upon fermionization (in contrast to our conventions, where such terms remain local).

[3]More generally, we could have inserted factors $e^{i\theta n_{a,\uparrow}}$ in Eq. (3.19) and $e^{i(\theta+\pi)n_{a,\downarrow}}$ in Eq. (3.20) to maintain on-site anticommutation. The choice $\theta = 0$ that we adopted is particularly convenient for symmetries.

	clock	parafermion	spinful fermion
$\mathbb{Z}_4$ breakable explicitly?	yes	no (locality)	yes
$\mathbb{Z}_4$ breakable spontaneously?	yes	yes ($\langle \alpha_a^2 \rangle \neq 0$)	yes
$\mathbb{Z}_4^2$ breakable explicitly?	yes	no (locality)	no (locality)
$\mathbb{Z}_4^2$ breakable spontaneously?	yes	no (statistics)	no (statistics)

Table 32: Comparison of $\mathbb{Z}_4$-symmetry robustness in various representations. For the case of spinful fermions, the locality and statistics conditions listed in the right column reduce to the familiar statement that fermion-parity conservation can be broken neither spontaneously nor explicitly.

Thus $\mathbb{Z}_4^2$ sends $f_{a,\alpha} \to -f_{a,\alpha}$ and represents global fermion parity conservation—which can be broken neither explicitly nor spontaneously in a system of physical fermions. By contrast, $\mathbb{Z}_4$ itself *can* be readily broken (explicitly or spontaneously) provided $\mathbb{Z}_4^2$ remains intact. Table 32 summarizes the varying robustness of $\mathbb{Z}_4$ symmetry in the clock, parafermionic, and fermionic representations.

Second, $\mathcal{T}_{\text{elec}} \equiv \mathbb{Z}_4 \mathcal{T}$ acts according to

$$\mathcal{T}_{\text{elec}} f_{a,\alpha} \mathcal{T}_{\text{elec}}^{-1} = i\sigma_{\alpha\beta}^y f_{a,\beta}; \tag{3.23}$$

here and below $\sigma^{x,y,z}$ denote the usual Pauli matrices [4]. One can recognize $\mathcal{T}_{\text{elec}}$ as electronic time-reversal symmetry that satisfies $\mathcal{T}_{\text{elec}}^2 = -1$ when acting on single-particle states. Third, $U_{\text{spin}} \equiv \mathbb{Z}_4 \mathcal{C}$ corresponds to a π spin rotation, i.e.,

$$U_{\text{spin}} f_{a,\alpha} U_{\text{spin}}^\dagger = \sigma_{\alpha\beta}^y f_{a,\beta}. \tag{3.24}$$

The set $\mathcal{T}_{\text{elec}}$, U_{spin}, and $\mathbb{Z}_4$ provides a convenient basis of symmetries in the fermionic representation. While $\mathbb{Z}_4$ generally acts nontrivially on the fermions, a simplification is possible in the low-density limit where $\langle n_{a,\alpha} \rangle \ll 1$. Here one can approximate $\mathbb{Z}_4$ by dropping the density-dependent phases acquired by the fermions. The resulting operation, which we label $\overline{\mathbb{Z}}_4$, yields a simpler transformation

$$\overline{Q} f_{a,\alpha} \overline{Q}^\dagger = i\sigma_{\alpha\beta}^z f_{a,\beta}, \text{(low-density approx. of } \mathbb{Z}_4) \tag{3.25}$$

---

[4]We inserted the factors $e^{-i\frac{\pi}{4}}$ in Eqs. (3.19) and (3.20) simply to recover the familiar form of electronic time-reversal in Eq. (3.23); without these factors the i on the right side would be absent.

	$\mathcal{T}_{\text{elec}} = \mathbb{Z}_4\mathcal{T}$	$U_{\text{spin}} = \mathbb{Z}_4 C$	$\overline{\mathbb{Z}}_4$
$f \rightarrow$	$i\sigma^y f$	$\sigma^y f$	$i\sigma^z f$

Table 33: Action of composite symmetries $\mathcal{T}_{\text{elec}}$ and U_{spin} along with $\overline{\mathbb{Z}}_4$ on spinful fermions. Remarkably, $\mathcal{T}_{\text{elec}}$ implements electronic time-reversal symmetry with $\mathcal{T}_{\text{elec}}^2 = -1$ while U_{spin} implements a π spin rotation. In the last column $\overline{\mathbb{Z}}_4$ is an approximation of the exact $\mathbb{Z}_4$ symmetry (see Table 31) valid in the low-fermion-density limit; this operation implements a π spin rotation about a different axis.

that represents π spin rotation about a different axis. Symmetry transformations under $\mathcal{T}_{\text{elec}}$, U_{spin}, and $\overline{\mathbb{Z}}_4$ appear in Table 33.

Dual fermions

One can of course straightforwardly generalize Eqs. (3.17) through (3.21) to instead fermionize the *dual* representation of the clock model. To this end we first define dual hard-core bosons

$$\tilde{b}_{\tilde{a},\uparrow} = \left[\mu_{\tilde{a}}\frac{1 - v_{\tilde{a}}^2}{4} + H.c.\right] + i\left[\mu_{\tilde{a}}\frac{v_{\tilde{a}}^\dagger - v_{\tilde{a}}}{4} + H.c.\right] \tag{3.26}$$

$$\tilde{b}_{\tilde{a},\downarrow} = \left[\frac{1 - v_{\tilde{a}}^2}{4}\mu_{\tilde{a}} + H.c.\right] + i\left[\frac{v_{\tilde{a}}^\dagger - v_{\tilde{a}}}{4}\mu_{\tilde{a}} + H.c.\right], \tag{3.27}$$

where $\tilde{a} = a + \frac{1}{2}$ labels dual-lattice sites. Dual fermions are then given by

$$\tilde{f}_{\tilde{a},\uparrow} = e^{-i\frac{\pi}{4}}\tilde{S}_{\tilde{a}}\tilde{b}_{\tilde{a},\uparrow}, \tag{3.28}$$

$$\tilde{f}_{\tilde{a},\downarrow} = e^{-i\frac{\pi}{4}}\tilde{S}_{\tilde{a}}e^{i\pi\tilde{n}_{\tilde{a},\uparrow}}\tilde{b}_{\tilde{a},\downarrow}, \tag{3.29}$$

with

$$\tilde{S}_{\tilde{a}} = e^{i\pi\sum_{\tilde{b}<\tilde{a}}(\tilde{n}_{\tilde{b},\uparrow} + \tilde{n}_{\tilde{b},\downarrow})} = \prod_{\tilde{b}<\tilde{a}} v_{\tilde{b}}^2 = \sigma_a^2\sigma_{-\infty}^2. \tag{3.30}$$

Clock-model duality [Eq. (3.7)] non-locally transforms our original spinful fermions $f_{a,\alpha}$ into these dual fermions $\tilde{f}_{\tilde{a},\alpha}$. The situation should be contrasted to the para-fermion representation, where duality merely implements a spatial translation. It is also worth contrasting to the Majorana-fermion representation of the Ising model, where Ising duality similarly corresponds to a spatial translation of the Majorana operators (as opposed to non-locally mapping to a new set of fermions).

The clock-operator fermionization described so far allows one to directly express lattice $\mathbb{Z}_4$ parafermions as non-local combinations of either fermions or dual fermions.

Interestingly, it is also possible to express parafermions in terms of a *local* product of fermions and dual fermions—reflecting the roughly self-dual nature of the parafermion operators alluded to earlier. The latter form resembles the factorization identified in Ref. [70] of $\mathbb{Z}_4$ parafermions into two sets of fermions that exhibit nontrivial commutation relations with one another. We relegate explicit expressions linking parafermions and fermions to Section 3.11 (see also Sec. 3.3).

Spin-1/2 representation and alternative fermionization schemes

There are numerous alternative mappings that relate $\mathbb{Z}_4$ clock operators to spin-1/2 or fermionic degrees of freedom. Among these, different choices may be convenient for revealing particular properties. This section briefly outlines an approach that yields the same spinful fermion operators as Sec. 3.2, but through a very different route. Sections 3.9 and 3.10 present additional details about this mapping and several other schemes, including that of Refs. [62, 108].

We begin by expressing the clock operators σ_a, τ_a in terms of spin-1/2 degrees of freedom via [62, 108]

$$\sigma_a = \frac{1+i}{2}\left(s^z_{a+\frac{1}{4}} + is^z_{a-\frac{1}{4}}\right), \tag{3.31}$$

$$\tau_a = \frac{1}{2}\left(s^x_{a+\frac{1}{4}} + s^x_{a-\frac{1}{4}}\right) + \frac{1}{2}\left(s^x_{a+\frac{1}{4}} - s^x_{a-\frac{1}{4}}\right)s^z_{a+\frac{1}{4}}s^z_{a-\frac{1}{4}}, \tag{3.32}$$

where $s^{x,y,z}$ denote Pauli matrices that reside at sites $a \pm \frac{1}{4}$. Next, we perform the familiar Ising-model duality mapping that trades in these variables for dual spins $t^{x,y,z}$ living on integer as well as half-integer sites,

$$t^x_a = s^z_{a-\frac{1}{4}}s^z_{a+\frac{1}{4}}, \qquad t^z_a = \prod_{a'<a}s^x_{a'}. \tag{3.33}$$

'Exchange' and 'transverse-field' clock-model couplings take on a particular simple form in this language:

$$-J(\sigma^\dagger_a\sigma_{a+1} + H.c.) = -J\left(t^x_a t^x_{a+\frac{1}{2}} + t^x_{a+\frac{1}{2}}t^x_{a+1}\right),$$
$$-f(\tau_a + \tau^\dagger_a) = -f\left(t^z_{a-\frac{1}{2}}t^z_a + t^z_a t^z_{a+\frac{1}{2}}\right), \tag{3.34}$$

and in particular precisely coincide with couplings in the 1D XY model. (References [62, 108] used a somewhat different mapping to a spin-1/2 model as discussed in Section 3.10.) Since clock-model duality interchanges the J and f terms, Eqs. (3.34) naively suggest that such a duality transformation is implemented as a

global $\pi/2$ rotation of t spins around the y axis. We caution, however, that this interpretation only holds for specific Hamiltonians and is not dictated by conditions of symmetry and locality; see Section 3.9.

Let us now employ a Jordan-Wigner transformation to define complex fermions

$$\mathbf{c}_a = \frac{1}{2}(t_a^y - it_a^z) \prod_{a'<a} t_{a'}^x \tag{3.35}$$

and then introduce spinful fermions $\mathbf{d}_{a,\alpha}$ via a Bogoliubov transformation:

$$\mathbf{d}_{a,\alpha} = \frac{i}{\sqrt{8}}\left(-\mathbf{c}_a - \mathbf{c}_a^\dagger - \mathbf{c}_{a+\frac{1}{2}} + \mathbf{c}_{a+\frac{1}{2}}^\dagger\right) + \frac{\alpha}{\sqrt{8}}\left(-\mathbf{c}_{a-\frac{1}{2}} - \mathbf{c}_{a-\frac{1}{2}}^\dagger - \mathbf{c}_a + \mathbf{c}_a^\dagger\right). \tag{3.36}$$

On the right side, $\alpha = +1$ for spin up and -1 for spin down. Somewhat lengthy but straightforward algebra sketched in Section 3.10 reveals that a local canonical transformation,

$$\mathbf{f}_{a,\alpha} = e^{-i\frac{\pi}{4}(1+\alpha)} \exp\left(-i\frac{\pi}{2}\mathbf{d}_{a,-\alpha}^\dagger \mathbf{d}_{a,-\alpha}\right) \mathbf{d}_{a,\alpha}, \tag{3.37}$$

yields operators that are identical to $f_{a,\alpha}$ up to a boundary term that squares to unity.

An alternative set of fermions can be formed by defining $\tilde{\mathbf{c}}_a = U\mathbf{c}_a U^\dagger$, where U implements a global $\pi/2$ spin rotation around t^y. Note that $\mathbf{c}_a$ and $\tilde{\mathbf{c}}_a$ are nonlocally related—the Jordan-Wigner string consists solely of t^x operators in the former but t^z operators in the latter. Since U is precisely the spin rotation that swaps the two lines of Eq. (3.34), it is natural to expect that $\tilde{\mathbf{c}}_a$ fermions closely relate to the dual fermions $\tilde{f}_{a,\alpha}$ of Sec. 3.2. Let $\tilde{\mathbf{d}}_{a,\alpha}$ and $\tilde{\mathbf{f}}_{a,\alpha}$ denote spinful fermions defined analogously to Eqs. (3.36) and (3.37). On the level of single-fermion operators, $\tilde{f}_{a,\alpha}$ and $\tilde{\mathbf{f}}_{a,\alpha}$ are related nonlocally. Nevertheless, Hamiltonians for which clock-model duality corresponds to a spin rotation take on an identical form when expressed in terms of either set of operators, though this relation breaks down for more generic models.

3.3 Mappings Between Phases

Hamiltonians

The remainder of this paper primarily explores *translationally invariant* fermionic phases and their clock/parafermion counterparts. All of the phases that we will discuss can be accessed microscopically from limits of (or in some cases weak perturbations to) the Hamiltonian

$$H = -J \sum_{a=1}^{N-1}(\sigma_a^\dagger \sigma_{a+1} + \sigma_{a+1}^\dagger \sigma_a - \lambda\sigma_a^2\sigma_{a+1}^2) - f\sum_{a=1}^{N}(\tau_a + \tau_a^\dagger - \lambda\tau_a^2) \tag{3.38}$$

for an N-site clock chain. Equation (3.38) corresponds to the well-studied Ashkin-Teller model [9], which exhibits a variety of ordered and disordered gapped phases, novel critical points, and extended critical phases (see, e.g., Refs. [3, 62, 108, 109]). Throughout we assume non-negative J, f couplings and take open boundary conditions to highlight nontrivial edge physics that arises in certain regimes. Since duality interchanges the J and f terms, the Hamiltonian is self-dual at $J = f$ for any λ.

In terms of parafermions, the model becomes

$$H = -J \sum_{a=1}^{N-1} [(e^{i\frac{\pi}{4}} \alpha_{2a}^\dagger \alpha_{2a+1} + H.c.) + \lambda \alpha_{2a}^2 \alpha_{2a+1}^2]$$
$$- f \sum_{a=1}^{N} [(e^{i\frac{\pi}{4}} \alpha_{2a-1}^\dagger \alpha_{2a} + H.c.) + \lambda \alpha_{2a-1}^2 \alpha_{2a}^2] . \tag{3.39}$$

The first and second lines favor competing dimerization patterns for the parafermion operators.

For spinful fermions it is useful to partition the Hamiltonian as $H = H_0 + H_\lambda$, where H_λ contains the terms proportional to λ in the Ashkin-Teller model. Implicitly summing repeated spin indices and neglecting unimportant overall constants, H_0 can be expressed as

$$H_0 = -J \sum_{a=1}^{N-1} \left(\hat{t}_a^{\alpha,\beta} f_{a,\alpha}^\dagger f_{a+1,\beta} + i\hat{\Delta}_a^{\alpha,\beta} f_{a,\alpha}^\dagger f_{a+1,\beta}^\dagger + H.c. \right) + 2f \sum_{a=1}^{N} f_{a,\alpha}^\dagger f_{a,\alpha} . \tag{3.40}$$

The f coupling simply yields a chemical potential for the fermions. In the J term, $\hat{t}_a^{\alpha,\alpha'}$ and $\hat{\Delta}_a^{\alpha,\alpha'}$ encode spin- and density-dependent hoppings and triplet pairings, respectively. We explicitly have

$$\begin{aligned}
\hat{t}_a^{\alpha,\alpha} &= 1 - n_{a,-\alpha} - n_{a+1,-\alpha} , \\
\hat{t}_a^{\alpha,-\alpha} &= \alpha[2n_{a,-\alpha} n_{a+1,\alpha} - n_{a,-\alpha} - n_{a+1,\alpha}] , \\
\hat{\Delta}_a^{\alpha,\alpha} &= \alpha[n_{a,-\alpha} - n_{a+1,-\alpha}] , \\
\hat{\Delta}_a^{\alpha,-\alpha} &= [n_{a,-\alpha} + n_{a+1,\alpha} - 2n_{a,-\alpha} n_{a+1,\alpha} - 1] .
\end{aligned} \tag{3.41}$$

The λ terms yield nontrivial four-fermion interactions:

$$H_\lambda = \lambda J \sum_{a=1}^{N-1} (if_{a,\uparrow}^\dagger + f_{a,\uparrow})(f_{a,\downarrow}^\dagger + if_{a,\downarrow})(if_{a+1,\uparrow}^\dagger + f_{a+1,\uparrow})(f_{a+1,\downarrow}^\dagger + if_{a+1,\downarrow})$$
$$+ \lambda f \sum_{a=1}^{N} (2n_{a,\uparrow} - 1)(2n_{a,\downarrow} - 1) . \tag{3.42}$$

	$\mathbb{Z}_4$	C	$\mathcal{T}$
$\phi \to$	$\phi + \pi/2$	$-\phi$	ϕ
$\theta \to$	θ	$-\theta$	$-\theta$

Table 34: Symmetry properties of bosonized fields used to construct long-wavelength expansions of clock operators, parafermions, and fermions.

View from the long-wavelength limit

It will prove exceedingly useful to obtain a bosonized description of H that filters out all but the long-wavelength modes needed to describe the phases of interest. To this end we focus on the spinful-fermion representation and assume the low-density limit $n_{a,\alpha} \approx 0$ where $\mathbb{Z}_4$ symmetry is well-approximated by $\overline{\mathbb{Z}}_4$. Consider first the $\lambda = 0$ limit. Upon retaining only the density-independent pieces from Eqs. (3.41), H_0 reduces to a free-fermion Hamiltonian

$$\overline{H}_0 = -J \sum_{a=1}^{N-1} \left(f_{a,\alpha}^\dagger f_{a+1,\alpha} - i f_{a,\alpha}^\dagger \sigma_{\alpha\beta}^x f_{a+1,\beta}^\dagger + H.c. \right) + 2f \sum_{a=1}^{N} f_{a,\alpha}^\dagger f_{a,\alpha}. \quad (3.43)$$

When $f = J$ the spectrum becomes gapless at zero momentum; low-energy excitations are captured by one right- and one left-moving fermion mode, $\psi_{R/L}$.

A bosonized description of this critical point arises from the identification

$$\begin{aligned}
i(f_\uparrow - f_\downarrow^\dagger) &\sim \psi_R \sim e^{i(\phi+\theta)}, \\
f_\uparrow + f_\downarrow^\dagger &\sim \psi_L \sim e^{i(\phi-\theta)},
\end{aligned} \quad (3.44)$$

where ϕ, θ are continuum fields satisfying

$$[\phi(x), \theta(x')] = i\pi\Theta(x' - x). \quad (3.45)$$

(Our bosonization recipe closely follows that employed by Ref. [36].) For later use we note that $\partial_x\theta/\pi$ yields the spin density since

$$f_\uparrow^\dagger f_\uparrow - f_\downarrow^\dagger f_\downarrow \sim \psi_R^\dagger \psi_R + \psi_L^\dagger \psi_L \sim \partial_x\theta/\pi, \quad (3.46)$$

while

$$e^{i\pi \sum_{a,\alpha} f_{a,\alpha}^\dagger f_{a,\alpha}} = e^{i\pi \sum_a [f_\uparrow^\dagger f_\uparrow - f_\downarrow^\dagger f_\downarrow]} = e^{i \int_x \partial_x\theta} \quad (3.47)$$

correspondingly specifies the total fermion parity in a region of the chain.

Table 34 catalogues symmetry properties of the bosonized fields inferred from Eq. (3.44). [Technically, Eq. (3.44) yield the action of $\overline{\mathbb{Z}}_4$ instead of $\mathbb{Z}_4$, though as we will see below this distinction is immaterial in the long-wavelength limit. We caution, however, that Eq. (3.44) can be used to relate microscopic fermion operators to continuum fields only in the low-density limit; outside of this regime one must exploit symmetry to find the bosonized form of a given lattice operator.] With these symmetries in hand we can deduce the low-energy expansion for operators in various other representations. Order and disorder operators correspond to

$$\sigma_a \sim e^{i\phi}, \qquad \mu_{a+\frac{1}{2}} = \prod_{b < a + \frac{1}{2}} \tau_b \sim e^{-i\theta/2}. \qquad (3.48)$$

Note that the right-hand sides not only yield consistent symmetry properties, but are also faithful to the clock-operator commutation relations. Similarly expanding our two parafermion representations—which again arise from attaching either a string of τ or $\tau^\dagger$ to σ—gives

$$\alpha_a \sim e^{i(\phi - \theta/2)}, \qquad \alpha'_a \sim e^{i(\phi + \theta/2)}. \qquad (3.49)$$

As a useful sanity check, doubling the string yields precisely the continuum limit of spinful fermions derived in Eqs. (3.44); cf. the lattice picture provided in Sec. 3.2.

From a dual perspective, one essentially views μ as the elementary spin operator and σ as the string. The dual analogue of Eq. (3.48) is then

$$\mu_{a+\frac{1}{2}} \sim e^{i\tilde{\phi}}, \qquad \sigma_a \sigma^\dagger_{-\infty} = \prod_{b < a} \nu_{b + \frac{1}{2}} \sim e^{-i\tilde{\theta}/2} \qquad (3.50)$$

with $[\tilde{\phi}(x), \tilde{\theta}(x')] = i\pi\Theta(x' - x)$ as in Eq. (3.45). Clearly the original continuum ϕ, θ fields and their duals are related by

$$\tilde{\phi}(x) = -\theta(x)/2, \qquad \tilde{\theta}(x) = -2[\phi(x) - \phi(-\infty)]. \qquad (3.51)$$

Attaching a string of ν or $\nu^\dagger$ to μ yields essentially the same long-wavelength limit of parafermion operators as before. Doubling this string, however, generates the continuum limit of our dual fermions:

$$\tilde{\psi}_R \sim e^{i(\tilde{\phi} + \tilde{\theta})}, \qquad \tilde{\psi}_L \sim e^{i(\tilde{\phi} - \tilde{\theta})}. \qquad (3.52)$$

In Sec. 3.2 we noted that parafermions can be expressed as local combinations of fermions and dual fermions on the lattice. This relation becomes particularly simple in the long-wavelength limit. Using Eq. (3.51) one immediately obtains

$$\alpha_a \sim \psi_R^\dagger \tilde{\psi}_L^\dagger, \qquad \alpha'_a \sim \psi_L^\dagger \tilde{\psi}_R, \qquad (3.53)$$

very similar to Ref. [70].

Returning to the critical Hamiltonian, the bosonized form of Eq. (3.43) reads $\overline{\mathcal{H}}_0 = \int_x \frac{v_0}{2\pi}[(\partial_x\phi)^2 + (\partial_x\theta)^2]$ with $v_0 \propto J$. Turning on $\lambda \neq 0$ and resurrecting interaction terms from H_0 that were neglected in Eq. (3.43) generically modifies the low-energy Hamiltonian to

$$\mathcal{H} = \int_x \left\{ \frac{v}{2\pi}[g(\partial_x\phi)^2 + g^{-1}(\partial_x\theta)^2] - \kappa_1 \cos(4\phi) - \kappa_2 \cos(2\theta) \right\}. \tag{3.54}$$

Here v is a renormalized velocity; g is the Luttinger parameter characterizing the interaction strength ($g = 1$ corresponds to free fermions, while $g < 1$ and $g > 1$ respectively indicate repulsive and attractive interactions); and the $\kappa_{1,2}$ terms are the leading harmonics consistent with symmetries and locality. Effective Hamiltonians of this form have been studied in related contexts in Refs. [55, 68, 87, 111]. We can appeal to self-duality of the microscopic Hamiltonian at $J = f$ to further constrain $\mathcal{H}$. In particular, here the continuum Hamiltonian must take the same form in terms of either ϕ, θ or their duals $\tilde{\phi}, \tilde{\theta}$. Using Eq. (3.51) we thus obtain $\kappa_1 = \kappa_2$ and $g = 2$. The latter constraint guarantees that the two cosines—which swap under duality—are both marginal at the self-dual critical point. Upon rescaling $\phi \to \phi/\sqrt{2}$ and $\theta \to \sqrt{2}\theta$, $\mathcal{H}$ maps onto one of the manifestly self-dual theories analyzed in Ref. [63]. There, non-Abelian bosonization techniques showed that the self-dual model exhibits a 'hidden' continuous $U(1)$ symmetry.

Breaking self-duality spoils these relations and can drive the system into various possible gapped phases that we explore next, both from a continuum and microscopic viewpoint. The phases that arise depend sensitively on the signs of κ_1 and κ_2. In the $\lambda = 0$ limit we must have $\kappa_1, \kappa_2 > 0$ so that the familiar ferromagnetic and paramagnetic phases of the clock model are 'nearby' (see below). We will show, however, that turning on λ provides access to phases driven by $\kappa_1, \kappa_2 < 0$ as well.

Phases driven by $\kappa_2 > 0$

With relevant $\kappa_2 > 0$ the $\cos(2\theta)$ term pins θ to 0 modulo π. In terms of clock spins, the disorder operator then condenses ($\langle \mu \rangle \neq 0$), yielding a trivial paramagnet. Microscopically, the paramagnetic state arises most simply from the Ashkin-Teller model at $J = \lambda = 0$, where the unique ground state is $|\tau = 1, \ldots, 1\rangle$. One sees from Eq. (3.39) that the corresponding parafermion system dimerizes in a trivial manner that gaps out the entire chain, including the ends. Finally, according to Eq. (3.40) spinful fermions realize the vacuum with no fermions present. The first column of Fig. 34 summarizes the properties of this regime in all three representations.
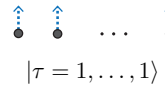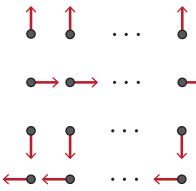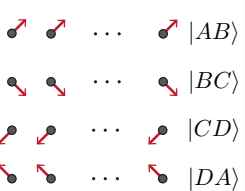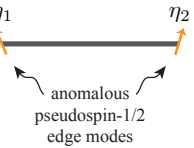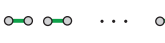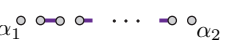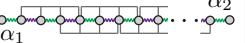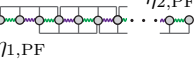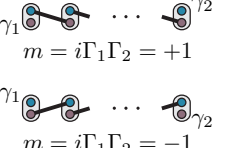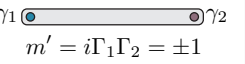
Hamiltonian parameters	$J = \lambda = 0, f \neq 0$	$f = \lambda = 0, J \neq 0$	$J, f \neq 0, \lambda = 1$ with $J' \neq 0$	$J, f \neq 0, \lambda = 1$ with $f' \neq 0$
Bosonized perturbation	$-\cos(2\theta)$	$-\cos(4\phi)$	$+\cos(4\phi)$	$+\cos(2\theta)$
Clock τ σ	Paramagnet $|\tau = 1, \ldots, 1\rangle$	Ferromagnet $\;|A\rangle$ $\;|B\rangle$ $\;|C\rangle$ $\;|D\rangle$	Canted ferromagnet $\;|AB\rangle$ $\;|BC\rangle$ $\;|CD\rangle$ $\;|DA\rangle$	SPT $\eta_1 \quad \eta_2$ anomalous pseudospin-1/2 edge modes
Parafermion	Trivial	Topological $\alpha_1 \quad \alpha_2$	Topological $\alpha_1 \quad \alpha_2$	SPT $\eta_{1,\mathrm{PF}} \quad \eta_{2,\mathrm{PF}}$
Spinful fermion	Fermion vacuum	Topological superconductor + symmetry breaking $\gamma_1 \quad \gamma_2$ $m = i\Gamma_1\Gamma_2 = +1$ $\gamma_1 \quad \gamma_2$ $m = i\Gamma_1\Gamma_2 = -1$	Topological superconductor + symmetry breaking $\gamma_1 \quad \gamma_2$ $m' = i\Gamma_1\Gamma_2 = \pm 1$	SPT (TRITOPS) $\gamma_{1\uparrow} \quad \gamma_{2\uparrow}$ $\gamma_{1\downarrow} \quad \gamma_{2\downarrow}$

Figure 34: Correspondence between gapped phases in the clock, $\mathbb{Z}_4$ parafermion, and spinful fermion representations. The first and second rows respectively indicate the microscopic Hamiltonian parameters and associated bosonized perturbations that generate the phases summarized in each column. Phases in the first and second columns are dual to one another, as are the phases in the third and fourth columns.

Phases driven by $\kappa_1 > 0$

When κ_1 is relevant and positive, the $\cos(4\phi)$ term pins ϕ to 0 modulo $\pi/2$. Implications of the pinning depend strongly on which degrees of freedom are regarded as physical. According to Eq. (3.48), a system of clock spins spontaneously breaks $\mathbb{Z}_4$ symmetry and realizes a four-fold-degenerate ferromagnetic state characterized by the local order parameter $\langle \sigma \rangle = \pm 1$ or $\pm i$. Such ferromagnetic order can be accessed straightforwardly from the $f = \lambda = 0$ limit of the Ashkin-Teller model, which admits broken-symmetry ground states

$$|A\rangle = |\sigma = 1, \ldots, 1\rangle, \qquad |B\rangle = |\sigma = i, \ldots, i\rangle,$$
$$|C\rangle = |\sigma = -1, \ldots, -1\rangle, \qquad |D\rangle = |\sigma = -i, \ldots, -i\rangle. \tag{3.55}$$

A parafermion chain, by contrast, realizes the topological phase introduced by Fend-

ley [34]. From Eq. (3.39) and Fig. 34 one sees that at $f = \lambda = 0$ the parafermions dimerize in a pattern that gaps the interior but leaves behind an 'unpaired' zero-energy mode at each edge. These parafermion zero modes encode a four-fold degeneracy that can not be lifted by any perturbation that is local from the parafermion viewpoint. Physical ground states in this representation correspond to $\mathbb{Z}_4$-preserving Schrödinger-cat superpositions of clock states defined in Eq. (3.55).

$$-\cos(2\theta) \qquad\qquad -\cos(4\phi) \qquad\qquad -\cos(2\theta)$$

Figure 35: Domain configuration used to extract zero-mode operators from the bosonized theory.

Although the parafermion zero-mode operators are easily identified from the microscopic Hamiltonian, it is instructive to recover their form also from the low-energy bosonized point of view. Figure 35 sketches a domain configuration in which trivial phases gapped by $-\cos(2\theta)$ (recall Sec. 3.3) flank a central region gapped by $-\cos(4\phi)$. For compactness we choose a gauge where θ pins to 0 in the left domain, but parametrize $\phi = \pi\hat{a}/2$ in the central domain and $\theta = \pi\hat{b}$ in the right domain. Here $\hat{a}, \hat{b}$ are integer-valued operators that obey the commutator $[\hat{a}, \hat{b}] = 2i/\pi$ inherited from Eq. (3.45). Using Eq. (3.49), parafermion operators acting at the left and right domain walls respectively project to

$$\alpha_1 = e^{i\frac{\pi}{2}\hat{a}}, \qquad \alpha_2 = e^{i\frac{\pi}{2}(\hat{a}-\hat{b})}, \tag{3.56}$$

which are the continuum counterpart of the lattice parafermion zero modes.

A system of spinful fermions splits the difference between the clock and parafermion realizations: half of the degeneracy has a topological origin, while the other half is encoded in the local order parameter

$$m \equiv \langle i\psi_R\psi_L + H.c.\rangle \sim \langle\cos(2\phi)\rangle = \pm 1, \tag{3.57}$$

signaling spontaneous breaking of electronic time-reversal $\mathcal{T}_{\text{elec}}$, U_{spin}, and $\mathbb{Z}_4$. Similar phases have been captured previously in both 1D systems [68, 89, 100]—most notably Fe chains proximitized by a Pb superconductor [26, 33, 51, 82, 83, 88, 94]—and proximitized quantum-spin-Hall edges [87, 111]. Even at $f = \lambda = 0$, the surviving pieces of the microscopic fermion Hamiltonian in Eq. (3.40) appear nontrivial

due to the interactions implicit in the J term. (Recall the density dependence in $\hat{t}, \hat{\Delta}$.) In terms of dual fermions $\tilde{f}_{a,\alpha}$, the $f = \lambda = 0$ model is of course quadratic. Changing from fermions to dual fermions, however, requires a non-local change of basis. Alternatively, one can tame these interactions with a judicious *local* basis change,

$$f_{a,\uparrow} = \frac{e^{-i\frac{\pi}{4}}}{2}(c_a + c_a^\dagger + d_a - d_a^\dagger), \tag{3.58}$$

$$f_{a,\downarrow} = \frac{e^{-i\frac{\pi}{4}}}{2}(d_a + d_a^\dagger + c_a - c_a^\dagger), \tag{3.59}$$

where c_a, d_a are canonical fermions with symmetry properties given in Table 35. In this basis the Hamiltonian becomes

$$H_{f=\lambda=0} = -J \sum_{a=1}^{N-1}(m_a c_a^\dagger + c_a)(c_{a+1} - m_{a+1}c_{a+1}^\dagger) + H.c.$$

$$\tag{3.60}$$

with

$$m_a = e^{i\pi d_a^\dagger d_a} = -f_a^\dagger \sigma^x f_a + (i f_{a,\uparrow}^\dagger f_{a,\downarrow}^\dagger + H.c.) \tag{3.61}$$

operators that commute with the Hamiltonian for any a [see Section 3.11 for an alternate derivation of Eq. (3.60)]. Note that in clock language we have $m_a = \sigma_a^2$.

By symmetry, m_a is the lattice analogue of the continuum order parameter in Eq. (3.57). We note that one cannot obtain this microscopic order parameter by using Eqs. (3.44) in conjunction with Eq. (3.57) because the former relations holds only in the low-density limit, which is not relevant here; recall the discussion below Eq. (3.47). In terms of the original spinful fermions, m_a receives contributions from the magnetization along x and singlet pairing with an imaginary coefficient— both of which share common symmetry properties. For simplicity we will refer to m_a as just 'magnetization' in what follows. The energy is minimized by choosing either $m_a = +1$ or -1 uniformly across the entire chain. Focusing on such uniform configurations and replacing $m_a \to m$, the Hamiltonian further simplifies to

$$H_{f=\lambda=0} \to -2J \sum_{a=1}^{N-1}(mc_a^\dagger + c_a)(c_{a+1} - mc_{a+1}^\dagger). \tag{3.62}$$

Equation (3.62) can be recognized as the trivially solvable limit of the Kitaev chain in the topological phase [58], but with one crucial distinction: in our case the model arose from *spontaneous* breaking of symmetries, most notably electronic

	$\mathcal{T}_{\text{elec}} = \mathbb{Z}_4\mathcal{T}$	$U_{\text{spin}} = \mathbb{Z}_4 C$	$\mathbb{Z}_4$
$c \rightarrow$	$ic^\dagger$	$ic^\dagger$	$ie^{i\pi d^\dagger d}c^\dagger$
$d \rightarrow$	$-id^\dagger$	$-id^\dagger$	$-ie^{i\pi c^\dagger c}d^\dagger$
$\gamma_1 \rightarrow$	$m\gamma_1$	γ_1	$m\gamma_1$
$\gamma_2 \rightarrow$	$m\gamma_2$	$-\gamma_2$	$-m\gamma_2$
$\Gamma_1 \rightarrow$	$p\Gamma_1$	Γ_1	$p\Gamma_1$
$\Gamma_2 \rightarrow$	$p\Gamma_2$	$-\Gamma_2$	$-p\Gamma_2$

Table 35: Symmetry properties for the microscopic fermions c_a, d_a defined through the basis change in Eqs. (3.58) and (3.59). The middle two lines summarize the transformations for the symmetry-enriched Majorana zero mode operators [Eq. (3.63) and (3.64)] that arise in the fermionic representation of the Ashkin-Teller model at $f = \lambda = 0$. The quantity $m = i\Gamma_1\Gamma_2 = \pm 1$, which is odd under all three symmetries in the table, is the order parameter whose condensation catalyzes the topological phase. Finally, the last two lines list the transformations for $\Gamma_{1,2}$. The factor $p = i\gamma_1\gamma_2$ is required to preserve anticommutation between Γ_j and γ_j.

time reversal. Consequently, the phase of matter realized here is distinct from that of the Kitaev chain. (See, e.g., Ref. [23] for a general discussion of the classification of short-range entangled phases with spontaneous symmetry breaking.) The Hamiltonian supports 'symmetry-enriched edge Majorana zero modes' described by

$$\gamma_1 = e^{i\frac{\pi}{4}(m+1)}c_1^\dagger + e^{-i\frac{\pi}{4}(m+1)}c_1 \,, \tag{3.63}$$

$$\gamma_2 = e^{i\frac{\pi}{4}(m-1)}c_N^\dagger + e^{-i\frac{\pi}{4}(m-1)}c_N \,, \tag{3.64}$$

whose form depends on the magnetization order parameter. These zero modes satisfy the usual Majorana algebra $\gamma_i^2 = 1, \gamma_i = \gamma_i^\dagger$, and $\{\gamma_1, \gamma_2\} = 0$, but transform nontrivially under electronic time-reversal symmetry,

$$\mathcal{T}_{\text{elec}} : \gamma_j \rightarrow m\gamma_j, \tag{3.65}$$

reflecting the intertwined symmetry-breaking order and topological physics. One can not sweep away the m in Eq. (3.65) by any redefinition of the Majorana operators that preserves their algebra. More physically, since each edge hosts only one Majorana mode, the m factor is required by the fact that $\mathcal{T}_{\text{elec}}^2$ must send $\gamma_j \rightarrow -\gamma_j$. In Sec. 3.6 we will argue on general grounds that proximitized Fe chains provide a concrete physical realization of our modified Kitaev-chain Hamiltonian.

Projecting the total-fermion-parity operator [Eq. (3.22)] into the ground-state manifold yields

$$P_{\text{tot}} \equiv e^{i\pi \sum_a (n_{a,\uparrow} + n_{a,\downarrow})} \rightarrow mp , \tag{3.66}$$

where we defined

$$p = i\gamma_1 \gamma_2 . \tag{3.67}$$

Equation (3.66) further illustrates the intertwinement of symmetry and topology: Flipping m while leaving p constant changes the total parity. This type of magnetization reversal is thus naturally implemented by fermionic operators, which one can efficiently obtain by decomposing

$$m = i\Gamma_1 \Gamma_2. \tag{3.68}$$

Here $\Gamma_{1,2}$ are Majorana operators that we take to additionally obey $\{\Gamma_i, \gamma_j\} = 0$; they simultaneously flip the magnetization *and* total parity as desired. Together, γ_j and Γ_j form a complete set of low-energy operators describing this fermionic phase (see Table 35 for their symmetry properties). We emphasize that $\Gamma_{1,2}$, in contrast to $\gamma_{1,2}$, are generally *not* local operators since they change the magnetization across the entire system. Locality therefore dictates that Γ_j can only appear in the Hamiltonian when the system becomes sufficiently small that the magnetization becomes a fluctuating quantum degree of freedom. We will encounter such 'small' systems in Sec. 3.4.

It is worth noting that while the factor of m in Eq. (3.65) is unavoidable, the form of the parity operator above depends on our specific definition of $\gamma_{1,2}$. One could instead define $\gamma_1' = \gamma_1$ and $\gamma_2' = m\gamma_2$, yielding a more standard expression $P_{\text{tot}} = i\gamma_1'\gamma_2'$. Magnetization flips would then more naturally be implemented by bosonic operators. This alternate convention is, however, less convenient for understanding hybridization of symmetry-enriched Majorana modes that will be discussed later.

Interestingly, one can reassemble the four Majorana operators characterizing the low-energy subspace into a single pair of $\mathbb{Z}_4$ parafermion zero modes:

$$\alpha_1 = -e^{i\frac{\pi}{4}(m-1)}\gamma_1 , \tag{3.69}$$

$$\alpha_2 = -e^{-i\frac{\pi}{4}[p(m+1)+1]}\Gamma_2 . \tag{3.70}$$

These expressions arise upon translating the microscopic zero-mode operators from the parafermion representation into fermionic language and projecting into the low-energy subspace. Such a reorganization is always possible for *any* quartet of Majorana operators. Some caution is thus warranted when invoking a parafermion

interpretation of the physics, particularly when the operators are non-local (as is the case for α_2 above when the fermion system is 'large'). Section 3.4 elaborates on the issue.

Here too we can recover the zero-mode structure from the low-energy bosonized theory. Consider again the setup from Fig. 35, and respectively write $\theta = 0$, $\phi = \pi\hat{a}/2$, and $\theta = \pi\hat{b}$ in the left, central, and right domains. In the present context $\hat{a}, \hat{b}$ determine the central domain's magnetization and total fermion parity according to

$$m = e^{i\pi\hat{a}}, \quad P_{\text{tot}} = e^{i\pi\hat{b}}, \tag{3.71}$$

where we used Eq. (3.47) for the parity operator. The bosonized analogue of Eqs. (3.63) and (3.64) are

$$\gamma_1 = \sqrt{2}\cos\left[\frac{\pi}{2}\left(\hat{a} - \frac{1}{2}\right)\right], \tag{3.72}$$

$$\gamma_2 = -i\sqrt{2}\cos\left[\frac{\pi}{2}\left(\hat{a} + \frac{1}{2}\right)\right]e^{i\pi\hat{b}}. \tag{3.73}$$

Both operators are local in the sense that γ_1 involves only projections of physical fermions $\psi_{R/L} \sim e^{i(\phi\pm\theta)}$ evaluated at the left domain wall, while γ_2 similarly involves fermions evaluated at the right domain wall. Moreover, using Eq. (3.71) we have $p = i\gamma_1\gamma_2 = mP_{\text{tot}}$, in harmony with Eqs. (3.66) and (3.67). The remaining pair of Majorana operators can be written

$$\Gamma_1 = \cos\left[\frac{\pi}{2}\left(\hat{a} - \hat{b} + \frac{1}{2}\right)\right] - \cos\left[\frac{\pi}{2}\left(\hat{a} + \hat{b} + \frac{1}{2}\right)\right] \tag{3.74}$$

$$\Gamma_2 = \cos\left[\frac{\pi}{2}\left(\hat{a} - \hat{b} - \frac{1}{2}\right)\right] + \cos\left[\frac{\pi}{2}\left(\hat{a} + \hat{b} - \frac{1}{2}\right)\right], \tag{3.75}$$

which involve not only domain-wall fermions, but also the operator $e^{i\int_{x\in\text{central domain}}\partial_x\theta/2} \sim e^{i\frac{\pi}{2}\hat{b}}$ that flips the central domain's magnetization. This definition of $\Gamma_{1,2}$ reflects a gauge choice and is certainly not unique: Any rotation among Γ_1 and Γ_2 that preserves the magnetization constitutes an equally valid set of operators. Equations (3.74) and (3.75) yield $i\Gamma_1\Gamma_2 = m$, consistent with the decomposition in Eq. (3.68). Using Eqs. (3.69) and (3.70) to repackage the bosonized form of the Majorana operators into $\mathbb{Z}_4$ parafermion zero modes precisely reproduces the parafermion operators from Eq. (3.56).

The Majorana representation of the zero modes is far less compact compared to the parafermion representation; cf. Eqs. (3.56) and (3.72) through (3.75). Nevertheless,

the former provides a much more natural description for an electronic system as it clearly partitions the topological and non-topological parts of the degeneracy. A similar viewpoint was very recently stressed by Mazza et al. [68]. We also note while some references (e.g., the review in Ref. [6]) discussed domain walls in quantum-spin-Hall edges with spontaneously broken time-reversal in terms of $\mathbb{Z}_4$ parafermions, it is now clear that the physics is more accurately described in terms of symmetry-enriched Majorana modes.

The form of the Hamiltonians in Eqs. (3.60) and (3.62) implies that the ground states, and in fact all energy eigenstates, have a free-fermion character despite the obviously interacting nature of the original fermionic Hamiltonian in Eq. (3.43). (More precisely, for any fixed configuration of m_a's the Hamiltonian is quadratic.) This observation connects with the recent work of Meichanetzidis et al. [69] that inferred free-fermion eigenstates from an analytic solution of the $f = 0$ fixed point combined with an interesting numerical diagnostic for the general case [103]. In terms of the clock-model states in Eq. (3.55), the total-even-parity fermionic ground states correspond to $|A\rangle + |C\rangle$, $|B\rangle + |D\rangle$ while the odd-parity states are $|A\rangle - |C\rangle$, $|B\rangle - |D\rangle$ (to see this, recall that $P_{\text{tot}} = Q^2 = \prod_a \tau_a^2$).

Figure 34, second column, summarizes the results from this subsection.

Phases driven by $\kappa_1 < 0$

When κ_1 is relevant and negative, ϕ locks to $\pi/4$ modulo $\pi/2$, leading to physics similar to what we encountered in Sec. 3.3 for positive κ_1. Clock spins once again realize a broken-symmetry phase with four degenerate ground states, parafermions form a topological phase where the degeneracy is fully protected, and fermions enter a topological state hosting a partially protected degeneracy encoded through symmetry-enriched Majorana zero modes. These states are distinct, however, from those of Sec. 3.3, at least in the presence of C symmetry. The bosonized theory encodes this distinction as follows. To smoothly interpolate between phases driven by $\kappa_1 > 0$ and $\kappa_1 < 0$, one could in principle replace $-\kappa_2 \cos(4\phi) \rightarrow -\kappa_2 \cos(4\phi - \phi_0)$ and then continuously sweep ϕ_0 between 0 and π. However, C symmetry permits *only $\phi_0 = 0$ or π*, thereby obstructing the interpolation; similar arguments appear in Ref. [74] in the context of symmetry-protected topological phases.

Pinning of ϕ to $\pi/4$ modulo $\pi/2$ implies that clock spins spontaneously break $\mathbb{Z}_4$ symmetry by developing a canted ferromagnetic polarization $\langle \sigma \rangle = (1 \pm i)/2$ or $(-1 \pm i)/2$. By modifying the 'root states' $|A, B, C, D\rangle$ defined in Eq. (3.55), we can

construct trial wavefunctions

$$|AB\rangle = \prod_a \frac{1 + \tau_a}{\sqrt{2}} |A\rangle, \qquad |BC\rangle = \prod_a \frac{1 + \tau_a}{\sqrt{2}} |B\rangle$$
$$|CD\rangle = \prod_a \frac{1 + \tau_a}{\sqrt{2}} |C\rangle, \qquad |DA\rangle = \prod_a \frac{1 + \tau_a}{\sqrt{2}} |D\rangle \tag{3.76}$$

with precisely these expectation values [5]. For example, in $|AB\rangle$ any site is equally likely to be found with $\sigma = 1$ or i (and similarly for $|BC\rangle$, etc.). Two closely related properties are worth noting: (*i*) these trial states involve no antiparallel σ bonds at any distance and (*ii*) the $(1 + \tau_a)$ factors ensure that the wavefunctions contain no $\tau = -1$ components. States with these characteristics are exact ground states of the Ashkin-Teller model [Eq. (3.38)] at $\lambda = 1$, independent of f/J. At $\lambda = 1$ the J term penalizes antiparallel nearest-neighbor σ bonds but does not distinguish parallel and 90° bonds, while the f term penalizes $\tau = -1$ but does not differentiate other τ states. See Fig. 36 for an illustration. Trial states in Eq. (3.76) incur no such penalties, and are thus indeed ground states.

Other ground states exist as well—a consequence of an 'accidental' U(1) symmetry supported by the Ashkin-Teller model in this limit [62]. In fact at $\lambda = 1$ the Ashkin-Teller model is known to reside at the edge of an extended 'critical fan' in the phase diagram [62]. To move away from criticality we therefore additionally incorporate a second-neighbor interaction

$$\delta H = -J' \sum_{a=1}^{N-2} (\sigma_a^\dagger \sigma_{a+2} + \sigma_{a+2}^\dagger \sigma_a - \sigma_a^2 \sigma_{a+2}^2) \tag{3.77}$$

with $J' > 0$. The above perturbation spoils the accidental U(1) by penalizing second-neighbor antiparallel σ bonds (similar to the J term), leaving our trial canted ferromagnet states as unique ground states. Exact diagonalization numerics summarized in Fig. 37 support this scenario; see caption for details. As a further check, DMRG calculations were performed on a 400-site system using ITensor [6]. With $J' = 0$, DMRG exhibited characteristics of a gapless system, predicting a gap several orders of magnitude below the J, f couplings. When a small J' perturbation was added, DMRG instead converged to the expected canted ground states [7] while

---

[5]These trial states do not form an orthogonal set on a finite chain, though any nontrivial overlaps vanish as $1/2^N$.

[6]Calculations performed using the ITensor C++ library, http://itensor.org/

[7]More precisely, with $\mathbb{Z}_4$ symmetry enforced, DMRG returns Schrodinger-cat superpositions of the states in Eq. (3.76). Adding a small $\mathbb{Z}_4$-breaking perturbation of the form $e^{i\frac{\pi}{4}}\sigma_j + H.c.$ to a single site j, however, yields one of the physical canted product states.

$$H = -[(\sigma_1^\dagger \sigma_2 + H.c.) - \lambda \sigma_1^2 \sigma_2^2] \qquad\qquad H = -(\tau + \tau^\dagger - \lambda \tau^2)$$
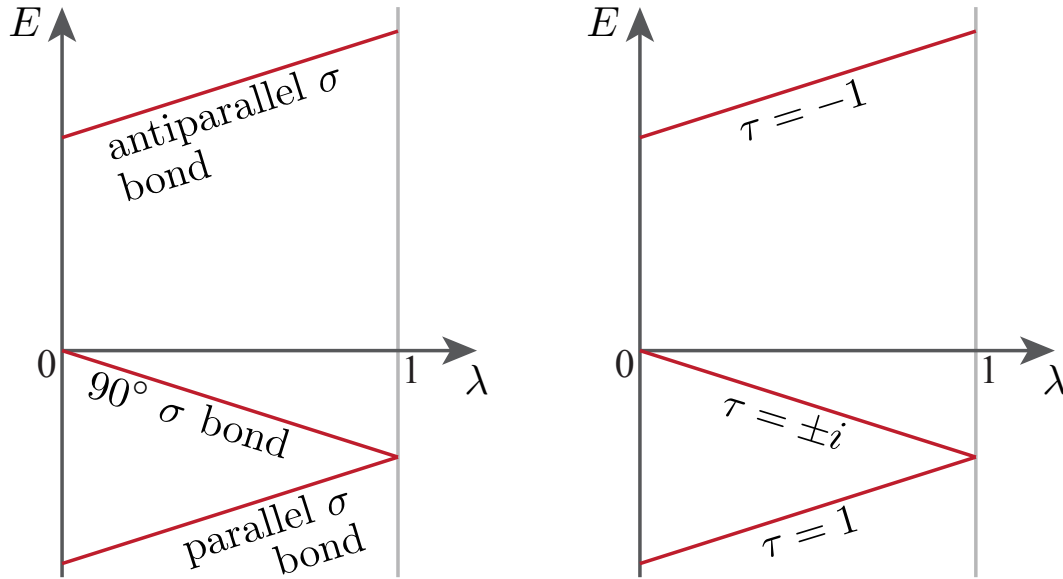
Figure 36: Energies versus λ obtained from the Hamiltonians shown at the top of the figure. The left plot represents the energy for a single J bond in the Ashkin-Teller model, Eq. (3.38). As λ increases from zero, the energy difference between parallel σ bonds (i.e., $\sigma_1^\dagger \sigma_2 = 1$) and $90°$ σ bonds ($\sigma_1^\dagger \sigma_2 = \pm i$) decreases. At $\lambda = 1$ these states become degenerate; the Hamiltonian then penalizes antiparallel σ bonds ($\sigma_1^\dagger \sigma_2 = -1$) but does not distinguish other configurations. The right plot similarly represents the energy for a single f term in the Ashkin-Teller model. Here the energy difference between $\tau = 1$ and $\tau = \pm i$ states diminishes with λ until they become degenerate at $\lambda = 1$; the Hamiltonian then penalizes $\tau = -1$ states but does not differentiate other configurations. As discussed in Secs. 3.3 and 3.3, the $\lambda = 1$ limit is useful for accessing canted-ferromagnet and symmetry-protected topological phases for clock spins, and by extension the analogous phases for parafermions and spinful fermions.
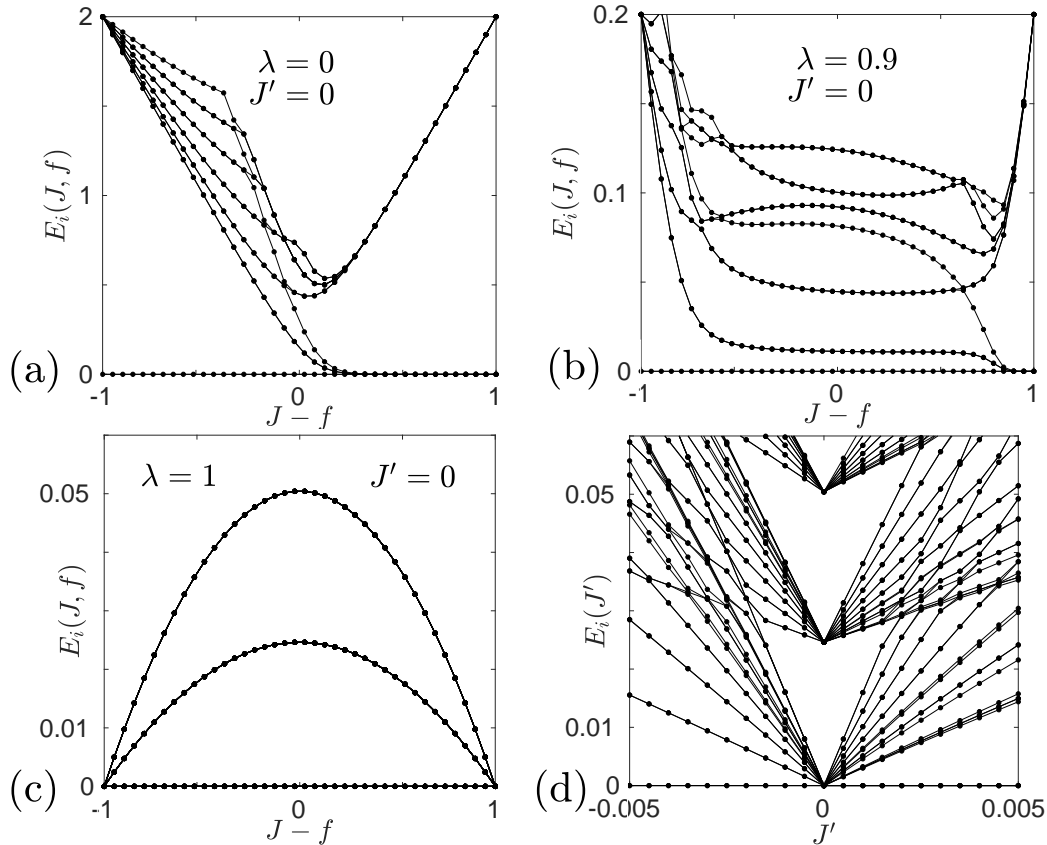
Figure 37: Low-energy spectra of the perturbed Ashkin-Teller model $H + \delta H$ given in Eqs. (3.38) and (3.77) for a chain of $N = 10$ sites with open boundary conditions. All spectra are shifted such that the ground states sit at zero energy, independent of parameters. (a) The 'vanilla' clock model corresponding to $\lambda = J' = 0$ undergoes a phase transition at $J = f$ separating the paramagnetic ($f > J$) from the ordered ($J > f$) phase. In a finite system, we find a unique ground state in the former and an (approximately) four-fold-degenerate ground state in the latter. (b) For non-zero λ, there is a finite region around $J = f$ where the spectrum remains relatively flat, and which we interpret as a finite-size avatar of the critical fan [62]. (c) At $\lambda = 1$ the spectrum is highly degenerate for arbitrary J and f. For $N \in [2, 10]$ the ground-state degeneracy grows as $2N + 1$. (d) Turning on non-zero J' immediately lifts this degeneracy; for $J' > 0$ only a four-fold-degenerate ground state remains as expected for the canted-ferromagnet phase.

predicting a gap of order J'. These results strongly suggest that the Hamiltonian is indeed gapped so long as $J' > 0$.

Translating into parafermion language, δH becomes

$$\delta H = -J' \sum_{a=1}^{N-2} \left[(i\alpha_{2a}^{\dagger} \alpha_{2a+1} \alpha_{2a+2}^{\dagger} \alpha_{2a+3} + H.c.) \right.$$
$$\left. - \alpha_{2a}^2 \alpha_{2a+1}^2 \alpha_{2a+2}^2 \alpha_{2a+3}^2 \right]. \tag{3.78}$$

See Fig. 34 for an illustration of the full set of couplings for the parafermion chain arising from both δH and the Ashkin-Teller model at $\lambda = 1$. Our prior analysis allows us to deduce some general features of the parafermion phase realized here: First, ground states necessarily correspond to $\mathbb{Z}_4$-preserving superpositions of clock states in Eq. (3.76), and second, the chain must host edge $\mathbb{Z}_4$ parafermion zero modes. (Upon breaking C this phase smoothly connects to the topological phase discussed in Sec. 3.3; since parafermion zero modes obviously exist in the latter case, they must also survive in the former by continuity. Restoring C can not change this conclusion.) Explicitly constructing lattice zero-mode operators is nevertheless nontrivial given that the Hamiltonian no longer consists of a sum of commuting terms [8].

We will content ourselves with capturing the zero modes within a bosonized framework. Let us take a domain configuration akin to Fig. 35, with outer regions again gapped by $-\cos(2\theta)$ but with the central region gapped by $+\cos(4\phi)$ instead of $-\cos(4\phi)$. We parametrize the low-energy sector with integer-valued operators $\hat{a}, \hat{b}$ by writing $\theta = 0$, $\phi = \pi/4 + \pi\hat{a}/2$, and $\theta = \pi\hat{b}$ in the left, middle, and right regions. Note in particular the $\pi/4$ shift in ϕ compared to the parametrization adopted in Sec. 3.3. The zero modes we seek follow from projecting parafermions evaluated at domain walls, and then introducing phase factors to ensure that the resulting low-energy operators fourth to unity; this procedure yields parafermion zero modes $\alpha_{1,2}$ given precisely by Eq. (3.56). What, then, is the distinction between the parafermion analogue of the conventional ferromagnetic and canted ferromagnetic phases? The answer lies in the symmetry properties of the zero modes. In particular, under C the zero modes obtained in Sec. 3.3 transform as $\alpha_j \to \alpha_j^{\dagger}$, while in the present case they transform as $\alpha_j \to -i\alpha_j^{\dagger}$—a consequence of the $\pi/4$ shift mentioned above. Without C symmetry this distinction vanishes, consistent with our earlier arguments.

---

[8]We expect that localized 'strong zero mode' operators that commute with the full microscopic Hamiltonian—and thus guarantee at least four-fold degeneracy of *all* eigenstates—do not actually exist, similar to the situations encountered in Refs. [4, 34, 49, 52, 76]. 'Weak zero modes', which arise from projections of local operators and ensure degeneracy only among ground states, certainly exist and are captured by the bosonization description that follows.

For spinful fermions, two ground states arise from Majorana zero modes while the other two reflect spontaneous symmetry breaking. A more obvious distinction from Sec. 3.3 emerges here: The local order parameter

$$\bar{m} \equiv \langle \psi_R \psi_L + H.c. \rangle \sim \langle \sin(2\phi) \rangle = \pm 1 \tag{3.79}$$

again breaks $\mathcal{T}_{\text{elec}}$ and $\mathbb{Z}_4$ but, contrary to Eq. (3.57), preserves U_{spin}. We can readily obtain the zero-mode structure from the continuum bosonized theory, following exactly the same procedure as for parafermions above. Within this framework our four Majorana zero mode operators once again take the form in Eqs. (3.72) through (3.75) and similarly satisfy $p = i\gamma_1\gamma_2 = \bar{m}P_{\text{tot}}$ and $\bar{m} = i\Gamma_1\Gamma_2$. Moreover, the Majorana operators transform under $\mathcal{T}_{\text{elec}}$ and $\mathbb{Z}_4$ precisely as in Table 35 (with $m \to \bar{m}$); they are invariant under U_{spin}, however, because the ground states now preserve that symmetry.

We can again interpret the physics in terms of a Kitaev-chain-like model arising from spontaneous symmetry breaking. The microscopic order parameter can be written as

$$\bar{m}_a = i(c_a d_a - d_a^\dagger c_a^\dagger) = -f_a^\dagger \sigma^y f_a, \tag{3.80}$$

corresponding to a magnetization along y. The above expression arises from fermionizing $\sigma^2(\tau - \tau^\dagger)/2$, which has the same symmetry properties as Eq. (3.79). Because $\bar{m}_a$ no longer commutes with the lattice Hamiltonian, an exact microscopic analysis is nonetheless more nontrivial than in Sec. 3.3 and will not be pursued here.

The canted phase and its parafermionic and fermionic counterparts are summarized in the third column of Fig. 34; note the close relation to the phases from the second column.

Phases driven by $\kappa_2 < 0$

With relevant $\kappa_2 < 0$ the $\cos(2\theta)$ term pins θ to $\pi/2$ modulo π. It is tempting to conclude that clock spins then form a trivial, symmetric gapped phase as found in Sec. 3.3 for $\kappa_2 > 0$, since the pinning once again condenses the disorder operator μ. However, one can not smoothly interpolate between phases driven by $\kappa_2 > 0$ and $\kappa_2 < 0$ without violating symmetries. Let us first apply the same logic as in the previous subsection: A term of the form $-\kappa_2 \cos(2\theta - \theta_0)$ can only have $\theta_0 = 0$ or π unless both C and $\mathcal{T}$ are explicitly broken, which precludes symmetrically bridging the two phases via continuous evolution of θ_0 [74]. We could alternatively connect the phases by (*i*) starting from the trivial regime gapped by $\kappa_2 > 0$, (*ii*) ramping

up a 'large' $\cos(\phi - \phi_0)$ perturbation for some constant ϕ_0, (*iii*) sweeping κ_2 from positive to negative, and (*iv*) turning off the $\cos(\phi - \phi_0)$ term. The system follows a unique ground state throughout this path, yet along the way maximally breaks $\mathbb{Z}_4$ and possibly other symmetries depending on ϕ_0. By 'maximally', we mean that $\mathbb{Z}_4$ and $\mathbb{Z}_4^2$ are both violated. To better understand this second scenario, suppose that we replace $\cos(\phi - \phi_0)$ with $\cos(2\phi)$—which also breaks $\mathbb{Z}_4$ but preserves $\mathbb{Z}_4^2$. Here, passing from (*i*) to (*ii*) incurs an Ising-type phase transition at which the order parameter $e^{i\phi}$ condenses into one of two spontaneously chosen values. The $\cos(\phi - \phi_0)$ term, by contrast, circumvents criticality by favoring a unique state. An identical distinction arises between the $\beta^2 = 2\pi$ and 4π theories discussed in Ref. [63]; in our conventions, the self-dual Sine-Gordon models described there model the deformation from the $\cos(2\theta)$-dominated phase to the $\cos(q\phi)$-dominated phase, where q is an integer.

The observations above suggest that $\kappa_2 < 0$ germinates a symmetry-protected topological phase (SPT). We will show that this is indeed the case not only for clock spins, but also for parafermions and fermions.

Recall that phases driven by $\kappa_2 < 0$ and $\kappa_1 < 0$ are dual to one another, and that the $\kappa_1 < 0$ state arises microscopically from the Ashkin-Teller Hamiltonian at $\lambda = 1$ supplemented by δH in Eq. (3.77). Dualizing the perturbed Ashkin-Teller model thus immediately yields a parent Hamiltonian for the phases of interest here. In the Ashkin-Teller parts, dualizing merely swaps $J \leftrightarrow f$. At $\lambda = 1$ the swap is inconsequential insofar as ground states are concerned, since these pieces merely penalize $\tau = -1$ configurations and antiparallel nearest-neighbor σ bonds for any f/J (see again Fig. 36). The dual of δH takes the form

$$\widetilde{\delta H} = -f' \sum_{a=1}^{N-1} (\tau_a \tau_{a+1} + \tau_a^\dagger \tau_{a+1}^\dagger - \tau_a^2 \tau_{a+1}^2). \tag{3.81}$$

For $f' > 0$, which we assume throughout, $\widetilde{\delta H}$ additionally penalizes nearest-neighbor configurations with $(\tau_a, \tau_{a+1}) = (1, -1), (-1, 1), (i, i)$, or $(-i, -i)$.

We can modify the 'root state' $|\tau = 1, \ldots, 1\rangle$ to construct an exact ground state of our new perturbed Ashkin-Teller model. For reasons that will become clear shortly, we label the wavefunction

$$| \downarrow\uparrow \rangle = \prod_{a=1}^{N-1} \frac{1 + \sigma_a^\dagger \sigma_{a+1}}{\sqrt{2}} |\tau = 1, \ldots, 1\rangle \, ; \tag{3.82}$$

note the dual relation to the canted-ferromagnet states defined in Eq. (3.76). The $(1 + \sigma_a^\dagger \sigma_{a+1})$ product generates an entangled state that, by construction, projects away all antiparallel σ bonds. Nontrivial elements in the product take the form $\sigma_{a_1}^\dagger \sigma_{a_1+1} \sigma_{a_2}^\dagger \sigma_{a_2+1} \cdots \sigma_{a_m}^\dagger \sigma_{a_m+1}$ where all a_i's are distinct. Crucially, such terms produce neither $\tau = -1$ configurations nor $(\tau_a, \tau_{a+1}) = (i, i)$ or $(-i, -i)$ pairs. (Obtaining $\tau = -1$ contributions would require σ_a^2 factors, while the latter pairs would require $\sigma_a^\dagger \sigma_{a+1}^\dagger$ or $\sigma_a \sigma_{a+1}$; none of these appear.) So $|\downarrow\uparrow\rangle$ maximally satisfies both the $\lambda = 1$ Ashkin-Teller model and $\widetilde{\delta H}$, and hence is a ground state as claimed.

For any site away from the edges, configurations with $\tau = 1, i$, and $-i$ all occur in $|\downarrow\uparrow\rangle$. Acting with σ or $\sigma^\dagger$ in the bulk thus necessarily takes the system out of the ground state, e.g., by mixing in $\tau = -1$ components penalized by the Ashkin-Teller terms. Boundaries behave differently. The leftmost two sites involve only $(\tau_1, \tau_2) = (1, 1), (1, i), (i, 1)$, and $(i, -i)$ pairs, and the rightmost two sites involve only $(\tau_{N-1}, \tau_N) = (1, 1), (1, -i), (-i, 1)$, and $(i, -i)$ pairs. We can therefore twist the edge spins without energy cost, yielding three additional ground states

$$|\uparrow\uparrow\rangle = \sigma_1|\downarrow\uparrow\rangle, \quad |\downarrow\downarrow\rangle = \sigma_N^\dagger|\downarrow\uparrow\rangle, \quad |\uparrow\downarrow\rangle = \sigma_1 \sigma_N^\dagger|\downarrow\uparrow\rangle. \tag{3.83}$$

For later use, observe that the generator Q of $\mathbb{Z}_4$ symmetry acts in the ground-state subspace as follows:

$$\begin{aligned} Q|\uparrow\uparrow\rangle &= i|\uparrow\uparrow\rangle, & Q|\downarrow\downarrow\rangle &= -i|\downarrow\downarrow\rangle, \\ Q|\downarrow\uparrow\rangle &= |\downarrow\uparrow\rangle, & Q|\uparrow\downarrow\rangle &= |\uparrow\downarrow\rangle. \end{aligned} \tag{3.84}$$

Our construction shows that each boundary of the clock chain hosts a degenerate pseudospin-1/2 degree of freedom, which we describe with Pauli matrices η_1^μ and η_2^μ. (Arrows in the kets above designate $\eta_{1,2}^z$ eigenvalues.) The pseudospins are locally distinguishable by Hermitian operators $i(\tau - \tau^\dagger)$ since $\langle \eta_1^z \eta_2^z | i(\tau_1 - \tau_1^\dagger) | \eta_1^z \eta_2^z \rangle = \eta_1^z$ and $\langle \eta_1^z \eta_2^z | i(\tau_N - \tau_N^\dagger) | \eta_1^z \eta_2^z \rangle = \eta_2^z$. These expectation values, together with Eqs. (3.83) and (3.84), enable us to relate pseudospins and microscopic operators projected into the ground-state subspace with a projector $\mathcal{P}$:

$$\mathcal{P} i(\tau_1 - \tau_1^\dagger)\mathcal{P} = \eta_1^z, \qquad\qquad \mathcal{P} i(\tau_N - \tau_N^\dagger)\mathcal{P} = \eta_2^z, \tag{3.85}$$

$$\mathcal{P}\sigma_1\mathcal{P} = (\eta_1^x + i\eta_1^y)/2, \qquad\qquad \mathcal{P}\sigma_N\mathcal{P} = (\eta_2^x + i\eta_2^y)/2, \tag{3.86}$$

$$\mathcal{P}Q\mathcal{P} = e^{i\frac{\pi}{4}(\eta_1^z + \eta_2^z)}. \tag{3.87}$$

Table 36 summarizes the pseudospin symmetry properties that follow from these relations.

	$\mathbb{Z}_4$	C	$\mathcal{T}$
$\eta_j^x \to$	$-\eta_j^y$	η_j^x	η_j^x
$\eta_j^y \to$	η_j^x	$-\eta_j^y$	η_j^y
$\eta_j^z \to$	η_j^z	$-\eta_j^z$	$-\eta_j^z$
	$\mathcal{T}_{\text{elec}} = \mathbb{Z}_4\mathcal{T}$	$U_{\text{spin}} = \mathbb{Z}_4 C$	$\mathbb{Z}_4$
$\gamma_{j\uparrow} \to$	$\gamma_{j\downarrow}$	$\gamma_{j\downarrow}$	$\gamma_{j\downarrow}$
$\gamma_{j\downarrow} \to$	$-\gamma_{j\uparrow}$	$\gamma_{j\uparrow}$	$-\gamma_{j\uparrow}$

Table 36: Symmetry transformations for the SPT edge degrees of freedom in the clock realization (top) and spinful-fermion realization (bottom). Here $j = 1$ and 2 respectively correspond to the left and right boundaries.

Abandoning C and $\mathcal{T}$ allows the boundary degeneracy to be lifted through local edge perturbations of the form $h_z(\eta_1^z + \eta_2^z)$, while discarding $\mathbb{Z}_4$ permits a perturbation $h_x(\eta_1^x + \eta_2^x)$ that likewise spoils the degeneracy. The symmetry-protection of the edge degeneracy seen here fully corroborates the analysis of the bulk given in the beginning of this subsection. In Section 3.13 we further show that the edge modes are anomalous (in all representations) in the presence of either $\mathbb{Z}_4\mathcal{T}$, or $\mathbb{Z}_4$ and C, thus proving that the system forms an SPT.

Suppose next that parafermions form the physical degrees of freedom. Figure 34 sketches the parafermion-chain couplings for this case [including $\widetilde{\delta H}$, which takes the same form as Eq. (3.78) but translated by one site]. The ground states in Eq. (3.84) are already eigenstates of the $\mathbb{Z}_4$ generator Q, and so form a physical basis also in this realization. Physical low-energy operators should, however, now derive from projections of parafermionic rather than clock degrees of freedom. Specifically, the microscopic operators to be projected become

$$
\begin{aligned}
&- e^{-i\frac{\pi}{4}} \alpha_1^\dagger \alpha_2 + H.c. = i(\tau_1 - \tau_1^\dagger), \\
&- e^{-i\frac{\pi}{4}} \alpha_{2N-1}^\dagger \alpha_{2N} + H.c. = i(\tau_N - \tau_N^\dagger) \\
&\alpha_1 = \sigma_1, \quad \alpha_{2N} = e^{i\frac{\pi}{4}} Q^\dagger \sigma_N,
\end{aligned}
\tag{3.88}
$$

which give rise to edge operators that we label $\eta_{j,\text{PF}}^\mu$. At the left boundary the projection is unmodified compared to the clock case; hence $\eta_{1,\text{PF}}^\mu = \eta_1^\mu$. The factor of $Q^\dagger$ appearing in α_{2n} does modify the structure of the edge mode at the right boundary, yielding

$$
\eta_{2,\text{PF}}^z = \eta_2^z, \qquad \eta_{2,\text{PF}}^{x,y} = e^{-i\frac{\pi}{4}\eta_1^z} \eta_2^{x,y} .
\tag{3.89}
$$

Notice that $\eta_{1,\mathrm{P}F}^{x,y}$ and $\eta_{2,\mathrm{P}F}^{x,y}$ do not commute—a remnant of the nonlocal parafermionic commutation relations. We stress that locality prevents these operators from appearing in the Hamiltonian by themselves. The *only* local operators that can remove the edge degeneracy in the parafermion SPT realization take the form $h_{z,1}\eta_{1,\mathrm{P}F}^{z}$ and $h_{z,2}\eta_{2,\mathrm{P}F}^{z}$, which require breaking C and $\mathcal{T}$. In other words, the $\mathbb{Z}_4$-breaking route to connecting the trivial and SPT phases discussed earlier for clock spins is inaccessible because $\mathbb{Z}_4$ can never be broken explicitly in a parafermion system.

We treat the spinful-fermion realization analogously. Since fermions arise from attaching a 'doubled' string to clock operators (Fig. 32), the edge modes take the same form as for the parafermion chain but with $e^{-i\frac{\pi}{4}\eta_1^z} \to e^{-i\frac{\pi}{2}\eta_1^z} = -i\eta_1^z$ in Eq. (3.89). [That is, the fermionic counterpart of Eq. (3.88) involves Q^2 instead of $Q^\dagger$.] One can conveniently parametrize the resulting edge modes as follows,

$$\eta_1^z = i\gamma_{1\downarrow}\gamma_{1\uparrow}, \quad \eta_2^z = i\gamma_{2\downarrow}\gamma_{2\uparrow} \tag{3.90}$$

$$\eta_1^x + i\eta_1^y = \gamma_{1\uparrow} - i\gamma_{1\downarrow} \tag{3.91}$$

$$-i\eta_1^z(\eta_2^x + i\eta_2^y) = \gamma_{2\downarrow} - i\gamma_{2\uparrow}, \tag{3.92}$$

where $\gamma_{j\alpha}$ are Majorana-fermion operators. Table 36 lists their transformation properties under the symmetry generators $\mathcal{T}_{\mathrm{elec}}$, U_{spin}, and $\mathbb{Z}_4$ that are natural for the fermionic representation. Most importantly, we see that *the pair of Majorana modes at each end form a Kramers doublet under electronic time reversal*—which immediately implies that the SPT in this representation corresponds to a time-reversal-invariant topological superconductor (TRITOPS) [19, 27, 40, 41, 57, 92, 112].

Two additional observations further illuminate the edge physics. First, our fermionization algorithm yields the relation

$$S_a^z \equiv \frac{\hbar}{2}(f_{a,\uparrow}^\dagger f_{a,\uparrow} - f_{a,\downarrow}^\dagger f_{a,\downarrow}) = -i\frac{\hbar}{4}(\tau_a - \tau_a^\dagger), \tag{3.93}$$

where S_a^z denotes the z-component of the electronic spin at site a. Upon combining with Eq. (3.85) we obtain

$$\mathcal{P}S_1^z\mathcal{P} = -\frac{\hbar}{4}(i\gamma_{1\downarrow}\gamma_{1\uparrow}), \quad \mathcal{P}S_N^z\mathcal{P} = -\frac{\hbar}{4}(i\gamma_{2\downarrow}\gamma_{2\uparrow}). \tag{3.94}$$

Thus each edge hosts a fractional spin $\pm\hbar/4$, which is another known signature of a TRITOPS phase [19, 57]. It is illuminating to view this result also in bosonization. In our bosonized theory the edge can be modeled by taking a TRITOPS phase gapped

by $+\cos(2\theta)$ bordered by trivial phases gapped by $-\cos(2\theta)$. Using Eq. (3.46), we see that the resulting $\pi/2$ kinks in θ at the domain walls bind fractional spin in agreement with our lattice calculation. Interestingly, an identical domain structure arises in the bosonized description of a quantum-spin-Hall edge gapped by regions with opposite magnetization. In that context the domain walls bind $e/2$ fractional charge [91], which we now see is a precise analogue of fractional spin at a TRITOPS edge. Yet another instance in which fractional spin binds to the edge of a 1D model occurs in the Haldane phase [1, 31, 43], which was analyzed using similar bosonization methods in Ref. [74]. Note that the status of the Haldane phase as an SPT is subtle when viewed as arising from electrons; see Refs. [8, 78]. By contrast, time-reversal-symmetry alone protects TRITOPS as a nontrivial SPT.

Second, the total fermion parity operator obeys

$$P_{\text{tot}} = Q^2 \rightarrow \gamma_{1\downarrow}\gamma_{1\uparrow}\gamma_{2\downarrow}\gamma_{2\uparrow}. \tag{3.95}$$

Equation (3.84) then implies that $|\downarrow\uparrow\rangle$ and $|\uparrow\downarrow\rangle$ have even parity while $|\uparrow\uparrow\rangle$ and $|\downarrow\downarrow\rangle$ have odd parity. It is now clear that the edge Majorana modes cycle through the ground states by simultaneously flipping the total fermion parity and fractional edge spins. Electronic time-reversal by itself suffices to preserve the boundary degeneracy and SPT order; in principle U_{spin} can also protect the topological phase but is a less natural symmetry to impose on an electronic system. Finally, as in the parafermion realization breaking $\mathbb{Z}_4$ does not destroy the SPT, in this case because $\mathbb{Z}_4^2$ can never be broken explicitly.

The final column of Fig. 34 summarizes the SPT's in each representation.

Hybrid order

It is also possible to stabilize phases with both $\langle e^{2i\phi}\rangle \neq 0$ *and* $\langle e^{i\theta}\rangle \neq 0$. In clock language such 'hybrid order' translates into the square of order and disorder operators condensing simultaneously—i.e., $\langle\sigma^2\rangle \neq 0$ and $\langle\mu^2\rangle \neq 0$—while σ itself fluctuates wildly. Clock spins thus spontaneously break $\mathbb{Z}_4$ but preserve $\mathbb{Z}_4^2$, yielding only two degenerate ground states. For simplicity, we will concentrate on hybrid orders that preserve C and $\mathcal{T}$ symmetries, which admit a particularly simple microscopic parent Hamiltonian given by

$$H_{\text{hybrid order}} = -J_2 \sum_{a=1}^{N-1} \sigma_a^2 \sigma_{a+1}^2 - f_2 \sum_{a=1}^{N} \tau_a^2. \tag{3.96}$$

We assume $J_2, f_2 > 0$ throughout this subsection. Equation (3.96) corresponds to the Ashkin-Teller model with only the λ terms retained, and is trivially solvable since σ^2 and τ^2 commute.

For any f_2/J_2, ground states have $\tau_a^2 = 1$ for all a and Ising-like ferromagnetic order with either $\sigma_a^2 = +1$ or -1 uniformly across the chain. The ground-state wavefunctions can be written in a similar form as the canted-ferromagnet states in Eq. (3.76):

$$|+\rangle = \prod_a \frac{1 + \tau_a^2}{\sqrt{2}} |\sigma = 1, \ldots, 1\rangle \tag{3.97}$$

$$|-\rangle = \prod_a \frac{1 + \tau_a^2}{\sqrt{2}} |\sigma = i, \ldots, i\rangle. \tag{3.98}$$

The $(1 + \tau_a^2)$ factors simultaneously disorder σ and project out $\tau_a^2 = -1$ configurations. As desired, both states are $C, \mathcal{T}$-symmetric and yield $\langle \sigma \rangle = 0$, while $\tau^2|\pm\rangle = |\pm\rangle$ and $\sigma^2|\pm\rangle = \pm|\pm\rangle$. When $J_2 = f_2$ the Hamiltonian is self-dual; one can also view the phase itself as self-dual for general f_2/J_2, in the sense that swapping $f_2 \leftrightarrow J_2$ yields exactly the same order. We show in Section 3.12 that duality indeed leaves the above states invariant, modulo a trivial basis transformation.

Equation (3.49) implies that the associated parafermion system realizes a 'parafermion condensate' phase with $\langle \alpha^2 \rangle \neq 0$ [4, 17, 77]. The parent Hamiltonian in this representation becomes

$$H_{\text{hybrid order}} = J_2 \sum_{a=1}^{N-1} \alpha_{2a}^2 \alpha_{2a+1}^2 + f_2 \sum_{a=1}^{N} \alpha_{2a-1}^2 \alpha_{2a}^2, \tag{3.99}$$

which is an example of the commuting-projector models from Ref. [17], and can also be viewed as a simpler variant of the parafermion-condensate model introduced by Motruk et al. [77]. The two ground states correspond to $\mathbb{Z}_4$-preserving superpositions $|\tilde{+}\rangle = (|+\rangle + |-\rangle)/\sqrt{2}$ and $|\tilde{-}\rangle = (|+\rangle - |-\rangle)/\sqrt{2}$ that are locally indistinguishable and satisfy $Q|\tilde{\pm}\rangle = \pm|\tilde{\pm}\rangle$. Operators $\alpha^2 \propto \sigma^2\mu^2$ acting *anywhere* in the chain toggle between the ground states. As emphasized in Refs. [4, 17, 77], the system exhibits a protected degeneracy yet lacks edge zero modes.

In the spinful-fermion realization, the two-fold degeneracy arises entirely from spontaneous symmetry breaking. The order parameter m from the bosonized theory in fact takes the same form given in Eq. (3.57). This symmetry breaking emerges transparently from the fermionic representation of Eq. (3.96), which can be conveniently

Hamiltonian parameters	$J_2, f_2 \neq 0$
Clock σ^2 ⇑	Ising-like ferromagnet
Parafermion $= f_2$ $= J_2$	Parafermion condensate
Spinful fermion	Symmetry breaking only $m = \pm 1$

Figure 38: Summary of phases stabilized by the equivalent Hamiltonians of Eqs. (3.96), (3.99), and (3.100). In the spinful-fermion realization, the system forms a topologically trivial strong-pairing superconductor with spontaneous symmetry breaking.

expressed as

$$H_{\text{hybrid order}} = - J_2 \sum_{a=1}^{N-1} m_a m_{a+1} - f_2 \sum_{a=1}^{N} (2n_{a,\uparrow} - 1)(2n_{a,\downarrow} - 1). \qquad (3.100)$$

Here $m_a = \sigma_a^2 = -f_a^\dagger \sigma^x f_a + (i f_{a,\uparrow}^\dagger f_{a,\downarrow}^\dagger + H.c.)$ is the microscopic clock order parameter re-expressed in terms of fermions [cf. Eq. (3.61)]. To maximally satisfy the f_2 term we project into the sector where both spin species on a given site are either occupied or unoccupied. In effect, the projection strongly pairs the fermions into bosons that can be conveniently described with spin-singlet Cooper-pair operators $b_a = f_{a,\uparrow} f_{a,\downarrow}$. Within this low-energy subspace, the order parameter projects to $m_a \to i(b_a^\dagger - b_a)$. Clearly the system can now also maximally satisfy the J_2 term by condensing $\langle i(b_a^\dagger - b_a) \rangle = \pm 1$. We thereby obtain a strong-pairing superconductor in which the fermions spontaneously develop an s-wave pairing potential with imaginary coefficient, thus breaking electronic time-reversal as well as U_{spin} and $\mathbb{Z}_4$.

Figure 38 summarizes the phases highlighted in this subsection.

3.4 Experimental Implications

How much non-Abelian-anyon physics survives in 1D electronic systems?

At this point we have studied in detail the exact mapping between parafermions and spinful fermions, relating symmetries and various phases of matter in these representations. In Secs. 3.3 and 3.3 we found that a parafermion chain with unpaired $\mathbb{Z}_4$ parafermion zero modes translates into an electronic topological superconductor that hosts symmetry-enriched Majorana zero modes and spontaneously breaks time-reversal symmetry. A natural question arises in light of this connection: to what extent does the non-Abelian-anyon physics encoded through parafermion zero modes survive in the latter strictly 1D fermionic setting? We will specifically address the survival of the three signature properties of non-Abelian anyons highlighted in the introduction: (*i*) the existence of *locally indistinguishable* ground states produced by the anyons, (*ii*) non-Abelian braiding that 'rigidly' rotates the system within the ground-state manifold, and (*iii*) nontrivial fusion rules that specify the different types of quasiparticles that the anyons can form when they coalesce. To bolster connection to experiment, in our treatment of the electronic setting below we will at most enforce $\mathcal{T}_{\mathrm{elec}} = \mathbb{Z}_4\mathcal{T}$ symmetry and *not* separately enforce $\mathbb{Z}_4$ (which is unnatural in that realization).

Concerning property (*i*), a pair of $\mathbb{Z}_4$ parafermion zero modes yields four locally indistinguishable ground states. The corresponding electron system certainly does not preserve this characteristic; Majorana modes generate two locally indistinguishable ground states, but the other two ground states reflect order-parameter configurations that local measurements readily distinguish. We note that this point is well-appreciated by previous works on related electronic systems; see, e.g., Refs. [55, 68, 89, 111].

To address property (*ii*) we will first summarize non-Abelian braiding in the parafermion realization, which is known to be richer than in conventional Majorana systems [12, 24, 29, 44, 47, 65, 104]. Imagine four $\mathbb{Z}_4$ parafermion zero modes $\alpha_{1,\ldots,4}$ realized at defects in a parent fractional-quantum-Hall fluid; see Fig. 39(a). For a given fixed overall $\mathbb{Z}_4$ charge, the system admits four degenerate ground states, and arbitrary superpositions of these states are physically permissible. Braiding, as implemented, e.g., in Fig. 39(a), rotates the system within this manifold. One specifically finds that swapping α_j and α_{j+1} sends $\alpha_j \rightarrow \alpha_{j+1}$ and $\alpha_{j+1} \rightarrow i\alpha_j^\dagger\alpha_{j+1}^2$,
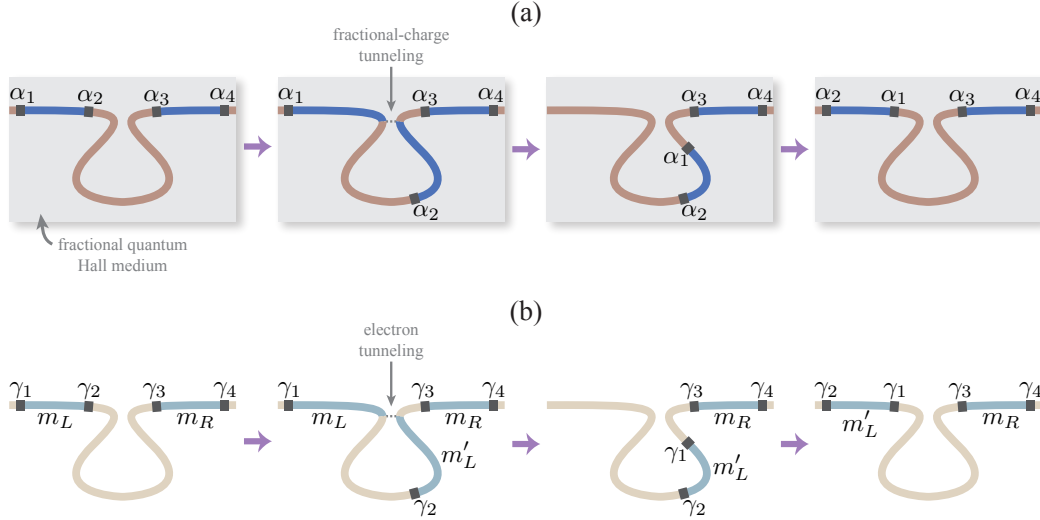
Figure 39: Sample braiding protocol in (a) a $\mathbb{Z}_4$ parafermion platform and (b) its electronic counterpart. In (a) $\mathbb{Z}_4$ parafermion zero modes $\alpha_{1,\dots,4}$ arise at line defects in a parent fractional-quantum-Hall medium. The sequence shown braids $\alpha_{1,2}$ (other braids proceed similarly). The electron equivalent in (b) hosts two strictly 1D topological superconductors with spontaneously chosen magnetizations $m_{L/R}$ and symmetry-enriched Majorana zero modes $\gamma_{1,\dots,4}$. Here the panels sketch a braid of $\gamma_{1,2}$—which is *not* described by parafermionic braid matrices. Differences in braiding properties can be traced to the second panels above: in (a) the dashed line represents a parafermion coupling that is non-local when mapped to fermions. Thus the Hamiltonian implementing parafermionic braid transformations is unphysical in the electronic realization. Braiding $\gamma_{1,2}$ does nevertheless allow for additional freedom compared to conventional Majorana platforms, since the initial and final magnetizations, m_L and m'_L, need not coincide.

[9] which is implemented by the unitary braid operator

$$U_{j,j+1} = \exp\left\{\frac{i\pi}{8}[2(e^{i\frac{\pi}{4}}\alpha_j^\dagger\alpha_{j+1} + H.c.) - i(\alpha_j^\dagger\alpha_{j+1})^2]\right\}. \tag{3.101}$$

The equivalent 1D electronic setup, sketched in Fig. 39(b), features a pair of topological superconductors each with spontaneous time-reversal symmetry breaking. The left superconductor hosts symmetry-enriched Majorana zero modes $\gamma_{1,2}$, magnetization $m_L = i\Gamma_1\Gamma_2$, and fermion parity $P_{\text{tot},L} = m_L(i\gamma_1\gamma_2)$; the right superconductor similarly hosts Majorana modes $\gamma_{3,4}$, magnetization $m_R = i\Gamma_3\Gamma_4$, and

---

[9]We focused on one particular chirality for the braid here. Moreover, in the more general case the operators could transform as $\alpha_j \to e^{-i\frac{\pi}{2}k}\alpha_{j+1}$, $\alpha_{j+1} \to e^{i\frac{\pi}{2}(1-k)}\alpha_j^\dagger\alpha_{j+1}^2$ for integer k [29, 65]. We have taken $k = 0$ for simplicity.

parity $P_{\text{tot},R} = m_R(i\gamma_3\gamma_4)$. In this realization, physical wavefunctions, i.e., non-Schrödinger-cat states with fixed global fermion parity, take the form

$$|\psi\rangle = a\,|m_L, P_{\text{tot},L}; m_R, P_{\text{tot},R}\rangle$$
$$+ b\,|m_L, -P_{\text{tot},L}; m_R, -P_{\text{tot},R}\rangle \tag{3.102}$$

for some complex a, b. Compared to the parafermion case, we now have eight states instead of four, since only global $\mathbb{Z}_4^2$ charge needs to be fixed, though the allowed superpositions are strongly restricted by the need to avoid cat states.

Braiding symmetry-enriched Majorana zero modes can induce rotations that are forbidden in conventional Majorana platforms yet still differ fundamentally from those in the parafermion realization. Consider adiabatically swapping $\gamma_{i,j}$ such that the instantaneous Hamiltonian $H(t)$ does not explicitly break time-reversal symmetry at any point during the exchange. The time-evolution operator implementing the braid is $U_{i,j}^{\text{elec}}(t_i, t_f) = T e^{i \int_{t_i}^{t_f} dt H(t)}$. Here T denotes time ordering, and we take $t_i = -\infty$ and $t_f = +\infty$ as appropriate for an adiabatic process. Applying time reversal yields $\mathcal{T}_{\text{elec}} U_{i,j}^{\text{elec}}(t_i, t_f) \mathcal{T}_{\text{elec}}^{-1} = [U_{i,j}^{\text{elec}}(t_f, t_i)]^{\dagger}$. On the right side, Hermitian conjugation reverses the braid chirality but so does swapping $t_i \leftrightarrow t_f$. These factors thus 'cancel', so that the braid operator satisfies

$$\mathcal{T}_{\text{elec}} U_{i,j}^{\text{elec}} \mathcal{T}_{\text{elec}}^{-1} = U_{i,j}^{\text{elec}} \;. \tag{3.103}$$

For a similar analysis see Ref. [38]. Equation (3.103) together with parity conservation allow us to infer the braiding properties of symmetry-enriched Majorana modes. All results below have been verified by explicit calculations similar to those in Ref. [29].

Figure 39(b) sketches an exchange of γ_1 and γ_2. The first step of the braid extends the left magnetized region into the lower loop. Crucially, the magnetization m_L' in the loop segment can either align or anti-align with the original magnetization m_L depending on details of the junction Hamiltonian. If $m_L' = m_L$ then the braid preserves the magnetization, and we obtain a standard Majorana exchange that acts as

$$U_{1,2}^{\text{elec}} \gamma_1 (U_{1,2}^{\text{elec}})^{\dagger} = -s\gamma_2, \quad U_{1,2}^{\text{elec}} \gamma_2 (U_{1,2}^{\text{elec}})^{\dagger} = s\gamma_1 \tag{3.104}$$

for some sign s [7, 28, 50]. As usual, the extra minus sign acquired by one of the Majorana operators is necessary to ensure conservation of parity $P_{\text{tot},L}$ for the left topological region. By applying time reversal to Eq. (3.104) using Table 35 and Eq. (3.103), one finds that the left and right sides are consistent only if s does not

depend on magnetization. Taking $s = +1$ for concreteness, the associated braid matrix then reads

$$U_{1,2}^{\text{elec}} = e^{\frac{\pi}{4}\gamma_1\gamma_2} \quad \text{(mag.-preserving braid)} . \tag{3.105}$$

If $m_L' = -m_L$ then the braid flips the magnetization. In this case conservation of $P_{\text{tot},L}$ dictates that the Majorana operators (written in our conventions) transform slightly differently from above:

$$U_{1,2}^{\text{elec}}\gamma_1(U_{1,2}^{\text{elec}})^\dagger = s'\gamma_2, \quad U_{1,2}^{\text{elec}}\gamma_2(U_{1,2}^{\text{elec}})^\dagger = s'\gamma_1 \tag{3.106}$$

with some sign s'. Consistency with time reversal now requires $s' = m_L$ (or $s' = -m_L$, but we focus on the former for simplicity). This transformation is implemented by

$$U_{1,2}^{\text{elec}} = \frac{1}{\sqrt{2}}(e^{-i\frac{\pi}{4}}\Gamma_1\gamma_1 + e^{i\frac{\pi}{4}}\Gamma_2\gamma_2) \quad \text{(mag.-flipping braid)} . \tag{3.107}$$

Note that in addition to transforming $\gamma_{1,2}$, $U_{1,2}^{\text{elec}}$ also sends $\Gamma_1 \to p\Gamma_2$ and $\Gamma_2 \to p\Gamma_1$, yielding the required magnetization flip $m_L \to -m_L$. We stress that Eq. (3.107) can not describe an adiabatic closed cycle in a Majorana system with explicit time-reversal symmetry breaking, for which the initial and final magnetizations would necessarily coincide.

Other braids can be analyzed similarly. The braid matrix $U_{3,4}^{\text{elec}}$ governing the exchange of γ_3 and γ_4 clearly conforms to a straightforward generalization of Eqs. (3.105) and (3.107). Swapping zero modes $\gamma_{2,3}$ that reside on different topological segments, however, naturally preserves both magnetizations. We find that consistency with time reversal yields

$$U_{2,3}^{\text{elec}} = \exp\left[\frac{\pi}{8}(1 + m_L - m_R + m_L m_R)\gamma_2\gamma_3\right] . \tag{3.108}$$

One can readily verify using Table 35 that Eqs. (3.105), (3.107), and (3.108) all satisfy Eq. (3.103).

To directly compare the parafermion and electronic braid matrices, we will now recast Eq. (3.101) in terms of Majorana operators γ_j and Γ_j using exact mappings that generalize Eqs. (3.69) and (3.70) to the case with four parafermion zero modes. Section 3.14 sketches this exercise. For $U_{1,2}$ we obtain

$$U_{1,2} = \exp\left\{\frac{i\pi}{4}\left[i(\gamma_2\Gamma_1 + \gamma_1\Gamma_2) - \frac{1}{2}P_{\text{tot},L}\right]\right\} , \tag{3.109}$$

which is clearly very different from $U_{1,2}^{\text{elec}}$. The first two pieces in the exponent swap local Majorana operators $\gamma_{1,2}$ with the non-local operators $\Gamma_{1,2}$; consequently, when acting on generic physical fermion wavefunctions $|\psi\rangle$, $U_{1,2}$ generates cat states that superpose $m_L = \pm 1$ configurations (see Section 3.14). A similar conclusion holds for $U_{3,4}$. For $U_{2,3}$ we find

$$U_{2,3} = \exp\left\{\frac{i\pi}{4}\left[(m_L + m_R)i\gamma_2\gamma_3 - \frac{1}{2}m_L m_R\right]\right\},\qquad(3.110)$$

which preserves the magnetizations and thus does not generate cat states. Nevertheless $U_{2,3}$ and $U_{2,3}^{\text{elec}}$ still differ qualitatively, and in fact the latter generates a finer protected rotation of the $\gamma_{2,3}$ zero-mode operators compared to the former.

The stark contrast between parafermion and electronic braid matrices seen here may appear surprising given that exact mappings bridge the two representations. This difference originates from the fact that the physical Hamiltonian governing the exchange in the parafermion realization becomes non-local when translated into fermion language. Specifically, the dashed line from Fig. 39(a), second panel, represents a coupling between parafermions at opposite edges of the loop, which microscopically arises from tunneling of fractional charge through the intervening quantum-Hall fluid. Mapping this term to spinful fermions generates an 'uncanceled' string across the entire loop below—yielding an unphysical process in this representation. Instead the analogous physical coupling in the electronic realization arises from ordinary electron tunneling (along with coupling between the magnetizations) across the upper part of the loop; see Fig. 39(b) [10].

The situation for fusion, property (*iii*), is different. Fusion brings two zero modes together, thereby intentionally removing any topologically protected degeneracies that arise when the zero modes are far apart. In the context of fusion properties, the distinction between the parafermion and electronic realizations is thus naturally blurred. Consider a parafermion platform and let X denote a domain-wall defect that binds a $\mathbb{Z}_4$ parafermion zero mode. These non-Abelian defects obey the fusion rule

$$X \times X \sim I + q_1 + q_2 + q_3\,,\qquad(3.111)$$

indicating that two defects can annihilate, corresponding to the identity fusion channel I, or form three different nontrivial quasiparticle types $q_{1,2,3}$. We will explore this fusion rule further by examining the setup from Fig. 310(a) that hybridizes the pair

---

[10]Our discussion here applies equally well to the braiding scheme proposed in Ref. [87] in the quantum-spin-Hall setting.

$\alpha_{1,2}$ as well as the pair $\alpha_{3,4}$. The figure indicates the bosonized perturbation gapping out each region; most importantly, the central domain is gapped by $-\cos(2\theta - \theta_0)$, where θ_0 represents a 'knob' that we will use to probe the parafermionic fusion characteristics.

In Section 3.15 we show that hybridization between $\alpha_{1,2}$ can be described by the Hamiltonian

$$H_{1,2} = -t \left[e^{i\frac{\pi-\theta_0}{4}} \alpha_1^\dagger \alpha_2 + H.c. \right] \tag{3.112}$$

for some real coupling t that we take to be postive (hybridization between $\alpha_{3,4}$ can be treated similarly). When $\theta_0 = 0$ $H_{1,2}$ admits a unique ground state with $e^{i\frac{\pi}{4}} \alpha_1^\dagger \alpha_2 = 1$, corresponding to the identity fusion channel in Eq. (3.111); excited states with $e^{i\frac{\pi}{4}} \alpha_1^\dagger \alpha_2 = \pm i, -1$ correspond to the three possible nontrivial quasiparticles $q_{1,2,3}$. Figure 310(b) plots the energy spectrum for $H_{1,2}$ as a function of θ_0. Crucially, all level crossings are protected by the (unbreakable) $\mathbb{Z}_4$ symmetry exhibited by the parafermion platform, thus strongly constraining the system's response to θ_0 sweeps. As an example, imagine starting from the ground state with $\theta_0 = 0$ and then adiabatically winding θ_0 by 2π. This cycle returns the Hamiltonian to its original form—which is clear from Fig. 310(a) [11]—but maps the ground state into an excited state. The system re-enters its ground state only after sweeping θ_0 by a total of 8π. This anomalous periodicity reflects the fact that *winding θ_0 cycles the system among the four possible fusion channels in Eq.* (3.111). The pumping cycle reviewed here is a cousin of the generalized fractional Josephson effect discussed for parafermions in fractional-quantum-Hall systems in Refs. [24, 25, 29, 65].

Below we will turn to the equivalent electronic setup and identify an analogous 8π-periodic pumping cycle that, remarkably, represents a purely 1D manifestation of nontrivial parafermionic fusion rules. We will also draw connections with closely related work in Refs. [87, 111] in the context of interacting quantum-spin-Hall edges, viewed from a new perspective in light of our mappings.

Imprint of parafermionic fusion rules in a 1D electron system

Figure 311(a) shows the strictly 1D electronic counterpart of the parafermion platform from Fig. 310(a). Recall that the outer segments gapped by $-\cos(2\theta)$ form trivial, $\mathcal{T}_{\text{elec}}$-invariant gapped phases that smoothly connect to the fermion vacuum. The central region gapped by $-\cos(2\theta - \theta_0)$ interpolates between a trivial phase (at

---

[11] Shifting θ_0 by 2π also returns the hybridization Hamiltonian $H_{1,2}$ to its original form, when followed by a gauge transformation $\alpha_2 \to i\alpha_2$. The key point is that $e^{i\frac{\pi}{4}} \alpha_1^\dagger \alpha_2$ is a conserved quantity; once fixed, the eigenvalue thus can not readjust to accommodate shifts in θ_0.

(a)

(b)
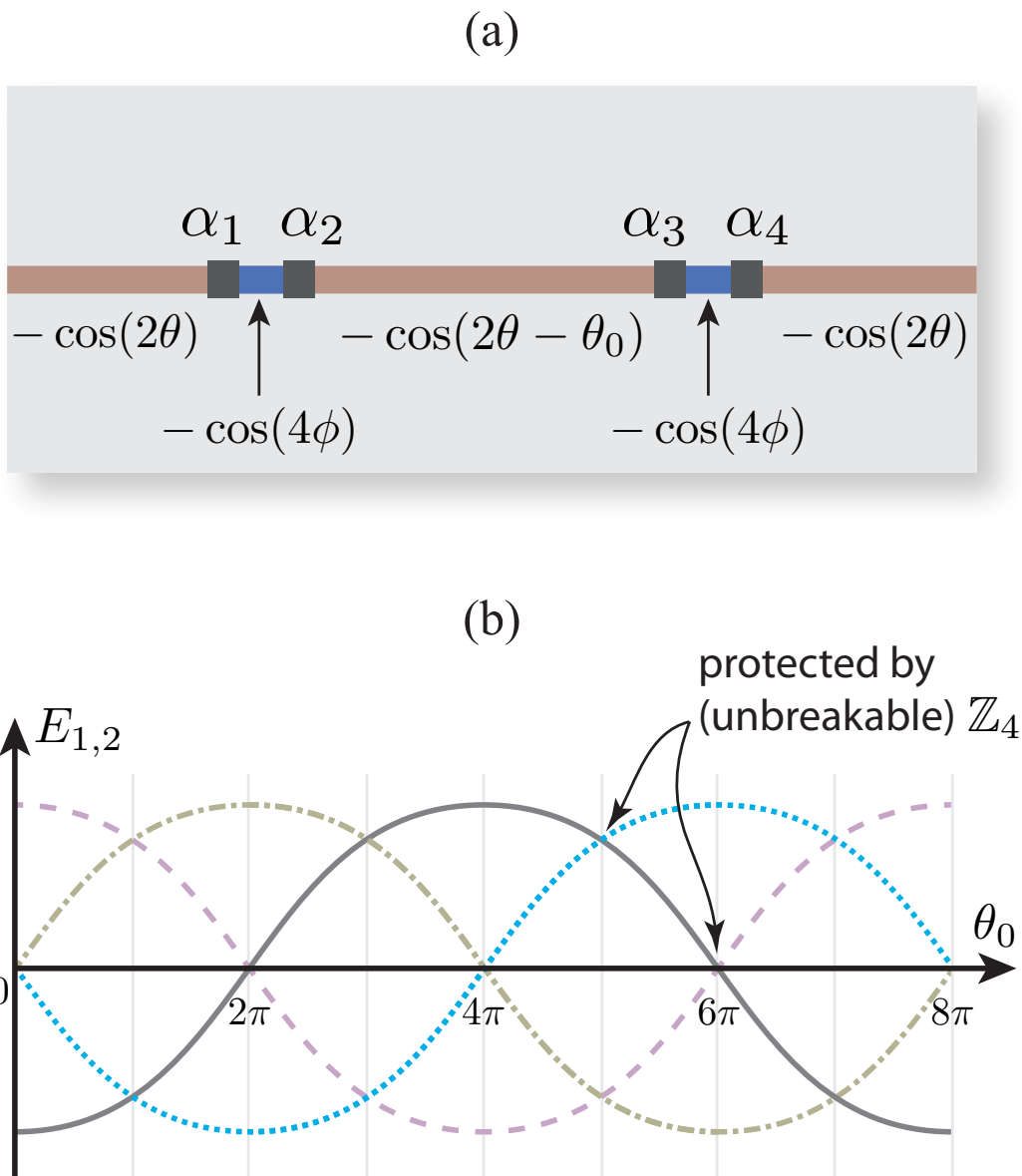
Figure 310: (a) Setup used for fusion in a $\mathbb{Z}_4$ parafermion platform. Parafermions α_1 and α_2 hybridize on the left, and similarly for α_3 and α_4 on the right. We label the bosonized perturbations gapping each region; note in particular the shift θ_0 in the central region, which modulates the parafermion couplings. (b) Energies $E_{1,2}$ for the hybridized parafermions $\alpha_{1,2}$ versus θ_0. All level crossings are protected by the parafermion platform's unbreakable $\mathbb{Z}_4$ symmetry. For a given θ_0 the different energy levels correspond to the four possible fusion channels for the non-Abelian defects binding the parafermions. Adiabatically winding θ_0 cycles the system among these four fusion channels, leading to an anomalous 8π-periodic response even though the underlying Hamiltonian is 2π periodic.
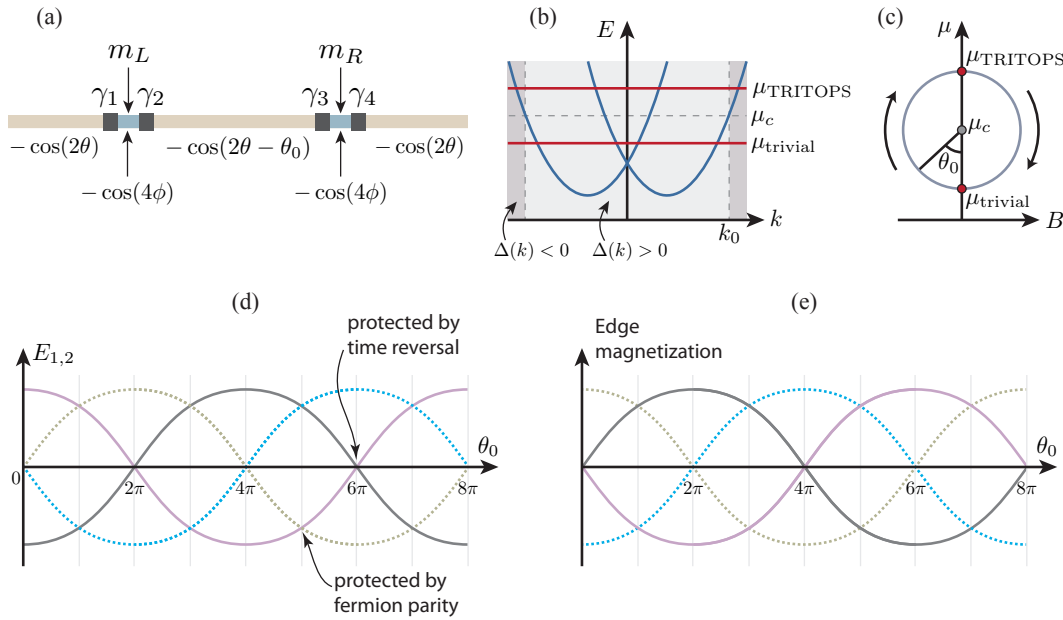
Figure 311: (a) Electronic counterpart of the fusion setup from Fig. 310(a). Outer regions form a trivial phase smoothly connected to the electron vacuum. The central region interpolates between a trivial phase at $\theta_0 = 0$ and TRITOPS phase at $\theta_0 = \pi$, and can be realized experimentally by a spin-orbit-coupled wire with an s-wave pair potential $\Delta(k)$ that changes sign at some momentum k_0. (b) Band structure for such a wire along with chemical potentials corresponding to trivial and TRITOPS phases. In this realization one can wind θ_0 by 2π by varying the chemical potential μ and an applied magnetic field B along the cycle shown in (c). Hybridization of the symmetry-enriched Majorana operators $\gamma_{1,2}$ and fluctuating quantum magnetization degree of freedom m_L yields the energy spectrum versus θ_0 sketched in (d). The levels are similar to those in the parafermion platform [Fig. 310(b)] except that crossings at $\theta_0 = \pi$ mod 2π are protected by fermion parity whereas those at $\theta_0 = 0$ mod 2π are protected by electronic time-reversal symmetry. Provided these crossings are maintained, the system inherits the parafermion platform's 8π-periodic pumping cycle—an imprint of nontrivial parafermionic fusion rules in our strictly 1D electron setting. The pumping cycle can be detected experimentally by measuring the magnetization at the edge, which as (e) illustrates is also 8π periodic. Magnetization for a given curve in (d) is shown with the same line type in (e).

$\theta_0 = 0$) and a $\mathcal{T}_{\text{elec}}$-invariant TRITOPS phase (at $\theta_0 = \pi$) via a path that explicitly breaks $\mathcal{T}_{\text{elec}}$. For a practical implementation of this region, we envision a spin-orbit-coupled wire with a momentum-dependent s-wave pairing potential that changes sign at some momentum k_0. As Fig. 311(b) illustrates, trivial and TRITOPS phases arise depending on whether the outer Fermi momentum is smaller or larger than k_0 [42, 84, 93, 107, 112]. One can, moreover, smoothly tune between these phases by varying the chemical potential μ and a $\mathcal{T}_{\text{elec}}$-breaking magnetic field B along the path shown in Fig. 311(c)—which in bosonized language winds θ_0 by 2π. Note that the B field generically induces both a Zeeman term *and* an imaginary component to the s-wave pair potential, thus preempting a phase transition.

The 'small' adjacent $-\cos(4\phi)$ regions in Fig. 311(a) exhibit magnetizations that now form fluctuating quantum degrees of freedom. Consequently, the Majorana operators Γ_j that we used to decompose the magnetizations become physical operators that can appear in the Hamiltonian, in addition to the symmetry-enriched Majorana operators γ_j. Focusing on the left region, we describe hybridization of these operators by an effective Hamiltonian

$$H_{1,2}^{\text{elec}} = H_t + H_{\mathbb{Z}_4\text{-breaking}} . \tag{3.113}$$

The first term,

$$H_t = -t\left[\cos\left(\frac{\theta_0}{4}\right) i(\gamma_1\Gamma_2 + \gamma_2\Gamma_1) - \sin\left(\frac{\theta_0}{4}\right) i(\gamma_1\Gamma_1 + \gamma_2\Gamma_2)\right], \tag{3.114}$$

represents Eq. (3.112) rewritten in terms of fermions using Eqs. (3.69) and (3.70). At both $\theta_0 = 0$ and $\theta_0 = \pi$, H_t preserves $\mathcal{T}_{\text{elec}}$ symmetry [12]. The second term, $H_{\mathbb{Z}_4\text{-breaking}}$, encodes additional allowed couplings that violate $\mathbb{Z}_4$ symmetry and hence are unphysical in the parafermion context; we assume that this piece also preserves $\mathcal{T}_{\text{elec}}$ at $\theta_0 = 0$. For any θ_0 the Hamiltonian commutes with $P_{\text{tot},L} = (i\gamma_1\gamma_2)(i\Gamma_1\Gamma_2)$.

Suppose for now that $H_{\mathbb{Z}_4\text{-breaking}} = 0$. Figure 311(d) sketches the resulting energies $E_{1,2}$ versus θ_0; solid and dashed curves respectively correspond to states with $P_{\text{tot},L} = +1$ and -1. By construction the energies are identical to those in Fig. 310(b), though the nature of the eigenstates changes. At $\theta_0 = 0$, H_t energy eigenstates have $i\gamma_1\Gamma_2 = \pm1$ and $i\gamma_2\Gamma_1 = \pm1$. The many-body spectrum correspondingly features

---

[12]At $\theta_0 = 0$ the Majorana operators transform under $\mathcal{T}_{\text{elec}}$ precisely as in Table 35 from Sec. 3.3. At $\theta_0 = \pi$, however, the domain configuration differs from that analyzed in Sec. 3.3, so here one obtains the modified transformations $\gamma_1 \to m\gamma_1$, $\gamma_2 \to -m\gamma_2$, $\Gamma_1 \to -p\Gamma_2$, and $\Gamma_2 \to p\Gamma_1$ under $\mathcal{T}_{\text{elec}}$.

non-degenerate states with energies $\pm 2t$ along with a degenerate Kramers doublet of states at zero energy. Increasing θ_0 breaks $\mathcal{T}_{\text{elec}}$ and eliminates the degeneracy until time-reversal symmetry is revived at $\theta_0 = \pi$. To understand the $\theta_0 = \pi$ spectrum it is convenient to employ a rotated basis $\gamma_\pm = (\gamma_1 \pm \gamma_2)/\sqrt{2}$ and $\Gamma_\pm = (\Gamma_1 \pm \Gamma_2)/\sqrt{2}$. The t term then becomes

$$H_t(\theta_0 = \pi) = \sqrt{2} ti\gamma_-\Gamma_- . \tag{3.115}$$

Notice that $i\gamma_+\Gamma_+$—which is odd under $\mathcal{T}_{\text{elec}}$—does not appear in the Hamiltonian, i.e., the system supports a fermionic zero mode corresponding to the hallmark Majorana Kramers pair for a TRITOPS phase [13]. The many-body spectrum thus contains levels at $\pm\sqrt{2}t$, each with two degenerate states carrying opposite fermion parity. Further increasing θ_0 to 2π yields a spectrum identical to that at $\theta_0 = 0$, except with the $P_{\text{tot},L}$ eigenvalues reversed.

As a technical aside, the opposite $P_{\text{tot},L}$ eigenvalues at $\theta_0 = 0$ and 2π may seem surprising. Clearly the bosonized Hamiltonian is identical at $\theta_0 = 0$ and 2π, so the energies and eigenstates must also be identical at these points. The resolution is that in our conventions the bosonized fermion-parity operator $e^{i\int_x \partial_x\theta}$ across the left $-\cos(4\phi)$ region projects to $P_{\text{tot},L}$ at $\theta_0 = 0$ but $-P_{\text{tot},L}$ at $\theta_0 = 2\pi$ [14]; thus opposite $P_{\text{tot},L}$ eigenvalues are actually required. The virtue of this convention is that tracking the evolution of states in response to θ_0 sweeps becomes particularly transparent.

Turning on $H_{\mathbb{Z}_4\text{-breaking}} \neq 0$ of course non-universally modifies the energies in Fig. 311(d). Nevertheless, the level crossings at $\theta_0 = 0 \mod 2\pi$ remain protected by $\mathcal{T}_{\text{elec}}$, whereas the crossings at $\theta_0 = \pi \mod 2\pi$ are unbreakable due to fermion-parity protection. (Breaking $\mathcal{T}_{\text{elec}}$ can only shift the the latter degeneracy points to different θ_0 values but can not turn them into avoided crossings.) Consequently, despite the obliteration of $\mathbb{Z}_4$ symmetry, our 1D electronic system inherits the parafermion platform's anomalous 8π-periodic pumping cycle, so long as $\mathcal{T}_{\text{elec}}$ is preserved at $\theta_0 = 0 \mod 2\pi$.

We can understand the pumping process physically as follows. Suppose the system starts in its unique ground state at $\theta_0 = 0$. Due to conservation of $P_{\text{tot},L}$, adiabatically

---

[13] While it is illuminating to describe the Majorana Kramers pair using our effective Hamiltonian that couples γ_i and Γ_i, its existence more fundamentally arises from the TRITOPS state. That is, the 'small' $-\cos(4\phi)$ region functions as a quantum dot that houses the Majorana Kramers pair that is guaranteed to exist due to the adjacent TRITOPS region.

[14] For an explicit example, at either $\theta_0 = 0$ or 2π, the ground state is unique and must have θ pinned to the same value on both sides of the 'small' $-\cos(4\phi)$ region (twists in θ cost energy in such geometries). Thus ground-state projection yields $e^{i\int_x \partial_x\theta} \to 1$. From Eq. (3.114), however, one can readily see that $P_{\text{tot},L} = (i\gamma_1\gamma_2)(i\Gamma_1\Gamma_2)$ projects to $+1$ at $\theta_0 = 0$ but -1 at $\theta_0 = 2\pi$.

winding θ_0 to 2π necessarily evolves the system to an excited state in which the fermion parity in the left $-\cos(4\phi)$ region has flipped (recall the relation between fermion parity and $P_{\text{tot},L}$ noted above). That is, the $0 \to 2\pi$ sweep pumps a fermion between the left and right $-\cos(4\phi)$ regions, producing a state that generically exhibits a non-zero magnetization even though the ending Hamiltonian preserves $\mathcal{T}_{\text{elec}}$. Subsequently sweeping θ_0 from 2π to 4π restores the original fermion parities. Time-reversal symmetry, however, now prevents the system from returning to the ground state. Restoring the ground state requires winding θ_0 by a total of 8π. One can experimentally probe this anomalous pumping cycle by measuring the magnetization at the edge of the wire, which exhibits the same 8π periodicity. Figure 311(e) sketches possible magnetization curves colored according to the corresponding branch in Fig. 311(d). Note that dispensing with $\mathcal{T}_{\text{elec}}$ still yields a nontrivial 4π-periodic cycle; in this case the pumping process becomes very similar to that introduced in Ref. [57] (see also Ref. [15]).

The specific electronic setup examined so far makes the connection to parafermions explicit and also allows one to capture the 8π-periodic pumping cycle within a very simple effective Hamiltonian. However, the requirements for implementing the cycle in practice can be distilled into a few basic ingredients shared by a much broader class of superconducting systems:

- A generic family of electron Hamiltonians $H(\theta_0)$, where θ_0 is an adiabatic parameter such that $H(\theta_0 + 2\pi) = H(\theta_0)$. By 'generic' we mean that $H(\theta_0)$ should contain no accidental degeneracies.

- $H(\theta_0)$ describes a phase that preserves electronic time-reversal symmetry if and only if $\theta_0 = 0 \mod \pi$. At these θ_0 points time reversal guarantees Kramers degeneracy for states with odd electron number.

- A single fermion zero mode—or equivalently, a pair of Majorana zero modes— at each end of the system when $\theta_0 = \pi \mod 2\pi$. Due to time-reversal invariance at this point, the zero mode must be anomalous.

- A set of four many-body sub-gap states whose evolution is constrained by the first three items above. These sub-gap states must be separated from the continuum for any value of θ_0 so that an adiabatic pumping cycle is well-defined.

(Once these items are satisfied, one can actually break time-reversal symmetry at $\theta_0 = \pi \mod 2\pi$ without spoiling the 8π periodicity, consistent with the preceding discussion.) Perhaps most importantly, the 'small' $-\cos(4\phi)$ regions [Fig. 311(a)] bordering our spin-orbit-coupled wire are inessential. Any source of sub-gap states—e.g., band bending at the edges—can satisfy the last item in this list. In this modified picture, the symmetry-enriched Majorana modes and fluctuating magnetization degree of freedom are simply adiabatically deformed into a pair of fermions encoding those sub-gap states. Further intuition can be gained by comparing with the more familiar 4π-periodic fractional Josephson effect [58] arising in junctions formed by a pair of topological superconductors with explicitly broken time-reversal symmetry. There, the nontrivial 4π-periodic cycle is conveniently understood as arising from Majorana modes that hybridize across a finite-width barrier in the junction; the effect survives equally well, however, if the barrier width shrinks to zero—so long as a sub-gap localized state persists. The latter sub-gap state is continuously connected to the hybridized Majorana modes in the finite-barrier situation, just as the sub-gap states in our problem are connected to the symmetry-enriched Majorana modes and magnetization degree of freedom.

References [87, 111] introduced a quite different platform satisfying the above properties, namely a Josephson junction realized at a quantum-spin-Hall edge. The quantum-spin-Hall setup is described by the same bosonized perturbations from Fig. 311(a), but with $\theta \leftrightarrow \phi$ (in the notation of Ref. [111]) and the adiabatic parameter θ_0 replaced by the superconducting-phase difference $\Delta\varphi$ across the junction. The $\cos(4\theta)$ terms in the barrier regions of the Josephson junction reflect two-particle backscattering; when relevant, these perturbations catalyze spontaneous time-reversal symmetry breaking with a magnetization order parameter $\cos(2\theta)$— very similar to the order parameter in our problem. Electronic time-reversal symmetry is present at $\Delta\varphi = 0$ and π, and at the latter value the barrier binds a single fermionic zero mode. Moreover, the necessary sub-gap levels can arise from Andreev bound states in a 'wide' junction. These properties, in conjunction with arbitrarily weak interactions, conspire to yield an 8π-periodic Josephson current.

Figure 312 summarizes the relation between our strictly 1D realization and the analogous quantum-spin-Hall setup. In the latter setting, the anomalous Josephson effect can also be naturally viewed as arising from hybridization of symmetry-enriched Majorana modes with a quantum magnetization degree of freedom— similar to Refs. [46, 90, 105] which analyzed the junction coupled to an impurity
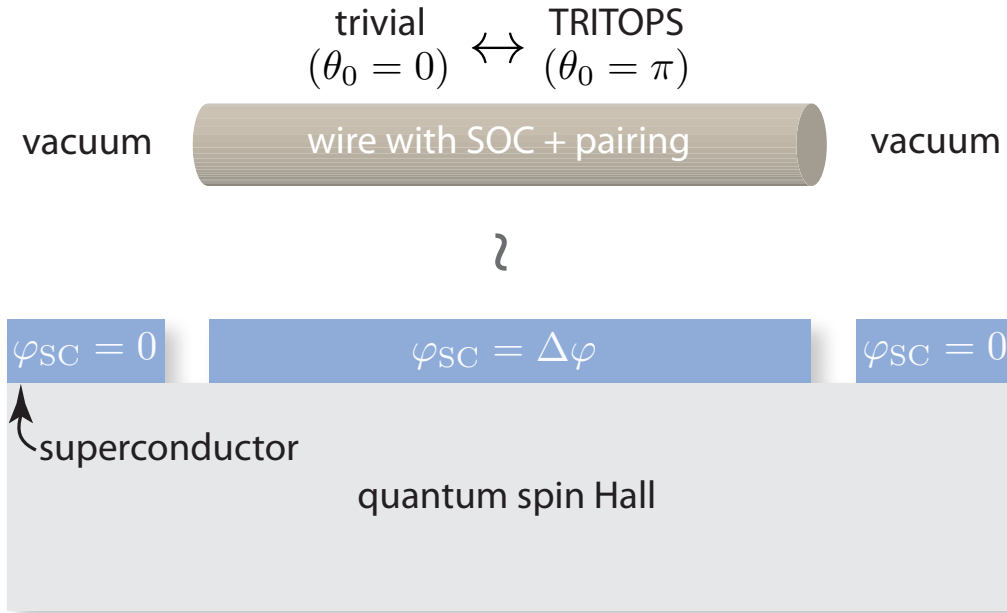
Figure 312: Connection between our strictly 1D electronic system (top) and a quantum-spin-Hall Josephson junction (bottom). The outer vacuum regions in the 1D setting correspond to segments of the Josephson junction with superconducting phase $\varphi_{SC} = 0$. The wire with spin-orbit-coupling (SOC) and momentum-dependent s-wave pairing corresponds to the central part of the junction with phase $\varphi_{SC} = \Delta\varphi$. Varying the adiabatic parameter θ_0 in the 1D system yields an 8π-periodic edge magnetization, while varying $\Delta\varphi$ yields an 8π-periodic Josephson current.

spin. Our exact mappings clarify the precise connection between these electronic setups and a system hosting bona fide $\mathbb{Z}_4$ parafermions: the hybridized sub-gap states mediating the anomalous pumping cycles are in one-to-one correspondence with fusion channels of non-Abelian defects binding $\mathbb{Z}_4$ parafermion zero modes. Given our general discussion in Sec. 3.4, which applies equally well to the strict 1D and quantum-spin-Hall platforms, we expect that this is the maximal extent to which non-fractionalized electron systems inherit non-Abelian $\mathbb{Z}_4$-parafermion physics.

We conclude this section with a discussion of the alternative fusion setup shown in Fig. 313. Compared to our previous setups, the $\cos(2\theta)$ and $\cos(4\phi)$ regions have essentially swapped roles. Note especially that the central domain in the figure is gapped by $-\cos(4\phi - \phi_0)$, where ϕ_0 is the control parameter that we wish to vary. For the parafermion realization in Fig. 313(a), Section 3.15 shows that parafermions
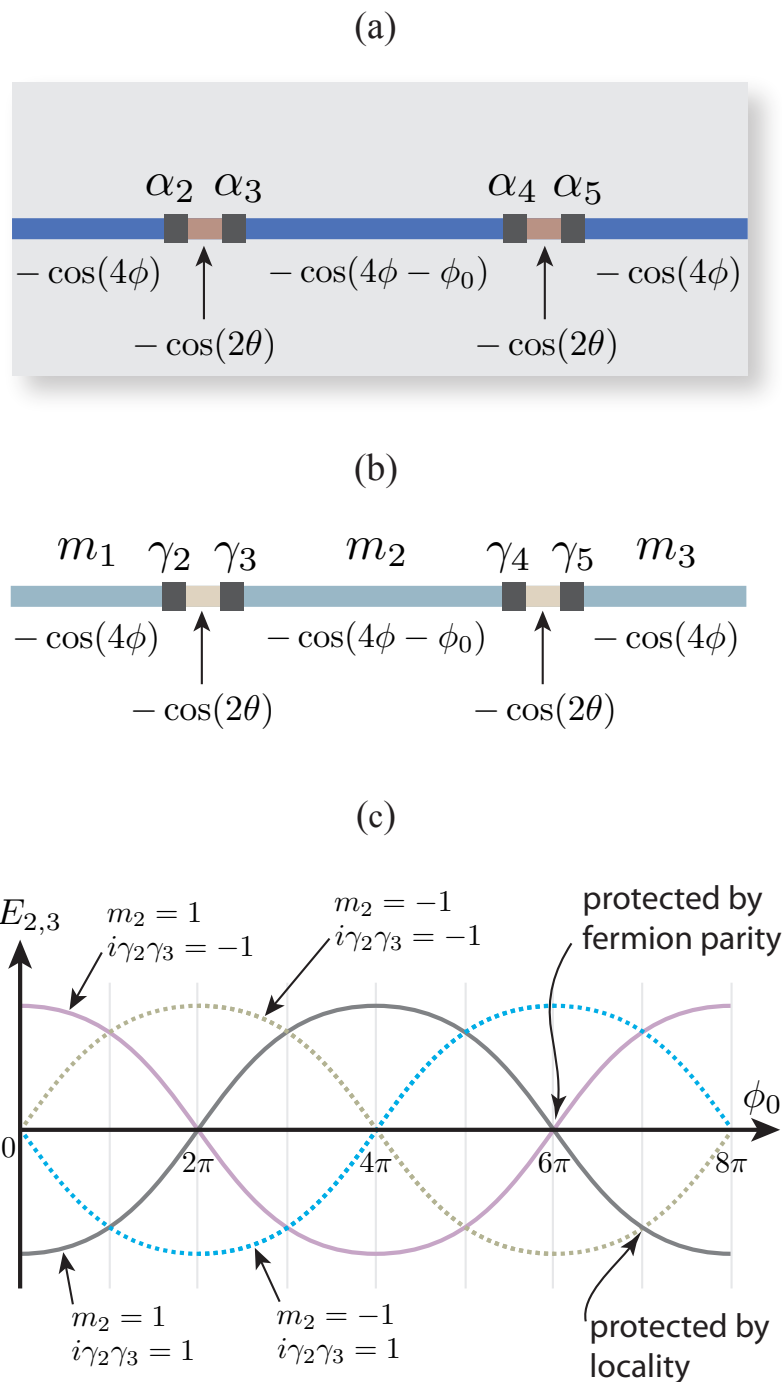
Figure 313: Variation of Figs. 310(a) and 311(a) for (a) a parafermion platform and (b) the corresponding electron system. Here a pumping process is carried out by varying the parameter ϕ_0 in the interactions governing the central region. In (b), $m_{1,2,3}$ denote spontaneously chosen magnetizations for the adjacent domains. (c) Energy spectrum describing hybridization of symmetry-enriched Majorana modes $\gamma_{2,3}$ at the left junction in (b), assuming fixed $m_1 = +1$. All level crossings are protected by either locality or fermion-parity considerations. The electronic system therefore exhibits an anomalous 8π-periodic response to ϕ_0 even when all symmetries are abandoned.

$\alpha_{2,3}$ at the left junction hybridize according to

$$H_{2,3} = -t \left[e^{i\frac{\pi+\phi_0}{4}} \alpha_2^\dagger \alpha_3 + H.c. \right],$$ (3.116)

which takes a nearly identical form to Eq. (3.112). Modulating ϕ_0 thus also cycles the system among the four possible fusion channels in Eq. (3.111), in turn generating a robust 8π-periodic response even though the microscopic Hamiltonian is 2π periodic. Fusing parafermions across regions gapped by $\cos(4\phi)$ versus $\cos(2\theta)$ evidently makes little difference.

The electronic realization in Fig. 313(b) nevertheless differs starkly from Fig. 311(a) because pairs of symmetry-enriched Majorana modes now hybridize across *trivial* domains. The outer regions gapped by $-\cos(4\phi)$ exhibit spontaneously chosen magnetizations m_1 and m_3 determined by $\langle\cos(2\phi)\rangle = \pm 1$, while the central region gapped by $-\cos(4\phi - \phi_0)$ exhibits a magnetization

$$m_2 = \langle\cos(2\phi - \phi_0/2)\rangle = \pm 1$$ (3.117)

whose microscopic meaning evolves with ϕ_0. For example, m_2 corresponds to a magnetization along x at $\phi_0 = 0$ but along y at $\phi_0 = \pi$; see Eqs. (3.61) and (3.80).

Converting $H_{2,3}$ into fermionic language using the dictionary from Section 3.14 yields [15],

$$H_{2,3} = -t \left[(m_1 + m_2) \cos\left(\frac{\phi_0}{4}\right) + (1 - m_1 m_2) \sin\left(\frac{\phi_0}{4}\right) \right] i\gamma_2 \gamma_3 .$$ (3.118)

For simplicity let us fix the magnetization in the leftmost region to $m_1 = +1$. Figure 313(c) sketches the energy levels $E_{2,3}$ versus ϕ_0 for the four remaining sectors labeled by $m_2 = \pm 1$ and $i\gamma_2\gamma_3 = \pm 1$. The level crossings at $\phi_0 = 0 \mod 2\pi$ arise from states with opposite fermion parity and are therefore protected. Furthermore, the crossings at $\phi_0 = \pi \mod 2\pi$ arise from macroscopically distinct states carrying opposite m_2 magnetizations, and can not be lifted by virtue of locality. Thus all level crossings are protected, implying that the electronic system *automatically* inherits the parafermion platform's 8π-periodic response without any symmetry enforcement required (as long as the microscopic Hamiltonian remains invariant under $\phi_0 \to \phi_0 + 2\pi$). An alternative way of viewing the resilience of the 8π periodicity is to observe that m_1, m_2, and $i\gamma_2\gamma_3$ are conserved quantities in $H_{2,3}$,

---

[15]Despite appearances, the hybridization Hamiltonian $H_{2,3}$ is also 2π periodic in ϕ_0, both in the parafermionic and fermionic representations. In the fermionic case, the periodicity reflects the fact that sending $\phi_0 \to \phi_0 + 2\pi$ shifts $m_2 \to -m_2$ and $\gamma_3 \to m_2\gamma_3$.

and must remain so even in the presence of arbitrary physical perturbations: The magnetization-flipping operators Γ_j are non-local in the present setting, and there are no other sources of low-energy fermions that can flip $i\gamma_2\gamma_3$. Spoiling the 8π periodicity requires shrinking the magnetized domains so that the order parameters become fluctuating quantum degrees of freedom and additional Majorana operators can provide a mechanism for fermion-parity switching.

The 8π-periodic cycle proceeds as follows: Start from the unique ground state at $\phi_0 = 0$. Winding ϕ_0 by 4π rotates the central domain's magnetization by a full 2π around the z axis [recall Eq. (3.117) and the comments just below], but also pumps a fermion to the junction—yielding an excited state. One must wind ϕ_0 by 4π a second time to recover the original ground state. The absolute robustness of this process is not without a price: implementing the cycle requires strong correlation together with interactions that can be tuned to twist ϕ_0.

Reference [89] examined a somewhat similar setup consisting of a Josephson junction formed by topological superconductors with spontaneous time-reversal symmetry breaking. These authors predicted an 8π-periodic Josephson effect protected by time-reversal symmetry. We would like to point out, however, that *within a fixed order-parameter sector*, time reversal does not protect level crossings in the spectrum. We expect that in such systems anomalous periodicity should either be protected by a symmetry that is present within a given order-parameter sector, or enjoy absolute protection due to locality constraints as found above.

3.5 Extension to higher parafermions

Our results for the $\mathbb{Z}_4$ case can be efficiently extended to arbitrary $\mathbb{Z}_{2M}$ parafermions, where M is any positive integer. In this section we outline a general fermionization scheme, then posit models that capture analogues of the four types of phases summarized in Fig. 34, and finally develop anomalous pumping cycles that reveal nontrivial fusion properties for higher parafermions.

Fermionization procedure

It is useful to introduce bosonic $\mathbb{Z}_{2M}$ clock variables σ_a, τ_a as an intermediary between parafermions and fermions. These unitary operators are now taken to satisfy

$$\sigma_a^{2M} = \tau_a^{2M} = 1, \quad \sigma_a\tau_a = e^{i\frac{\pi}{M}}\tau_a\sigma_a . \tag{3.119}$$

We will consider a $\mathbb{Z}_{2M}$ symmetry that sends

$$\sigma_a \to e^{i\frac{\pi}{M}}\sigma_a, \qquad \tau_a \to \tau_a \tag{3.120}$$

along with $\mathcal{T}$ and C symmetries that act exactly as in Eqs. (3.5) and (3.6). These clock variables can be nonlocally combined to form unitary $\mathbb{Z}_{2M}$ parafermion operators

$$\alpha_{2a-1} = \sigma_a\mu_{a-\frac{1}{2}}, \qquad \alpha_{2a} = e^{-i\frac{\pi}{2M}}\sigma_a\mu_{a+\frac{1}{2}}, \tag{3.121}$$

where $\mu_{a+\frac{1}{2}} = \prod_{b<a+\frac{1}{2}} \tau_b$ as before. These parafermions obey

$$\alpha_a^{2M} = 1, \qquad \alpha_a\alpha_{b>a} = e^{i\frac{\pi}{M}}\alpha_b\alpha_a. \tag{3.122}$$

Next, we would like to relate $\mathbb{Z}_{2M}$ clock variables to fermions. In analogy with Sec. 3.2, fermion anticommutation at long separation can be obtained by binding σ to the Mth power of the string μ, but the local structure requires some additional work. Each clock site now hosts a $2M$-dimensional Hilbert space. For $\mathbb{Z}_4$, the dimension matches that for two species of fermions, facilitating a complete fermionization of the clock operators as carried out in Sec. 3.2. A similar matching occurs when $M = 2^{k-1}$ (k is an integer), which in principle allows a complete fermionization into k species of fermions. At other M values, however, this relation breaks down.

To cover all M's in one formalism, we will thus follow a variant of the route adopted for the $\mathbb{Z}_4$ case in Sec. 3.3. In particular, there we utilized an explicit separation into a fermionic sector (described by a single species c_a) coupled to a $\mathbb{Z}_2$ magnetization order parameter $m_a = e^{i\pi d_a^\dagger d_a} = \sigma_a^2$. When generalizing to the $\mathbb{Z}_{2M}$ case, we will again employ a single fermion species C_a, but promote the magnetization m_a to a unitary $\mathbb{Z}_M$ order parameter $O_a = \sigma_a^2$ whose eigenvalues are cycled by a conjugate unitary operator $\mathcal{D}_a$, i.e.,

$$O_a^M = \mathcal{D}_a^M = 1, \qquad O_a\mathcal{D}_a = e^{i\frac{2\pi}{M}}\mathcal{D}_a O_a. \tag{3.123}$$

In this way the clock-spin Hilbert-space dimension is faithfully recovered for all M. The explicit mapping to these variables follows from

$$\sigma_a = B_a + O_a B_a^\dagger, \tag{3.124}$$

$$\tau_a = e^{i\frac{\pi}{M}B_a^\dagger B_a}\mathcal{D}_a, \tag{3.125}$$

where B_a are hard-core bosons that commute with $O_a, \mathcal{D}_a$. One can readily verify that the decomposition above preserves the properties in Eq. (3.119). Finally, we introduce spinless fermions via

$$C_a \equiv B_a e^{i\pi \sum_{b<a} B_b^\dagger B_b} = B_a \prod_{b<a} \tau_b^M. \tag{3.126}$$

	$\mathbb{Z}_{2M}$	C	$\mathcal{T}$
$\sigma \rightarrow$	$e^{i\frac{\pi}{M}}\sigma$	$\sigma^\dagger$	$\sigma^\dagger$
$\tau \rightarrow$	τ	$\tau^\dagger$	τ
$B \rightarrow$	$e^{i\frac{\pi}{M}}B$	$BO^\dagger$	$BO^\dagger$
$O \rightarrow$	$e^{i\frac{2\pi}{M}}O$	$O^\dagger$	$O^\dagger$
$\mathcal{D} \rightarrow$	$\mathcal{D}$	$\mathcal{D}^\dagger e^{-i\frac{2\pi}{M}C^\dagger C}$	$\mathcal{D}e^{i\frac{2\pi}{M}C^\dagger C}$
$C \rightarrow$	$e^{i\frac{\pi}{M}}C$	$CO^\dagger$	$CO^\dagger$

Table 37: Transformation properties for $\mathbb{Z}_{2M}$ clock variables and the operators used to decompose them through Eqs. (3.124), (3.125), and (3.126).

The order parameter O_a can also be rewritten in terms of fermions, as in the case for Z_4 parafermions, though if M is not a power of 2 we will need to project out the excess states in the Hilbert space.

Section 3.16 inverts Eqs. (3.124) and (3.125) and, in the special case of $\mathbb{Z}_4$, relates the operators above to the c_a and d_a fermions used in Sec. 3.3; specifically, we show that

$$\mathcal{D}_a = (d_a + d_a^\dagger)(c_a^\dagger - c_a), \tag{3.127}$$

$$C_a = \frac{1 - m_a}{2}c_a + \frac{1 + m_a}{2}c_a^\dagger. \tag{3.128}$$

Table 37 enumerates the symmetry properties for the original clock variables along with operators defined in Eqs. (3.124) through (3.126). From the table one sees that in the fermionic representation, $(\mathbb{Z}_{2M})^M$ is the $\mathbb{Z}_2$ symmetry associated with conservation of global fermion parity. We also observe that the composite anti-unitary symmetry $\mathcal{T}' \equiv \mathbb{Z}_{2M}\mathcal{T}$ is a generalization of electronic time-reversal symmetry for which $(\mathcal{T}')^2$ has eigenvalues $e^{i\frac{2\pi}{M}l}$ (l is an integer).

With this general fermionization algorithm in hand, we will now explore the correspondence between various phases in the clock, parafermion, and fermion representations. It is worth keeping in mind, however, that many different fermionization schemes are possible as alluded to above and will generally yield different fermionic phases from what we describe below; pursuing such alternative representations is certainly interesting but left to future work.

Paramagnetic and ferromagnetic phases

It is simplest to first examine the $\mathbb{Z}_{2M}$ clock model

$$H = -J \sum_{a=1}^{N-1} (\sigma_a^\dagger \sigma_{a+1} + H.c.) - f \sum_{a=1}^{N} (\tau_a + H.c.) . \qquad (3.129)$$

The $J = 0$ and $f = 0$ limits provide trivially solvable realizations of the non-degenerate paramagnetic state and $2M$-fold degenerate ferromagnetic phase, respectively. In terms of $\mathbb{Z}_{2M}$ parafermions H becomes [34]

$$H = -J \sum_{a=1}^{N-1} (e^{i\frac{\pi}{2M}} \alpha_{2a}^\dagger \alpha_{2a+1} + H.c.) - f \sum_{a=1}^{N} (e^{i\frac{\pi}{2M}} \alpha_{2a-1}^\dagger \alpha_{2a} + H.c.) . \qquad (3.130)$$

At $J = 0$ all parafermions dimerize yielding a unique ground state; at $f = 0$ the parafermions form a topological phase with unpaired parafermion zero modes that encode a robust degeneracy consisting of $2M$ locally indistinguishable states.

The fermionized Hamiltonian reads

$$\begin{aligned} H = &-J \sum_{a=1}^{N-1} [(C_a^\dagger - O_a^\dagger C_a)(C_{a+1} + O_{a+1}C_{a+1}^\dagger) + H.c.] \\ &- f \sum_{a=1}^{N} (e^{i\frac{\pi}{M}C_a^\dagger C_a} \mathcal{D}_a + H.c.) . \end{aligned} \qquad (3.131)$$

In the $J = 0$ limit, the ground state has $\mathcal{D}_a = 1$ and $C_a^\dagger C_a = 0$ for all sites. Hence, the trivial parafermion phase corresponds to the fermionic vacuum with a vanishing order parameter $\langle O_a \rangle = 0$. The $f = 0$ Hamiltonian closely resembles Eq. (3.60), though recall that the c_a and C_a fermions do not coincide at $M = 2$. Here the energy is minimized by uniformly condensing the order parameter, i.e., taking $\langle O_a \rangle = e^{i\frac{2\pi}{M}n}$ for some arbitrary integer n. The fermions then enter a topological phase with symmetry-enriched Majorana end states whose wavefunctions again depend on the precise order-parameter configuration. Just like the $\mathbb{Z}_4$ case, topological degeneracy encoded by parafermion zero modes becomes a mixture of 2-fold topological degeneracy and M-fold symmetry-breaking degeneracy.

We can also appeal to a long-wavelength approach to recover these phases, following a straightforward generalization of Sec. 3.3. Using bosonized variables ϕ, θ that satisfy the commutator in Eq. (3.45), clock order and disorder operators can now be expanded as $\sigma \sim e^{i\phi}, \mu \sim e^{-i\theta/M}$. Inserting these expansions into Eqs. (3.121) and (3.126) yields $\alpha \sim e^{i(\phi - \theta/M)}$ for long-wavelength parafermions and $\psi_{R/L} \sim e^{i(\phi \pm \theta)}$

for long-wavelength fermions. The bosonized Hamiltonian takes the form

$$\mathcal{H} = \int_x \left\{ \frac{v}{2\pi} [g(\partial_x \phi)^2 + g^{-1}(\partial_x \theta)^2] - \kappa_1 \cos(2M\phi) - \kappa_2 \cos(2\theta) \right\} . \qquad (3.132)$$

Relevant $\kappa_1 > 0$ and $\kappa_2 > 0$ couplings respectively generate the ferromagnetic and paramagnetic phases in clock language. Next we turn to the phases stabilized by relevant couplings of the opposite sign, which are generalizations of the canted and SPT phases explored previously for the $\mathbb{Z}_4$ case.

Canted and SPT phases

The canted-ferromagnet phase discussed in Sec. 3.3 generalizes to a state with $\langle \sigma_a \rangle \sim e^{i\frac{\pi}{M}(k+\frac{1}{2})}$ for integer k, i.e., the clock spins orient 'halfway' between adjacent σ_a eigenvalues. We construct trial wavefunctions that exhibit this ordering as

$$|e^{i\frac{\pi}{M}(k+\frac{1}{2})}\rangle = \prod_a \frac{1 + \tau_a}{\sqrt{2}} |\sigma = e^{i\frac{\pi}{M}k}, e^{i\frac{\pi}{M}k}, \ldots \rangle . \qquad (3.133)$$

These states contain no $\tau = -1$ components; moreover, all nearest-neighbor bonds involve only configurations with $\sigma_a^\dagger \sigma_{a+1} = 1, e^{i\frac{\pi}{M}}$, or $e^{-i\frac{\pi}{M}}$. Our trial wavefunctions are therefore exact ground states of the Hamiltonian

$$H_{\text{canted}} = -\sum_{a=1}^{N-1} \mathcal{P}_{\sigma_a^\dagger \sigma_{a+1}=1, e^{i\frac{\pi}{M}}, e^{-i\frac{\pi}{M}}} + \sum_{a=1}^{N} \mathcal{P}_{\tau_a=-1} , \qquad (3.134)$$

where $\mathcal{P}_\kappa$ projects onto states satisfying property κ. In the $\mathbb{Z}_4$ limit H_{canted} is equivalent to the Ashkin-Teller model at $f = 0$ and $\lambda = 1$, which contains many other ground states as well. Thus we should again add a perturbation akin to δH in Eq. (3.77) that leaves the canted states as the only ground states. (The specific form of the interaction is not important for us.)

In the absence of C symmetry, the canted and ferromagnet states can be smoothly connected. The parafermion counterpart of these clock phases must therefore share exactly the same symmetry-independent topological characteristics—i.e., both phases must support a $2M$-fold robust ground-state degeneracy. An identical conclusion holds for the fermion realization: Both phases yield Majorana end states whose structure depends on the order parameter, but with a different expectation value $\langle O_a \rangle = \langle \sigma_a^2 \rangle \sim e^{i\frac{\pi}{M}(2k+1)}$ in the canted state.

The dual of H_{canted} is given by

$$H_{\text{SPT}} = -\sum_{a=1}^{N} \mathcal{P}_{\tau_a=1, e^{i\frac{\pi}{M}}, e^{-i\frac{\pi}{M}}} + \sum_{a=1}^{N-1} \mathcal{P}_{\sigma_a^\dagger \sigma_{a+1}=-1} . \qquad (3.135)$$

The four wavefunctions $|\eta_1^z \eta_2^z\rangle$ defined for the $\mathbb{Z}_4$ case in Eqs. (3.82) and (3.83) are unfrustrated ground states of H_{SPT} for any M. One can always add a perturbation $\widetilde{\delta H}$ to ensure that no other ground states exist; we will assume that such a perturbation has been included. The resulting four-fold degeneracy again arises from pseudospin-1/2 edge degrees of freedom $\vec{\eta}_{1,2}$ for the clock chain. These edge modes can be related to microscopic operators projected into the ground-state manifold:

$$\mathcal{P} \frac{i(\tau_1 - \tau_1^\dagger)}{\sin \pi/M} \mathcal{P} = \eta_1^z, \qquad\qquad \mathcal{P} \frac{i(\tau_N - \tau_N^\dagger)}{\sin \pi/M} \mathcal{P} = \eta_2^z \tag{3.136}$$

$$\mathcal{P} \sigma_1 \mathcal{P} = (\eta_1^x + i\eta_1^y)/2, \qquad\qquad \mathcal{P} \sigma_N \mathcal{P} = (\eta_2^x + i\eta_2^y)/2, \tag{3.137}$$

which straightforwardly generalize Eqs. (3.85) and (3.86).

The parafermion and fermion realizations exhibit edge zero modes as well, though the statistics of the boundary operators naturally changes compared to the clock case. (The transcription between representations can be carried out using the same procedure adopted in Sec. 3.3.). In particular, for the fermion case the edge degrees of freedom can be described by a pair of Majorana zero modes at each end, precisely as for the TRITOPS phase found in the $\mathbb{Z}_4$ limit. For any representation, the edge zero modes are robust in the presence of $\mathbb{Z}_{2M}$, C, and $\mathcal{T}$ but can be eliminated when all breakable symmetries are abandoned—strongly suggesting the onset of an SPT phase for any $M \geq 2$.

Anomalous $\mathbb{Z}_{2M}$ pumps

The parafermion fusion setups in Figs. 310(a) and 313(a) extend straightforwardly to the $\mathbb{Z}_{2M}$ case by simply replacing $\cos(4\phi) \to \cos(2M\phi)$ and $\cos(4\phi - \phi_0) \to \cos(2M\phi - \phi_0)$ in the appropriate domains. For the generalized Fig. 310(a), coupling of parafermions $\alpha_{1,2}$ is governed by

$$H_{1,2} = -t \left[e^{i\frac{\pi - \theta_0}{2M}} \alpha_1^\dagger \alpha_2 + H.c. \right]. \tag{3.138}$$

Eigenstates of $H_{1,2}$ have $e^{i\frac{\pi}{2M}} \alpha_1^\dagger \alpha_2 = e^{i\frac{\pi}{M}n}$ with $n = 0, \ldots, 2M - 1$, yielding energies

$$E_n(\theta_0) = -2t \cos\left(\frac{n\pi}{M} - \frac{\theta_0}{2M} \right) \tag{3.139}$$

that are each $4M\pi$-periodic in θ_0. Level crossings occur only at $\theta_0 = 0 \mod \pi$; they are all protected by an unbreakable $\mathbb{Z}_{2M}$ symmetry in this realization—implying a $4M\pi$-periodic response to θ_0 sweeps. Once again, this anomalous periodicity reflects the fact that shifting θ_0 by 2π cycles the system among the $2M$ available

fusion channels for the corresponding non-Abelian defects. For the generalized Fig. 313(a), parafermions $\alpha_{2,3}$ couple via

$$H_{2,3} = -t\left[e^{i\frac{\pi+\phi_0}{2M}}\alpha_2^\dagger\alpha_3 + H.c.\right]. \tag{3.140}$$

Identical logic applied to this setup implies a $4M\pi$-periodic response to ϕ_0 sweeps as well.

The fermionic setups from Figs. 311(a) and 313(b) admit the same $\mathbb{Z}_{2M}$ generalization, though here we must also promote the magnetizations m_i to $\mathbb{Z}_M$ order parameters O_i. As in our analysis of the $\mathbb{Z}_4$ case, we will allow for additional physical perturbations in this setting, e.g., those that break $\mathbb{Z}_{2M}$ symmetry. If the level crossings that underlie the anomalous periodicity for the parafermion platform persist, then the $4M\pi$-periodic response survives; otherwise the periodicity will be reduced.

Consider the generalized Fig. 311(a) first. Suppose for now that the Hamiltonian is given by Eq. (3.138) re-expressed in terms of fermions, so that the energies are again given by Eq. (3.139). At $\theta_0 = 0$, the $n = 0$ and $n = M$ levels are non-degenerate, while all other energy levels form doublets comprised of states with $n = p$ and $n = -p \mod 2M$. This structure persists even in the presence of additional perturbations provided the Hamiltonian preserves $\mathcal{T}' = \mathbb{Z}_{2M}\mathcal{T}$—which guarantees degeneracy of the doublets via a generalization of Kramer's theorem. At $\theta_0 = \pi$ the Hamiltonian describes the boundary between the fermionic vacuum and the SPT phase described in the previous subsection. This interface hosts a single Dirac-fermion zero mode and, accordingly, all energy levels in Eq. (3.139) are doubly degenerate. The resulting level crossings at $\theta_0 = \pi$ are protected by fermion parity and remain robust to arbitrary local perturbations. Hence, the fermionic system retains the anomalous $4M\pi$-periodic response to θ_0 sweeps provided $\mathcal{T}'$ symmetry is enforced at $\theta_0 = 0 \mod 2\pi$.

Finally, consider the generalized Fig. 313(b). Just as for the $\mathbb{Z}_4$ limit, locality and fermion-parity constraints alone guarantee an anomalous $4M\pi$-periodic response to ϕ_0 (no special symmetries required). The Hamiltonian governing the left junction in the figure can only depend on $i\gamma_2\gamma_3$ and the order parameters $O_{1,2}$, all of which are necessarily conserved quantities in the effective low-energy description. Eliminating the level crossings that underlie the anomalous periodicity would require either transitioning between macroscopically distinct order-parameter configurations, or a source of low-energy fermions to flip $i\gamma_2\gamma_3$. Neither process is available in our

setup. We can see this result explicitly by rewriting Eq. (3.140) in the fermionic representation:

$$H_{2,3} = -2t \cos\left[\frac{\pi}{M}(\hat{q}_1 - \hat{q}_2) + \frac{\phi_0}{2M}\right] i\gamma_2\gamma_3, \qquad (3.141)$$

where we introduced integer-valued operators $\hat{q}_{1,2}$ that specify the order parameters via $O_{1,2} = e^{i\frac{2\pi}{M}\hat{q}_{1,2}}$. As deduced on general grounds, Eq. (3.141) predicts energies that are $4M\pi$ periodic in ϕ_0, with each branch corresponding to fixed order-parameter and parity configurations. Transitions between these levels are therefore forbidden.

As an aside, Eq. (3.141) in the $M = 2$ limit describes precisely the same setup as Eq. (3.118), though the Hamiltonians look rather different. In terms of the magnetizations appropriate for the $\mathbb{Z}_4$ case, we have $e^{i\frac{\pi}{2}\hat{q}_{1,2}} = [(1 + m_{1,2}) + i(1 - m_{1,2})]/2$. Using this relation and sending $\gamma_2 \to m_1\gamma_2$ in Eq. (3.141) reproduces Eq. (3.118), i.e., they indeed provide equivalent descriptions.

Figure 314 summarizes the structure of the energy levels in both fermionic platforms considered above, specializing to the $M = 3$ case.

3.6 Discussion

We have established an exact correspondence between $\mathbb{Z}_{\text{even}}$ parafermion chains and 1D fermionic systems, using clock spins as an intermediary. From the clock viewpoint, our formalism extends the familiar fermionization of the Ising model into a much broader class of discrete spin systems. We were most interested, however, in understanding how the physics of bona fide parafermions, which (to our knowledge) require a fractionalized host, filters into the fermionic realm.

Most of our effort centered around the $\mathbb{Z}_4$ case. There we introduced a judicious fermionization algorithm that maps $\mathbb{Z}_4$ parafermions to ordinary spinful electrons, a result foreshadowed by earlier works on anomalous quantum-spin-Hall edge modes [87, 111]. Moreover, we saw that symmetries of the parafermion system can be repackaged into familiar operations for fermions—notably electronic time reversal and global spin rotations. Phases for $\mathbb{Z}_4$ parafermions, in turn, translate into physically relevant electronic states as summarized in Fig. 34: The trivial gapped parafermion phase maps to an electronic insulator; the topological phase with unpaired parafermion zero modes [34] maps to a topological superconductor hosting symmetry-enriched Majorana zero modes whose structure intertwines with a spontaneously chosen magnetization order parameter; and an SPT phase for parafermions maps to the widely studied time-reversal-invariant topological superconductor (TRITOPS) for electrons.
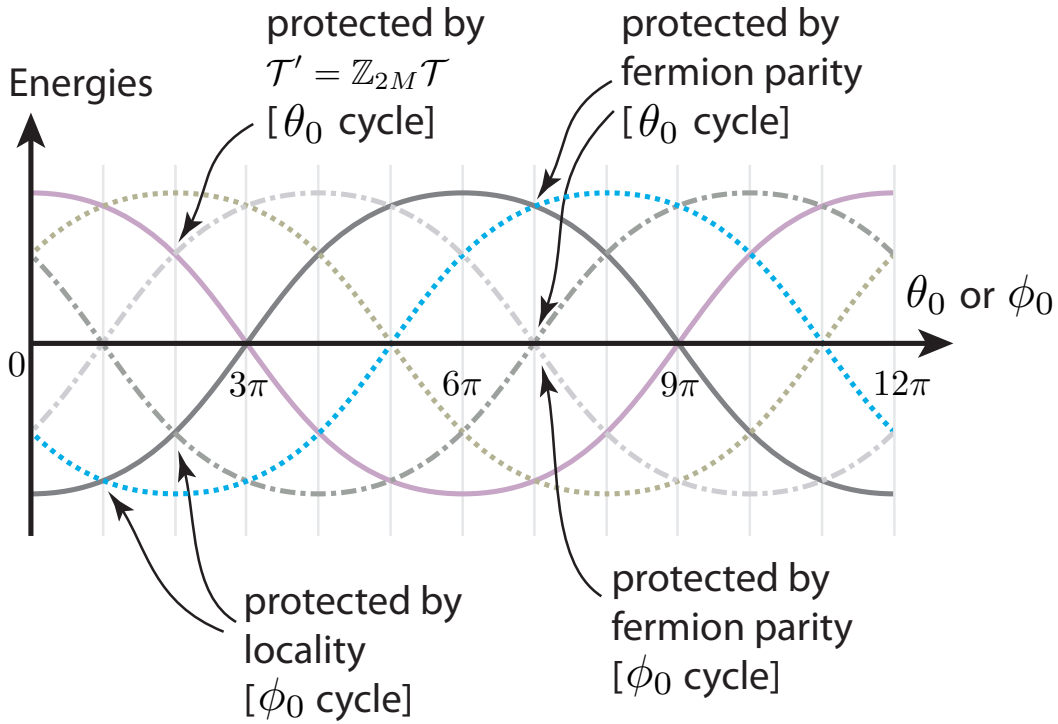
Figure 314: Energies versus pumping parameters θ_0 or ϕ_0 for the fermionic setups in Figs. 311(a) and 313(b), generalized to the $\mathbb{Z}_6$ case (i.e., $M = 3$). For the generalized Fig. 311(a), the level crossings at $\theta_0 = 0 \mod 2\pi$ are protected by the antiunitary symmetry $\mathcal{T}' = \mathbb{Z}_{2M}\mathcal{T}$, while level crossings at $\theta_0 = \pi \mod 2\pi$ exhibit fermion-parity protection. As long as these level crossings are maintained, the system exhibits an anomalous 12π-periodic response to θ_0 sweeps. For the generalized Fig. 313(b), the level crossings at zero energy are fermion-parity protected; all others occur between states with different order-parameter configurations and are protected by locality. The system thus generically exhibits 12π-periodic response to ϕ_0, with no additional symmetries required. These enlarged periodicities are an imprint of the nontrivial fusion rules in the corresponding $\mathbb{Z}_6$ parafermion platforms.

Interestingly, symmetry-enriched Majorana zero modes may have already been experimentally realized in proximitized Fe chains [33, 51, 83, 88, 94]. The Fe-chain Hamiltonian of course differs markedly from the toy models studied in Sec. 3.3, but shares the all-important feature of spontaneous time-reversal symmetry breaking. Majorana zero modes appearing in Fe chains must then conform to Eq. (3.65) on very general grounds, indicating symmetry enrichment in the sense defined in this paper. The precise connection to parafermion physics highlights a surprising new perspective on these experiments.

Our exact mappings further enabled a rigorous comparison between non-Abelian-anyon physics arising from $\mathbb{Z}_4$ parafermion zero modes and from symmetry-enriched Majorana modes. We showed that their braiding properties differ starkly and pinpointed the origin of this distinction (the parafermion braiding Hamiltonian becomes nonlocal when mapped to fermions). Symmetry-enriched Majorana modes do, nevertheless, underlie braid transformations that can not arise in conventional Majorana systems, since the order parameter need not return to its original value under an adiabatic closed cycle of the Hamiltonian. It is unclear whether this additional flexibility offers any advantages for quantum computing, though this question certainly warrants serious consideration.

Fusion properties arising from $\mathbb{Z}_4$ parafermion zero modes are more directly inherited by electrons in the following sense. Parafermion platforms admit a pumping cycle that returns the Hamiltonian to its original form but cycles the system among four possible 'fusion channels' for the parafermions—yielding an anomalous 8π-periodic response. Precisely the same 8π periodicity can be harnessed in the corresponding 1D electronic setting. We introduced 'weak' and 'strong' implementations that can both be understood in terms of hybridization of symmetry-enriched Majorana modes. The 'weak' version (summarized in Fig. 311) cyclically modulates a wire between TRITOPS and trivial phases; provided time-reversal symmetry is maintained at certain points of the cycle, the magnetization at the ends of the system exhibits 8π periodicity. This phenomenon is a cousin of the 8π-periodic Josephson effect that can arise at a quantum-spin-Hall edge [46, 87, 90, 105, 111]. The 'strong' version (Fig. 313) realizes an anomalous 8π-periodic pumping cycle that eschews symmetry requirements altogether, but necessitates strong correlation together with tunable interactions. Implementation in proximitized Fe chains poses a tantalizing possibility worth exploring in detail.

We generalized our $\mathbb{Z}_4$ results by using a modified algorithm that recasts $\mathbb{Z}_{2M}$

parafermions in terms of a single species of fermions coupled to a $\mathbb{Z}_M$ order parameter. Weak and strong anomalous pumping cycles, now with $4M\pi$ periodicity, were identified also in this broader setting. Experimental connections are less obvious compared to the $\mathbb{Z}_4$ case, however, and would be useful to develop in future work. One potentially promising avenue is to explore an array of wires with a Z_M rotational symmetry (similar to the bundles examined in Ref. [60]) that is spontaneously broken, yielding a nontrivial interplay with Majorana zero modes. It is natural to also ask about Z_{odd} parafermions. Our fermionization approach does not readily extend to this case due to a 'mismatch' in Hilbert-space dimensions. Nevertheless, it would be interesting to pursue variations of our approach, for instance that map Z_{odd} parafermions to fermions with a constrained Hilbert space.

The classifications of interacting gapped 1D phases from Refs. [21, 35, 96, 102] strongly constrain the kinds of non-Abelian-anyon defects that 1D systems can support. Specifically, these works capture only 'Ising' defects that trap Majorana zero modes. One of the general messages of our work is that the interplay between Majorana modes and local order parameters can nonetheless enrich their properties as summarized above. In light of this perspective, it would be interesting to revisit earlier works aimed at mimicking parafermion physics in strictly 1D setups [60, 61, 86, 101]: might such setups provide additional platforms for symmetry-enriched Majorana modes? Pursuing realizations of symmetry-enhanced non-Abelian defects using cold atoms poses another natural direction: building, e.g., off of Ref. [45]. Cold-atoms proposals for obtaining genuine parafermions do exist [67], but the requisite topologically ordered host platforms have not yet been demonstrated.

We conclude by highlighting several other future directions. A more exhaustive dictionary linking phases for parafermions and fermions would certainly be welcome. We have focused on a select few examples, and there are likely deeper insights to be gained from other such correspondences. Majorana zero modes can also of course arise in two-dimensional topological superconductors. Can one harvest a fruitful interplay with order-parameter physics also in this setting? On a more formal level, we saw that a duality transformation for clock spins maps fermions onto dual fermions, which (roughly) are related to one another by attaching a parafermion [recall, e.g., Eq. (3.53)]. It is interesting to ask whether a similar nontrivial connection between fermions and dual fermions can exist in higher dimensions [71, 72, 79, 98, 106]. Explorations along these lines may contribute to the growing 'duality web' that has recently been established in $(2 + 1)$-dimensional

field theories [20, 39, 53, 54, 56, 80, 81, 97].

3.7 Expressing hard-core bosons in terms of $\mathbb{Z}_4$ clock operators

Inverting Eqs. (3.15) and (3.16) is nontrivial since the expansion of σ_a involves terms that are both linear and cubic in hard-core boson operators. We perform the inversion by first assembling linear combinations that cancel the cubic components. Some algebra yields

$$\sigma \left(\frac{1 - \tau^2}{2} \right) + H.c. = b_\uparrow^\dagger + b_\uparrow \tag{3.142}$$

$$\left(\frac{1 - \tau^2}{2} \right) \sigma + H.c. = b_\downarrow^\dagger + b_\downarrow \tag{3.143}$$

$$\sigma \left(\frac{\tau^\dagger - \tau}{2} \right) + H.c. = i(b_\uparrow^\dagger - b_\uparrow) \tag{3.144}$$

$$\left(\frac{\tau^\dagger - \tau}{2} \right) \sigma + H.c. = i(b_\downarrow^\dagger - b_\downarrow), \tag{3.145}$$

where for notational simplicity we suppressed the site label a. From here it is straightforward to take superpositions that isolate $b_\uparrow$ and $b_\downarrow$, yielding Eqs. (3.17) and (3.18) from the main text.

3.8 Symmetry properties of spinful fermions

In this section we derive the action of $\mathbb{Z}_4$, $\mathcal{T}$, and $\mathcal{C}$ symmetries on spinful fermions. The string S_a is invariant under each of these operations; thus all the action arises from the bosons and the additional phase factors in Eqs. (3.19) and (3.20).

Consider first $\mathbb{Z}_4$. The following relations, which can be obtained from Eqs. (3.15) and (3.16), are helpful for evaluating this symmetry:

$$i\sigma \left(\frac{1 - \tau^2}{2} \right) + H.c. = -ie^{i\pi n_\downarrow}(b_\uparrow^\dagger - b_\uparrow) \tag{3.146}$$

$$i \left(\frac{1 - \tau^2}{2} \right) \sigma + H.c. = ie^{i\pi n_\uparrow}(b_\downarrow^\dagger - b_\downarrow) \tag{3.147}$$

$$i\sigma \left(\frac{\tau^\dagger - \tau}{2} \right) + H.c. = e^{i\pi n_\downarrow}(b_\uparrow^\dagger + b_\uparrow) \tag{3.148}$$

$$i \left(\frac{\tau^\dagger - \tau}{2} \right) \sigma + H.c. = -e^{i\pi n_\uparrow}(b_\downarrow^\dagger + b_\downarrow). \tag{3.149}$$

(We continue to suppress site indices for simplicity.) Using the above together with Eqs. (3.4), (3.17), and (3.18), one sees that the hard-core bosons transform under

$\mathbb{Z}_4$ as

$$Qb_\uparrow Q^\dagger = ie^{i\pi n_\downarrow}b_\uparrow, \quad Qb_\downarrow Q^\dagger = -ie^{i\pi n_\uparrow}b_\downarrow. \tag{3.150}$$

The fermions transform in an identical fashion:

$$Qf_\uparrow Q^\dagger = ie^{i\pi n_\downarrow}f_\uparrow, \quad Qf_\downarrow Q^\dagger = -ie^{i\pi n_\uparrow}f_\downarrow. \tag{3.151}$$

The action of time-reversal $\mathcal{T}$ on hard-core bosons follows straightforwardly from Eqs. (3.5), (3.17), and (3.18); we find

$$\mathcal{T}b_\uparrow\mathcal{T} = b_\downarrow, \quad \mathcal{T}b_\downarrow\mathcal{T} = b_\uparrow. \tag{3.152}$$

In this case the phase factors in Eqs. (3.19) and (3.20) result in a more nontrivial action on the fermions,

$$\mathcal{T}f_\uparrow\mathcal{T} = ie^{i\pi n_\uparrow}f_\downarrow, \quad \mathcal{T}f_\downarrow\mathcal{T} = ie^{i\pi n_\downarrow}f_\uparrow. \tag{3.153}$$

An analogous situation arises for charge conjugation C. For the bosons we obtain the simple transformation

$$Cb_\uparrow C = b_\downarrow, \quad Cb_\downarrow C = b_\uparrow, \tag{3.154}$$

which yields

$$Cf_\uparrow C = e^{i\pi n_\uparrow}f_\downarrow, \quad Cf_\downarrow C = e^{i\pi n_\downarrow}f_\uparrow \tag{3.155}$$

for the fermions.

3.9 Spin-$1/2$ representations and symmetries

To better understand the structure behind our fermionization, and compare to earlier works, it is instructive to express the clock operators σ_a, τ_a in terms of spin-1/2 degrees of freedom. References [62, 108] employed one possible decomposition given by

$$\sigma_a = \frac{1+i}{2}(s^z_{a+\frac{1}{4}} + is^z_{a-\frac{1}{4}}), \tag{3.156}$$

$$\tau_a = \frac{1}{2}(s^x_{a+\frac{1}{4}} + s^x_{a-\frac{1}{4}}) + \frac{1}{2}(s^x_{a+\frac{1}{4}} - s^x_{a-\frac{1}{4}})s^z_{a+\frac{1}{4}}s^z_{a-\frac{1}{4}}.$$

The inverse relationship is

$$s^z_{a-\frac{1}{4}} = -\frac{1+i}{2}(\sigma_a - i\sigma_a^\dagger),$$ (3.157)

$$s^z_{a+\frac{1}{4}} = \frac{1-i}{2}(\sigma_a + i\sigma_a^\dagger),$$ (3.158)

$$s^x_{a-\frac{1}{4}} = \frac{1}{2}\left(\tau_a + \tau_a^\dagger + \sigma_a^2(\tau_a - \tau_a^\dagger)\right),$$ (3.159)

$$s^x_{a+\frac{1}{4}} = \frac{1}{2}\left(\tau_a + \tau_a^\dagger - \sigma_a^2(\tau_a - \tau_a^\dagger)\right).$$ (3.160)

In these variables the Ashkin-Teller model, Eq. (3.38), maps onto two coupled transverse-field Ising models:

$$H = -J\sum_a (s^z_{a+\frac{1}{4}}s^z_{a+1+\frac{1}{4}} + s^z_{a-\frac{1}{4}}s^z_{a+1-\frac{1}{4}})$$ (3.161)

$$-f\sum_a (s^x_{a+\frac{1}{4}} + s^x_{a-\frac{1}{4}})$$

$$+\lambda\sum_a (Js^z_{a-\frac{1}{4}}s^z_{a+\frac{1}{4}}s^z_{a+1-\frac{1}{4}}s^z_{a+1+\frac{1}{4}} + fs^x_{a-\frac{1}{4}}s^x_{a+\frac{1}{4}}).$$

Next we will show that this spin-1/2 model admits two useful alternative forms: 'Spin model A' exhibits translation symmetry, with duality implemented as a non-symmorphic spin rotation. 'Spin model B' is invariant under a continuous spin-rotation symmetry, with duality instead implemented as a translation.

Spin model A

Suppose that we perform the familiar Ising-model duality transformation that trades in $s^{x,y,z}_{a\pm\frac{1}{4}}$ variables for dual spins $t^{x,y,z}$ living on integer as well as half-integer sites:

$$t^x_a = s^z_{a-\frac{1}{4}}s^z_{a+\frac{1}{4}} \qquad\qquad t^z_a = \prod_{a'<a} s^x_{a'}.$$ (3.162)

(In the second expression, the variable a' in the product runs over all integers and half-integers.) The Ashkin-Teller model then takes the form

$$H_{J,f} = -J\sum_a (t^x_{a-\frac{1}{2}}t^x_a + t^x_a t^x_{a+\frac{1}{2}})$$ (3.163)

$$-f\sum_a (t^z_{a-\frac{1}{2}}t^z_a + t^z_a t^z_{a+\frac{1}{2}})$$

$$+\lambda\sum_a (Jt^x_a t^x_{a+1} + ft^z_{a-\frac{1}{2}}t^z_{a+\frac{1}{2}}).$$

For later convenience, on the left side we have explicitly displayed the J, f couplings as subscripts of H. The λ terms only involve operators on the same sublattice

(integer or half-odd-integer sites). Translations $T : a \rightarrow a + 1$ and inversions $\mathcal{I}$ that preserve these sublattices leave $H_{J,f}$ invariant. We also introduce the 'half-translation' $T_{\frac{1}{2}} : a \rightarrow a + \frac{1}{2}$, which interchanges the sublattices, and a $\frac{\pi}{2}$ spin rotation $U = \exp\left[i\frac{\pi}{4}t_y\right]$. The model of Eq. (3.163) satifies

$$H_{J,f}[\boldsymbol{t}] = H_{f,J}[T_{\frac{1}{2}}U\boldsymbol{t}U^{-1}T_{\frac{1}{2}}^{-1}] , \tag{3.164}$$

i.e., duality is realized as a local spin rotation combined with a change of sublattice. This implementation of duality is specific to the Ashkin-Teller Hamiltonian and does not hold for more generic models that are only constrained by $\mathbb{Z}_4$, $\mathcal{C}$ and $\mathcal{T}$ symmetries. We already encountered an example of such a term in Eq. (3.77). Specifically, we find

$$\sigma_a^{\dagger}\sigma_{a+2} + H.c. = [t_{a+\frac{1}{2}}^x t_{a+\frac{3}{2}}^x][t_a^x t_{a+1}^x + t_{a+1}^x t_{a+2}^x] , \tag{3.165}$$

$$\tau_a\tau_{a+1} + H.c. = [t_a^z t_{a+1}^z - t_a^y t_{a+1}^y][t_{a-\frac{1}{2}}^z t_{a+\frac{1}{2}}^z + t_{a+\frac{1}{2}}^z t_{a+\frac{3}{2}}^z]$$

$$+ [t_a^z t_{a+1}^z + t_a^y t_{a+1}^y][1 + t_{a-\frac{1}{2}}^z t_{a+\frac{3}{2}}^z] .$$

Clock-model duality interchanges the expressions on the left side, but the corresponding terms on the right side are clearly not related by $T_{\frac{1}{2}}U$. In contrast, for the last term in Eq. (3.77), the symmetry operation $T_{\frac{1}{2}}U$ does implement duality, i.e.,

$$\sigma_a^2\sigma_{a+2}^2 = t_a^x t_{a+2}^x ,$$

$$\tau_a^2\tau_{a+1}^2 = t_{a-\frac{1}{2}}^z t_{a+\frac{3}{2}}^z .$$

To connect to the treatment in the main text, it is convenient to bosonize this spin model according to

$$t_y \sim \partial_x\phi + (-1)^x \sin 2\phi , \tag{3.166}$$

$$t_z \pm it_x \sim e^{\mp i\theta}[(-1)^x + \sin 2\phi] . \tag{3.167}$$

This expansion results in an effective low-energy Hamiltonian

$$\mathcal{H} = \int_x \left\{ \frac{v}{2\pi}[g(\partial_x\phi)^2 + g^{-1}(\partial_x\theta)^2] \right.$$

$$\left. - \kappa_1 \cos(4\phi) - \kappa_2 \cos(2\theta) \right\} \tag{3.168}$$

that has same form as Eq. (3.54), though the relation between g, κ_1, κ_2 and microscopic parameters of the Ashkin-Teller model is different. Firstly, for $\lambda = 0$

and $J = f$, Eq. (3.163) is a pure XY model, which in the convention defined by Eqs. (3.166) and (3.167) corresponds to $g = 1$ and $\kappa_1 = \kappa_2 = 0$. Taking $J \neq f$ but $\lambda = 0$ introduces an Ising anisotropy with $\kappa_2 \sim J - f$. When instead $\lambda \neq 0$ but $J = f$, Eq. (3.163) is symmetric under $T_{\frac{1}{2}}U$, which acts as $\phi \to \phi + \pi/2, \theta \to \theta + \pi/2$—implying that $\kappa_2 = 0$. Finally, for generic J, f, λ all terms in Eq. (3.168) are present. The broken translation symmetry would appear to permit the additional term $\sim \cos 2\phi$, but that is forbidden by $\mathcal{I}$.

In this formulation of the Ashkin-Teller model, all phases discussed in Sec. 3.3 are readily identified. The ferromagnetic and paramagnetic phases of the clock model are driven by κ_2. When $\kappa_2 < 0$, θ is pinned to $\pi/2 \mod \pi$ and $\langle t^x \rangle \neq 0$ while for $\kappa_2 > 0$ it is pinned to $0 \mod \pi$ and consequently $\langle t^z \rangle \neq 0$. The phases driven by κ_1 are characterized by magnetization in the y direction ($\kappa_1 < 0$) or by valence-bond order ($\kappa_1 > 0$). Finally, 'hybrid order' can be read off from the $\lambda \to \infty$ limit of Eq. (3.163) and amounts to $\langle t^x \rangle \neq 0$ on integer sites and $\langle t^z \rangle \neq 0$ on half-integer sites.

Spin model B

We now return to Eq. (3.161) and perform the Ising-model duality of Eq. (3.162) for *half* of the spins, i.e., $s'^x_{a-1/4} = s^z_{a-\frac{1}{4}} s^z_{a-1-\frac{1}{4}}$ and $s'^z_{a-\frac{1}{4}} = \prod_{a'<a} s^x_{a'-\frac{1}{4}}$ (the product now runs only over integer sites a'). The Ashkin-Teller Hamiltonian becomes

$$H_{J,f} = - J \sum_a (s^z_{a+\frac{1}{4}} s^z_{a+1+\frac{1}{4}} + s'^x_{a-\frac{1}{4}}) - f \sum_a (s^x_{a+\frac{1}{4}} + s^z_{a-\frac{1}{4}} s'^z_{a+1-\frac{1}{4}})$$
$$+ \lambda \sum_a (J s'^z_{a+\frac{1}{4}} s'^z_{a+1+\frac{1}{4}} s^x_{a+1-\frac{1}{4}} + f s^z_{a-\frac{1}{4}} s^z_{a+1-\frac{1}{4}} s'^x_{a+\frac{1}{4}}) . \quad (3.169)$$

A second application of Eq. (3.162), this time for all s and s', yields [62, 108]

$$H_{J,f} = - J \sum_a (t'^x_{a-\frac{1}{2}} t'^x_a + t'^z_{a-\frac{1}{2}} t'^z_a - \lambda t'^y_{a-\frac{1}{2}} t'^y_a) \quad (3.170)$$
$$- f \sum_a (t'^z_a t'^z_{a+\frac{1}{2}} + t'^x_a t'^x_{a+\frac{1}{2}} - \lambda t'^y_a t'^y_{a+\frac{1}{2}}) .$$

This formulation is invariant under continuous global spin rotations about t'^y and satisfies

$$H_{J,f}[\boldsymbol{t'}] = H_{f,J}[T_{\frac{1}{2}} \boldsymbol{t'} T_{\frac{1}{2}}^{-1}] , \quad (3.171)$$

i.e., duality is implemented as a translation. Bosonizing as before, one finds

$$\mathcal{H} = \int_x \left\{ \frac{v'}{2\pi} [g'(\partial_x \phi')^2 + g'^{-1}(\partial_x \theta')^2] - \kappa'_1 \cos(4\theta') - \kappa'_2 \cos(2\phi') \right\} \quad (3.172)$$

with $\kappa_2' \sim J - f$. It follows that the low-energy descriptions of spin models A and B are related by interchanging ϕ and θ.

3.10 Alternative fermionization schemes

The spin-1/2 representations of Section 3.9 provide an alternative route to fermionizing clock Hamiltonians by using the conventional Jordan-Wigner transformation. The form of Eq. (3.163) suggests introducing spinless Jordan-Wigner fermions as

$$\mathbf{c}_a' = \frac{1}{2}(t_a^z - it_a^x) \prod_{a' < a} t_{a'}^y \ . \tag{3.173}$$

When these fermions are bosonized via $\mathbf{c}_a' \sim e^{ik_F a} e^{i(\theta + \phi)} + e^{-ik_F a} e^{i(\theta - \phi)}$, the Pauli operators take the form given in Eqs. (3.166) and (3.167), and the low-energy Hamiltonian is the one of Eq. (3.168). Note that the bosonization convention employed above differs from that in Sec. 3.3, which is useful since the low-energy descriptions obtained in the two approaches then exactly match up.

Spinful fermions

To connect to the fermionization performed in the main text, it is instructive to adopt the alternative convention

$$\mathbf{c}_a = \frac{1}{2}(t_a^y - it_a^z) \prod_{a' < a} t_{a'}^x \ . \tag{3.174}$$

This is related to the one above by a global spin rotation—a highly non-local transformation on the fermions. Using Eqs. (3.156) and (3.162) we find for integer a

$$\mathbf{c}_a = \frac{i}{2}(\sigma_a + \sigma_a^\dagger) \tau_a^\dagger \prod_{a' < a} \tau_{a'}^2 \ ,$$

$$\mathbf{c}_{a+\frac{1}{2}}^\dagger - \mathbf{c}_{a+\frac{1}{2}} = \frac{1+i}{2}(\sigma_a + i\sigma_a^\dagger)\tau_a^2 \prod_{a' < a} \tau_{a'}^2 \ ,$$

$$\mathbf{c}_{a-\frac{1}{2}}^\dagger + \mathbf{c}_{a-\frac{1}{2}} = -\frac{1-i}{2}(\sigma_a - i\sigma_a^\dagger)\tau_a^2 \prod_{a' < a} \tau_{a'}^2 \ ,$$

where we omitted a boundary term s_0^z. Note that the spinful fermions introduced in Sec. 3.2 have exactly the same structure, i.e., a string of τ^2's that is terminated by an odd power of σ operators. This similarity implies a local relationship between the two kinds of fermions, which we already provided explicitly in Eqs. (3.36) and (3.37).

Dual fermions

To connect to the dual fermions of Sec. 3.2, recall that the spin-1/2 representation of Eq. (3.163) implements duality as a $\pi/2$ rotation combined with a half-translation. This suggests that the spinful fermions $\tilde{\mathbf{f}}_{a,\alpha}$ defined by replacing c_a in Eqs. (3.36) and (3.37) by

$$\tilde{c}_a = T_{\frac{1}{2}} U c_a U^{-1} T_{\frac{1}{2}}^{-1} = \frac{1}{2}(t^y_{a+\frac{1}{2}} + it^x_{a+\frac{1}{2}}) \prod_{a'<a+\frac{1}{2}} t^z_{a'} \tag{3.175}$$

correspond to the dual fermions introduced in the main text. Indeed, for the Ashkin-Teller model one finds

$$
\begin{aligned}
H_{J,f}[\tilde{f}_\alpha] &= H_{f,J}[f_\alpha] = H_{f,J}[\mathbf{f}_\alpha] \\
&= H_{J,f}[T_{\frac{1}{2}} U \mathbf{f}_\alpha U^{-1} T_{\frac{1}{2}}^{-1}] = H_{J,f}[\tilde{\mathbf{f}}_\alpha],
\end{aligned} \tag{3.176}
$$

where the third equality holds due to Eq. (3.164). This relationship breaks down, e.g., in the presence of the perturbation described by Eq. (3.165). Unlike $\mathbf{f}_\alpha$ and f_α, the single-particle operators $\tilde{\mathbf{f}}_\alpha$ and $\tilde{f}_\alpha$ are related non-locally as noted in the main text.

3.11 Explicit map between $\mathbb{Z}_4$ parafermions and fermions

Here we furnish explicit maps that fermionize the $\mathbb{Z}_4$ parafermion operators defined in Eq. (3.9). We first use Eqs. (3.15) through (3.21) to write σ_a and $\sigma_a \tau_a$ in terms of fermions:

$$\sigma_a = S_a[(\bar{w}f^\dagger_{a,\downarrow} + wf_{a,\uparrow}) + (\bar{w}f^\dagger_{a,\uparrow} - wf_{a,\uparrow})n_{a,\downarrow} - (wf_{a,\downarrow} + \bar{w}f^\dagger_{a,\downarrow})n_{a,\uparrow}] \tag{3.177}$$

$$\sigma_a \tau_a = S_a[\bar{w}(f^\dagger_{a,\downarrow} - f_{a,\uparrow}) + (\bar{w}f_{a,\uparrow} - wf^\dagger_{a,\uparrow})n_{a,\downarrow} + (wf_{a,\downarrow} - \bar{w}f^\dagger_{a,\downarrow})n_{a,\uparrow}], \tag{3.178}$$

where $w = e^{i\frac{\pi}{4}}$. These expressions simplify considerably upon introducing Majorana operators and projectors as follows:

$$f_{a,\alpha} = \bar{w}(\gamma_{a,1\alpha} + i\gamma_{a,2\alpha})/2 \tag{3.179}$$

$$\mathcal{P}_{a,1\pm} = \frac{1}{2}(1 \pm i\gamma_{a,1\downarrow}\gamma_{a,2\uparrow}) \tag{3.180}$$

$$\mathcal{P}_{a,2\pm} = \frac{1}{2}(1 \pm i\gamma_{a,1\uparrow}\gamma_{a,2\downarrow}). \tag{3.181}$$

We then obtain

$$\sigma_a = S_a[\mathcal{P}_{a,1+}\gamma_{a,1\uparrow} - i\mathcal{P}_{a,1-}\gamma_{a,2\downarrow}] \tag{3.182}$$

$$\bar{w}\sigma_a \tau_a = \frac{S_a}{\sqrt{2}}e^{\frac{\pi}{2}i(\mathcal{P}_{a,2+}-1)}(\gamma_{a,1\downarrow} - \gamma_{a,2\uparrow}). \tag{3.183}$$

As an aside, Eq. (3.182) provides an alternative means of recovering Eq. (3.60) directly from the clock model. The fermionic operators c_a and d_a are respectively given by $c_a = \frac{1}{2}(\gamma_{a,1\uparrow} + i\gamma_{a,2\downarrow})$ and $d_a = \frac{1}{2}(\gamma_{a,1\downarrow} + i\gamma_{a,2\uparrow})$. Moreover, $P_{a,1+}$ and $P_{a,1-}$ project onto the magnetization sectors $m_a = -1$ and $m_a = +1$, respectively, while the strings combine to yield a simple multiplicative factor of $m_a(i\gamma_{a,1\uparrow}\gamma_{a,2\downarrow})$.

The parafermion operators $\alpha_{2a-1}, \alpha_{2a}$ arise from Eq. (3.182), (3.183) multiplied by the disorder operator $\mu_{a-\frac{1}{2}}$, respectively. Both cases contain a factor

$$S_a \mu_{a-\frac{1}{2}} = \mu_{a-\frac{1}{2}}^\dagger = e^{-i\frac{\pi}{2}\sum_{b<a}(n_{b,\uparrow}-n_{b,\downarrow}+2n_{b,\uparrow}n_{b,\downarrow})}$$

$$= e^{-i\frac{\pi}{4}\sum_{b<a}[1+i\gamma_{b,1\uparrow}\gamma_{b,2\uparrow}(2+i\gamma_{b,1\downarrow}\gamma_{b,2\downarrow})]}. \tag{3.184}$$

Putting everything together yields

$$\alpha_{2a-1} = \frac{1}{2}e^{-i\frac{\pi}{4}\sum_{b<a}[1+i\gamma_{b,1\uparrow}\gamma_{b,2\uparrow}(2+i\gamma_{b,1\downarrow}\gamma_{b,2\downarrow})]}[\mathcal{P}_{a,1+}\gamma_{a,1\uparrow} - i\mathcal{P}_{a,1-}\gamma_{a,2\downarrow}] \tag{3.185}$$

$$\alpha_{2a} = \frac{1}{\sqrt{2}}e^{-i\frac{\pi}{4}\sum_{b<a}[1+i\gamma_{b,1\uparrow}\gamma_{b,2\uparrow}(2+i\gamma_{b,1\downarrow}\gamma_{b,2\downarrow})]}e^{\frac{\pi}{2}i(\mathcal{P}_{a,2+}-1)}(\gamma_{a,1\downarrow} - \gamma_{a,2\uparrow}). \tag{3.186}$$

Equations (3.185) and (3.186) explicitly relate parafermions to non-local products of fermions. We will now derive an alternative decomposition that involves local combinations of fermions and dual fermions. To this end define the dual analogue of Eqs. (3.179) through (3.181),

$$\tilde{f}_{\tilde{a},\alpha} = \bar{w}(\tilde{\gamma}_{\tilde{a},1\alpha} + i\tilde{\gamma}_{\tilde{a},2\alpha})/2 \tag{3.187}$$

$$\tilde{\mathcal{P}}_{\tilde{a},1\pm} = \frac{1}{2}(1 \pm i\tilde{\gamma}_{\tilde{a},1\downarrow}\tilde{\gamma}_{\tilde{a},2\uparrow}) \tag{3.188}$$

$$\tilde{\mathcal{P}}_{\tilde{a},2\pm} = \frac{1}{2}(1 \pm i\tilde{\gamma}_{\tilde{a},1\uparrow}\tilde{\gamma}_{\tilde{a},2\downarrow}), \tag{3.189}$$

as well as the dual analogue of Eq. (3.182),

$$\mu_{\tilde{a}} = \tilde{S}_{\tilde{a}}[\tilde{\mathcal{P}}_{\tilde{a},1+}\tilde{\gamma}_{\tilde{a},1\uparrow} - i\tilde{\mathcal{P}}_{\tilde{a},1-}\tilde{\gamma}_{\tilde{a},2\downarrow}], \tag{3.190}$$

where $\tilde{a} = a + \frac{1}{2}$. The string in the above equation reads

$$\tilde{S}_{\tilde{a}} = \prod_{\tilde{b}<\tilde{a}} \nu_{\tilde{b}}^2 = \sigma_a^2 = i\gamma_{a,1\downarrow}\gamma_{a,2\uparrow}. \tag{3.191}$$

Here we neglected the termination of the ν^2 string; that is, we discarded a $\sigma_{-\infty}^2$ factor. To obtain the right-hand side, we used Eq. (3.182) to express $\tilde{S}_{\tilde{a}}$ as a purely local

product of the original fermions. One can similarly express the string in Eqs. (3.182) and (3.183) as a local product of dual fermions:

$$S_a = \mu^2_{\tilde{a}-1} = i\tilde{\gamma}_{\tilde{a}-1,1\downarrow}\tilde{\gamma}_{\tilde{a}-1,2\uparrow}. \tag{3.192}$$

We can now obtain the desired form of the parafermion operators,

$$\begin{aligned}
\alpha_{2a-1} &= \sigma_a\mu_{\tilde{a}-1} \\
&= [\mathcal{P}_{a,1+}\gamma_{a,1\uparrow} + i\mathcal{P}_{a,1-}\gamma_{a,2\downarrow}](\tilde{\mathcal{P}}_{\tilde{a}-1,2+} - \tilde{\mathcal{P}}_{\tilde{a}-1,2-}) \\
&\quad \times [\tilde{\mathcal{P}}_{\tilde{a}-1,1+}\tilde{\gamma}_{\tilde{a}-1,1\uparrow} - i\tilde{\mathcal{P}}_{\tilde{a}-1,1-}\tilde{\gamma}_{\tilde{a}-1,2\downarrow}] \tag{3.193} \\
\alpha_{2a} &= \bar{w}\sigma_a\mu_{\tilde{a}} \\
&= \bar{w}[\mathcal{P}_{a,1+}\gamma_{a,1\uparrow} - i\mathcal{P}_{a,1-}\gamma_{a,2\downarrow}](\mathcal{P}_{a,2+} - \mathcal{P}_{a,2-}) \\
&\quad \times [\tilde{\mathcal{P}}_{\tilde{a},1+}\tilde{\gamma}_{\tilde{a},1\uparrow} - i\tilde{\mathcal{P}}_{\tilde{a},1-}\tilde{\gamma}_{\tilde{a},2\downarrow}]. \tag{3.194}
\end{aligned}$$

The factor $\mu_{\tilde{a}-1}$ above involves a string $\tilde{S}_{\tilde{a}-1} = \sigma^2_{a-1}$. To derive Eq. (3.193) we equivalently wrote this string as $\tilde{S}_{\tilde{a}-1} = \sigma^2_a\nu^2_{\tilde{a}-1}$, expressed σ^2_a in terms of a local product of fermions using Eq. (3.191), and expressed $\nu^2_{\tilde{a}-1}$ in terms of dual fermions. Similarly, the σ_a in Eq. (3.194) involves a string $S_a = \mu^2_{\tilde{a}-1}$ which we can rewrite as $\tau^2_a\mu^2_{\tilde{a}}$. Here we expressed $\mu^2_{\tilde{a}}$ as a local product of dual fermions using Eq. (3.192) and wrote τ^2_a in terms of fermions. We adopted this approach to express the parafermions as products of fermion operators living on a single site and dual fermions living on another.

3.12 Self-duality of the hybrid-order ground states

As discussed in Sec. 3.3, ground states of the Hamiltonian $H_{\text{hybrid order}} = -J_2 \sum_a \sigma^2_a\sigma^2_{a+1} - f_2 \sum_a \tau^2_a$ can be expressed as

$$|+\rangle = \prod_a \frac{1 + \tau^2_a}{\sqrt{2}} |\sigma = 1, \ldots, 1\rangle \tag{3.195}$$

$$|-\rangle = \prod_a \frac{1 + \tau^2_a}{\sqrt{2}} |\sigma = i, \ldots, i\rangle \tag{3.196}$$

for any positive couplings f_2, J_2. Our goal here is to show that these states take essentially the same form after a duality transformation.

For this purpose, one can profitably view $|\pm\rangle$ as follows: Start from 'root states' $|\sigma = 1, \ldots, 1\rangle$ and $|\sigma = i, \ldots, i\rangle$ that satisfy the J_2 term, and then apply $(1 + \tau^2_a)$ factors that project away $\tau^2_a = -1$ configurations to satisfy the f_2 term. (Choosing root states $|\sigma = -1, \ldots, -1\rangle$ and $|\sigma = -i, \ldots, -i\rangle$ produces the same end result.)

From a dual viewpoint, we can construct one ground state by taking the root state $|\tau = 1, \ldots, 1\rangle$ that satisfies the f_2 term, and then applying $(1 + \sigma_a^2 \sigma_{a+1}^2)$ factors to satisfy J_2. The corresponding wavefunction reads

$$|\tilde{\mp}\rangle = \prod_a \frac{1 + \sigma_a^2 \sigma_{a+1}^2}{\sqrt{2}} |\tau = 1, \ldots, 1\rangle \qquad (3.197)$$

and obeys $Q|\tilde{\mp}\rangle = |\tilde{\mp}\rangle$ (as usual Q is the $\mathbb{Z}_4$ generator). Taking the root state $|\tau = -1, 1, \ldots, 1\rangle$—which also satisfies f_2—yields a second ground state

$$|\tilde{\mp}\rangle = \prod_a \frac{1 + \sigma_a^2 \sigma_{a+1}^2}{\sqrt{2}} |\tau = -1, 1, \ldots, 1\rangle = \sigma_1^2 |\tilde{\mp}\rangle \qquad (3.198)$$

with $Q|\tilde{\mp}\rangle = -|\tilde{\mp}\rangle$. Despite appearances, $|\tilde{\pm}\rangle$ represent product states for the clock chain. Applying the basis change $|\tau = 1\rangle = \frac{1}{2} \sum_\sigma |\sigma\rangle$ allows us to write

$$\frac{|\tilde{\mp}\rangle + |\tilde{\mp}\rangle}{\sqrt{2}} = \frac{1}{2^N} \sum_{\sigma_1, \ldots, \sigma_N} \frac{1 + \sigma_1^2}{\sqrt{2}} \prod_a \frac{1 + \sigma_a^2 \sigma_{a+1}^2}{\sqrt{2}} |\sigma_1, \ldots, \sigma_N\rangle. \qquad (3.199)$$

The $(1 + \sigma_1^2)$ factor restricts the σ_1 sum to ± 1; the product $(1 + \sigma_a^2 \sigma_{a+1}^2)$ then propagates this same restriction to all other sites. We therefore obtain the relation

$$\frac{|\tilde{\mp}\rangle + |\tilde{\mp}\rangle}{\sqrt{2}} = |+\rangle, \qquad (3.200)$$

while analogous logic yields

$$\frac{|\tilde{\mp}\rangle - |\tilde{\mp}\rangle}{\sqrt{2}} = |-\rangle. \qquad (3.201)$$

Duality indeed merely introduces a basis change. The situation should be contrast to the broken-symmetry canted-ferromagnet states defined in Eq. (3.76), which dualize into ground states of an SPT phase [Eqs. (3.82) and (3.83)].

3.13 Zero-mode anomalies in the SPT phases

This Section rigorously shows that the $\kappa_2 < 0$ states discussed in Sec. 3.3 correspond to SPT phases. To do so, we will appeal to the theory of projective representations for SPT's put forward by Refs. [21–23]. The relevant symmetries are $\mathbb{Z}_4$, C, and $\mathcal{T}$. Generators of these symmetries—which we respectively denote by Q, c, and t—form a linear representation of the symmetry group when acting on physical degrees of freedom. For example, take $\mathbb{Z}_4$. In the clock representation, we can choose σ eigenstates as physical kets; Q 'winds' these states according to

$$|\sigma = 1\rangle \rightarrow |\sigma = -i\rangle \rightarrow |\sigma = -1\rangle$$
$$\rightarrow |\sigma = i\rangle \rightarrow |\sigma = 1\rangle. \qquad (3.202)$$

This action leads to an example of a linear representation: the matrix representation of the symmetry generator Q,

$$N(Q) = \begin{bmatrix} 0 & 0 & 0 & 1 \\ 1 & 0 & 0 & 0 \\ 0 & 1 & 0 & 0 \\ 0 & 0 & 1 & 0 \end{bmatrix}, \tag{3.203}$$

obeys the same multiplication rules as the symmetry generators themselves. That is,

$$N(g)N(h) = N(gh), \tag{3.204}$$

where g, h are symmetry-group elements and N is the corresponding matrix representation. When considering $\mathbb{Z}_4$ alone, one has $g = Q^a$ and $h = Q^b$ for integers a, b, though Eq. (3.204) defines a linear representation for general symmetry groups as well.

For an SPT, an interesting loophole arises: the edge modes are anomalous and carry a *projective* representation of the symmetry group. Specifically, if $M(g)$ is the matrix representation that specifies how the edge modes transform under a symmetry element g, then

$$M(g)M(h) = \omega(g, h)M(gh). \tag{3.205}$$

Here ω is a phase factor that cannot be gauged to 1 by a phase redefinition of the form $M(g) \rightarrow M'(g) = e^{i\theta_g} M(g)$. In what follows we will show that the edge zero modes in the $\kappa_2 < 0$ phases indeed transform projectively under appropriate symmetries, indicating that the bulk forms an SPT.

We will first address the clock representation (see below for an extension to the fermion and parafermion cases). Let us focus on the left zero mode, which as discussed in Section 3.3 encodes a twofold degeneracy corresponding to pseudospin-1/2 states with $\eta_1^z = \pm 1$. According to Eq. (3.87), the action of Q on the zero mode is given by the operator $e^{i\frac{\pi}{4}\eta_1^z}$, which yields the matrix representation

$$M(Q) = \begin{bmatrix} e^{i\frac{\pi}{4}} & 0 \\ 0 & e^{-i\frac{\pi}{4}} \end{bmatrix}. \tag{3.206}$$

Although $Q^4 = 1$ by definition, the matrix above satisfies $[M(Q)]^4 = -1$. In this case the -1 on the right side can be gauged away by defining $M'(Q) = e^{i\frac{\pi}{4}} M(Q)$. Then $M'(Q)^4 = M'(Q^4) = 1$, yielding a linear representation. Hence the clock chain does *not* form an SPT if $\mathbb{Z}_4$ alone is present.

Suppose that we instead enforce the combination $\mathbb{Z}_4\mathcal{T}$. The symmetry properties from Table 36 imply that $\mathcal{T}$ transforms the zero mode according to the matrix

$$M(t) = \begin{bmatrix} 0 & 1 \\ 1 & 0 \end{bmatrix} \mathcal{K}, \tag{3.207}$$

where $\mathcal{K}$ denotes complex conjugation, reflecting antiunitary of $\mathcal{T}$. The matrix representation of the generator Qt follows as

$$M(Qt) = \begin{bmatrix} 0 & e^{i\frac{\pi}{4}} \\ e^{-i\frac{\pi}{4}} & 0 \end{bmatrix} \mathcal{K}. \tag{3.208}$$

Similar to the case of $\mathbb{Z}_4$ by itself, we see that $[M(Qt)]^4 = -1$ even though $(Qt)^4 = 1$. Crucially, however, here there is no phase factor that we can append to remove the -1. Thus the zero mode transforms projectively under $\mathbb{Z}_4\mathcal{T}$, and the clock chain forms an SPT in the presence of this composite symmetry.

Alternatively, the clock chain can form an SPT protected by $\mathbb{Z}_4$ and C. Under C symmetry σ eigenstates transform as

$$|\sigma = 1\rangle \rightarrow |\sigma = 1\rangle, \quad |\sigma = -1\rangle \rightarrow |\sigma = -1\rangle \tag{3.209}$$

$$|\sigma = i\rangle \rightarrow |\sigma = -i\rangle, \quad |\sigma = -i\rangle \rightarrow |\sigma = i\rangle. \tag{3.210}$$

Furthermore, C transforms the zero mode according to

$$M(c) = \begin{bmatrix} 0 & 1 \\ 1 & 0 \end{bmatrix}, \tag{3.211}$$

where we again used the symmetry properties from Table 36. It is useful to now associate σ eigenstates with the four compass directions; from this viewpoint $\mathbb{Z}_4$ effects a rotation while C yields a reflection. The corresponding symmetry group is D_8, the dihedral group on 4 elements. In order for the zero modes to transform as a linear representation with respect to $\mathbb{Z}_4$ and C symmetries, we must be able to deform the matrices in Eqs. (3.206) and (3.211) so that

$$[M(Q)]^4 = M(Q^4) = 1 \tag{3.212}$$

$$[M(c)]^2 = M(c^2) = 1 \tag{3.213}$$

$$M(c)M(Q)M(c) = M(cQc = Q^{-1}) = M(Q)^{-1}. \tag{3.214}$$

In the last line we invoked properties of the dihedral group. Such a deformation is impossible—no matter what phases we append to $M(Q)$ and $M(c)$, we can not

simultaneously satisfy all three conditions above. So the zero modes indeed transform projectively in the presence of $\mathbb{Z}_4$ and C, again guaranteeing an SPT for the clock chain.

Note that *both* $\mathbb{Z}_4$ and C symmetries must be enforced for the conclusion above to apply, as similar logic shows that the combination $\mathbb{Z}_4 C$ by itself does not protect the SPT. However, an SPT does emerge upon supplementing $\mathbb{Z}_4 C$ with $\mathbb{Z}_4^2$, which together form the group $\mathbb{Z}_2 \times \mathbb{Z}_2$. The associated matrix representations are

$$M(Qc) = \begin{bmatrix} 0 & e^{i\frac{\pi}{4}} \\ e^{-i\frac{\pi}{4}} & 0 \end{bmatrix}, \quad M(Q^2) = \begin{bmatrix} i & 0 \\ 0 & -i \end{bmatrix}. \tag{3.215}$$

A linear representation arises if we can redefine the matrices such that

$$[M(Q^2)]^2 = M(Q^4) = 1 \tag{3.216}$$

$$[M(Qc)]^2 = M((Qc)^2) = 1 \tag{3.217}$$

$$M(Q^2)M(Qc) = M(Qc)M(Q^2), \tag{3.218}$$

which again is impossible.

We can readily extend these results to the parafermion and fermion realizations. Above we saw that the clock-chain SPT can be protected by (*i*) $\mathbb{Z}_4 \mathcal{T}$, (*ii*), $\mathbb{Z}_4$ and C, or (*iii*) $\mathbb{Z}_4 C$ and $\mathbb{Z}_4^2$. For parafermions and fermions, some of these symmetries are enforced automatically—thus weakening the symmetry requirements for obtaining an SPT in these realizations. Parafermions realize $\mathbb{Z}_4$ automatically, so that we need only impose $\mathcal{T}$ or C. Fermions realize $\mathbb{Z}_4^2$ automatically—which corresponds to global fermion parity—though $\mathbb{Z}_4$ itself can be broken. Thus electronic time reversal $\mathcal{T}_{\text{elec}} = \mathbb{Z}_4 \mathcal{T}$ or spin rotation symmetry $U_{\text{spin}} = \mathbb{Z}_4 C$ protect the fermionic SPT. Incidentally, the existence of an SPT in the latter context is clear even without the analysis in this section, since the fermions realize the well-studied TRITOPS phase.

3.14 Parafermion braid matrices in fermion language

As noted in Sec. 3.4, rewriting parafermion braid matrices in terms of Majorana operators enables a direct comparison with braid matrices that arise in the spinful-fermion realization. Adapting the machinery from Sec. 3.3 yields the following

dictionary:

$$\alpha_1 = -e^{i\frac{\pi}{4}(m_L-1)}\gamma_1 \tag{3.219}$$

$$\alpha_2 = -e^{-i\frac{\pi}{4}[p_L(m_L+1)+1]}\Gamma_2 \tag{3.220}$$

$$\alpha_3 = -e^{i\frac{\pi}{4}[m_R-m_L+p_L(m_L+1)]}\gamma_3\gamma_2\Gamma_1 \tag{3.221}$$

$$\alpha_4 = -e^{-i\frac{\pi}{4}[p_R(m_R+1)-p_L(m_L+1)+m_L]}\Gamma_1\Gamma_4\gamma_2. \tag{3.222}$$

Here α_j and γ_j denote zero-mode operators in Fig. 39; $p_L = i\gamma_1\gamma_2$ and $p_R = i\gamma_3\gamma_4$; and $m_L = i\Gamma_1\Gamma_2$ and $m_R = i\Gamma_3\Gamma_4$ denote the magnetizations in Fig. 39(b). The total fermion parities in the left and right topological segments are $P_{\text{tot},L} = m_L p_L$ and $P_{\text{tot},R} = m_R p_R$, respectively. Inserting the decomposition above into Eq. (3.101) yields the braid matrices given in Eqs. (3.109) and (3.110) from Sec. 3.4.

To see that the parafermionic braid matrix $U_{1,2}$ generates cat states when acting on physical fermion wavefunctions, consider its action on states $|m_L, P_{\text{tot},L}\rangle$ for the left topological segment:

$$|m_L = 1, P_{\text{tot},L} = 1\rangle \rightarrow e^{i\frac{3\pi}{8}} |m_L = -1, P_{\text{tot},L} = 1\rangle$$

$$|m_L = 1, P_{\text{tot},L} = -1\rangle \rightarrow e^{i\frac{\pi}{8}} |m_L = 1, P_{\text{tot},L} = -1\rangle$$

$$|m_L = -1, P_{\text{tot},L} = 1\rangle \rightarrow e^{i\frac{3\pi}{8}} |m_L = 1, P_{\text{tot},L} = 1\rangle$$

$$|m_L = -1, P_{\text{tot},L} = -1\rangle \rightarrow e^{i\frac{\pi}{8}} |m_L = -1, P_{\text{tot},L} = -1\rangle.$$

The total parity is preserved under $U_{1,2}$ as expected, though the magnetization flips in the $P_{\text{tot},L} = +1$ sector. Applying $U_{1,2}$ to a physical fermion state

$$|\psi\rangle = a\,|m_L, P_{\text{tot},L}; m_R, P_{\text{tot},R}\rangle + b\,|m_L, -P_{\text{tot},L}; m_R, -P_{\text{tot},R}\rangle$$

then yields a cat state whenever a and b are both nonzero.

3.15 Derivation of parafermion fusion Hamiltonians

We will now analyze Fig. 310(a) and derive the minimal Hamiltonian coupling parafermions α_1 and α_2. Following Sec. 3.3, we parametrize the pinned bosonized fields in the adjacent domains as follows: $\theta = 0$ on the left, $\phi = \pi\hat{a}/2$ between $\alpha_{1,2}$, and $\theta = \pi\hat{b} + \theta_0/2$ in the central region. With these definitions (in particular, including the $\theta_0/2$ shift) $\hat{a}, \hat{b}$ are once again integer-valued operators that define parafermions via $\alpha_1 = e^{i\frac{\pi}{2}\hat{a}}$ and $\alpha_2 = e^{i\frac{\pi}{2}(\hat{a}-\hat{b})}$, precisely as in Eq. (3.56).

Now consider the bosonized perturbation

$$H_{1,2} = -2t\cos\left[\frac{\theta(x_2) - \theta(x_1)}{2}\right], \tag{3.223}$$

where x_1 sits just to the left of α_1 while x_2 sits just to the right of α_2. This coupling cycles ϕ in the intervening region among adjacent pinned values and is physical provided $\alpha_{1,2}$ are close to one another. Note also that $H_{1,2}$ preserves $\mathbb{Z}_4, C$, and $\mathcal{T}$—which are present at least when $\theta_0 = 0 \mod \pi$. Away from these special θ_0 values we can in principle introduce a non-universal shift inside of the cosine in $H_{1,2}$, though such a shift is benign for our purposes. We will also ignore higher harmonics, i.e., terms like $\cos[\theta(x_2) - \theta(x_1)]$, since they also do not affect our conclusions. Projecting $H_{1,2}$ into the low-energy subspace yields

$$
\begin{aligned}
H_{1,2} &\to -2t \cos\left(\frac{\pi}{2}\hat{b} + \frac{\theta_0}{4}\right) \\
&= -t\left[e^{i\frac{\pi-\theta_0}{4}}\alpha_1^\dagger \alpha_2 + H.c.\right],
\end{aligned}
\tag{3.224}
$$

corresponding to Eq. (3.112) from the main text.

One can similarly examine the parafermion setup from Fig. 313(a). Here we parametrize the pinned bosonized fields as $\phi = \pi\hat{a}/2$ on the left, $\theta = \pi\hat{b}$ between $\alpha_{2,3}$, and $\phi = \pi\hat{c}/2 + \phi_0/4$ in the middle domain ($\hat{a}, \hat{b}, \hat{c}$ are integer-valued operators). In this case the parafermion operators are given by $\alpha_2 = e^{i\frac{\pi}{2}(\hat{a}-\hat{b})}$ and $\alpha_3 = e^{i\frac{\pi}{2}(\hat{c}-\hat{b})}$. Define a bosonized perturbation that cycles θ between adjacent pinned values:

$$
H_{2,3} = -2t \cos[\phi(x_3) - \phi(x_2)]
\tag{3.225}
$$

with x_2 now taken just to the left of α_2 and x_3 taken just to the right of α_3. This term projects to

$$
\begin{aligned}
H_{2,3} &\to -2t \cos\left[\frac{\pi}{2}(\hat{c} - \hat{a}) + \frac{\phi_0}{4}\right] \\
&= -t\left[e^{i\frac{\pi+\phi_0}{4}}\alpha_2^\dagger \alpha_3 + H.c.\right].
\end{aligned}
\tag{3.226}
$$

3.16 Dictionary for higher parafermions

In this section we will invert Eqs. (3.124) and (3.125) so that we can express fermions and order-parameter operators in terms of clock variables. This exercise will enable us to relate the fermions in the $M = 2$ limit to the alternate set of fermions that we obtained for the $\mathbb{Z}_4$ case in Sec. 3.3.

As we already observed, the order parameter O_a is easily related to clock operators by squaring Eq. (3.124), which yields

$$
O_a = \sigma_a^2.
\tag{3.227}
$$

Next we will solve for the hard-core bosons B_a. It is useful to observe that

$$\tau_a^M = e^{i\pi B_a^\dagger B_a}, \tag{3.228}$$

which follows from Eqs. (3.125) and (3.123). Using this relation in conjunction with Eq. (3.124), we have

$$\sigma_a = B_a + O_a B_a^\dagger \tag{3.229}$$

$$\sigma_a \tau_a^M = -B_a + O_a B_a^\dagger \tag{3.230}$$

and hence

$$B_a = \frac{1}{2}\sigma_a(1 - \tau_a^M). \tag{3.231}$$

Substituting our expression for B_a into Eq. (3.125) yields

$$\mathcal{D}_a = \tau\left[\left(\frac{1+\tau^M}{2}\right) + e^{-i\frac{\pi}{M}}\left(\frac{1-\tau^M}{2}\right)\right]. \tag{3.232}$$

One can readily verify that $\mathcal{D}_a$ and O_a commute with B_a, as assumed in our decomposition. Finally, combining Eqs. (3.228) and (3.231) allows us to write C_a fermions defined in Eq. (3.126) as

$$C_a = \frac{1}{2}\sigma_a(1 - \tau_a^M)\prod_{a'<a}\tau_{a'}^M. \tag{3.233}$$

We now specialize to $\mathbb{Z}_4$, i.e., $M = 2$, with the intention of relating operators $O_a, \mathcal{D}_a, C_a$ to the fermions c_a, d_a defined in Eqs. (3.58) and (3.59). The order parameter part is trivial, since $O_a \to m_a = e^{i\pi d_a^\dagger d_a}$ [recall Eq. (3.61)]. As an intermediate step for the other pieces, we use Eqs. (3.15) and (3.16) to express $\mathcal{D}_a$ and B_a in terms of hard-core spinful bosons:

$$\mathcal{D}_a = e^{i\pi n_{a,\downarrow}} = e^{i\pi f_{a,\downarrow}^\dagger f_{a,\downarrow}} \tag{3.234}$$

$$B_a = n_{a,\downarrow}b_{a,\uparrow}^\dagger + (1 - n_{a,\downarrow})b_{a,\uparrow}. \tag{3.235}$$

Using Eq. (3.59) in the first equation immediately gives

$$\mathcal{D}_a = (d_a + d_a^\dagger)(c_a^\dagger - c_a). \tag{3.236}$$

The string that relates C_a fermions to B_a bosons [see Eq. (3.126)] is built from

$$e^{i\pi B_a^\dagger B_a} = e^{i\pi(n_{a,\downarrow}+n_{a,\uparrow})}, \tag{3.237}$$

and thus has exactly the same form as the string in Eq. (3.21) that relates spinful fermions $f_{a,\alpha}$ to $b_{a,\alpha}$. Thus, C_a should be locally related to $f_{a,\alpha}$ fermions, and in turn c_a, d_a fermions. Equation (3.235) together with Eqs. (3.19), (3.20), (3.58), and (3.59) specifically yield

$$C_a = \frac{1 - m_a}{2}c_a + \frac{1 + m_a}{2}c_a^\dagger. \tag{3.238}$$

3.17 Acknowledgments

BIBLIOGRAPHY

[1] Ian Affleck, Tom Kennedy, Elliott H. Lieb, and Hal Tasaki. Valence bond ground states in isotropic quantum antiferromagnets. *Comm. Math. Phys.*, 115 (3):477–528, 1988. URL https://projecteuclid.org:443/euclid.cmp/1104161001.

[2] Ramon Aguado. Majorana quasiparticles in condensed matter. *Riv. Nuovo Cimento*, 40:523, 2017. doi: 10.1393/ncr/i2017-10141-9.

[3] F. C. Alcaraz, M. N. Barber, M. T. Batchelor, R. J. Baxter, and G. R. W. Quispel. Surface exponents of the quantum XXZ, Ashkin-Teller and Potts models. *Journal of Physics A: Mathematical and General*, 20(18):6397, 1987. URL http://stacks.iop.org/0305-4470/20/i=18/a=038.

[4] A. Alexandradinata, N. Regnault, Chen Fang, Matthew J. Gilbert, and B. Andrei Bernevig. Parafermionic phases with symmetry breaking and topological order. *Phys. Rev. B*, 94:125103, Sep 2016. doi: 10.1103/PhysRevB.94.125103. URL https://link.aps.org/doi/10.1103/PhysRevB.94.125103.

[5] Jason Alicea. New directions in the pursuit of Majorana fermions in solid state systems. *Reports on Progress in Physics*, 75(7):076501, 2012. doi: 10.1088/0034-4885/75/7/076501. URL http://stacks.iop.org/0034-4885/75/i=7/a=076501.

[6] Jason Alicea and Paul Fendley. Topological phases with parafermions: theory and blueprints. *Annual Review of Condensed Matter Physics*, 7:119, 2016. doi: 10.1146/annurev-conmatphys-031115-011336.

[7] Jason Alicea, Yuval Oreg, Gil Refael, Felix von Oppen, and Matthew P. A. Fisher. Non-Abelian statistics and topological quantum information processing in 1D wire networks. *Nat. Phys.*, 7(5):412–417, 05 2011. doi: 10.1038/nphys1915.

[8] F. Anfuso and A. Rosch. String order and adiabatic continuity of haldane chains and band insulators. *Phys. Rev. B*, 75:144420, Apr 2007. doi: 10.1103/PhysRevB.75.144420. URL https://link.aps.org/doi/10.1103/PhysRevB.75.144420.

[9] J. Ashkin and E. Teller. Statistics of two-dimensional lattices with four components. *Phys. Rev.*, 64:178–184, Sep 1943. doi: 10.1103/PhysRev.64.178. URL https://link.aps.org/doi/10.1103/PhysRev.64.178.

[10] Maissam Barkeshli and Xiao-Liang Qi. Topological nematic states and non-Abelian lattice dislocations. *Phys. Rev. X*, 2:031013, Aug 2012. doi: 10.1103/PhysRevX.2.031013.

[11] Maissam Barkeshli and Xiao-Liang Qi. Synthetic topological qubits in conventional bilayer quantum Hall systems. *Phys. Rev. X*, 4:041035, Nov 2014. doi: 10.1103/PhysRevX.4.041035. URL http://link.aps.org/doi/10.1103/PhysRevX.4.041035.

[12] Maissam Barkeshli, Chao-Ming Jian, and Xiao-Liang Qi. Twist defects and projective non-Abelian braiding statistics. *Phys. Rev. B*, 87:045130, Jan 2013. doi: 10.1103/PhysRevB.87.045130.

[13] Maissam Barkeshli, Parsa Bonderson, Meng Cheng, and Zhenghan Wang. Symmetry fractionalization, defects, and gauging of topological phases. *Phys. Rev. B*, 100:115147, Sep 2019. doi: 10.1103/PhysRevB.100.115147. URL https://link.aps.org/doi/10.1103/PhysRevB.100.115147.

[14] C. W. J. Beenakker. Search for Majorana fermions in superconductors. *Annu. Rev. Con. Mat. Phys.*, 4:113–136, 2013. doi: 10.1146/annurev-conmatphys-030212-184337.

[15] Erez Berg, Michael Levin, and Ehud Altman. Quantized pumping and topology of the phase diagram for a system of interacting bosons. *Phys. Rev. Lett.*, 106:110405, Mar 2011. doi: 10.1103/PhysRevLett.106.110405. URL https://link.aps.org/doi/10.1103/PhysRevLett.106.110405.

[16] H. Bombin. Topological order with a twist: Ising anyons from an Abelian model. *Phys. Rev. Lett.*, 105:030403, Jul 2010. doi: 10.1103/PhysRevLett.105.030403.

[17] Roberto Bondesan and Thomas Quella. Topological and symmetry broken phases of Z_N parafermions in one dimension. *J. Stat. Mech.*, 2013(10): P10024, 2013. URL http://stacks.iop.org/1742-5468/2013/i=10/a=P10024.

[18] Alessio Calzona, Tobias Meng, Maura Sassetti, and Thomas L. Schmidt. $\mathbb{z}_4$ parafermions in one-dimensional fermionic lattices. *Phys. Rev. B*, 98:201110, Nov 2018. doi: 10.1103/PhysRevB.98.201110. URL https://link.aps.org/doi/10.1103/PhysRevB.98.201110.

[19] Alberto Camjayi, Liliana Arrachea, Armando Aligia, and Felix von Oppen. Fractional spin and Josephson effect in time-reversal-invariant topological superconductors. *Phys. Rev. Lett.*, 119:046801, Jul 2017. doi: 10.1103/PhysRevLett.119.046801. URL https://link.aps.org/doi/10.1103/PhysRevLett.119.046801.

[20] Jing-Yuan Chen, Jun Ho Son, Chao Wang, and S. Raghu. Exact boson-fermion duality on a 3D Euclidean lattice. *Phys. Rev. Lett.*, 120:016602, Jan 2018. doi: 10.1103/PhysRevLett.120.016602. URL https://link.aps.org/doi/10.1103/PhysRevLett.120.016602.

[21] Xie Chen, Zheng-Cheng Gu, and Xiao-Gang Wen. Complete classification of one-dimensional gapped quantum phases in interacting spin systems. *Phys. Rev. B*, 84:235128, Dec 2011. doi: 10.1103/PhysRevB.84.235128.

[22] Xie Chen, Zheng-Cheng Gu, and Xiao-Gang Wen. Classification of gapped symmetric phases in one-dimensional spin systems. *Phys. Rev. B*, 83:035107, Jan 2011. doi: 10.1103/PhysRevB.83.035107. URL https://link.aps.org/doi/10.1103/PhysRevB.83.035107.

[23] Xie Chen, Zheng-Cheng Gu, Zheng-Xin Liu, and Xiao-Gang Wen. Symmetry protected topological orders and the group cohomology of their symmetry group. *Phys. Rev. B*, 87:155114, Apr 2013. doi: 10.1103/PhysRevB.87.155114. URL https://link.aps.org/doi/10.1103/PhysRevB.87.155114.

[24] Meng Cheng. Superconducting proximity effect on the edge of fractional topological insulators. *Phys. Rev. B*, 86:195126, Nov 2012. doi: 10.1103/PhysRevB.86.195126. URL https://link.aps.org/doi/10.1103/PhysRevB.86.195126.

[25] Meng Cheng and Roman Lutchyn. Fractional Josephson effect in number-conserving systems. *Phys. Rev. B*, 92:134516, Oct 2015. doi: 10.1103/PhysRevB.92.134516. URL https://link.aps.org/doi/10.1103/PhysRevB.92.134516.

[26] T.-P. Choy, J. M. Edge, A. R. Akhmerov, and C. W. J. Beenakker. Majorana fermions emerging from magnetic nanoparticles on a superconductor without spin-orbit coupling. *Phys. Rev. B*, 84:195442, Nov 2011. doi: 10.1103/PhysRevB.84.195442.

[27] Suk Bum Chung, Joshua Horowitz, and Xiao-Liang Qi. Time-reversal anomaly and Josephson effect in time-reversal-invariant topological superconductors. *Phys. Rev. B*, 88:214514, Dec 2013. doi: 10.1103/PhysRevB.88.214514. URL https://link.aps.org/doi/10.1103/PhysRevB.88.214514.

[28] David J. Clarke, Jay D. Sau, and Sumanta Tewari. Majorana fermion exchange in quasi-one-dimensional networks. *Phys. Rev. B*, 84:035120, Jul 2011. doi: 10.1103/PhysRevB.84.035120.

[29] David J. Clarke, Jason Alicea, and Kirill Shtengel. Exotic non-Abelian anyons from conventional fractional quantum Hall states. *Nature Commun.*, 4:1348, 2013. doi: 10.1038/ncomms2340.

[30] Sankar Das Sarma, Michael Freedman, and Chetan Nayak. Majorana zero modes and topological quantum computation. *NPJ Quantum Information*, 1:15001, 2015. doi: 10.1038/npjqi.2015.1.

[31] Marcel den Nijs and Koos Rommelse. Preroughening transitions in crystal surfaces and valence-bond phases in quantum spin chains. *Phys. Rev. B*, 40:4709–4734, Sep 1989. doi: 10.1103/PhysRevB.40.4709. URL https://link.aps.org/doi/10.1103/PhysRevB.40.4709.

[32] Steven R. Elliott and Marcel Franz. *Colloquium* : Majorana fermions in nuclear, particle, and solid-state physics. *Rev. Mod. Phys.*, 87:137–163, Feb 2015. doi: 10.1103/RevModPhys.87.137.

[33] Benjamin E. Feldman, Mallika T. Randeria, Jian Li, Sangjun Jeon, Yonglong Xie, Zhijun Wang, Ilya K. Drozdov, B. Andrei Bernevig, and Ali Yazdani. High-resolution studies of the Majorana atomic chain platform. *Nature Physics*, 13:286, 2017. doi: 10.1038/nphys3947.

[34] Paul Fendley. Parafermionic edge zero modes in $\mathbb{Z}_n$-invariant spin chains. *J. Stat. Mech.*, 2012(11):11020, 2012. doi: 10.1088/1742-5468/2012/11/P11020.

[35] Lukasz Fidkowski and Alexei Kitaev. Effects of interactions on the topological classification of free fermion systems. *Phys. Rev. B*, 81:134509, Apr 2010. doi: 10.1103/PhysRevB.81.134509.

[36] Matthew P. A. Fisher and Leonid I. Glazman. Transport in a one-dimensional luttinger liquid. In L L. Sohn, Kouwenhoven L.P., and Schön G., editors, *Mesoscopic Electron Transport*, volume 345 of *NATO ASI Series (Series E: Applied Sciences)*. Springer, Dordrecht, 1997.

[37] E. Fradkin and L. P. Kadanoff. Disorder variables and parafermions in two-dimensional statistical mechanics. *Nucl. Phys. B*, 170:1, 1980. doi: 10.1016/0550-3213(80)90472-1.

[38] Pin Gao, Ying-Ping He, and Xiong-Jun Liu. Symmetry-protected non-Abelian braiding of Majorana Kramers pairs. *Phys. Rev. B*, 94:224509, Dec 2016. doi: 10.1103/PhysRevB.94.224509. URL https://link.aps.org/doi/10.1103/PhysRevB.94.224509.

[39] Hart Goldman and Eduardo Fradkin. Loop models, modular invariance, and three-dimensional bosonization. *Phys. Rev. B*, 97:195112, May 2018. doi: 10.1103/PhysRevB.97.195112. URL https://link.aps.org/doi/10.1103/PhysRevB.97.195112.

[40] Arbel Haim, Anna Keselman, Erez Berg, and Yuval Oreg. Time-reversal-invariant topological superconductivity induced by repulsive interactions in quantum wires. *Phys. Rev. B*, 89:220504, Jun 2014. doi: 10.1103/PhysRevB.89.220504. URL https://link.aps.org/doi/10.1103/PhysRevB.89.220504.

[41] Arbel Haim, Erez Berg, Karsten Flensberg, and Yuval Oreg. No-go theorem for a time-reversal invariant topological phase in noninteracting systems coupled to conventional superconductors. *Phys. Rev. B*, 94:161110, Oct 2016. doi: 10.1103/PhysRevB.94.161110. URL https://link.aps.org/doi/10.1103/PhysRevB.94.161110.

[42] Arbel Haim, Konrad Wölms, Erez Berg, Yuval Oreg, and Karsten Flensberg. Interaction-driven topological superconductivity in one dimension. *Phys. Rev. B*, 94:115124, Sep 2016. doi: 10.1103/PhysRevB.94.115124. URL https://link.aps.org/doi/10.1103/PhysRevB.94.115124.

[43] F. D. M. Haldane. Nonlinear field theory of large-spin heisenberg antiferromagnets: Semiclassically quantized solitons of the one-dimensional easy-axis néel state. *Phys. Rev. Lett.*, 50:1153–1156, Apr 1983. doi: 10.1103/PhysRevLett.50.1153. URL https://link.aps.org/doi/10.1103/PhysRevLett.50.1153.

[44] Matthew B. Hastings, Chetan Nayak, and Zhenghan Wang. Metaplectic anyons, Majorana zero modes, and their computational power. *Phys. Rev. B*, 87:165421, Apr 2013. doi: 10.1103/PhysRevB.87.165421.

[45] Haiping Hu, Fan Zhang, and Chuanwei Zhang. Majorana doublets, flat bands, and dirac nodes in *s*-wave superfluids. *Phys. Rev. Lett.*, 121:185302, Nov 2018. doi: 10.1103/PhysRevLett.121.185302. URL https://link.aps.org/doi/10.1103/PhysRevLett.121.185302.

[46] Hoi-Yin Hui and Jay D. Sau. 8π-periodic dissipationless ac Josephson effect on a quantum spin Hall edge via a quantum magnetic impurity. *Phys. Rev. B*, 95:014505, Jan 2017. doi: 10.1103/PhysRevB.95.014505. URL https://link.aps.org/doi/10.1103/PhysRevB.95.014505.

[47] Adrian Hutter and Daniel Loss. Quantum computing with parafermions. *Phys. Rev. B*, 93:125105, Mar 2016. doi: 10.1103/PhysRevB.93.125105. URL https://link.aps.org/doi/10.1103/PhysRevB.93.125105.

[48] Adrian Hutter, James R. Wootton, and Daniel Loss. Parafermions in a kagome lattice of qubits for topological quantum computation. *Phys. Rev. X*, 5:041040, Dec 2015. doi: 10.1103/PhysRevX.5.041040. URL https://link.aps.org/doi/10.1103/PhysRevX.5.041040.

[49] Fernando Iemini, Christophe Mora, and Leonardo Mazza. Topological phases of parafermions: A model with exactly solvable ground states. *Phys. Rev. Lett.*, 118:170402, Apr 2017. doi: 10.1103/PhysRevLett.118.170402. URL https://link.aps.org/doi/10.1103/PhysRevLett.118.170402.

[50] D. A. Ivanov. Non-Abelian statistics of half-quantum vortices in *p*-wave superconductors. *Phys. Rev. Lett.*, 86:268–271, Jan 2001. doi: 10.1103/PhysRevLett.86.268.

[51] Sangjun Jeon, Yonglong Xie, Jian Li, Zhijun Wang, B. Andrei Bernevig, and Ali Yazdani. Distinguishing a Majorana zero mode using spin-resolved measurements. *Science*, 358(6364):772, 2017. doi: 10.1126/science.aan3670.

[52] Adam S. Jermyn, Roger S. K. Mong, Jason Alicea, and Paul Fendley. Stability of zero modes in parafermion chains. *Phys. Rev. B*, 90:165106, Oct 2014. doi: 10.1103/PhysRevB.90.165106.

[53] Shamit Kachru, Michael Mulligan, Gonzalo Torroba, and Huajia Wang. Bosonization and mirror symmetry. *Phys. Rev. D*, 94:085009, Oct 2016. doi: 10.1103/PhysRevD.94.085009. URL https://link.aps.org/doi/10.1103/PhysRevD.94.085009.

[54] Shamit Kachru, Michael Mulligan, Gonzalo Torroba, and Huajia Wang. Nonsupersymmetric dualities from mirror symmetry. *Phys. Rev. Lett.*, 118:011602, Jan 2017. doi: 10.1103/PhysRevLett.118.011602. URL https://link.aps.org/doi/10.1103/PhysRevLett.118.011602.

[55] C L Kane and Fan Zhang. The time reversal invariant fractional Josephson effect. *Physica Scripta*, 2015(T164):014011, 2015. URL http://stacks.iop.org/1402-4896/2015/i=T164/a=014011.

[56] Andreas Karch and David Tong. Particle-vortex duality from 3D bosonization. *Phys. Rev. X*, 6:031043, Sep 2016. doi: 10.1103/PhysRevX.6.031043. URL http://link.aps.org/doi/10.1103/PhysRevX.6.031043.

[57] Anna Keselman, Liang Fu, Ady Stern, and Erez Berg. Inducing time-reversal-invariant topological superconductivity and fermion parity pumping in quantum wires. *Phys. Rev. Lett.*, 111:116402, Sep 2013. doi: 10.1103/PhysRevLett.111.116402. URL https://link.aps.org/doi/10.1103/PhysRevLett.111.116402.

[58] Alexei Yu Kitaev. Unpaired Majorana fermions in quantum wires. *Sov. Phys.–Uspeki*, 44(10S):131, October 2001. doi: 10.1070/1063-7869/44/10S/S29.

[59] Alexei Yu Kitaev. Fault-tolerant quantum computation by anyons. *Ann. Phys.*, 303:2–30, 2003. doi: 10.1016/S0003-4916(02)00018-0.

[60] Jelena Klinovaja and Daniel Loss. Parafermions in an interacting nanowire bundle. *Phys. Rev. Lett.*, 112:246403, Jun 2014. doi: 10.1103/PhysRevLett.112.246403. URL http://link.aps.org/doi/10.1103/PhysRevLett.112.246403.

[61] Jelena Klinovaja and Daniel Loss. Time-reversal invariant parafermions in interacting Rashba nanowires. *Phys. Rev. B*, 90:045118, Jul 2014. doi: 10.1103/PhysRevB.90.045118. URL http://link.aps.org/doi/10.1103/PhysRevB.90.045118.

[62] Mahito Kohmoto, Marcel den Nijs, and Leo P. Kadanoff. Hamiltonian studies of the $d = 2$ Ashkin-Teller model. *Phys. Rev. B*, 24:5229–5241, Nov 1981. doi: 10.1103/PhysRevB.24.5229. URL https://link.aps.org/doi/10.1103/PhysRevB.24.5229.

[63] P. Lecheminant, Alexander O. Gogolin, and Alexander A. Nersesyan. Criticality in self-dual sine-Gordon models. *Nuclear Physics B*, 639(3): 502 – 523, 2002. doi: http://dx.doi.org/10.1016/S0550-3213(02)00474-1. URL http://www.sciencedirect.com/science/article/pii/S0550321302004741.

[64] Martin Leijnse and Karsten Flensberg. Introduction to topological super-conductivity and Majorana fermions. *Semicond. Sci. Technol.*, 27:124003, 2012.

[65] Netanel H. Lindner, Erez Berg, Gil Refael, and Ady Stern. Fractionalizing Majorana fermions: Non-Abelian statistics on the edges of Abelian quantum Hall states. *Phys. Rev. X*, 2:041002, Oct 2012. doi: 10.1103/PhysRevX.2.041002.

[66] R. M. Lutchyn, E. P. A. M. Bakkers, L. P. Kouwenhoven, P. Krogstrup, C. M. Marcus, and Y. Oreg. Majorana zero modes in superconductor-semiconductor heterostructures. *Nature Reviews Materials*, 3(5):52–68, 2018. ISSN 2058-8437. doi: 10.1038/s41578-018-0003-1. URL https://doi.org/10.1038/s41578-018-0003-1.

[67] M. F. Maghrebi, S. Ganeshan, D. J. Clarke, A. V. Gorshkov, and J. D. Sau. Parafermionic zero modes in ultracold bosonic systems. *Phys. Rev. Lett.*, 115:065301, Aug 2015. doi: 10.1103/PhysRevLett.115.065301. URL https://link.aps.org/doi/10.1103/PhysRevLett.115.065301.

[68] Leonardo Mazza, Fernando Iemini, Marcello Dalmonte, and Christophe Mora. Nontopological parafermions in a one-dimensional fermionic model with even multiplet pairing. *Phys. Rev. B*, 98:201109, Nov 2018. doi: 10.1103/PhysRevB.98.201109. URL https://link.aps.org/doi/10.1103/PhysRevB.98.201109.

[69] Konstantinos Meichanetzidis, Christopher J. Turner, Ashk Farjami, Zlatko Papić, and Jiannis K. Pachos. Free-fermion descriptions of parafermion chains and string-net models. *Phys. Rev. B*, 97:125104, Mar 2018. doi: 10.1103/PhysRevB.97.125104. URL https://link.aps.org/doi/10.1103/PhysRevB.97.125104.

[70] D. Meidan, E. Berg, and Ady Stern. Classification of topological phases of parafermionic chains with symmetries. *Phys. Rev. B*, 95:205104, May 2017. doi: 10.1103/PhysRevB.95.205104. URL https://link.aps.org/doi/10.1103/PhysRevB.95.205104.

[71] Max A. Metlitski. *S*-duality of $u(1)$ gauge theory with $\theta = \pi$ on non-orientable manifolds: Applications to topological insulators and superconductors. 2015.

[72] Max A. Metlitski and Ashvin Vishwanath. Particle-vortex duality of two-dimensional Dirac fermion from electric-magnetic duality of three-dimensional topological insulators. *Phys. Rev. B*, 93:245151, Jun 2016. doi: 10.1103/PhysRevB.93.245151. URL http://link.aps.org/doi/10.1103/PhysRevB.93.245151.

[73] Roger S. K. Mong, David J. Clarke, Jason Alicea, Netanel H. Lindner, and Paul Fendley. Parafermionic conformal field theory on the lattice. *Journal of Physics A: Mathematical and Theoretical*, 47(45):452001, 2014.

[74] Arianna Montorsi, Fabrizio Dolcini, Rita C. Iotti, and Fausto Rossi. Symmetry-protected topological phases of one-dimensional interacting fermions with spin-charge separation. *Phys. Rev. B*, 95:245108, Jun 2017. doi: 10.1103/PhysRevB.95.245108. URL https://link.aps.org/doi/10.1103/PhysRevB.95.245108.

[75] G. Moore and N. Read. Nonabelions in the fractional quantum Hall effect. *Nucl. Phys. B*, 360:362, 1991.

[76] N. Moran, D. Pellegrino, J. K. Slingerland, and G. Kells. Parafermionic clock models and quantum resonance. *Phys. Rev. B*, 95:235127, Jun 2017. doi: 10.1103/PhysRevB.95.235127. URL https://link.aps.org/doi/10.1103/PhysRevB.95.235127.

[77] Johannes Motruk, Erez Berg, Ari M. Turner, and Frank Pollmann. Topological phases in gapped edges of fractionalized systems. *Phys. Rev. B*, 88:085115, Aug 2013. doi: 10.1103/PhysRevB.88.085115. URL https://link.aps.org/doi/10.1103/PhysRevB.88.085115.

[78] Sanjay Moudgalya and Frank Pollmann. Fragility of symmetry-protected topological order on a hubbard ladder. *Phys. Rev. B*, 91:155128, Apr 2015. doi: 10.1103/PhysRevB.91.155128. URL https://link.aps.org/doi/10.1103/PhysRevB.91.155128.

[79] David F. Mross, Jason Alicea, and Olexei I. Motrunich. Explicit derivation of duality between a free Dirac cone and quantum electrodynamics in (2 + 1) dimensions. *Phys. Rev. Lett.*, 117:016802, Jun 2016. doi: 10.1103/PhysRevLett.117.016802. URL http://link.aps.org/doi/10.1103/PhysRevLett.117.016802.

[80] David F. Mross, Jason Alicea, and Olexei I. Motrunich. Symmetry and duality in bosonization of two-dimensional Dirac fermions. *Phys. Rev. X*, 7:041016, Oct 2017. doi: 10.1103/PhysRevX.7.041016. URL https://link.aps.org/doi/10.1103/PhysRevX.7.041016.

[81] Jeff Murugan and Horatiu Nastase. Particle-vortex duality in topological insulators and superconductors. *Journal of High Energy Physics*, 2017(5): 159, May 2017. ISSN 1029-8479. doi: 10.1007/JHEP05(2017)159. URL https://doi.org/10.1007/JHEP05(2017)159.

[82] S. Nadj-Perge, I. K. Drozdov, B. A. Bernevig, and Ali Yazdani. Proposal for realizing Majorana fermions in chains of magnetic atoms on a superconductor. *Phys. Rev. B*, 88:020407, Jul 2013. doi: 10.1103/PhysRevB.88.020407.

[83] Stevan Nadj-Perge, Ilya K. Drozdov, Jian Li, Hua Chen, Sangjun Jeon, Jungpil Seo, Allan H. MacDonald, B. Andrei Bernevig, and Ali Yazdani. Observation of Majorana fermions in ferromagnetic atomic chains on a superconductor. *Science*, 346(6209):602–607, 2014. doi: 10.1126/science.1259327.

[84] Sho Nakosai, Jan Carl Budich, Yukio Tanaka, Björn Trauzettel, and Naoto Nagaosa. Majorana bound states and nonlocal spin correlations in a quantum wire on an unconventional superconductor. *Phys. Rev. Lett.*, 110:117002, Mar 2013. doi: 10.1103/PhysRevLett.110.117002. URL https://link.aps.org/doi/10.1103/PhysRevLett.110.117002.

[85] Chetan Nayak, Steven H. Simon, Ady Stern, Michael Freedman, and Sankar Das Sarma. Non-Abelian anyons and topological quantum computation. *Rev. Mod. Phys.*, 80:1083–1159, Sep 2008.

[86] Yuval Oreg, Eran Sela, and Ady Stern. Fractional helical liquids in quantum wires. *Phys. Rev. B*, 89:115402, Mar 2014. doi: 10.1103/PhysRevB. 89.115402. URL http://link.aps.org/doi/10.1103/PhysRevB.89. 115402.

[87] Christoph P. Orth, Rakesh P. Tiwari, Tobias Meng, and Thomas L. Schmidt. Non-Abelian parafermions in time-reversal-invariant interacting helical systems. *Phys. Rev. B*, 91:081406, Feb 2015. doi: 10.1103/PhysRevB.91. 081406.

[88] Remy Pawlak, Marcin Kisiel, Jelena Klinovaja, Tobias Meier, Shigeki Kawai, Thilo Glatzel, Daniel Loss, and Ernst Meyer. Probing atomic structure and Majorana wavefunctions in mono-atomic Fe chains on superconducting Pb surface. *NPJ Quantum Information*, 2:16035, 2016. doi: 10.1038/npjqi.2016. 35.

[89] Christopher J. Pedder, Tobias Meng, Rakesh P. Tiwari, and Thomas L. Schmidt. Missing Shapiro steps and the 8π-periodic Josephson effect in interacting helical electron systems. *Phys. Rev. B*, 96:165429, Oct 2017. doi: 10.1103/PhysRevB.96.165429. URL https://link.aps.org/doi/10.1103/PhysRevB.96.165429.

[90] Yang Peng, Yuval Vinkler-Aviv, Piet W. Brouwer, Leonid I. Glazman, and Felix von Oppen. Parity anomaly and spin transmutation in quantum spin Hall

Josephson junctions. *Phys. Rev. Lett.*, 117:267001, Dec 2016. doi: 10.1103/PhysRevLett.117.267001. URL https://link.aps.org/doi/10.1103/PhysRevLett.117.267001.

[91] Xiao-Liang Qi, Taylor L. Hughes, and Shou-Cheng Zhang. Fractional charge and quantized current in the quantum spin Hall state. *Nature Physics*, 4:273, 2008. doi: 10.1038/nphys913.

[92] Xiao-Liang Qi, Taylor L. Hughes, S. Raghu, and Shou-Cheng Zhang. Time-reversal-invariant topological superconductors and superfluids in two and three dimensions. *Phys. Rev. Lett.*, 102:187001, May 2009. doi: 10.1103/PhysRevLett.102.187001. URL https://link.aps.org/doi/10.1103/PhysRevLett.102.187001.

[93] Xiao-Liang Qi, Taylor L. Hughes, and Shou-Cheng Zhang. Topological invariants for the Fermi surface of a time-reversal-invariant superconductor. *Phys. Rev. B*, 81:134508, Apr 2010. doi: 10.1103/PhysRevB.81.134508. URL https://link.aps.org/doi/10.1103/PhysRevB.81.134508.

[94] Michael Ruby, Falko Pientka, Yang Peng, Felix von Oppen, Benjamin W. Heinrich, and Katharina J. Franke. End states and subgap structure in proximity-coupled chains of magnetic adatoms. *Phys. Rev. Lett.*, 115:197204, Nov 2015. doi: 10.1103/PhysRevLett.115.197204. URL https://link.aps.org/doi/10.1103/PhysRevLett.115.197204.

[95] Masatoshi Sato and Satoshi Fujimoto. Majorana fermions and topology in superconductors. *Journal of the Physical Society of Japan*, 85(7):072001, 2016. doi: 10.7566/JPSJ.85.072001.

[96] Norbert Schuch, David Pérez-García, and Ignacio Cirac. Classifying quantum phases using matrix product states and projected entangled pair states. *Phys. Rev. B*, 84:165139, Oct 2011. doi: 10.1103/PhysRevB.84.165139.

[97] Nathan Seiberg, T. Senthil, Chong Wang, and Edward Witten. A duality web in 2+1 dimensions and condensed matter physics. *Annals of Physics*, 374:395 – 433, 2016. ISSN 0003-4916. doi: http://dx.doi.org/10.1016/j.aop.2016.08.007. URL http://www.sciencedirect.com/science/article/pii/S0003491616301531.

[98] Dam Thanh Son. Is the composite fermion a Dirac particle? *Phys. Rev. X*, 5:031027, Sep 2015. doi: 10.1103/PhysRevX.5.031027. URL http://link.aps.org/doi/10.1103/PhysRevX.5.031027.

[99] Tudor D. Stanescu and Sumanta Tewari. Majorana fermions in semiconductor nanowires: Fundamentals, modeling, and experiment. *J. Phys.: Condens. Matter*, 25:233201, 2013.

[100] E. M. Stoudenmire, Jason Alicea, Oleg A. Starykh, and Matthew P.A. Fisher. Interaction effects in topological superconducting wires supporting Majorana fermions. *Phys. Rev. B*, 84:014503, Jul 2011. doi: 10.1103/PhysRevB. 84.014503. URL https://link.aps.org/doi/10.1103/PhysRevB.84. 014503.

[101] A. M. Tsvelik. $\mathbb{Z}_N$ parafermion zero modes without fractional quantum Hall effect. unpublished, 2014.

[102] Ari M. Turner, Frank Pollmann, and Erez Berg. Topological phases of one-dimensional fermions: An entanglement point of view. *Phys. Rev. B*, 83(7): 075102, Feb 2011.

[103] Christopher J. Turner, Konstantinos Meichanetzidis, Zlatko Papic, and Jiannis K. Pachos. Optimal free descriptions of many-body theories. *Nature Communications*, 8:14926, 2017. doi: 10.1038/ncomms14926.

[104] Abolhassan Vaezi. Fractional topological superconductor with fractionalized Majorana fermions. *Phys. Rev. B*, 87:035132, Jan 2013. doi: 10.1103/ PhysRevB.87.035132.

[105] Yuval Vinkler-Aviv, Piet W. Brouwer, and Felix von Oppen. $\mathbb{Z}_4$ parafermions in an interacting quantum spin Hall Josephson junction coupled to an impurity spin. *Phys. Rev. B*, 96:195421, Nov 2017. doi: 10.1103/PhysRevB. 96.195421. URL https://link.aps.org/doi/10.1103/PhysRevB.96. 195421.

[106] Chong Wang and T. Senthil. Dual Dirac liquid on the surface of the electron topological insulator. *Phys. Rev. X*, 5:041031, Nov 2015. doi: 10. 1103/PhysRevX.5.041031. URL http://link.aps.org/doi/10.1103/ PhysRevX.5.041031.

[107] Chris L. M. Wong and K. T. Law. Majorana Kramers doublets in $d_{x^2-y^2}$-wave superconductors with Rashba spin-orbit coupling. *Phys. Rev. B*, 86:184516, Nov 2012. doi: 10.1103/PhysRevB.86.184516. URL https://link.aps. org/doi/10.1103/PhysRevB.86.184516.

[108] Masanori Yamanaka, Yasuhiro Hatsugai, and Mahito Kohmoto. Phase diagram of the Ashkin-Teller quantum spin chain. *Phys. Rev. B*, 50:559–562, Jul 1994. doi: 10.1103/PhysRevB.50.559. URL https://link.aps.org/ doi/10.1103/PhysRevB.50.559.

[109] Sung-Kil Yang. $Z_4 \times Z_4$ symmetry and parafermion operators in the self-dual critical Ashkin-Teller model. *Nuclear Physics B*, 285(Supplement C):639 – 650, 1987. doi: https://doi.org/10.1016/0550-3213(87)90359-2. URL http://www.sciencedirect.com/science/article/pii/ 0550321387903592.

[110] Yi-Zhuang You and Xiao-Gang Wen. Projective non-Abelian statistics of dislocation defects in a $\mathbb{Z}_N$ rotor model. *Phys. Rev. B*, 86:161107, Oct 2012. doi: 10.1103/PhysRevB.86.161107.

[111] Fan Zhang and C. L. Kane. Time-reversal-invariant Z_4 fractional Josephson effect. *Phys. Rev. Lett.*, 113:036401, Jul 2014. doi: 10.1103/PhysRevLett. 113.036401.

[112] Fan Zhang, C. L. Kane, and E. J. Mele. Time-reversal-invariant topological superconductivity and Majorana Kramers pairs. *Phys. Rev. Lett.*, 111:056402, Aug 2013. doi: 10.1103/PhysRevLett.111.056402. URL https://link. aps.org/doi/10.1103/PhysRevLett.111.056402.

Chapter 4

TIME-CRYSTALLINE TOPOLOGICAL SUPERCONDUCTORS

4.1 Introduction

Periodically driven quantum systems evade certain constraints imposed in equilibrium. For instance, 'time crystals' that spontaneously break time-translation symmetry in the sense envisioned in Refs. [29, 34] cannot arise in equilibrium [33], yet can emerge with periodic driving. In periodically driven time crystals *any* physical (i.e., non-cat) state evolves with a subharmonic of the drive frequency [11, 15, 36]. The canonical realization consists of disordered Ising spins that collectively flip after each drive period, thereby requiring two periods to recover their initial state. Experiments have detected signatures of time crystallinity both in driven cold atoms [30, 38] and solid-state spin systems [7, 22, 25].

As a second, deeply related example, consider a one-dimensional (1D) free-fermion topological superconductor hosting Majorana end modes [16], each described by a Hermitian operator γ. If γ adds energy E then $\gamma^\dagger$ adds $-E$, while Hermiticity requires that these be equivalent. In equilibrium the unique solution is $E = 0$—corresponding to the well-studied Majorana zero modes. Periodically driving with frequency Ω additionally permits 'Floquet Majorana modes' carrying $E = \Omega/2$ since energy is then only conserved mod Ω [14]. Floquet Majorana modes have been proposed to facilitate more efficient quantum information processing compared to equilibrium systems [2, 4, 5]. Moreover, they encode a topological flavor of time-translation symmetry breaking in that Floquet Majorana operators change sign each drive cycle, thus also requiring two periods to recover their initial form.

We merge the phenomena above by exploring periodically driven 1D topological superconductors generated upon coupling Cooper-paired electrons to doubled-periodicity time-crystalline Ising spins. Such 'time-crystalline topological superconductors' intertwine bulk time-translation symmetry breaking and topological physics, yielding anomalous *quadrupled-periodicity* Floquet Majorana modes that categorically can not arise in free-fermion platforms. We propose implementation via quantum-dot arrays (see Fig. 41) reminiscent of setups utilized in Refs. [8, 12, 28] for engineering equilibrium Majorana zero modes. We derive and analyze an exactly solvable, physically intuitive model for time-crystalline topological superconductiv-
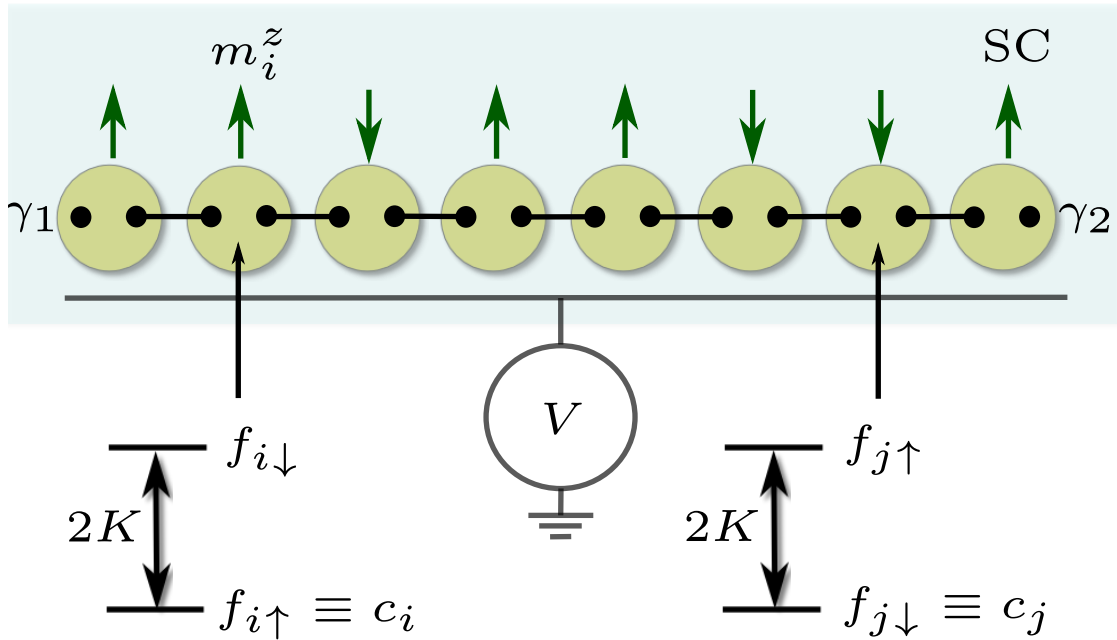
Figure 41: Proximitized quantum-dot array coupled to Ising spins. The Ising spins polarize the dot electrons—effectively producing a system of spinless fermions c_j. In any Ising configuration, the fermions can realize topological superconductivity with unpaired Majorana zero modes $\gamma_{1,2}$ that intertwine with the adjacent spins.

ity and show that probing junctions between time-crystalline and static topological superconductors reveals the Floquet Majorana modes' quadrupled periodicity.

4.2 Model and Setup

Time-crystalline topological superconductors closely relate to equilibrium topological superconductors that spontaneously violate electronic time-reversal symmetry $\mathcal{T}$, which importantly satisfies $\mathcal{T}^2 = -1$. We thus begin by modeling the latter. Our setup, sketched in Fig. 41, consists of a superconductor coupled to a chain of quantum dots indexed by sites j, each hosting one active spinful level described by operators $f_{j\sigma}$ ($\sigma = \uparrow, \downarrow$ denotes spin); we assume that charging energy is quenched by coupling to the superconductor and can thus be neglected. A chain of Ising spins described by Pauli matrices m_j^z resides proximate to the quantum-dot array. We

model the setup with a $\mathcal{T}$-symmetric Hamiltonian $H = H_0 + H_f$, where

$$H_0 = \sum_j (-Jm_j^z m_{j+1}^z - Km_j^z f_j^\dagger \sigma^z f_j), \tag{4.1}$$

$$H_f = \sum_j [-\mu f_j^\dagger f_j - t(f_j^\dagger f_{j+1} + H.c.)$$

$$+ \alpha(if_j^\dagger \sigma^x f_{j+1} + H.c.) + \Delta(f_{j\uparrow} f_{j\downarrow} + H.c.)]. \tag{4.2}$$

In H_0, $J > 0$ ferromagnetically couples neighboring Ising spins and $K > 0$ couples the Ising and dot spins. Terms in H_f describe the chemical potential (μ), hopping (t), spin-orbit coupling (α), and proximity-induced pairing (Δ) for the quantum-dot electrons.

Suppose that the K term dominates and energetically enforces alignment of each electron spin with the nearest Ising spin. Only one of the two spinful levels in each dot remains active at low energies—effectively creating a system of spinless fermions described by operators

$$c_j = \frac{1}{2}\left[(1 + m_j^z)f_{j\uparrow} + (1 - m_j^z)f_{j\downarrow}\right], \tag{4.3}$$

as Fig. 41 illustrates. Time-reversal $\mathcal{T}$ sends $m_j^z \to -m_j^z$ and $c_j \to m_j^z c_j$, thus satisfying time-reversal symmetry. This intertwinement between spinless fermions and Ising spins is unavoidable; without it, c_j has no way of acquiring the required minus sign upon two applications of $\mathcal{T}$.

In Section 4.8 we project H onto the spinless-fermion subspace by integrating out high-energy fermionic modes, yielding an effective Hamiltonian

$$H_{\mathrm{eff}} = \sum_j [-Jm_j^z m_{j+1}^z - \mu' c_j^\dagger c_j$$

$$+ (t'_{m_j^z, m_{j+1}^z} c_j^\dagger c_{j+1} + \Delta'_{m_j^z, m_{j+1}^z} c_j c_{j+1} + H.c.)]. \tag{4.4}$$

Here $\mu' = -(K + \mu)$ is a renormalized chemical potential, while $t'_{m_j^z, m_{j+1}^z} = a + a^* m_j^z m_{j+1}^z$ and $\Delta'_{m_j^z, m_{j+1}^z} = bm_j^z - b^* m_{j+1}^z$ denote Ising-spin-dependent effective hopping and p-wave pairing amplitudes, with $a = (-t+i\alpha)/2$ and $b = (-t+i\alpha)\Delta/(K-\mu)$. The real part of a sets the hopping strength between sites with aligned Ising spins, which is directly inherited from spin-conserving tunneling in Eq. (4.2); the imaginary part similarly fixes the hopping when Ising spins anti-align, which is instead mediated by spin-orbit coupling α. Pairing in H_{eff} follows from second-order processes that involve virtual excitations out of the spinless-fermion subspace—hence

the $K - \mu$ energy denominator in b. Depending on the Ising configuration, either spin-conserving hopping or spin-orbit coupling virtually creates a doubly-occupied site of f fermions that then Cooper pair via the original s-wave Δ term, effectively mediating p-wave pairing of spinless fermions.

4.3 Phase Diagram

Equation (4.4) describes a strongly interacting system of Ising spins and fermions. Nevertheless, for any given Ising configuration the model reduces to free fermions. Consider first uniformly polarized all-up or all-down Ising spins. Here Eq. (4.4) maps to the familiar Kitaev chain [16] with uniform hopping strength $2|a| \cos \phi_a$ and pairing $\pm 2i|b| \sin \phi_b$, where $a = |a|e^{i\phi_a}$ and $b = |b|e^{i\phi_b}$. (Our derivation above yielded $\phi_a = \phi_b$, though it will be useful to now keep these phases independent.) Accordingly, the chain hosts edge Majorana zero modes provided the chemical potential intersects the band and pairing is finite, i.e., for $|\mu'| < 4|a||\cos \phi_a|$ and $\sin \phi_b \neq 0$ as sketched in Fig. 42(a).

To examine the fermionic ground state with random Ising spins—which is our main interest—we compute the correlation length ξ using the transfer-matrix technique; see, e.g, Ref. [19] and Section 4.9. This method allows us to map out phase boundaries by numerically searching for diverging ξ as we vary $\phi_{a,b}$; for our purposes a regular 400×400 grid of ϕ_a and ϕ_b values in the interval $[-\pi/2, \pi/2]$ is sufficient. [Exploiting $\xi(\phi_a, \phi_b) = \xi(-\phi_a, -\phi_b)$ halves the number of simulations]. Figure 42(b) illustrates representative results obtained for $\mu' = |b| = |a|/4$ and $N = 10^6$ sites. The data points indicate local maxima where ξ is typically of order 10^2 or larger, while it is of order unity elsewhere. We expect these peaks to represent true divergences in ξ when ϕ_a or ϕ_b are tuned continuously in the thermodynamic limit. Topological regions are easily identified via exact diagonalization on smaller systems and confirming the presence of edge Majorana zero modes. In Section 4.10 we analytically capture the topological phase for a restricted window of $\phi_{a,b}$ via the Born approximation.

For our quantum-dot setup, we expect $\phi_a = \phi_b$ [red line in Fig. 42(b)] and also $|a| \gg |b|$ since p-wave pairing encoded in b appears at second order in perturbation theory. Starting from the topological phase in this physical regime, Fig. 42(b) strongly suggests that we can deform parameters to $\phi_a = \pi/4$ and $\phi_b = -\pi/4$, $|a| = |b|$, and $\mu' = 0$ without encountering a divergent ξ. (See Section 4.9 for additional evidence.) This special point corresponds to the model's zero-correlation-
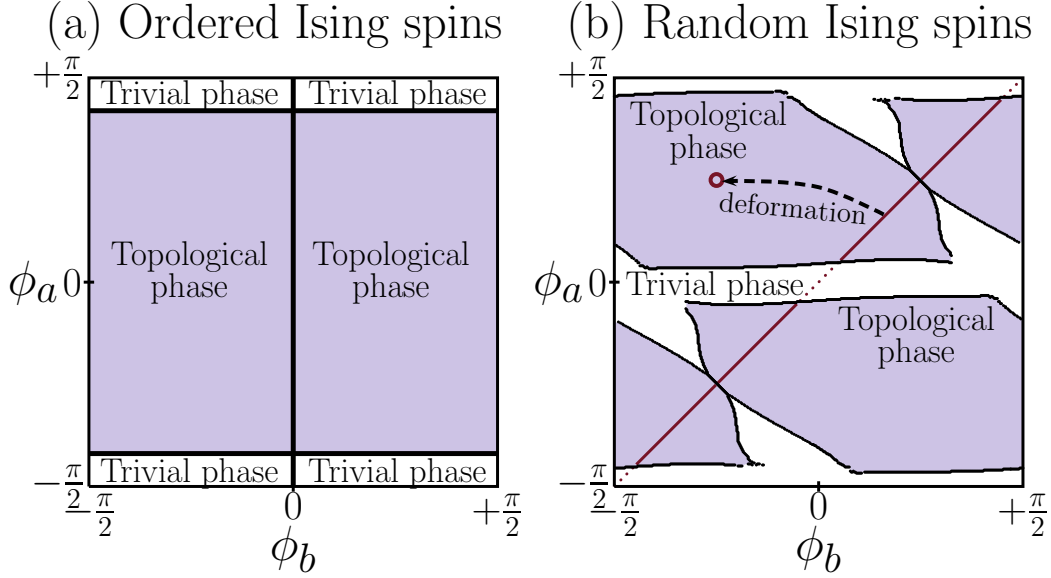
Figure 42: Phase diagram for Eq. (4.4) assuming (a) fully polarized and (b) random Ising spins. In (a) a nonzero chemical potential $\mu' = |a|$ generates the trivial phase, and the system is gapless along the thick black lines. Data in (b) were generated from transfer-matrix simulations at $\mu' = |b| = |a|/4$ with 10^6 sites. Data points indicate sharp peaks in the localization length, as expected at a topological phase transition. The red diagonal line $\phi_a = \phi_b$ is relevant for the physical quantum-dot setup from Fig. 41. As the dashed arrow illustrates, the topological phase along this line can be deformed to the zero-correlation-length limit with $\phi_a = \pi/4$, $\phi_b = -\pi/4$ (and also $|a| = |b|$, $\mu' = 0$) without crossing a phase boundary.

length limit. Here it is convenient to decompose the spinless fermions in terms of Majorana operators $\eta_{A,Bj}$ via $c_j = e^{-i\frac{\pi}{4}m_j^z}(\eta_{Bj} + i\eta_{Aj})$, whereupon Eq. (4.4) becomes

$$H'_{\text{eff}} = \sum_j (-Jm_j^z m_{j+1}^z - i\kappa s_{m_j^z, m_{j+1}^z} \eta_{Aj}\eta_{Bj+1}) \tag{4.5}$$

with $s_{m_i, m_j} = (1 - m_i + m_j + m_i m_j)/2 = \pm 1$ and $\kappa = 4\sqrt{2}|a|$. *For any choice of m_j^z's* the Majorana operators dimerize nontrivially as shown in Fig. 41, yielding Majorana zero modes

$$\begin{aligned}
\gamma_1 &\equiv \eta_{B1} = e^{i\frac{\pi}{4}m_1^z}c_1 + H.c. \\
\gamma_2 &\equiv \eta_{AN} = -ie^{i\frac{\pi}{4}m_N^z}c_N + H.c.
\end{aligned} \tag{4.6}$$

at the leftmost and rightmost sites. Notice the spin-fermion intertwinement inherent in the zero modes, which consequently evolve under $\mathcal{T}$ via

$$\gamma_1 \to m_1^z\gamma_1, \quad \gamma_2 \to -m_N^z\gamma_2, \tag{4.7}$$

again consistent with $\mathcal{T}^2 = -1$. All Hamiltonian eigenstates are at least fourfold degenerate in this limit: one factor of two arises because $\mathcal{T}$ flips all Ising spins, while the other reflects topological degeneracy encoded in the Majorana zero modes. The topological degeneracy of the fermionic ground states given a static Ising configuration persists even away from the special limit examined above, due to the finite gap for fermionic excitations. Moreover, Section 4.11 shows that Eq. (4.7) holds even when the zero-mode wavefunctions extend over many sites.

4.4 Adiabatic cycle

Next we generalize Eq. (4.1) to

$$H_0' = \sum_j [-J(\hat{\mathbf{n}} \cdot \mathbf{m}_j)(\hat{\mathbf{n}} \cdot \mathbf{m}_{j+1}) - K(\hat{\mathbf{n}} \cdot \mathbf{m}_j)f_j^\dagger \hat{\mathbf{n}} \cdot \boldsymbol{\sigma} f_j], \qquad (4.8)$$

where $\mathbf{m}, \boldsymbol{\sigma}$ denote vectors of Pauli matrices and the unit vector $\hat{\mathbf{n}} \equiv \cos\theta\hat{\mathbf{z}} + \sin\theta\hat{\mathbf{y}}$ determines the easy axis for the Ising spins. At either $\theta = 0$ or π, H_0' reduces to Eq. (4.1). Suppose that we again deform to the zero-correlation-length limit (which is possible for any θ) and then implement the following cycle: (*i*) Start with an arbitrary Ising spin configuration at $\theta = 0$, (*ii*) initialize the fermions into one of the topological-superconductor ground states, and finally (*iii*) adiabatically rotate the easy axis by winding θ from 0 to π.

Although the Hamiltonian returns to its original form, *the wavefunctions do not*. Rather, the cycle slowly rotates all Ising spins by π, while the fermions follow their instantaneous minimum-energy configuration given the adiabaticity. The initial ground state thereby transforms into its time-reversed counterpart. One rotation sends $m_j^z \to -m_j^z$, $f_j \to e^{i\frac{\pi}{2}\sigma^x} f_j$, and hence $c_j \to ic_j$. Majorana zero modes thus transform as $\gamma_1 \to m_1^z\gamma_1$ and $\gamma_2 \to m_N^z\gamma_2$, similar to the action of $\mathcal{T}$. Interestingly, two cycles return the Ising spins to their original form whereas *four cycles* are required to recover the initial zero-mode operators, e.g.,

$$\gamma_1 \to m_1^z\gamma_1 \to -\gamma_1 \to -m_1^z\gamma_1 \to \gamma_1. \qquad (4.9)$$

4.5 Time-crystalline topological superconductivity and detection

We now promote the adiabatic ground-state phenomenon described above to a dynamic phenomenon applicable to *arbitrary* physical states. To this end we apply a variation of the preceding cycle periodically with period T, thus generating time-crystalline topological superconductivity. We specifically consider a binary drive
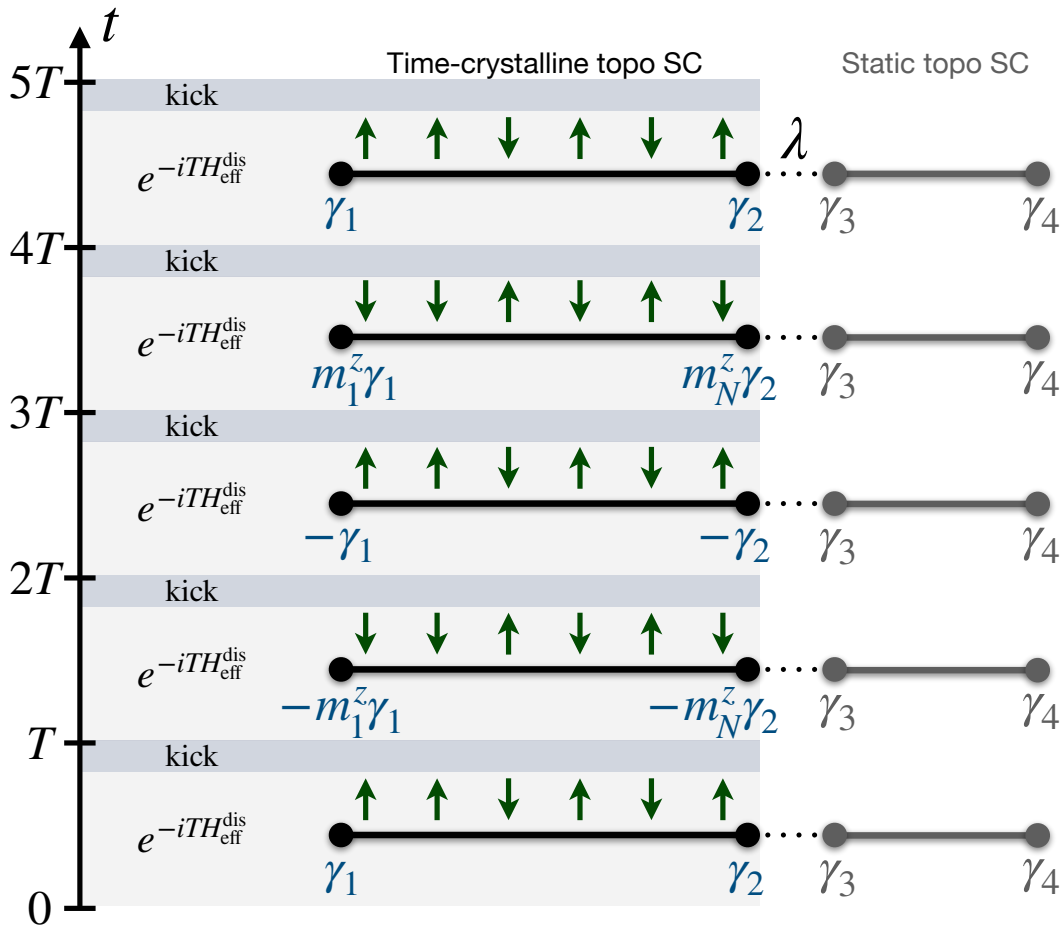
Figure 43: Time evolution for the time-crystalline topological superconductor generated by Eq. (4.10) at $\epsilon = 0$. Each period T globally flips all Ising spins, yielding doubled-periodicity bulk response, whereas the Floquet Majorana modes $\gamma_{1,2}$ exhibit quadrupled-periodicity response that can be probed in the junction with the static topological superconductor on the right. The inner Majorana modes $\gamma_{2,3}$ hybridize with coupling strength λ. Since γ_3 is static while γ_2 evolves nontrivially after each period T, the junction's energy inherits the latter's quadrupled periodicity.

such that the Floquet operator that evolves the system over a single period reads

$$U_T = e^{-i(\pi/2-\epsilon)\sum_j(m_j^x + c_j^\dagger c_j)} e^{-iTH_{\mathrm{eff}}^{dis}}. \tag{4.10}$$

The right exponential evolves the system with respect to a disordered, static Hamiltonian H_{eff}^{dis} that is the same as Eq. (4.4) but with J, a, b replaced with random site-dependent couplings J_j, a_j, b_j. We neglect randomness in the phases of a_j, b_j and treat J_j, a_j, b_j as independent random variables with magnitudes drawn from uniform distributions $[\bar{J} - \delta J, \bar{J} + \delta J], [\bar{a} - \delta a, \bar{a} + \delta a], [\bar{b} - \delta b, \bar{b} + \delta b]$. Disorder crucially introduces many-body localization (MBL) into the dynamics and prevents heating to infinite temperatures [1, 9, 13, 17, 23]. The left exponential in Eq. (4.10) performs an instantaneous 'kick' that (at least approximately) flips the Ising spins via a transverse magnetic field pulse and applies a potential to the spinless fermions—thereby mimicking evolution from our adiabatic cycle without the adiabaticity requirement.

The dynamics is analytically tractable at $\epsilon = 0$ and when H_{eff}^{dis} reduces to Eq. (4.5) with random couplings J_j, κ_j. Starting from any Ising configuration, the 'perfect' kick in U_T sends $m_j^z \to -m_j^z$ and thus flips all spins, signifying period-doubling time crystallinity in the spin sector. In the fermionic sector, $\gamma_{1,2}$ in Eq. (4.6) continue to commute with H_{eff}^{dis} despite the randomness. The kick, however, nontrivially transforms the Majorana edge operators so that $U_T\gamma_1 U_T^\dagger = m_1^z\gamma_1$ and $U_T\gamma_2 U_T^\dagger = m_N^z\gamma_2$. Precisely as illustrated in Eq. (4.9), $\gamma_{1,2}$ therefore require *four* drive periods to recover their initial form, i.e., they form the hallmark quadrupled-periodicity Floquet Majorana modes. Shaded regions of Fig. 43 summarize the evolution.

Quadrupled periodicity can be experimentally probed in junctions between time-crystalline and static topological superconductors as in the right side of Fig. 43, wherein γ_3 and γ_4 denote time-independent Majorana zero modes. Electron tunneling across the junction couples γ_2 with γ_3, producing a Hamiltonian term $H_{23} = i\lambda\gamma_2\gamma_3$ for some λ that may depend on the adjacent Ising spins. Consequently, the junction's energy density (among other local properties) directly manifests the quadrupled-periodicity built into the anomalous Floquet Majorana mode γ_2.

Rigidity against 'imperfect' drives is a crucial feature of time-crystalline phases [11, 15, 32, 36]. Here, such imperfection arises from taking $\epsilon \neq 0$ and H_{eff}^{dis} away from the zero-correlation-length limit, which spoils exact solvability and prompts us to turn to numerics.

4.6 Numerics

We employ time-evolving block decimation (TEBD), using a maximum bond dimension of $\chi = 50$, on a 20-site system with random Ising spins and parameters appropriate for our quantum-dot setup: $\phi_a = \phi_b = \pi/8$, $\bar{b} = \bar{a}/2$, $\bar{J} = \bar{a}/4$, $\mu' = 0$, $\delta a = \delta b = \delta J = \bar{a}/8$. Our simulations incorporate a decoupled, static zero-energy fermion c_0 that functions similarly to the static topological superconductor in Fig. 43. We initialize into a state that entangles the static fermion with the rest of the system. We then simulate the Floquet operator in Eq. (4.10) with $\bar{a}T = 2$ and $\bar{a}T = 0.2$, and with the kick shifted away from commensurability by $\epsilon = 0.2$ [1]. Despite the rather small system size, in both cases the bond dimension quickly saturated, and the truncation error was relatively coarse. To check robustness of our numerics we repeated the computations for maximum bond dimension $\chi = 25$, and the results agreed with those at $\chi = 50$.

Over a run of 60 Floquet evolutions and 150 disorder averages, we measure the Ising spin $\langle m^z_{j=10} \rangle$ in the middle of the system as well as $\langle c_0^\dagger c_1 \rangle$, where c_1 corresponds to the leftmost quantum dot. The former probes bulk time crystallinity while the latter probes the Floquet Majorana modes. Figure 42 plots the Fourier transform of both quantities as a function of frequency ω normalized by $\Omega = 2\pi/T$. For $\bar{a}T = 2$ the data show the rigidity characteristic of a time crystal: despite the imperfect drive, the bulk magnetization and edge fermion bilinear respectively remain peaked at $\omega = \Omega/2$ and $\omega = 3\Omega/4$ (as expected for doubled-periodicity Ising spins and quadrupled periodicity Floquet Majorana modes). By contrast, in our $\bar{a}T = 0.2$ simulations both peaks clearly shift due to non-zero ϵ, indicating an absence of rigid time-crystallinity for this case. We also ran exact numerics on a 7-site system and measured the level-spacing statistics of the U_T eigenvalues. At $\bar{a}T = 2$ the mean level spacing was approximately 0.39, close to the Poisson value 0.386 expected for MBL [21].

4.7 Discussion

The admixture of symmetry breaking and topology is known to generate new physics in static systems; examples include 8π-periodic Josephson effects [20, 37] and enrichment of Majorana braiding and fusion [6]. Our work establishes that driven systems can be similarly enriched by 'decorating' topological phases with spontaneous time-translation symmetry breaking. We specifically showed that 1D time-crystalline topological superconductors engineered from quantum-dot arrays host

---

[1] Calculations were performed using the ITensor Library, http://itensor.org.
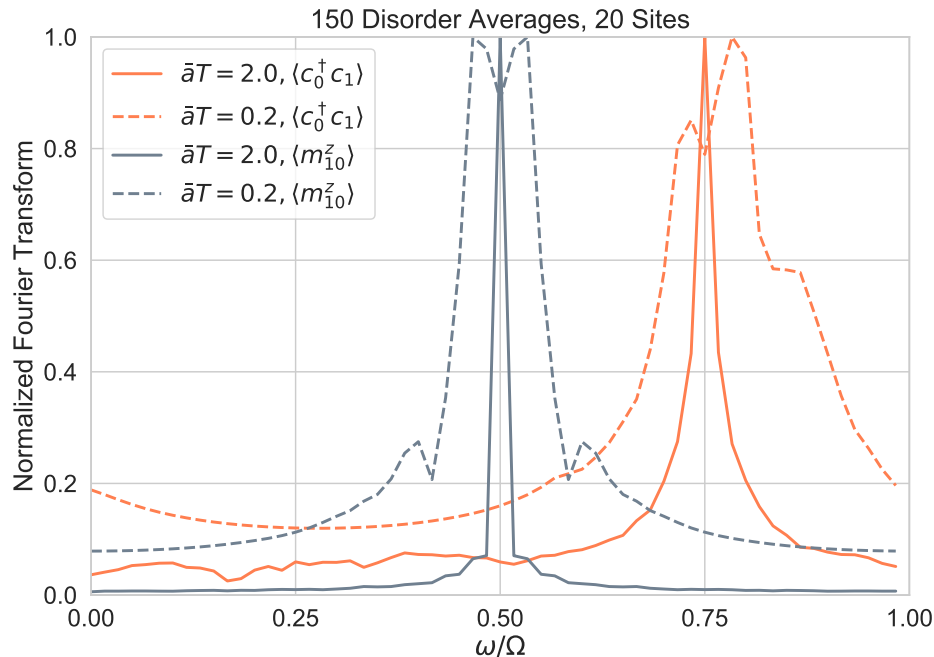
Figure 44: Fourier transform of the quantities shown in the legend following time evolution via Eq. (4.10) with $\epsilon = 0.2$ and parameters specified in the main text. Data are normalized by setting the maximum of each Fourier spectrum to 1, and frequency ω on the horizontal axis is normalized by $\Omega = 2\pi/T$, with T the drive period. Here m_{10}^z represents an Ising spin at the center of the chain, c_0 is an auxiliary zero-energy static fermion that enables probing the Floquet Majorana mode periodicity, and c_1 is the fermion at the left end of the quantum-dot chain. For initialization we use random Ising configurations and random fermionic states that entangle c_0 with the rest of the system. Runs were repeated 150 times for disorder averaging with maximum bond dimension $\chi = 50$; similar results were obtained with $\chi = 25$. For $\bar{a}T = 2$ sharp peaks persist at $\Omega/2$ and $3\Omega/4$—despite 'imperfect' driving generated by $\epsilon \neq 0$—indicating 'rigid' doubled-periodicity Ising spins and quadrupled-periodicity Floquet Majorana modes characteristic of time-crystalline topological superconductivity. For $\bar{a}T = 0.2$, the imperfect drive pushes the peak frequencies away from these quantized values, indicating a loss of rigid time crystallinity.

novel Floquet Majorana modes that display anomalously long periodicity not possible with free fermions. Exotic states of this type are not captured by the cohomology classification of interacting topological Floquet phases [10, 24, 26, 27, 31]. In future work, it would be interesting to explore similarly enriched *two-dimensional* (2D) phases. Driven spinless 2D $p+ip$ superconductors also support doubled-periodicity Floquet Majorana modes [3, 18, 35] and thus constitute natural candidate platforms. One could envision promoting spinless fermions in such systems to spinful fermions coupled to magnetic degrees of freedom as done here, possibly leading to new higher-dimensional adiabatic cycles, time-crystalline topological phases, and nontrivial pre-thermal regimes.

4.8 Derivation of effective spinless-fermion Hamiltonian

Here we derive the effective Hamiltonian given in Eq. (4.4) that describes the quantum dots and Ising spins in the limit of large K. We start from the original microscopic model $H = H_0 + H_f$ [recall Eq. (4.2)] and decompose the spinful fermions via

$$f_{j\uparrow} = \frac{1}{2}[(1 + m_j^z)c_j + (1 - m_j^z)d_j] \tag{4.11}$$

$$f_{j\downarrow} = \frac{1}{2}[(1 - m_j^z)c_j + (1 + m_j^z)d_j]. \tag{4.12}$$

Here c_j are precisely the low-energy fermionic degrees of freedom from Eq. (4.3) that minimize the energy of the K term, while d_j represent high-energy fermions that we wish to formally integrate out. In terms of c_j and d_j, we have

$$H_0 = \sum_j [-Jm_j^z m_{j+1}^z - K(c_j^\dagger c_j - d_j^\dagger d_j)] \tag{4.13}$$

and

$$\begin{aligned}
H_f = \sum_j \Big\{ &- \mu(c_j^\dagger c_j + d_j^\dagger d_j) \\
&+ [(-tP_{j1} + i\alpha P_{j2})(c_j^\dagger c_{j+1} + d_j^\dagger d_{j+1}) + H.c.] \\
&+ [(-tP_{j2} + i\alpha P_{j1})(c_j^\dagger d_{j+1} + d_j^\dagger c_{j+1}) + H.c.] \\
&+ \Delta m_j^z(c_j d_j + H.c.)\Big\}.
\end{aligned} \tag{4.14}$$

In Eq. (4.14) we introduced projectors

$$P_{j1} = \frac{1}{2}(1 + m_j^z m_{j+1}^z), \quad P_{j2} = \frac{1}{2}(1 - m_j^z m_{j+1}^z) \tag{4.15}$$

that project onto states where nearest-neighbor Ising spins are aligned and anti-aligned, respectively.

The formal elimination of d_j's is conveniently carried out within a (Euclidean) path-integral formalism, with the zero-temperature partition function given by

$$Z = \int \mathcal{D}d^\dagger \mathcal{D}d \mathcal{D}c^\dagger \mathcal{D}c e^{-S}, \tag{4.16}$$

where

$$S = \int_{-\infty}^{\infty} d\tau \left[\sum_j (c_j^\dagger \partial_\tau c_j + d_j^\dagger \partial_\tau d_j) + H \right] \tag{4.17}$$

is the imaginary-time action. Upon integrating over $d_j, d_j^\dagger$ (which can be done exactly since H is quadratic in fermions), the partition function can be written as

$$Z \propto \int \mathcal{D}c^\dagger \mathcal{D}c e^{-S_{eff}}$$

$$S_{eff} = \int_{-\infty}^{\infty} \frac{d\omega}{2\pi} \left[\sum_j (-i\omega c_j^\dagger c_j) + \mathcal{H}_{eff}(\omega) \right]. \tag{4.18}$$

In the low-frequency limit, i.e., $|\omega| \ll (K-\mu)$, we can neglect frequency dependence in $\mathcal{H}_{eff}$ to obtain an effective spinless-fermion Hamiltonian that takes the form of Eq. (4.4). Finally, upon truncating the chemical potential, hopping, and pairing matrix elements to leading nontrivial order in $1/(K-\mu)$, we obtain precisely the $\mu', t'_{m_j^z, m_{j+1}^z}, \Delta'_{m_j^z, m_{j+1}^z}$ couplings quoted in the main text.

4.9 Transfer-matrix details

To examine the fermionic ground state for random Ising spins we express the model of Eq. (4.4) in terms of transfer matrices. The equation of motion for $\psi_j = (c_j, c_j^\dagger)$ can be brought to the form

$$\begin{pmatrix} \psi_{j+1} \\ F_j^\dagger \psi_j \end{pmatrix} = T_j \begin{pmatrix} \psi_j \\ F_{j-1}^\dagger \psi_{j-1} \end{pmatrix}, \tag{4.19}$$

with

$$T_j = \begin{pmatrix} F_j^{-1}[E - \mu\sigma^z] & -F_j^{-1} \\ F_j^\dagger & 0 \end{pmatrix}, \tag{4.20}$$

$$F_j = \begin{pmatrix} t'_{m_j^z, m_{j+1}^z} & -\Delta'^*_{m_j^z, m_{j+1}^z} \\ \Delta'_{m_j^z, m_{j+1}^z} & -t'^*_{m_j^z, m_{j+1}^z} \end{pmatrix}. \tag{4.21}$$
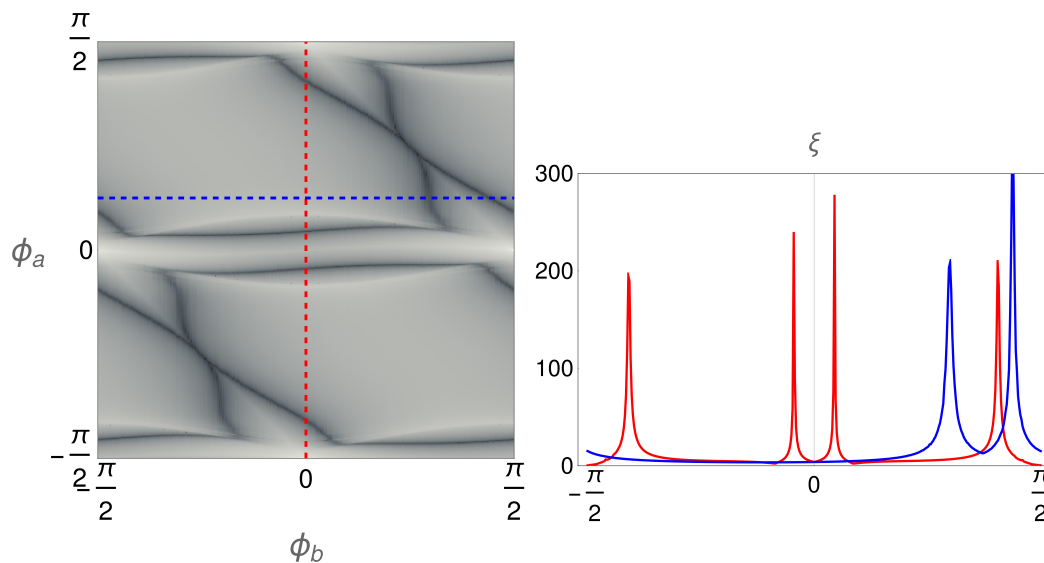
Figure 45: Transfer-matrix data for $\mu' = |b| = |a|/4$ and 10^6 sites. On the left we show a density map of $\log(\xi)$, with darker shades denoting larger ξ. The phase boundaries are readily apparent as narrow dark lines. The dashed lines denote two specific cuts for which we show ξ on a linear scale on the right. The very rapid divergence of ξ near specific points supports our identification of the phase boundaries.

The transfer matrix for an N-site chain is $Q = \prod_{j=1}^{N} T_j$, and the smallest positive eigenvalue of $\frac{1}{N} \log[QQ^\dagger]$ is the inverse localization length ξ^{-1} (see, e.g., [19]). In Fig. 45 we present the data from which the phase diagram in Fig. 42 of the main text is obtained. First, we show a two-dimensional density map of ξ on a logarithmic scale, which reveals the phase boundaries without any need for processing the data. Second, we show ξ on a linear scale for two representative cuts to illustrate the rapid growth of ξ near phase boundaries.

Finally, we detune the parameters of the models from the ones of Fig. 42—which relate to the microscopic model—towards the exactly solvable point $|a| = |b|$ and $\mu' = 0$; see Fig. 46. [In Figs. 45 and 46 we do not use the relation $\xi(\phi_a, \phi_b) = \xi(-\phi_a, -\phi_b)$ to halve the data points, contrary to Fig. 42(b) from the main text.] During this deformation the phase boundaries move substantially, but at the specific value $\phi_a = -\phi_b = \pi/4$ the system always remains in the same strongly localized topological phase. Consequently, the topological phase obtained with microscopically derived parameters indeed smoothly connects to the zero-correlation length limit $\phi_a = -\phi_b = \pi/4$, $|a| = |b|$, and $\mu' = 0$ as suggested by Fig. 42(b) from the main text.
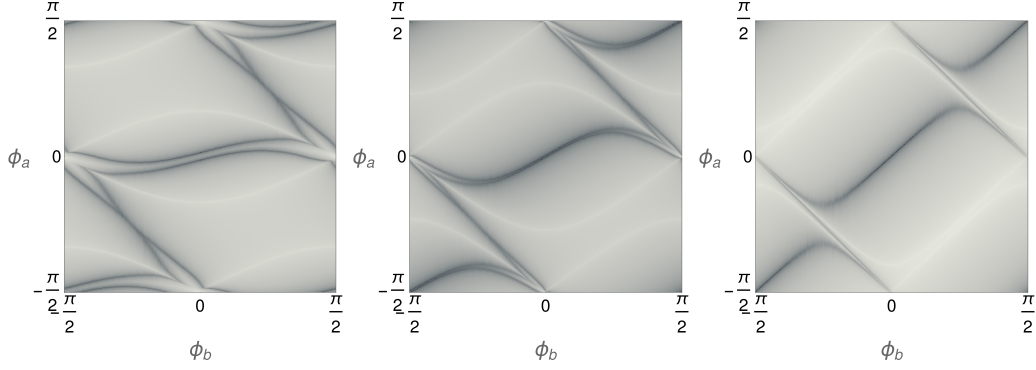
Figure 46: Density maps of $\log(\xi)$ for (left) $\mu' = |a|/8$ and $|b| = |a|/2$, (middle) $\mu' = |a|/20$ and $|b| = 3|a|/4$, and (right) $\mu' = |a|/50$ and $|b| = 0.95|a|$. The phase boundaries change significantly between these parameter values, but the special point $\phi_a = -\phi_b = \pi/4$ always remains deeply in the localized topological phase.

4.10 Majorana Zero Modes via the Born Approximation

For certain values of a, b, we can use the Born approximation to capture Majorana zero modes in the Hamiltonian of Eq. (4.4) with random m_j^z Ising configurations. In what follows we ignore the J term for simplicity. Suppose that we perform the gauge transformation

$$c_j \rightarrow e^{i\frac{\pi}{4}(1-m_1^z)}e^{-i\frac{\pi}{4}[1+\sum_{k<j}(1-m_k^z m_{k+1}^z)]}c_j, \qquad (4.22)$$

so that Eq. (4.4) becomes

$$H_{eff} = \sum_j[-\mu'c_j^\dagger c_j + (t''_{m_j^z,m_{j+1}^z}c_j^\dagger c_{j+1} + \Delta''_{m_j^z,m_{j+1}^z}c_j c_{j+1} + H.c.)]. \qquad (4.23)$$

The new hopping and pairing coefficients are given by

$$t''_{m_j^z,m_{j+1}^z} = \frac{(ae^{-i\frac{\pi}{4}} + c.c.)}{\sqrt{2}} + \frac{m_j^z m_{j+1}^z(ae^{i\frac{\pi}{4}} + c.c.)}{\sqrt{2}} \qquad (4.24)$$

$$\Delta''_{m_j^z,m_{j+1}^z} = \frac{(-be^{i\frac{\pi}{4}} + c.c.)}{\sqrt{2}} + \frac{m_j^z m_{j+1}^z(be^{-i\frac{\pi}{4}} + c.c.)}{\sqrt{2}}. \qquad (4.25)$$

As before we write $a = |a|e^{i\phi_a}$ and $b = |b|e^{i\phi_b}$. Notice that at $\phi_a = \pi/4$ and $\phi_b = -\pi/4$, which are the same phases used to access the zero-correlation limit, *the m_j^z dependence has been completely gauged out of the Hamiltonian for any $|a|, |b|$.* We immediately conclude that at these phases the system harbors edge Majorana zero modes regardless of the Ising configuration provided $|\mu'| < 2\sqrt{2}|a|$.

Suppose next that we deform away from this limit by writing $\phi_a = \pi/4 + \epsilon_a$ and $\phi_b = -\pi/4 + \epsilon_b$, where $|\epsilon_{a,b}| \ll 1$. The m_j^z dependence no longer drops out, and

for random Ising configurations can be viewed as generating weak disorder in the fermion hoppings and pairings. To lowest order in the Born approximation this disorder is treated by simply replacing $H_{\text{eff}} \to \overline{H_{\text{eff}}}$ with the overline indicating a disorder average over m_j^z configurations. Here and below we will assume that the m_j^z's are uncorrelated from site to site and have zero mean (as appropriate for the random Ising configurations that are our primary interest). The hopping and pairing strengths accordingly become

$$\overline{t''_{m_j^z, m_{j+1}^z}} = \sqrt{2}|a| \cos \epsilon_a, \quad \overline{\Delta''_{m_j^z, m_{j+1}^z}} = -\sqrt{2}|b| \cos \epsilon_b. \tag{4.26}$$

Within this approximation edge Majorana zero modes persist so long as $|\mu'| < 2\sqrt{2}|a| \cos \epsilon_a$.

Thus far we have made no assumptions about the relative strength of $|a|$ and $|b|$. Additional progress is possible if we specialize to the (most physically relevant) regime $|a| \gg |b|$, which we now assume. We continue to take $\phi_a = \pi/4 + \epsilon_a$ but now allow for general ϕ_b, and treat ϵ_a as well as the entire pairing term as perturbations. Within the lowest-order Born approximation the hopping and pairing strengths are now modified to

$$\overline{t''_{m_j^z, m_{j+1}^z}} = \sqrt{2}|a| \cos \epsilon_a, \tag{4.27}$$

$$\overline{\Delta''_{m_j^z, m_{j+1}^z}} = -\sqrt{2}|b| \cos(\phi_b + \pi/4). \tag{4.28}$$

At this order, edge Majorana zero modes appear when $|\mu'| < 2\sqrt{2}|a| \cos \epsilon_a$ *and* $\cos(\phi_b + \pi/4) \neq 0$. These criteria naively rule out Majorana zero modes when $\phi_b = \pi/4$. Nonzero pairing after disorder averaging is, however, generated at *second order* in the Born approximation (at least when $\epsilon_a \neq 0$), so that Majorana zero modes can still emerge as we show next.

Let $\phi_b = \pi/4$ and write the Hamiltonian as $H_{\text{eff}} = H_0 + H_1$, where all m_j^z-dependent terms are lumped into H_1. Explicitly, we have

$$H_0 = \sum_j [-\mu' c_j^\dagger c_j + (\bar{t} c_j^\dagger c_{j+1} + H.c.)] \tag{4.29}$$

$$H_1 = \sum_j m_j^z m_{j+1}^z (t_1 c_j^\dagger c_{j+1} + \Delta_1 c_j c_{j+1} + H.c.) \tag{4.30}$$

with $\bar{t} = \sqrt{2}|a| \cos \epsilon_a$, $t_1 = -\sqrt{2}|a| \sin \epsilon_a$, and $\Delta_1 = \sqrt{2}|b|$. To proceed we switch to first-quantized language, defining position-space Hamiltonian matrix elements

$\mathcal{H}_{0,1;jk}$ through

$$H_{0,1} = \sum_{j,k} \Psi_j^\dagger \mathcal{H}_{0,1;jk} \Psi_k, \tag{4.31}$$

where

$$\Psi_j^\dagger = \begin{bmatrix} c_j^\dagger & c_j \end{bmatrix} \tag{4.32}$$

is the Nambu spinor. In terms of the bare Green's function

$$G_{0;jk}(i\omega) = (i\omega - \mathcal{H}_0)_{jk}^{-1}, \tag{4.33}$$

the fermion self-energy at second order in the Born approximation reads

$$\Sigma_{jk} = \overline{\mathcal{H}_{1;jl} G_{0;lm}(i\omega = 0)\mathcal{H}_{1;mk}}. \tag{4.34}$$

Repeated indices are implicitly summed above. The prefactor $m_j^z m_{j+1}^z$ in $\mathcal{H}_1$ implies that the disorder average is nonzero only when we contract matrix elements corresponding to the same sites, i.e., when $jl = mk$ or $jl = km$.

Disorder averaging effectively restores translation invariance, so it is useful to pass to momentum space. For $\mathcal{H}_0$ we simply write

$$\mathcal{H}_{0;jk} = \int_p e^{ip(j-k)} \mathcal{H}_0(p). \tag{4.35}$$

The Fourier transform is

$$\mathcal{H}_0(p) = \frac{1}{2}(2\bar{t} \cos p - \mu')\tau^z, \tag{4.36}$$

where Pauli matrices $\tau^{x,y,z}$ act in Nambu space. For $\mathcal{H}_1$ we isolate the position-dependent magnetization by instead writing

$$\mathcal{H}_{1;jk} = m_j^z m_k^z \int_p e^{ip(j-k)} \tilde{\mathcal{H}}_1(p), \tag{4.37}$$

which yields

$$\tilde{\mathcal{H}}_1(p) = t_1 \cos p \, \tau^z + \Delta_1 \sin p \, \tau^y. \tag{4.38}$$

We can now express the self-energy as

$$\Sigma_{jk} = \overline{m_j^z m_l^z m_m^z m_k^z} \int_{p_1,p_2} e^{ip_1(j-l)} e^{ip_2(m-k)} \tilde{\mathcal{H}}_1(p_1) G_{0;lm}(i\omega = 0)\tilde{\mathcal{H}}_1(p_2). \tag{4.39}$$

The disorder average on the first line evaluates to

$$\overline{m_j^z m_l^z m_m^z m_k^z} = \delta_{jk}\delta_{lm} + \delta_{jm}\delta_{kl}. \tag{4.40}$$

The first pair of Kronecker deltas involve δ_{jk} and thus merely generate an on-site correction. We neglect this term and instead focus on the second pair of Kronecker deltas:

$$\Sigma_{jk} \rightarrow \int_{p_1,p_2} e^{i(p_1+p_2)(j-k)}\tilde{\mathcal{H}}_1(p_1)G_{0;kj}(i\omega = 0)\tilde{\mathcal{H}}_1(p_2). \tag{4.41}$$

Upon further Fourier transforming the Green's function we obtain

$$\Sigma_{jk} = \int_q e^{iq(j-k)}\Sigma(q) \tag{4.42}$$

$$\Sigma(q) = \int_{p_1,p_2} \tilde{\mathcal{H}}_1(p_1)G_0(i\omega = 0, p_1 + p_2 - q)\tilde{\mathcal{H}}_1(p_2). \tag{4.43}$$

It is useful to now decompose the self energy as

$$\Sigma(q) = \Sigma^z(q)\tau^z + \Sigma^y(q)\tau^y. \tag{4.44}$$

The $\Sigma^z(q)$ part encodes renormalization of the kinetic energy, while $\Sigma^y(q)$ encodes p-wave pairing. The latter is given by

$$\Sigma^y(q) = -2t_1\Delta_1 \int_{p_1,p_2} \frac{\sin(p_1 + p_2)}{2\bar{t}\cos(p_1 + p_2 - q) - \mu'} \tag{4.45}$$

$$= -\frac{t_1\Delta_1}{\bar{t}}f\left(\frac{\mu'}{2\bar{t}}\right)\sin q \tag{4.46}$$

for some nontrivial function $f(x)$ that satisfies $f(x \ll 1) \approx 1$. Provided t_1, Δ_1 are nonzero—which in turn requires nonzero ϵ_a and $|b|$—the pairing amplitude is finite, yielding unpaired Majorana modes if $|\mu'| < 2\sqrt{2}|a|\cos\epsilon_a$ as claimed. We note that the correlated nature of disorder in the tunneling and pairing terms in H_1 is essential to this outcome.

In our second-order Born analysis we set $\phi_b = \pi/4$ exactly. If we now take $\phi_b = \pi/4 + \epsilon_b$ (again with $\epsilon_b \ll 1$) then we can estimate the effective p-wave pairing amplitude Δ_{eff} by simply summing the contributions from Eqs. (4.28) and (4.46). [Technically, taking $\epsilon_b \neq 0$ also modifies Eq. (4.46), though this correction will be small compared to the contribution from Eq. (4.28).] We thereby obtain

$$\Delta_{\mathrm{eff}} \approx \sqrt{2}|b|\epsilon_b - \frac{t_1\Delta_1}{\bar{t}}f\left(\frac{\mu'}{2\bar{t}}\right)$$

$$\approx \sqrt{2}|b|\left[\epsilon_b + \epsilon_a f\left(\frac{\mu'}{2\sqrt{2}|a|}\right)\right], \tag{4.47}$$
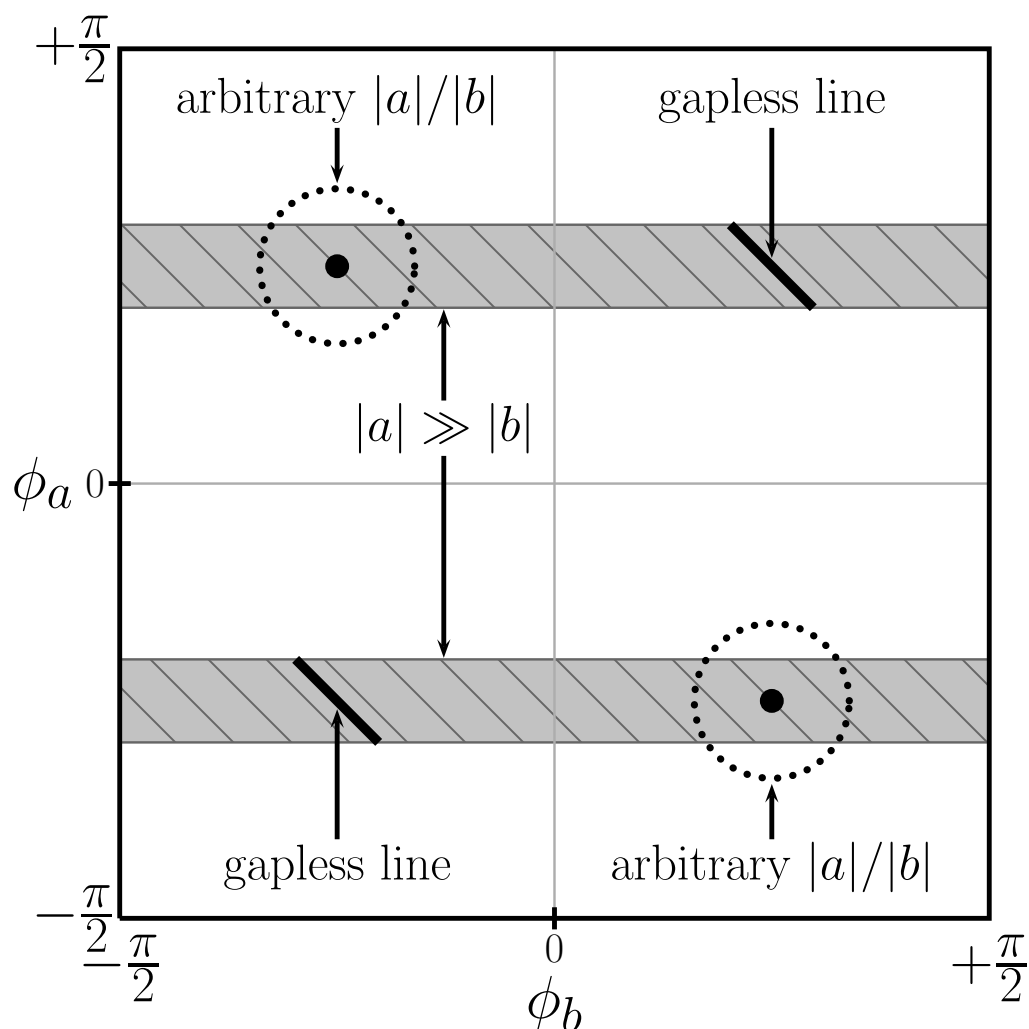
Figure 47: Summary of Born-approximation results. Shaded and circled regions denote $\phi_{a,b}$ values amenable to the Born approximation (assuming the regime of $|a|/|b|$ values indicated). Except for the gapless lines in the upper-right and lower-left quadrants, Majorana zero modes are predicted over a finite window of chemical potential throughout these regions, in agreement with transfer-matrix simulations.

where on the second line we used $t_1/\bar{t} \approx -\epsilon_a, \bar{t} \approx \sqrt{2}|a|$, and $\Delta_1 = \sqrt{2}|b|$. In the limit $\mu' \ll |a|$ we can further replace $f \to 1$; the pairing then vanishes when $\epsilon_b = -\epsilon_a$, which defines a gapless line along which Majorana modes are absent.

Figure 47 summarizes our Born-approximation results, which are fully consistent with our transfer-matrix simulations.

The Born approximation further elucidates the structure of the phase diagram.

After applying the gauge transformation in Eq. (4.22), the Hamiltonian in Eq. (4.23) exhibits purely real couplings. Hence an 'accidental' antiunitary $\mathcal{T}'$ symmetry that obeys $\mathcal{T}'^2 = +1$ becomes manifest. Majorana modes can therefore be classified as 'real' or 'imaginary' depending on whether they exhibit eigenvalues $+1$ or -1 under $\mathcal{T}'$. In the standard, uniform Kitaev chain Hamiltonian, the topological phase can be characterized by the relative sign of the hopping and pairing, $\mathrm{sgn}(t\Delta)$. Should this quantity be positive, the left Majorana zero mode is imaginary while its partner on the right end is real. If the sign is negative, the opposite is true.

Our system is more complex, in that the hopping and pairings depend nontrivially on the Ising configuration in a site-dependent fashion. However, the Born approximation smears out this nontrivial dependence, thereby generating uniform effective hopping and pairing. With $|a| \gg |b|$, $\phi_a = \pi/4 + \epsilon_a$, and $\phi_b = \pi/4 + \epsilon_b$, these quantities are given approximately by Eqs. (4.27) and (4.47). In particular, the effective pairing in Eq. (4.47) changes sign along the gapless lines sketched in Fig. 47—implying that the two topological phases meeting at that line exhibit Majorana zero modes with opposite $\mathcal{T}'$ eigenvalues. More generally, a first-order or continuous phase transition, or an intermediate state, necessarily separates these phases so long as $\mathcal{T}'$ persists.

4.11   Transformation of Majorana Zero Modes

In the main text we deformed our effective spinless-fermion Hamiltonian to the zero-correlation-length limit, yielding Eq. (4.5). Each Majorana zero mode in this limit localizes to a single site as shown in Fig. 41 and Eq. (4.6). Moreover, according to Eq. (4.7) each Majorana zero mode acquires a factor of the adjacent Ising spin, i.e., m_1^z or m_N^z, under time-reversal symmetry $\mathcal{T}$. This transformation rule raises a conundrum: away from the zero-correlation-length limit, the zero-mode wavefunctions extend into the bulk over a distance set by the correlation length, and thus 'sample' not just m_1^z or m_N^z, but many Ising spins. How does $\mathcal{T}$ transform the Majorana zero modes in this more generic situation? The normalization $\gamma^2 = 1$ together with Hermiticity implies that the zero-mode operators can only be multiplied by an operator with eigenvalues ± 1. This discreteness prohibits any perturbative corrections and the transformation in Eq. (4.7) in fact continues to hold more generally. It is instructive to see explicitly how this comes about by perturbing the Hamiltonian Eq. (4.5) away from the perfectly dimerized limit.

Consider the $\mathcal{T}$-invariant Hamiltonian

$$H''_{\text{eff}} = \sum_j \left(- Jm^z_j m^z_{j+1} - i\kappa s_{m^z_j,m^z_{j+1}} \eta_{Aj}\eta_{Bj+1} - i\kappa' \eta_{Aj}\eta_{Bj} \right) \tag{4.48}$$

corresponding to Eq. (4.5) modified by the κ' term—which spoils the perfect dimer-ization and yields a finite correlation length. We assume $|\kappa'| < |\kappa|$ so that the fermions remain in the topological phase, and also take κ' to be independent of m^z_j's since such a choice is compatible with $\mathcal{T}$. In contrast, $\mathcal{T}$ necessitates the nontrivial m^z dependence in the signs $s_{m^z_j,m^z_{j+1}}$. This m^z dependence can nevertheless be absorbed into the Majorana fermions by defining

$$\eta_{A,Bj} \equiv \left(\prod_{k<j} s_{m^z_k,m^z_{k+1}} \right) \tilde{\eta}_{A,Bj}, \tag{4.49}$$

where $\tilde{\eta}_{A,Bj}$ are a new set of Majorana operators. The Hamiltonian becomes

$$H''_{\text{eff}} = \sum_j \left(- Jm^z_j m^z_{j+1} - i\kappa \tilde{\eta}_{Aj}\tilde{\eta}_{Bj+1} - i\kappa' \tilde{\eta}_{Aj}\tilde{\eta}_{Bj} \right). \tag{4.50}$$

Couplings between Majorana fermions in this representation are manifestly independent of the Ising spins.

Because H''_{eff} only couples $\tilde{\eta}_{Ai}$ Majorana fermions to $\tilde{\eta}_{Bj}$ Majorana fermions, the Hamiltonian preserves an 'accidental' antiunitary symmetry $\mathcal{T}'$ (see also Appendix 4.10) that obeys $(\mathcal{T}')^2 = +1$ and sends

$$m^z_j \rightarrow m^z_j, \quad \tilde{\eta}_{Aj} \rightarrow -\tilde{\eta}_{Aj}, \quad \tilde{\eta}_{Bj} \rightarrow \tilde{\eta}_{Bj}. \tag{4.51}$$

The zero modes $\gamma_{1,2}$ can be defined such that they acquire either $+1$ or -1 eigenvalue under $\mathcal{T}'$, which sharply constrains their allowed form. Additionally incorporating Hermiticity and invoking continuity with the $\kappa' = 0$ limit allows us to write

$$\gamma_1 = \sum_j \phi_{Bj}\tilde{\eta}_{Bj} = \sum_j \phi_{Bj} \left(\prod_{k<j} s_{m^z_k,m^z_{k+1}} \right) \eta_{Bj} \tag{4.52}$$

$$\gamma_2 = S \sum_j \phi_{Aj}\tilde{\eta}_{Aj} = \sum_j \phi_{Aj} \left(\prod_{k\geq j} s_{m^z_k,m^z_{k+1}} \right) \eta_{Aj} \tag{4.53}$$

for real $\phi_{A,Bj}$ that localize exponentially to the ends of the chain and, importantly, do not depend on m^z_j. On the right sides we reverted back to $\eta_{A,Bj}$ operators to explicitly display the *non-local m^z_j dependence* in the zero-mode wavefunctions. In

the second line we introduced a factor $S = \prod_{\text{all sites } j} s_{m_j^z, m_{j+1}^z}$, which causes the string of $s_{m_k^z, m_{k+1}^z}$ signs to emanate from the right in the expression for γ_2. This convention is very natural since γ_2 localizes to the right end of the chain, and moreover correctly recovers the $\kappa' = 0$ limit of γ_2 from Eq. (4.6).

Physical time reversal $\mathcal{T}$ sends

$$\eta_{Aj} \rightarrow m_j^z \eta_{Aj}, \; \eta_{Bj} \rightarrow -m_j^z \eta_{Bj}, \tag{4.54}$$

$$s_{m_j^z, m_{j+1}^z} \rightarrow m_j^z m_{j+1}^z s_{m_j^z, m_{j+1}^z}. \tag{4.55}$$

Using these transformations to enact $\mathcal{T}$ on $\gamma_{1,2}$, one finds that the contribution of each term in the string of $s_{m_j^z, m_{j+1}^z}$ signs cancels with the next, except at the very ends of the chains. One thus recovers Eq. (4.7) as claimed.

4.12 Acknowledgments

BIBLIOGRAPHY

[1] Dmitry A. Abanin, Wojciech De Roeck, and François Huveneers. Theory of many-body localization in periodically driven systems. *Annals of Physics*, 372: 1 – 11, 2016. ISSN 0003-4916. doi: https://doi.org/10.1016/j.aop.2016.03. 010. URL http://www.sciencedirect.com/science/article/pii/ S000349161630001X.

[2] Bela Bauer, T. Pereg-Barnea, Torsten Karzig, Maria-Theresa Rieder, Gil Refael, Erez Berg, and Yuval Oreg. Topologically protected braiding in a single wire using floquet majorana modes, 2018.

[3] Zi bo Wang, Hua Jiang, Haiwen Liu, and X.C. Xie. Floquet majorana fermions in driven hexagonal lattice systems. *Solid State Communications*, 215-216:18 – 26, 2015. ISSN 0038-1098. doi: https://doi.org/10.1016/j.ssc.2015.04. 019. URL http://www.sciencedirect.com/science/article/pii/ S0038109815001532.

[4] Raditya Weda Bomantara and Jiangbin Gong. Simulation of non-abelian braiding in majorana time crystals. *Phys. Rev. Lett.*, 120:230405, Jun 2018. doi: 10.1103/PhysRevLett.120.230405. URL https://link.aps.org/doi/10. 1103/PhysRevLett.120.230405.

[5] Raditya Weda Bomantara and Jiangbin Gong. Quantum computation via floquet topological edge modes. *Phys. Rev. B*, 98:165421, Oct 2018. doi: 10. 1103/PhysRevB.98.165421. URL https://link.aps.org/doi/10.1103/ PhysRevB.98.165421.

[6] Aaron Chew, David F. Mross, and Jason Alicea. Fermionized parafermions and symmetry-enriched majorana modes. *Phys. Rev. B*, 98:085143, Aug 2018. doi: 10.1103/PhysRevB.98.085143. URL https://link.aps.org/doi/ 10.1103/PhysRevB.98.085143.

[7] Soonwon Choi, Joonhee Choi, Renate Landig, Georg Kucsko, Hengyun Zhou, Junichi Isoya, Fedor Jelezko, Shinobu Onoda, Hitoshi Sumiya, Vedika Khemani, Curt von Keyserlingk, Norman Y. Yao, Eugene Demler, and Mikhail D. Lukin. Observation of discrete time-crystalline order in a disordered dipolar many-body system. *Nature*, 543:221 EP –, Mar 2017. URL https://doi.org/10.1038/nature21426.

[8] T.-P. Choy, J. M. Edge, A. R. Akhmerov, and C. W. J. Beenakker. Majorana fermions emerging from magnetic nanoparticles on a superconductor without spin-orbit coupling. *Phys. Rev. B*, 84:195442, Nov 2011. doi: 10.1103/PhysRevB.84.195442. URL https://link.aps.org/doi/ 10.1103/PhysRevB.84.195442.

[9] Luca D'Alessio and Marcos Rigol. Long-time behavior of isolated periodically driven interacting lattice systems. *Phys. Rev. X*, 4:041048, Dec 2014. doi: 10. 1103/PhysRevX.4.041048. URL https://link.aps.org/doi/10.1103/PhysRevX.4.041048.

[10] Dominic V. Else and Chetan Nayak. Classification of topological phases in periodically driven interacting systems. *Phys. Rev. B*, 93:201103, May 2016. doi: 10.1103/PhysRevB.93.201103. URL https://link.aps.org/doi/10.1103/PhysRevB.93.201103.

[11] Dominic V. Else, Bela Bauer, and Chetan Nayak. Floquet time crystals. *Phys. Rev. Lett.*, 117:090402, Aug 2016. doi: 10.1103/PhysRevLett.117.090402. URL https://link.aps.org/doi/10.1103/PhysRevLett.117.090402.

[12] Ion C Fulga, Arbel Haim, Anton R Akhmerov, and Yuval Oreg. Adaptive tuning of majorana fermions in a quantum dot chain. *New Journal of Physics*, 15(4):045020, apr 2013. doi: 10.1088/1367-2630/15/4/045020. URL https://doi.org/10.1088%2F1367-2630%2F15%2F4%2F045020.

[13] David A. Huse, Rahul Nandkishore, Vadim Oganesyan, Arijeet Pal, and S. L. Sondhi. Localization-protected quantum order. *Phys. Rev. B*, 88:014206, Jul 2013. doi: 10.1103/PhysRevB.88.014206. URL https://link.aps.org/doi/10.1103/PhysRevB.88.014206.

[14] Liang Jiang, Takuya Kitagawa, Jason Alicea, A. R. Akhmerov, David Pekker, Gil Refael, J. Ignacio Cirac, Eugene Demler, Mikhail D. Lukin, and Peter Zoller. Majorana fermions in equilibrium and in driven cold-atom quantum wires. *Phys. Rev. Lett.*, 106:220402, Jun 2011. doi: 10.1103/PhysRevLett.106.220402. URL https://link.aps.org/doi/10.1103/PhysRevLett.106.220402.

[15] Vedika Khemani, Achilleas Lazarides, Roderich Moessner, and S. L. Sondhi. Phase structure of driven quantum systems. *Phys. Rev. Lett.*, 116:250401, Jun 2016. doi: 10.1103/PhysRevLett.116.250401. URL https://link.aps.org/doi/10.1103/PhysRevLett.116.250401.

[16] A Yu Kitaev. Unpaired majorana fermions in quantum wires. *Physics-Uspekhi*, 44(10S):131–136, oct 2001. doi: 10.1070/1063-7869/44/10s/s29. URL https://doi.org/10.1070%2F1063-7869%2F44%2F10s%2Fs29.

[17] Achilleas Lazarides, Arnab Das, and Roderich Moessner. Equilibrium states of generic quantum systems subject to periodic driving. *Phys. Rev. E*, 90: 012110, Jul 2014. doi: 10.1103/PhysRevE.90.012110. URL https://link.aps.org/doi/10.1103/PhysRevE.90.012110.

[18] Dillon T. Liu, Javad Shabani, and Aditi Mitra. Floquet majorana zero and π modes in planar josephson junctions, 2018.

[19] Angus MacKinnon. *Transfer Matrices and Disordered Systems*, pages 21–30. Springer Berlin Heidelberg, Berlin, Heidelberg, 2003. ISBN 978-3-540-45202-7. doi: 10.1007/978-3-540-45202-7_2. URL https://doi.org/10.1007/978-3-540-45202-7_2.

[20] Christoph P. Orth, Rakesh P. Tiwari, Tobias Meng, and Thomas L. Schmidt. Non-Abelian parafermions in time-reversal-invariant interacting helical systems. *Phys. Rev. B*, 91:081406, Feb 2015. doi: 10.1103/PhysRevB.91.081406.

[21] Arijeet Pal and David A. Huse. Many-body localization phase transition. *Phys. Rev. B*, 82:174411, Nov 2010. doi: 10.1103/PhysRevB.82.174411. URL https://link.aps.org/doi/10.1103/PhysRevB.82.174411.

[22] Soham Pal, Naveen Nishad, T. S. Mahesh, and G. J. Sreejith. Temporal order in periodically driven spins in star-shaped clusters. *Phys. Rev. Lett.*, 120:180602, May 2018. doi: 10.1103/PhysRevLett.120.180602. URL https://link.aps.org/doi/10.1103/PhysRevLett.120.180602.

[23] Pedro Ponte, Z. Papić, Fran çois Huveneers, and Dmitry A. Abanin. Many-body localization in periodically driven systems. *Phys. Rev. Lett.*, 114:140401, Apr 2015. doi: 10.1103/PhysRevLett.114.140401. URL https://link.aps.org/doi/10.1103/PhysRevLett.114.140401.

[24] Andrew C. Potter, Takahiro Morimoto, and Ashvin Vishwanath. Classification of interacting topological floquet phases in one dimension. *Phys. Rev. X*, 6:041001, Oct 2016. doi: 10.1103/PhysRevX.6.041001. URL https://link.aps.org/doi/10.1103/PhysRevX.6.041001.

[25] Jared Rovny, Robert L. Blum, and Sean E. Barrett. Observation of discrete-time-crystal signatures in an ordered dipolar many-body system. *Phys. Rev. Lett.*, 120:180603, May 2018. doi: 10.1103/PhysRevLett.120.180603. URL https://link.aps.org/doi/10.1103/PhysRevLett.120.180603.

[26] Rahul Roy and Fenner Harper. Abelian floquet symmetry-protected topological phases in one dimension. *Phys. Rev. B*, 94:125105, Sep 2016. doi: 10.1103/PhysRevB.94.125105. URL https://link.aps.org/doi/10.1103/PhysRevB.94.125105.

[27] Rahul Roy and Fenner Harper. Floquet topological phases with symmetry in all dimensions. *Phys. Rev. B*, 95:195128, May 2017. doi: 10.1103/PhysRevB.95.195128. URL https://link.aps.org/doi/10.1103/PhysRevB.95.195128.

[28] Jay D. Sau and S. Das Sarma. Realizing a robust practical majorana chain in a quantum-dot-superconductor linear array. *Nature Communications*, 3:964 EP –, Jul 2012. URL https://doi.org/10.1038/ncomms1966. Article.

[29] Alfred Shapere and Frank Wilczek. Classical time crystals. *Phys. Rev. Lett.*, 109:160402, Oct 2012. doi: 10.1103/PhysRevLett.109.160402. URL https://link.aps.org/doi/10.1103/PhysRevLett.109.160402.

[30] J. Smits, L. Liao, H. T. C. Stoof, and P. van der Straten. Observation of a space-time crystal in a superfluid quantum gas. *Phys. Rev. Lett.*, 121:185301, Oct 2018. doi: 10.1103/PhysRevLett.121.185301. URL https://link.aps.org/doi/10.1103/PhysRevLett.121.185301.

[31] C. W. von Keyserlingk and S. L. Sondhi. Phase structure of one-dimensional interacting floquet systems. i. abelian symmetry-protected topological phases. *Phys. Rev. B*, 93:245145, Jun 2016. doi: 10.1103/PhysRevB.93.245145. URL https://link.aps.org/doi/10.1103/PhysRevB.93.245145.

[32] C. W. von Keyserlingk, Vedika Khemani, and S. L. Sondhi. Absolute stability and spatiotemporal long-range order in floquet systems. *Phys. Rev. B*, 94:085112, Aug 2016. doi: 10.1103/PhysRevB.94.085112. URL https://link.aps.org/doi/10.1103/PhysRevB.94.085112.

[33] Haruki Watanabe and Masaki Oshikawa. Absence of quantum time crystals. *Phys. Rev. Lett.*, 114:251603, Jun 2015. doi: 10.1103/PhysRevLett.114.251603. URL https://link.aps.org/doi/10.1103/PhysRevLett.114.251603.

[34] Frank Wilczek. Quantum time crystals. *Phys. Rev. Lett.*, 109:160401, Oct 2012. doi: 10.1103/PhysRevLett.109.160401. URL https://link.aps.org/doi/10.1103/PhysRevLett.109.160401.

[35] Xiaosen Yang, Beibing Huang, and Zhengling Wang. Floquet topological superfluid and majorana zero modes in two-dimensional periodically driven fermi systems. *Scientific Reports*, 8(1):2243, 2018. ISSN 2045-2322. doi: 10.1038/s41598-018-20604-w. URL https://doi.org/10.1038/s41598-018-20604-w.

[36] N. Y. Yao, A. C. Potter, I.-D. Potirniche, and A. Vishwanath. Discrete time crystals: Rigidity, criticality, and realizations. *Phys. Rev. Lett.*, 118:030401, Jan 2017. doi: 10.1103/PhysRevLett.118.030401. URL https://link.aps.org/doi/10.1103/PhysRevLett.118.030401.

[37] Fan Zhang and C. L. Kane. Time-reversal-invariant Z_4 fractional josephson effect. *Phys. Rev. Lett.*, 113:036401, Jul 2014. doi: 10.1103/PhysRevLett.113.036401. URL https://link.aps.org/doi/10.1103/PhysRevLett.113.036401.

[38] J. Zhang, P. W. Hess, A. Kyprianidis, P. Becker, A. Lee, J. Smith, G. Pagano, I.-D. Potirniche, A. C. Potter, A. Vishwanath, N. Y. Yao, and C. Monroe. Observation of a discrete time crystal. *Nature*, 543:217 EP –, Mar 2017. URL https://doi.org/10.1038/nature21413.

Chapter 5

CONCLUSION

In this thesis, we have proposed different setups that enrich the already nontrivial physics of the Majorana mode. These setups all consist of heterostructures built from realtively well-understood phases of matter. Our work can be viewed as a sort of intermediate step between near-term and fully-fledged topological quantum computation: by harnessing systems already being developed for computation, we create testbeds for new, unexplored physics.

Our first project detailed a scheme to realize the SYK model by hybridizing Majorana nanowires and quantum dots. The SYK model is a theoetical goldmine for the study of holography and gravity; realizing this system in the laboratory will thus be of immense value. It is natural to ask the following question: if an implementation of the SYK model is created, what properties of the system should be studied? One quantity that will be of great interest to study is out of time ordered correlators, or OTOCs. In the SYK model, this quantity saturates a bound on how rapidly quantum chaos can grow in a system. Measuring this quantity remains a major challenge, due to the necessity of backwards-in-time measurement of operators.

Our second project, investigating the relationship between Z_4 parafermions and Majorana modes intertwined with symmetry breaking, has highlighted all sorts of new dualities and mappings between different phases of matter. Perhaps most striking is the technique to recover signatures of Z_4 parafermionic fusion in pumping cycles. Our result detailing the pumping cycle between the TRITOPS and trivial phase is extremely appealing in that no interactions are needed; the Z_4 character of the phases is revealed via free fermion physics. One many further consider extending our symmetry enrichment to more nontrivial phases and symmetries; for example, using two dimensional systems or quantum Hall phases.

Our final result, the time-crystalline topological superconductor, has illuminated a new direction in heterostructure creation. To the best of our knowledge, time crystals have never before been considered as tools to be exploited to enrich non-Abelian anyon physics. We show this avenue is extremely profitable, creating a new type of anomalous Majorana zero mode that cannot emerge in standard Majorana wire systems. We also detail experimental protocols to probe the anomalous character

of these zero modes in physical setups. This result begs the question of whether time crystals can be further exploited in more nontrivial settings, again perhaps in two-dimensional materials.

Our work here has only scratched the surface of what is possible with Majorana zero modes. We have employed well-known phases of matter to create exotic systems, but what if we were to use different ingredients, like quantum Hall systems, topological insulators, in place of our superconductors and ferromagnets? Our three projects are exciting results in what is potentially an extremely profitable line of research: using known phases of matter to enrich and probe properties of Majorana zero modes and other non-Abelian anyons.